



<https://theses.gla.ac.uk/>

Theses Digitisation:

<https://www.gla.ac.uk/myglasgow/research/enlighten/theses/digitisation/>

This is a digitised version of the original print thesis.

Copyright and moral rights for this work are retained by the author

A copy can be downloaded for personal non-commercial research or study,
without prior permission or charge

This work cannot be reproduced or quoted extensively from without first
obtaining permission in writing from the author

The content must not be changed in any way or sold commercially in any
format or medium without the formal permission of the author

When referring to this work, full bibliographic details including the author,
title, awarding institution and date of the thesis must be given

Enlighten: Theses

<https://theses.gla.ac.uk/>
research-enlighten@glasgow.ac.uk

**THE USE OF α/β LIQUID SCINTILLATION SPECTROMETRY IN MARINE
TRACER STUDIES**

Jacqueline Mary Pates

Scottish Universities Research and Reactor Centre

Presented as a thesis for the degree of
Doctor of Philosophy
in the University of Glasgow

March 1995

© J. M. Pates, 1995

ProQuest Number: 10992194

All rights reserved

INFORMATION TO ALL USERS

The quality of this reproduction is dependent upon the quality of the copy submitted.

In the unlikely event that the author did not send a complete manuscript and there are missing pages, these will be noted. Also, if material had to be removed, a note will indicate the deletion.



ProQuest 10992194

Published by ProQuest LLC (2018). Copyright of the Dissertation is held by the Author.

All rights reserved.

This work is protected against unauthorized copying under Title 17, United States Code
Microform Edition © ProQuest LLC.

ProQuest LLC.
789 East Eisenhower Parkway
P.O. Box 1346
Ann Arbor, MI 48106 – 1346

Theris
10194
Copy 1



TABLE OF CONTENTS

ACKNOWLEDGEMENTS	(i)
DECLARATION	(ii)
ABSTRACT	(iii)
GLOSSARY OF ABBREVIATIONS	(vi)
CHAPTER 1: INTRODUCTION	1
1.1 INTRODUCTION	1
1.2 LIQUID SCINTILLATION SPECTROMETRY	2
1.2.1 Radioactive decay	3
1.2.2 The liquid scintillation counter	5
1.2.2.1 Quenching	10
1.2.2.2 Background reduction	15
1.2.3 Liquid scintillation samples	20
1.2.3.1 The sample	21
1.2.3.2 The vial	21
1.2.3.3 The cocktail	24
1.3 ALPHA / BETA SEPARATION LSS	34
1.3.1 Pulse shape characteristics	35
1.3.2 Scintillation response	37
1.3.3 Pulse shape discrimination	39
1.3.4 Pulse shape discrimination applied to LSS	41
1.3.4.1 Energy resolution	42
1.3.4.2 Pulse shape resolution	44

1.3.4.3 α/β separation liquid scintillation spectrometers	45
1.4 URANIUM SERIES RADIONUCLIDES IN THE MARINE ENVIRONMENT	48
1.4.1 Geochemistry and Distribution	48
1.4.2 Radioactive Disequilibrium	52
1.4.3 Marine tracer studies	54
1.5 AIMS	60

CHAPTER 2: OPTIMIZATION OF COUNTING CONDITIONS AND COCKTAIL

DEVELOPMENT FOR ALPHA/BETA LSS	62
2.1 INTRODUCTION	62
2.1.1 The effect of cocktail composition	63
2.1.2 The effects of quenching	67
2.1.3 Other factors	69
2.2 EXPERIMENTAL	70
2.2.1 Determination of the optimum PDD setting	72
2.2.1.1 Manual determination	72
2.2.1.2 Instrumental determination	76
2.2.2 Cocktail development and optimization	76
2.2.3 Quenching	81
2.2.4 Other factors	82
2.3 RESULTS AND DISCUSSION	83
2.3.1 Cocktail optimization	83
2.3.2 Quenching	101
2.3.3 Other factors	112
2.4 CONCLUSIONS	115

CHAPTER 3: DEVELOPMENT OF AN α/β LIQUID SCINTILLATION SPECTROMETRY

METHOD FOR ^{234}Th ANALYSIS	117
3.1 INTRODUCTION	117
3.2 ANALYTICAL METHODS	118
3.2.1 Current methods of analysis	118
3.2.1.1 Gamma spectrometry	119
3.2.1.2 Gas proportional counting	121
3.2.1.3 ^{238}U analysis	124
3.2.2 LSS as an alternative method	126
3.3 DEVELOPMENT OF AN α/β LSS METHOD FOR ^{234}Th IN MARINE	
SAMPLES	127
3.3.1 Preparation of ^{234}Th and ^{230}Th spikes	128
3.3.2 Optimization of instrumental parameters	131
3.3.3 Optimization of chemical separation procedure	134
3.3.3.1 Dissolved ^{234}Th analysis	140
3.3.3.2 Suspended particulate ^{234}Th analysis	150
3.3.3.3 Extractive scintillators	153
3.3.3.4 Manganese dioxide columns	155
3.3.3.5 The effect of variable quenching	156
3.3.3.6 ^{238}U analysis	162
3.3.4 Quality control	163
3.4 CONCLUSIONS	178

CHAPTER 4: APPLICATIONS OF $^{234}\text{Th}/^{238}\text{U}$ DISEQUILIBRIUM IN THE MARINE

ENVIRONMENT	180
-------------	-----

CHAPTER 4: APPLICATIONS OF $^{234}\text{Th}/^{238}\text{U}$ DISEQUILIBRIUM IN THE MARINE ENVIRONMENT	180
4.1 INTRODUCTION	180
4.2 SURVEY OF APPLICATIONS	181
4.2.1 Sedimentary processes	181
4.2.2 Carbon fluxes	184
4.2.3 Reactive pollutants	188
4.3 APPLICATIONS OF THE α/β LSS ^{234}Th METHOD TO MARINE TRACER STUDIES	191
4.3.1 Partitioning of ^{234}Th in the Northeast Atlantic and Firth of Clyde	191
4.3.1.1 Introduction	191
4.3.1.2 Experimental methods	194
4.3.1.3 Northeast Atlantic: results and discussion	195
4.3.1.4 Firth of Clyde: results and discussion	209
4.3.2 Hydrothermal vents in the Mid-Atlantic Ridge	214
4.3.2.1 Introduction	214
4.3.2.2 Experimental methods	216
4.3.2.3 Results and discussion	218
4.4 CONCLUSIONS	224
 CHAPTER 5: CONCLUSIONS	 226
 REFERENCES	 229

LIST OF TABLES

Table 1.1: Safety and performance data for some LS solvents	26
Table 1.2: A comparison of different LS spectrometers and their performance with respect to α analysis	46
Table 2.1: Comparison of % spills for open and narrow windows, with and without background subtraction	79
Table 2.2: Cross-over characteristics and composition of the cocktails studied	84
Table 2.3: Water and mineral acid holding capacities of the DIN based cocktails	88
Table 2.4 Comparison of the α/β separation efficiency of $^{90}\text{Sr}/^{90}\text{Y}$ and ^{238}Pu in cocktails differing only in the secondary fluor	91
Table 2.5: Comparison of the 2250 CA α/β , the 2550 TR/AB	94
Table 2.6: The effect of varying solvent on the α/β separation properties of various secondary fluors	101
Table 2.7: Changes in optimum PDD and % spill _m for various β emitters with increasing quench by nitromethane	102
Table 2.8: Change in optimum PDD and misclassification with quenching for various quenching agents	108
Table 2.9: The effect of purging Ultima Gold™ AB with oxygen and nitrogen on α/β separation	112
Table 2.10: The effect of varying cocktail volume, vial type and vial volume on α/β separation	114
Table 3.1: Optimization of the E^2/B figure of merit for ^{234}Th	135

Table 3.2: Comparison of a selection of reported details of spike equilibration and iron (III) hydroxide precipitation procedures	141
Table 3.3: The effect of added iron concentration and stirring times on the recovery of ^{230}Th	142
Table 3.4: Effect of varying aluminium concentration and number of precipitations on the recovery of ^{230}Th	144
Table 3.5: Comparison of the effect of different elution acids on thorium recovery from nitrate form columns	146
Table 3.6: Comparison of the background and efficiency obtainable with 7 ml glass and plastic vials for ^{234}Th	149
Table 3.7: Comparison of the effectiveness of different hydrochloric acid strengths in redissolving ^{230}Th spike solutions	150
Table 3.8: Comparison of recovery of thorium from filter papers treated in various ways	151
Table 3.9: The recovery of ^{230}Th from spiked solutions using the extractive scintillator THOREX®	154
Table 3.10: The effect of quenching on ^{234}Th and ^{230}Th counting efficiencies	159
Table 3.11: Effect on errors of using the normal count mode (NCM) and low-level count mode (LLCM) with and without optimized windows	169
Table 3.12: The effect of counting time on the errors for duplicate estuarine samples	171
Table 3.13: The effect of sample volume on the errors associated with duplicate estuarine samples	173
Table 3.14: Reagent blanks counted on three occasions	176
Table 4.1: Results of ^{234}Th analysis for Northeast Atlantic samples collected during cruises CH97/92, CH101B/93 and CH105/93	196

Table 4.2: Rate of removal and residence times for ^{234}Th in the dissolved and particulate phases for Northeast Atlantic samples	202
Table 4.3: Rates of removal and residence times for ^{234}Th from the dissolved and particulate phases from a depth profile at station B in the Northeast Atlantic	207
Table 4.4: Results from sea loch samples and sampling cruises (CH101B/93 and 105/93) for Firth of Clyde samples	210
Table 4.5: Rate of removal and residence times for Firth of Clyde samples	212
Table 4.6: Results from hydrothermal vent samples collected at the MARK, TAG and Broken Spur sites	219

LIST OF FIGURES

Figure 1.1: Simplified circuit diagram of a liquid scintillation counter (after Kessler, 1989).	9
Figure 1.2: The spectrum of PPO compared to the sensitivity of a typical PMT (after Kessler, 1989).	30
Figure 1.3: Energy transfer in a liquid binary solution.	32
Figure 1.4: Schematic diagram of the relative contributions of radiative and non-radiative energy transfer between fluors (after Birks and Kuchela, 1961).	33
Figure 1.5: Liquid scintillation spectra of ^{241}Am and ^{36}Cl	38
Figure 1.6: Schematic representation of the zero-crossing method of pulse shape discrimination.	40
Figure 1.7: The natural decay series (major branching schemes).	49
Figure 1.8: Simple box model (after Cochran, 1992).	55
Figure 1.9: Partitioned box model for radionuclide scavenging (after Cochran, 1992).	58
Figure 2.1: Schematic representation of a cross-over plot.	73
Figure 2.2: Cross-over (A and B) and total spill (C and D) plots showing skewing of the apparent optimum PDD.	74
Figure 2.3: The ability of different polynomials to model cross-over plots.	75
Figure 2.4: 5th order polynomial fitted to data of varying resolution.	77
Figure 2.5: Cross-over (A and B) and total spill (C) plots for cocktail 08.	78
Figure 2.6: The effect on the % spill of using open and narrow windows, with and without background subtraction.	80
Figure 2.7: The relationship between surfactant concentration and % spill _m	85
Figure 2.8: The relationship between % spill _m and tSIE.	86

Figure 2.9: The relationship between surfactant concentration and tSIE.	86
Figure 2.10: PMT anode pulse shapes for A) cocktail 07 and B) cocktail 08.	89
Figure 2.11: Molecular structures for the fluors studied.	92
Figure 2.12: Comparison of different instruments with samples in Insta-Gel® XF + 20% naphthalene. A) 2250 CA α/β , B) 2550 TR/AB (a) and C) 2550 TR/AB (b).	93
Figure 2.13: The relationship between % spill _m and optimum PDD.	95
Figure 2.14: PMT anode pulse shapes for: A) cocktail M, B) cocktail L and C) cocktail J.	96
Figure 2.15: The effect on optimum PDD and % spill of two groups of secondary fluors.	97
Figure 2.16: The relationship between tSIE, % spill _m and optimum PDD.	98
Figure 2.17: $^{90}\text{Sr}/^{90}\text{Y}$ and ^{210}Po cross-over plots with increasing quenching by nitromethane. . .	104
Figure 2.18: PMT anode pulse shapes with increasing nitromethane quench. A) no added CH_3NO_2 , B) 35 μl and C) 100 μl CH_3NO_2	105
Figure 2.19: The change in % spill with increasing nitromethane quench at constant PDD for a range of β emitters.	107
Figure 2.20: Schematic of the effect of quenching on the misclassification of α events.	109
Figure 2.21: The effect on the optimum PDD and % spill of various quenching agents. A) nitromethane, B) acetone, C) carbon tetrachloride and D) 9M hydrochloric acid.	110
Figure 2.22: The effect on optimum PDD and % spill of purging Ultima Gold™ AB.	111
Figure 2.23: The effect of vial type on optimum PDD and % spill. A) 7 ml vials + 5 ml cocktail, B) 20 ml vials + 10 ml cocktail.	113
Figure 2.24: The effect of cocktail volume and size on optimum PDD and % spill.	114
Figure 3.1: Schematic of the principal decay schemes of ^{234}Th , $^{234\text{m}}\text{Pa}$ and ^{234}Pa	119
Figure 3.2: Typical procedures employed for ^{234}Th analysis of A) sediment (Aller and DeMaster, 1984) and B) seawater (Moran and Buesseler, 1993).	125

Figure 3.3: Spectrum from a seawater sample counted in the 2550 TR/AB (b) showing the ^{230}Th peak and the underlying $^{234}\text{Th}/^{234\text{m}}\text{Pa}$ continuum.	127
Figure 3.4: Separation procedure employed for spike preparation.	129
Figure 3.5: Decay and ingrowth of ^{234}Th in an unsupported and a supported situation respectively.	131
Figure 3.6: Instrumentally determined cross-over plot for ^{234}Th and ^{230}Th , showing the optimum PDD and the PDD employed, using the 2550 TR/AB (b).	132
Figure 3.7: Optimization of the β counting window and low-level option for ^{234}Th using the 2550 TR/AB (b).	137
Figure 3.8: The separation procedure developed and employed in the present work for the determination of ^{234}Th in seawater and marine particulate material.	138
Figure 3.9: The two types of filtration apparatus employed in the present work.	139
Figure 3.10: Sampling locations for samples HB (Helensburgh), AR (Arrochar) and LG (Carrick).	152
Figure 3.11: Manganese dioxide column apparatus.	157
Figure 3.12: The effect of quenching on counting efficiency for ^{234}Th (A) and ^{230}Th (B) in the NCM (a,c) and LLCM (b,d) using open (a,b) and optimized (c,d) windows.	161
Figure 3.13: Schematic representation of decay and ingrowth processes affecting the ^{234}Th activity in a sample before counting.	164
Figure 3.14: The variation in background standards between different vials and different counts.	175
Figure 3.15: Ingrowth of ^{234}Th into filtered estuarine water samples.	178
Figure 4.1: Two dimensional model of thorium scavenging (after McKee et al., 1984).	182
Figure 4.2: Schematic of the marine organic carbon cycle (after Chester, 1990).	185

Figure 4.3: Schematic of a multi-layer box model (after Buesseler, 1992a).	189
Figure 4.4: Location of Northeast Atlantic and Firth of Clyde sampling stations.	192
Figure 4.5: $^{234}\text{Th}/^{238}\text{U}$ activity ratios for the two transects: A) northern and B) southern.	199
Figure 4.6: $^{234}\text{Th}/^{238}\text{U}$ activity ratios for the depth profile sampled during cruise CH97/92 at Station B.	200
Figure 4.7: Rate of removal for ^{234}Th in the dissolved and particulate phase with increasing distance from land. A) northern transect and B) southern transect.	203
Figure 4.8: Residence times for ^{234}Th in the dissolved and particulates phases with increasing distance from land. A) northern transect and B) southern transect.	205
Figure 4.9: Rate of removal and residence times of dissolved and particulate ^{234}Th with increasing depth at Station B (cruise CH97/92).	208
Figure 4.10: $^{234}\text{Th}/^{238}\text{U}$ activity ratios for the Firth of Clyde samples vs. salinity.	212
Figure 4.11: Residence times for ^{234}Th in the dissolved and particulate phases for the Firth of Clyde samples vs. salinity.	213
Figure 4.12: Depth profiles of samples taken at the Mid-Atlantic Ridge. A) MARK site, B) TAG site and C) Broken Spur site.	222
Figure 4.13: Particulate ^{234}Th data from the TAG site for 1988 (from German et al., 1991a) and 1993.	223

ACKNOWLEDGEMENTS

I would like to thank my supervisors, Dr Gordon Cook and Dr Gus MacKenzie, for their valued support and help throughout the past three years. Also, Chuck Passo and other staff at Packard Instruments for their encouragement and the opportunity to partake in several trips to the US - often boosting flagging morale in the process. More formally, I would like to thank both the NERC and Packard Instruments for financial support during this work.

My parents, Jenny and Andy, who made me continue with my studies when I wanted to give up, are the best I could ask for. I also appreciate the support of my brother, William, and my sister, Lucy, also both there with love and encouragement and silliness.

The staff and students at the SURRC have been a source of friendship, fun and enthusiasm throughout my time there, which helped in the hard times that we all have. Most especially, I would like to thank Dr Paul McDonald, who helped get me started; Phil Naysmith and Alison Stuart, for always being willing to assist when needed; Bob Anderson, for teaching me so much about what liquid scintillation can and cannot do; Eleanor Logan, for going through it all at the same time, and providing a shoulder when needed and a giggle when needed more; and last, but not least, all the other students. Thanks!

And most of all - Gawen. You put up with the tears, grumpiness and lack of self-esteem. I hope it hasn't been too awful. Thank you with all my heart.

DECLARATION

Except where specific reference is made to other sources, the work presented in this thesis is the original work of the author. It has not been submitted, in part or in whole, for any other degree.

Certain of the results from Chapters 2 and 3 have been published elsewhere, in either peer-reviewed conference proceedings or journals.

Jacqueline M. Pates

ABSTRACT

Liquid scintillation spectrometry (LSS) is becoming an increasingly important tool in the analysis of both anthropogenic and naturally occurring radionuclides, partly due to the introduction of pulse shape discrimination (PSD) into commercial, β counting instruments. PSD allows α and β events, in the same sample, to be separated into different multi-channel analysers (MCAs), opening up the possibility for novel applications of the technique to be developed. PSD works by examining the duration of individual pulses as they reach the photomultiplier tube (PMT) anode, α pulses being longer than β pulses. The optimum pulse decay discriminator (PDD) setting is found by determining the misclassification of events over a range of settings for a pure α emitter and a pure β emitter, referred to as standards.

The objectives of this work were: to characterize an α/β LS spectrometer and optimize the separation of α from β events; to develop an aqueous accepting cocktail, suitable for the simultaneous determination of α and β emitters; develop a method using the instrument for the determination of ^{234}Th , in the presence of a ^{230}Th yield tracer, in marine samples; and to apply this method in marine tracer studies.

This work commences with a study of the factors affecting PSD and α/β separation. Although a comprehensive study had been made of the factors affecting both pulse shape and pulse height resolution for the single PMT, PERALS® instrument, no similar survey had previously been carried out on an instrument capable of both α and β analysis. It was found that cocktail composition was a critical factor in how efficiently the instrument was able to distinguish between α and β events. A comparison was made between several solvents, surfactants and fluors to examine the effects of individual components of the cocktail and to develop a cocktail specifically for α/β separation of aqueous samples. In order for PMT anode pulses to be sufficiently different between the two types

of event, the cocktail needed to contain a "slow" solvent (*i.e.* with a long decay constant), such as diisopropylnaphthalene (DIN), which produced significantly longer α than β pulses. However, the combination of a fast solvent with a slow fluor did not have the same effect on PMT anode pulse shapes. The optimum cocktail formulation found used DIN as the solvent and the fluors PPO and *bis*-MSB, and has been marketed by Packard Instruments as Ultima Gold® AB. Later work showed that POPOP may be a suitable alternative to the secondary fluor, *bis*-MSB.

Other factors examined included the effects of quenching, vial size, vial type, cocktail volume and the effects of purging the cocktail prior to counting. Quenching was shown to play a major role in α/β separation, with different quenching levels giving rise to different degrees of misclassification. Thus, if the level of misclassification in the standards is to accurately reflect that found in samples, it is essential to maintain constant levels of quenching throughout an experiment. In addition, different quenching agents were shown to have different effects on PMT anode pulse shapes, and consequently produce a variety of changes in the degree of misclassification. Glass vials produced better separation of α and β events than plastic vials. The cause of this difference remained unclear, but a possible explanation is interaction between the cocktail and the vial wall, resulting in altered pulse shapes. While vial size and cocktail volume had no significant effect on α/β separation, it should be remembered that they can affect both counting efficiency and the measurement of quenching. Purging the cocktail with oxygen-free gas did not affect PSD when the cocktail was based on DIN, as oxygen has a low solubility in this solvent.

Once the instrument and sample composition had been optimized for α/β separation, a novel technique was developed for the determination of ^{234}Th , in the presence of a ^{230}Th yield tracer, and optimized for the analysis of seawater and suspended marine particulate material. The chemical separation of thorium was based on established procedures, but various stages were re-examined with regard to both the sample matrices and the alternative counting technique. In particular, attention was

paid to the final sample preparation, the effects of quenching on counting efficiency and misclassification, and the use of electronic background reduction. The limit of detection for the method, for a 10 l sample, was found to be 0.08 dpm l⁻¹, which was sufficient for the applications studied in the present work. This figure could be reduced to 0.04 dpm l⁻¹ by the use of 20 l samples, or to 0.05 dpm l⁻¹ for 10 l samples, if a more modern instrument, with a lower β background, were employed.

The method was applied to two studies of the partitioning of thorium between the dissolved and particulate phases in the marine environment, one in the Northeast Atlantic and Firth of Clyde and the other in the hydrothermal vent fields of the Mid-Atlantic Ridge (MAR). The first showed that this method was capable of distinguishing the greater scavenging rates associated with the higher production that can occur in the region of an oceanic front. However, the samples taken from the Firth of Clyde were close to the detection limit for the technique, and there would have been an advantage in taking 20 l samples. The second study showed that the method can be used with samples collected using manganese dioxide cartridges. The large sample volumes (~ 100 l) and high counting efficiencies for LSS enabled the analysis to be conducted several weeks after sampling, upon completion of the cruise. However, little information could be gained on scavenging processes at hydrothermal vents as the manganese cartridges were shown to have scavenged thorium with highly variable efficiencies.

GLOSSARY OF ABBREVIATIONS

ADC	analogue-to-digital converter
AQC	automatic quench correction
<i>bis</i> -MSB	<i>p-bis</i> -(<i>o</i> -methylstyryl)-benzene
BGO	bismuth germanate
BNL	bottom nepheloid layer
butyl-PBD	2-(4'- <i>tert</i> -butylphenyl)-5-(4''-biphenyl)-1,3,4-oxadiazole
DBB	delay-before-burst
DIN	di-isopropylnapthalene
DIPE	di-isopropylether
DMA	9,10-dimethylantracene
DPA	9,10-diphenylantracene
ESCR	external standard channels ratio
ICP-MS	inductively coupled plasma-mass spectrometry
IOSDL	Institute of Oceanographic Sciences - Deacon Laboratory
LLCM	low-level count mode
LSC	liquid scintillation counting
LSS	liquid scintillation spectrometry
MAR	Mid-Atlantic Ridge
MCA	multi-channel analyser
NCM	normal count mode
α -NOPON	1,4- <i>bis</i> -[2-(5- α -naphthyloxazolyl)]-benzene
NWM	nominal molecular weight

PBBO	2-(4'-biphenyl)-6-phenylbenzoxazole
PDA	pulse decay analysis
PDD	pulse decay discriminator
PERALS®	Photon/Electron Rejecting Alpha Liquid Scintillation
PMT	photomultiplier tube
POPOP	1,4-di-[2-(5-phenyloxazolyl)]-benzene
PPO	2,5-diphenyloxazole
PSA	pulse shape analysis
PSD	pulse shape discrimination
PXE	phenylxylylene
QIP	quench indicator parameter
RPH	relative pulse height
SAP	stand-alone pump
SCR	sample channels ratio
SIE	spectral index of the external standard
SIS	spectral index of the sample
SQP(E)	spectral quench parameter (external)
SQP(I)	spectral quench parameter (internal)
SURRC	Scottish Universities Research and Reactor Centre
TD	time discriminator
TOPO	trioctyl phosphine oxide
TR-LSC™	Time-Resolved-LSC
TTA	thenoyltrifluoroacetone
tSIE	transformed spectral index of the external standard

CHAPTER 1: INTRODUCTION

1.1 INTRODUCTION

Liquid scintillation spectrometry or counting (LSS or LSC) is a method of determining the activity of a radioactive sample, whereby the sample is usually homogeneously mixed with a scintillating liquid called a cocktail. The focus of the work presented here was the simultaneous determination of α and β^- activity by LSS. The starting point of the study was the optimization of the separation of α from β^- events, including the development of a new LS cocktail specifically for α/β separation in aqueous samples, as none previously existed for this purpose. Thereafter, the objective was the development of an LS analytical method for the determination of ^{234}Th (β^- emitter) in the presence of ^{230}Th (α emitter) yield tracer. ^{234}Th is widely used as a tracer of marine processes, but existing analytical methods have certain disadvantages, which are discussed in detail later (section 3.2.2). LSS, utilizing α/β separation, could provide an alternative to the existing counting techniques, with some advantages, such as a reduction in sample volume.

The first commercial liquid scintillation (LS) counters were produced in 1953 by the Packard Instrument Company (Rapkin, 1970), after Raben and Bloembergen (1951) first used the technique of dissolving a radioactive sample in a scintillating solution. Liquid scintillation spectrometry, as a tool for radiochemical analysis, has undergone many changes since then, with the most rapid advances occurring during the last decade. Early instrumentation was restricted in its use, by a relatively high background and lack of spectral data, to counting high activities of ^3H , ^{14}C and ^{32}P (all pure β^- emitters) for biochemical/biomedical tracer studies (Peng, 1993). Until recently, radiocarbon dating has been the only "low-level" or environmental application of LSS in widespread use. Developments in electronics and the incorporation of multi-channel analysers (MCAs) have given LS counters a degree of spectroscopic capability, facilitating data interpretation and nuclide identification. These

developments, combined with the introduction of new photomultiplier tubes (PMTs) with lower levels of electronic noise and various background reduction features, such as pulse shape analysis (PSA) and anti-coincidence guards, mean that modern instruments have much lower limits of detection than earlier versions. Furthermore, commercial LS counters are now available with pulse shape discrimination (PSD) capability, allowing the simultaneous determination of α and β^- activities in a single sample. Thus, LSS is now a technique suitable for the analysis of a wide range of radionuclides at environmental levels (Noakes *et al.*, 1993).

1.2 LIQUID SCINTILLATION SPECTROMETRY

The origins of liquid scintillation counting (LSC) lie with Kallmann's realization in 1937 that organic materials, such as naphthalene, could be made to fluoresce (Oster, 1966), and his invention of a scintillation counter (Broser and Kallmann, 1947). Three years later Ageno *et al.* (1950) were using liquid scintillators to resolve the problems inherent in solid, organic scintillators, *i.e.* growing a crystal of the correct size and shape to be used in a detector. In the same year, Reynolds *et al.* (1950) built the first instrument designed specifically for use with liquid scintillators. Initially, liquid scintillators were used for the measurement of γ photons and high energy particles from sources external to the counter, as with whole body counters (*e.g.* Anderson, 1958), but with the introduction of ^{14}C labelled material into the scintillator (Raben and Bloembergen, 1951) came the birth of internal LSC. Hayes and Gould (1953) also recognized the potential of this technique for assaying weak β^- emitters, and used an instrument built by co-workers at the Los Alamos Scientific Laboratory (Hiebert and Watts, 1953) for the analysis of biological samples containing ^{14}C and ^3H . Soon afterwards, the first commercial instruments were being built by the Packard Instrument Company to the design of Hiebert and Watts (Packard, 1958; Horrocks, 1974).

Research in the field of liquid scintillation covers several areas. Firstly, the optimization of

sample composition, both in terms of the analyte and the scintillator, has mainly involved "trial and error" type experiments (*e.g.* Kallmann and Furst, 1951; Hayes *et al.*, 1955a). However, these studies have been complemented by more systematic approaches to defining the processes occurring in the scintillator (*e.g.* Birks, 1974). Quenching, which causes a decrease in counting efficiency and is a major problem affecting LS, has been another area in which much work has been done, including the examination of interference mechanisms (*e.g.* Furst and Kallmann, 1958) and ways in which to correct for this phenomenon (*e.g.* Bush, 1963). Finally, improvements in instrumentation and new counter technology have been pursued by both the manufacturers and users alike (*e.g.* Noakes *et al.*, 1974). However, before these areas can be discussed in any detail, it is necessary to quickly review some features of radioactive decay processes, as these are fundamental to the understanding of later work.

1.2.1 Radioactive decay

Alpha, β^- and γ radiation are all discussed at later stages in this work and, hence, these are the types of radioactive decay which are concentrated on in this section. However, it should be noted that LS can be used to detect most types of radioactive decay (Polach, 1992). It is only the basic principles which are reviewed here, using information from Keller (1988). A more detailed analysis can be found in texts such as Friedlander *et al.* (1981).

Alpha particles are essentially helium nuclei (*i.e.* two protons and two neutrons) emitted from the parent nucleus, as illustrated by the example in reaction 1.1, causing the mass number (A) to decrease by four, and the atomic number (Z) to decrease by two.



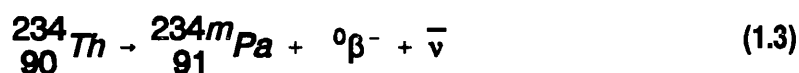
This type of decay occurs in the heavier elements with $Z > 83$, such as many of the nuclides in the natural decay series. Alpha particles have discrete, characteristic energies according to the emitting nuclide. For example, ${}^{210}\text{Po}$ emits a single α particle with energy 5.305 MeV and probability of 100%,

whereas ^{228}Th emits five different α particles, with energies ranging from 5.137 to 5.423 MeV and probabilities of emission ranging from 0.05% to 72.7%. The different energies result from decay into excited states of the daughter nucleus. Alpha particles have a mass of four a.m.u. and a charge of 2+, and are relatively heavy and slow moving (they move at approximately one twentieth the speed of light) compared to β^- particles.

Beta minus decay occurs in nuclides that are unstable due to an excess of neutrons. Beta particles are high energy electrons, formed by the conversion of a neutron into a proton (reaction 1.2)



An example of this type of decay is given in reaction 1.3



Beta particles have a charge of 1- and move at velocities approaching the speed of light. During the decay process there is a release of energy from the parent nucleus, which is shared between the β^- particle and the antineutrino ($\bar{\nu}$). As a result, β^- particles emitted in the decay of a given nuclide have a range of energies from 0 keV to the E_{max} for that nuclide, with a Maxwellian distribution, giving rise to the β^- spectrum.

In some instances, radioactive decay will result in the daughter nuclide occupying an excited state, and in most cases the excitation energy is rapidly lost by the emission of a γ photon. Many nuclides have a characteristic γ spectrum, resulting from emissions from different excited nuclear states. When the γ emission has a half-life of greater than 1 s, the excited state is referred to as a meta-stable state. An example of this type of radioactive emission is given in reaction 1.4



Alpha, β^- and γ radiations all lose their energy by ionizing the material through which they

pass. The linear rate at which they do so is referred to as the specific ionization or specific energy loss (dE/dr), which is defined as the rate of change in energy of the radiation with respect to distance. Alpha and β^- particles, being charged, interact with orbital electrons by electrostatic repulsion or attraction and, thus, have higher specific ionizations than γ photons. Beta minus particles result in the ionization of approximately 1 in every 1000 molecules encountered. Alpha particles, on the other hand, ionize virtually every molecule encountered, due to both their high charge and their relatively slow velocities. Both α and β^- particles lose energy continuously as they pass through a substance.

Gamma rays, being uncharged, have a probability of ionizing only 1 in every 1,000,000 molecules. They tend to lose all their energy in only a few interactions. These interactions can take one of three forms: the photoelectric effect, the Compton effect and pair production. The probability of each occurring varies with the γ photon energy and the atomic number of the absorbing material. The photoelectric effect is the result of interactions with electrons, dominantly in the K shell, but also in the L shell, causing them to be ejected from the atom. This process is dominant at low energies (up to 0.5 MeV in lead). Pair production is the result of the γ photon interacting with the electric field of a nucleus, causing the production of an electron-positron pair. In order for this process to occur, the γ ray energy must be greater than the theoretical limit of 1.022 MeV, and in lead this process dominates above 4 MeV. Gamma rays can also interact with valence electrons, scattering them as Compton electrons. In lead, this process is dominant at intermediate energies. The ejected electrons can cause further ionization, as they behave in the same way as β^- particles.

From this point onwards, β^- particles and decay will be referred to as β particles or decay, for the purpose of simplicity. All half-lives ($t_{1/2}$) and decay energies quoted in the text have been taken from Lederer and Shirley (1978).

1.2.2 The liquid scintillation counter

LSS enables the measurement of the activity of a sample that is intimately mixed with a

fluorescent liquid, called a cocktail, by quantifying the amount of light that is emitted by it, as a consequence of the interaction of the radiation. Ionizing radiation causes the excitation and ionization of molecules in its path, leading to the emission of a pulse of light, made up of photons, when de-excitation occurs. The photons are detected by PMTs and converted into electronic pulses. The specific luminescence (the number of photons per unit path length) is a function of the specific energy loss for the particle or photon (Voltz *et al.*, 1966) and, hence, the intensity of the pulse is proportional to the energy of the event. This proportionality allows the pulses to be classified according to pulse height (intensity) in an MCA to produce an energy spectrum.

Samples (either organic or aqueous) to be counted by LSS are mixed in a vial with an organic mixture called a scintillation cocktail. Cocktails are made up of several components: the solvent, surfactants or emulsifiers (aqueous holding cocktails only), and the fluors or scintillants. There may also be a secondary "solvent" such as naphthalene (which is a solid at room temperature and, hence, is not usually regarded as a solvent in the conventional usage of the term). The solvent absorbs most of the energy from the ionizing radiation. Excited solvent molecules transfer their excess energy to the fluors, which de-excite *via* photon emission. A more detailed discussion of the individual characteristics of each of these components is given in section 1.2.3.3. There is a wide range of cocktails available (both commercial and "home-made"), each suitable for different sample types. However, before turning to a discussion of the sample and cocktail, the mechanisms operating in the counter itself will be described.

The sample vial is positioned between two diametrically opposed PMTs, in a light tight sample chamber, surrounded by lead shielding. A PMT consists of an evacuated, cylindrical glass envelope. The internal face of the end window, termed the photocathode, is coated with a photosensitive material. As interactions of radioactive decay products occur with the constituents of the cocktail in the vial, photons are produced which strike the photocathode. The internal walls of the sample

chamber are coated with reflective material to increase the probability of this occurring. If the photon has sufficient energy to exceed the threshold energy of the photocathode, a number of photoelectrons will be produced proportional to the energy of the photon. The rate of photoelectron production, *i.e.* the response of the photocathode, has been estimated as 1-2.5 electrons/keV for organic scintillators (Lynch, 1975), but this number varies as both a function of the PMT and the cocktail, according to the spectral match (Brooks, 1979). Horrocks (1964a) estimated the energy dissipated in the cocktail to be 25-30 eV per photoelectron for electron excitation and 250-350 eV for α particle excitation. The reasons for this difference will be discussed in section 1.3.2.

The photoelectrons are accelerated and multiplied by a series of dynodes, which consist of electron releasing materials. When a dynode is struck on the front surface by an electron, it releases more electrons from the back face, resulting in a multiplication of the signal. Each dynode multiplies the number of incident electrons by a factor, M , which is given by equation 1.5 (Adams and Dams, 1970)

$$M = \delta g \quad (1.5)$$

where δ is the mean number of emitted secondary electrons per incident electron; and g is the probability of their capture by the next dynode. Electrons are progressively accelerated and multiplied down the length of the PMT by between 11 and 13 dynodes, each at a higher voltage than the previous one, resulting in an overall increase in the number of electrons by a factor of 10^6 - 10^8 (Adams and Dams, 1970). Finally, a cascade of electrons reaches the anode and can be detected as an electronic pulse. The amplification between the photon and the electronic pulse is linear, preserving the proportionality between event energy and pulse height (Horrocks, 1974).

Early PMTs had glass windows and caesium-antimony photocathodes. These were superseded by quartz, which has greater light transmission over a wider spectral range (Horrocks, 1974), and by bialkali (K_2CsSb) photocathodes. Dynodes are either coated with a caesium-antimony

mixture, as with the photocathode, or are made of a magnesium-silver alloy activated by oxygen or caesium vapour (Adams and Dams, 1970). All electronic components suffer from random electrical discharges or dark noise, which is related to the temperature of their surroundings. The older types of PMT were particularly prone to this and, therefore, the original LS counters required extensive refrigeration units in order to reduce noise and maintain an acceptable background (Stanley, 1980). Bialkali PMTs have the advantage of lower noise levels, even at higher temperatures (Rapkin, 1970). Now, cooling units are an optional extra, but are still useful, for instance in controlling chemiluminescence and maintaining counter electronic stability. The response of the photocathode varies across its face (Birks, 1964; Horrocks, 1974), with the centre portion being the most sensitive. For this reason, it is important that the sample vial is centrally positioned in the sample chamber and, hence, the need for special adapters for mini vials.

Two PMTs are used in order to discriminate against background caused by random electrical discharges. For an event to be accepted by the circuitry, it must be detected by both PMTs within a specific time, of the order of 20 ns, *i.e.* be coincident. This condition of coincidence was first used by Kallmann and Accardo (1950) and has been applied to virtually every LS counter produced since (Rapkin, 1970). (Usually this coincidence gate is fixed, but in some of the more modern instruments it is possible for the user to manually adjust this parameter. This feature may be desirable in the case of using a solid scintillator with a long decay time.) This condition should only be passed by events originating in the cocktail, and not by dark noise in the PMTs, which is unlikely to occur simultaneously in both PMTs, as shown by equation 1.6 (Horrocks, 1974)

$$N_c = 2\tau N_1 N_2 \quad (1.6)$$

where N_c is the number of coincident noise pulses; τ is the resolving time - typically 20 ns; and N_1 and N_2 are the number of noise events per unit time occurring in each of the PMTs respectively. If PMTs with a noise rate of 10,000 cpm are used, the number of coincident pulses will only be 0.07 cpm.

Some modern PMTs have been shown to have an even lower dark current. For example, in one study the RCA 4501-V4 PMT produced only 100 cpm at a normal working voltage (Guan and Xie, 1992). In some instruments, once a pulse has been accepted as being coincident, it must also pass a pulse height comparator (Kojola *et al.*, 1984). This system examines the relative heights of pulses detected in each PMT, rejecting as background those events with a ratio that is not close to unity, which would indicate that the event originated in one PMT and only a faint signal was being picked up by the other (Haas and Trigg, 1991).

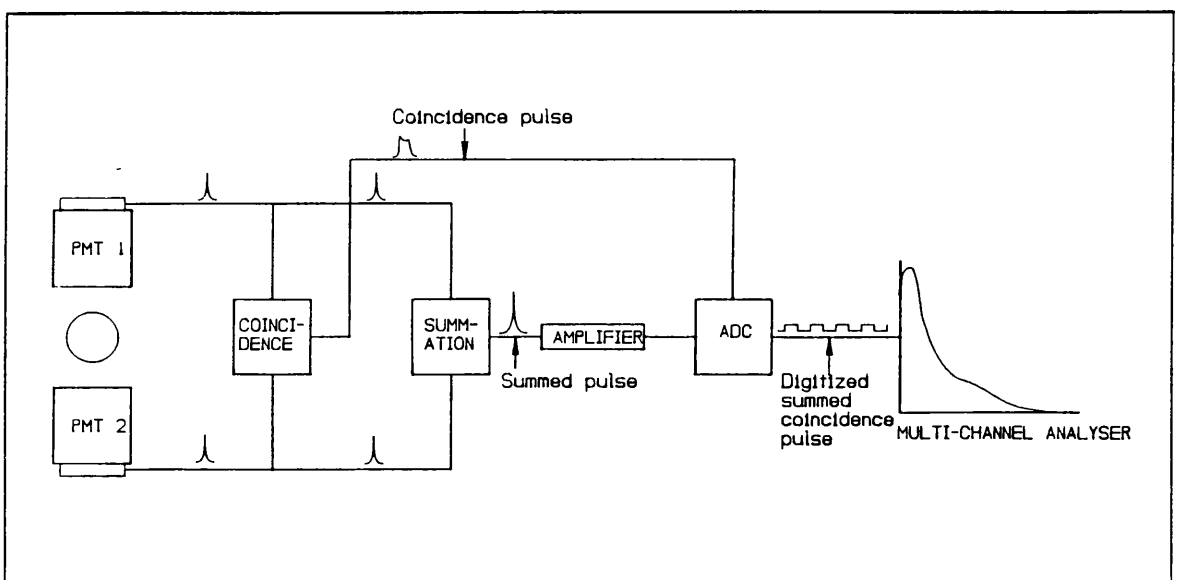


Figure 1.1: Simplified circuit diagram of a liquid scintillation counter (after Kessler, 1989).

The use of two PMTs not only serves to reduce background, but helps in the resolution of another problem. A photon emitted close to one PMT will cause a greater response in that photocathode than in the other and, if measures are not taken to compensate for this effect, the difference in observed pulse heights can cause a broadening of the spectrum (Rapkin, 1970). Therefore, in 1963 the Packard Instrument Company introduced pulse summation circuitry (Stanley, 1980) (Fig. 1.1) which electronically adds the PMT anode pulses together, thereby not only sharpening the spectrum, but also increasing the number of low energy events that pass the noise threshold (Horrocks, 1974). This feature has been generally adopted by all manufacturers.

The next stage in the circuitry is the amplification of the electronic pulse, before sending it to the single or multi-channel analyser. It is here that one of the major differences between instruments appears - either the amplification is linear or logarithmic. Originally, when single channel analysers were in use, logarithmic amplifiers (introduced by ANSitrone in 1964 (Rapkin, 1970)) had the advantage of being able to register the full energy spectrum of radionuclides with E_{max} ranging from that of ^3H (18.6 keV) to that of ^{32}P (1710 keV), without the need to alter either the high voltage or the gain on the PMTs, thus simplifying the counter controls. However, with the introduction of inexpensive, 4096 channel analysers, linear amplification no longer has this particular disadvantage.

After amplification, the pulse is allocated to a pulse height channel. The first instruments had a single channel, but this was increased to first two and then three counting channels (Rapkin, 1970). By the late 1970s, MCAs could be added to counters, as an extra feature to enhance research (*e.g.* Alessio *et al.*, 1976; Ediss, 1980), but were still not commonplace. The advent of analogue-to-digital converters (ADCs) and MCAs in standard, commercial counters had a radical effect on LSC. Now, the digitized, summed, coincidence pulses could be individually allocated to any one of 4096 channels. However, pre-set windows were still in use and free manipulation of the data was not possible (Polach *et al.*, 1983a). Therefore, in order to reap the full benefit of MCA technology, a windowless approach was suggested (Polach *et al.*, 1983a). Two approaches to counting are now commonly used: either preset windows as with older technology instruments; or full-spectrum counting, with windows or regions of interest being selected after the count has ended. Software programmes now allow repeated analysis of the spectra, regions of interest can be redefined at will, and data analysis is unconstrained by the paucity of information provided by the instrument (Polach, 1992).

1.2.2.1 Quenching

Quenching reduces the production of photons and the transmission of light to the PMTs. It causes a loss of counting efficiency and shifts the spectrum to lower energy. This effect is the result

of fewer photons reaching the photocathode with sufficient energy to produce a photoelectron. It is essential to know the efficiency with which a sample is counted accurately, but each nuclide is affected by quenching to a different degree, according to the E_{max} , and every cocktail has individual quench characteristics. Therefore, various methods for quench determination and correction have been derived, each with its advantages and disadvantages. Quenching falls into several different categories, which can be defined by their causes and effects.

Chemical quench occurs when excitation energy is transferred to the "wrong" molecules, such as those of impurities, that are unable to produce photons that can be detected by the PMTs, *i.e.* it increases the rate of non-productive energy transfer, with the net result that fewer photons are produced per decay event. Increasing the viscosity of the LS solvent has been shown to reduce the effect of quenching (ter Wiel, 1993), which implies that chemical quenching relies on the physical approach of a quenching molecule and an excited solvent or fluor molecule to interfere with energy transfer. Nitromethane (CH_3NO_2) and carbon tetrachloride (CCl_4) are extremely effective quenching agents which are often used in experiments studying the effects of quenching (*e.g.* Takiue *et al.*, 1991). These molecules are able to intercept excitation energy, as a result of their high electron affinities (Laustriat *et al.*, 1970). Sample molecules themselves cause chemical quenching, except when the radionuclide has been incorporated into one of the cocktail components, for example tritiated toluene. However, sample quenching can be reduced by minimizing sample volume and acid concentration. Aqueous samples are more prone to the effects of quenching than those that are dissolved in an organic medium, as the surfactants, required for homogeneous mixing of the aqueous sample, cause quenching in addition to that caused by the aqueous medium itself.

Oxygen is a very effective quenching agent, as it competes favourably with several energy transfer processes (Pringle *et al.*, 1953). In order for the oxygen molecule to compete effectively for the excitation energy (*i.e.* quench) it must have a rate parameter for the process that is equal to or

greater than the rate for the scintillator molecules. Birks (1970) has suggested that processes vulnerable to oxygen quenching are solvent-solute energy transfer and primary excitation of the solvent. Excited fluor molecules and molecules in the triplet state can also be quenched by oxygen, reducing the probability of photon emission and the size of the delayed component (section 1.3.1). Quenching by oxygen can be reduced by purging with oxygen-free nitrogen or argon.

Colour quench occurs when photons are absorbed by coloured material in the sample and is most commonly found in biological samples. This effect is particularly noticeable with yellow and red coloration, as liquid scintillators emit light in the ultra-violet region (Bush, 1963). Problems arise when a sample contains both colour and chemical quenching agents, as their effects on efficiency are different, as would be expected from their different mechanisms (Takiue *et al.*, 1991). This interference can be minimized in many environmental samples by ensuring that the sample has been fully oxidized and has no coloured impurities.

Concentration or self quenching is a function of the concentration of the fluorescing components of the cocktail, especially the fluors (Furst and Kallmann, 1958). Furst and Kallmann (1958) proposed a mechanism whereby an excited and an unexcited fluor molecule interact with one another to form an excited dimer (excimer). This species then decays without producing a detectable photon, thus reducing the scintillation efficiency of the cocktail.

Ionization quench is a result of the high density of ionized molecules along the tracks of particles with a high specific energy loss and can take two forms. Static quench is the reduction of the primary excitation efficiency by temporarily ionized or excited molecules, which compete with the internal conversion process that populates the $S_{1,x}$ energy level (Brooks, 1979). Dynamic quench is less effective, but is more persistent. Birks (1964) suggested that it is due to free radicals competing with the secondary energy transfer processes.

Over the years, several different methods of determining the degree of quenching, and hence

counting efficiency, have been employed. Initially, the internal standard method was used, as proposed by Hayes (1956). In this case, the sample was counted, a small aliquot of known activity material was added and the sample recounted. The efficiency could be determined according to equation 1.7 (Horrocks, 1974)

$$\text{Efficiency} = \frac{\text{cpm}(\text{standard} + \text{sample}) - \text{cpm}(\text{sample})}{\text{dpm}(\text{standard})} \quad (1.7)$$

This method has all the disadvantages inherent in adding material to a vial, such as the possibility of introducing a quenching agent and inaccuracies in pipetting, the need for two counts and, perhaps most important, the fact that the sample cannot be recounted once the standard has been added.

When instruments were introduced with two or more counting channels, the possibility arose for another method of quench correction (Rapkin, 1970). The samples channels ratio (SCR) method makes use of the shift in the energy spectrum to determine the degree of quenching (Bush, 1963). Two windows are chosen, one of which covers the low energy region of the spectrum, while the other covers either the high energy region or the full spectrum (Gibson, 1980). The accuracy of this method is dependent on having sufficient counts in each of the windows used and, thus, is of limited use for low activity samples. In order to find the counting efficiency of a particular sample, a series of standards is counted at different levels of quenching. The SCR is then plotted against efficiency to produce a calibration curve. This use of quench standards is necessary with all techniques other than internal standardization. Dahlberg (1982) combined the internal standard and SCR methods, to find the channels ratio of the added standard for low activity samples.

Two other examples of sample spectrum quenching parameters which have been used are: the SIS (Spectral Index of the Sample) and the SQP(I) (Spectral Quench Parameter of the Isotope). These parameters are both based on the average energy of the β spectrum (E_{av}). The SIS is defined by equation 1.8 (Kessler, 1989)

$$SIS = K \frac{\sum_{x=0}^u x * n(x)}{\sum_{x=0}^u n(x)} \quad (1.8)$$

where K is the normalized E_{av} factor, based on energy channels from X to ΔX ; $n(x)$ is the number of counts between X and ΔX (proportional to the total number of counts); x is the pulse height; and u is the end point of the spectrum. These parameters are still subject to the problems associated with low count rate, but are independent of sample volume (Ring and Everett, 1982).

In 1965, the first instrument with an external standard was brought out by Beckman Instruments (Rapkin, 1970). In this approach, a γ emitting source (usually ^{226}Ra , ^{137}Cs or ^{133}Ba) (Gibson, 1980) is brought into close proximity with the sample vial, inducing Compton electrons in the cocktail. These electrons then cause the production of photons in the same way as β particles, giving rise to an energy spectrum. In the method proposed by Higashimura *et al.* (1962), efficiency was simply correlated to the total number of counts due to the external standard. This method was then refined to the external standard channels ratio method (ESCR), which operates under the same principles as the SCR method, without the complications of low sample count rate. Instruments with the ESCR method of quench determination had a total of five counting channels (3 + 2) - three for sample counts and the remaining two for external standard counts (Rapkin, 1970).

While the ESCR would at first seem to be the ideal method of quench correction, it suffers from problems associated with variations in vial thickness and sample volume, and chemical and colour quenching produce different responses (Takiue *et al.*, 1991). The aim of the instrument manufacturers is to define a method of quench determination which is independent of cocktail volume and type and is insensitive to small variations in the vial dimensions, so that a single set of quench standards can be used for each radionuclide of interest. Therefore, various quench indicator

parameters (QIPs) have been introduced, making use of different aspects of the Compton electron spectrum.

The SIE (Spectral Index of the External standard) and SQP(E) (Spectral Quench Parameter of the External standard) are the external standard versions of the SIS and SQP(I) respectively. The SIE has now been replaced by the tSIE (transformed SIE) whereby the external standard spectrum is first mathematically transformed, before the calculations are performed. This procedure eliminates "wall effects" which create a secondary spectrum, caused by Compton electrons produced in the vicinity of the vial walls (De Filippis and van Cauter, 1985). tSIE is inversely proportional to quench, and has a range of 1000 units.

Another external standard QIP is based on the inflection point of the leading edge of the spectrum, *i.e.* the point at which the second derivative of the leading edge becomes equal to zero. As the spectrum is quenched the inflection point moves to the left. The difference between the quenched and the unquenched spectra gives rise to the H-number (H#) (Horrocks, 1976a), which is proportional to the degree of quenching. Instruments with H# as the QIP can also employ a method of automatic quench correction (AQC), whereby the spectrum is electronically restored to its unquenched position, negating the need for quench calibration curves (Burns and Steiner, 1991).

1.2.2.2 Background reduction

Interest in using LS for low-level or environmental applications increased rapidly from the point at which spectral processing and the possibility of background reduction became available. Radiocarbon dating has been performed extensively by LS since the discovery of a method for synthesizing benzene from sample carbon (Noakes *et al.*, 1963). Benzene can easily be counted by this technique as it can take the place of the solvent in the cocktail. It was this field that produced most early advances in further reducing the background of these instruments - a critical factor for low-level applications, as background has a large effect on the minimum detectable activity. In the early

1980s, the instrument manufacturers saw the potential for low-level applications and many more advances in background reduction have been made since then.

Before it is possible to understand the various mechanisms for background reduction in modern LS spectrometers, it is necessary to consider the various sources of spurious counts. Horrocks (1974) has discussed many of these sources in detail and Polach (1992) has produced a more concise summary. As previously mentioned, PMT dark noise and other forms of electronic noise are not significant in modern counters. Most background originates from radiation sources other than the sample. These can be cosmic rays, local γ emissions (usually caused by a poorly shielded external standard (section 1.2.2.1)), or natural radiation from the materials from which the counter, vials, *etc.* are constructed. Other sources of background are gas discharges (from residual gas in the PMTs), chemiluminescence, photoluminescence and static induced discharges.

Background can result from cosmic ray (*i.e.* high energy protons and γ photons) interactions with the PMTs, vial walls, *etc.* As these high energy particles or photons pass through the structure of the counter they are slowed, producing Cerenkov radiation. This radiation is in the form of ultra-violet photons, which can be detected by both PMTs, as a result of crosstalk - the piping of light from one PMT to the other by the vial walls, the light guide or through the sample (Horrocks, 1974). Crosstalk, which allows these background events to appear in coincidence, can be reduced by masking either the vials or the PMTs (Polach, 1992) with black tape or paint. Cerenkov radiation appears in a similar region of the energy spectrum as ^{14}C , as the photon yield is poor, despite being caused by high energy events (Horrocks, 1985). It is difficult to reduce this background by use of narrower windows or optical filters, as these will both reduce counts from the sample (Horrocks, 1974). This type of background is deemed to be unquenchable, as quenching conditions in the cocktail do not affect its spectrum. (Horrocks, 1985).

Quenchable background is derived from radiations which interact with the cocktail in the same

way as radiation emitted from the sample. These radiations include lead x-rays produced by the interaction of cosmic radiation with the shielding, low energy secondary electrons and γ photons (Horrocks, 1974). Quenching in the cocktail affects the energy distribution of this background, as the photons are produced by the cocktail (Alessio *et al.*, 1978; Horrocks, 1985).

A static electrical charge can build up on the vial walls during its placement in the counting chamber and its subsequent discharge will result in background counts. Plastic vials are particularly prone to this phenomenon, especially during periods of low humidity (Bond, 1984). This problem can be prevented by a delay before the count commences, after the vial has been positioned, or by the use of anti-static devices, which are present in some counters (Polach, 1992). Static can be neutralized by placing the vial in an ionized environment. The ionization can be caused either by an α emitting source (Rapkin, 1970) or by an electric field (Kessler, 1989), the latter being more common in modern instruments.

Chemiluminescence is the result of light-producing, chemical reactions in the vial. It is often caused by sample solubilizing agents, usually used in bioscience applications, or impurities in either the sample or the cocktail. It can be avoided by taking care with sample preparation, allowing the reaction to complete by storing the sample before counting or by cooling the sample during counting to reduce the reaction rate (Horrocks, 1974). Photoluminescence, caused by the excitation of vial materials by light, is best prevented by storing vials, caps and cocktails in a dark place (Polach, 1992).

Background reduction features in modern LS spectrometers aim to reduce the contribution of cosmic radiations to the instrument background. The best method of eliminating this component is by placing the counter underground, with the overlying rocks acting as very efficient shielding (Alessio *et al.*, 1976), or under a dam, as water has a lower natural activity than rocks (Polach *et al.*, 1988). However, this method is not convenient for routine users of LSS, and other methods have had to be found - most commonly by both active and passive shielding, and electronic PSA.

Most LS counters use a standard 5 cm thick lead shield, which leads to a compact design, in contrast to larger instruments with more extensive passive shielding (Polach, 1992). The passive shield reported by Kojola *et al.* (1984) consists of 20 cm lead, lined with copper and cadmium. Lead is effective at shielding a detector from high energy cosmic background, due to its high atomic number. However, as it slows γ photons by absorbing their energy a byproduct is the emission of lead K-shell x-rays at 75 and 85 keV (Adams and Dams, 1970). The use of thin layers of cadmium (~ 2 mm) and copper (~ 0.2 mm) prevents these x-rays from interacting with the detector. Cadmium absorbs the lead x-rays, while the copper absorbs the x-rays that the cadmium then emits. Other types of passive shield consist of 7.5 cm lead, lined with 4 cm stainless steel (Guan and Xie, 1992) and 20 cm iron (Einarsson, 1992).

The passive shield is normally used in conjunction with an active shield or anti-coincidence guard, which typically consists of a plastic or liquid scintillator or a NaI(Tl) detector. In theory, a cosmic ray will be detected by both the guard counter and the sample PMTs, whereas radioactive emissions from the sample will only be detected by the latter. Therefore, once an event has satisfied the coincidence condition for detection in both sample PMTs, it must pass an anti-coincidence condition, *i.e.* it should be detected only by these PMTs and not by the guard PMTs. The spectrometers described by both Guan and Xie (1992) and Einarsson (1992) use NaI(Tl) as an anti-coincidence shield. Alessio *et al.* (1976) and Kojola *et al.* (1984) both describe instruments utilizing a plastic scintillator, the latter being the first commercial instrument to incorporate this feature (the LKB Wallac QuantulusTM). NaI(Tl) anti-coincidence guards have been shown to have a greater effect on the background than a plastic scintillator of comparable volume, due to their greater detection efficiency for γ photons (Guan and Xie, 1992). However, the QuantulusTM shielding is capable of reducing the background to levels comparable with those that can be achieved by placing the instrument in an underground laboratory (Polach *et al.*, 1984).

The use of relatively large passive shields and anti-coincidence guards adds to the expense of an LS spectrometer, thus effectively eliminating this approach to background reduction for many laboratories which may have a wide variety of samples to assay and cannot afford a dedicated low background (low-level) counter. This logic supports the alternative approach to background reduction of using an electronic method of background rejection based upon PSA (Kessler, 1990; Burns and Steiner, 1991).

As previously mentioned, an incompletely evacuated PMT can lead to background production. This takes the form of small pulses, called after-pulses, occurring in the wake of a high energy, unquenchable background event, caused by the ionization of the gas (Horrocks, 1974). One type of PSA, variously termed 3-D spectrum analysis (van Cauter, 1986), time-resolved LSC (TR-LSC™) (Kessler, 1990) and burst-counting-circuitry (BCC) (Cook and Anderson, 1993), counts these after-pulses to distinguish between light produced by the cocktail and Cerenkov photons. The number of after-pulses is referred to as the pulse index (Passo and Kessler, 1993). By comparing the index and height of a given pulse with stored values of these parameters, the instrument decides whether or not to reject the event as background. A low energy event with several after-pulses would be rejected in this way. Usually, only after-pulses occurring more than 75 ns (the length of a typical, unquenched ^{14}C β pulse) after the start of the prompt pulse will be included in the count of after-pulses (van Cauter, 1986; Kessler, 1990). However, the start of after-pulse or burst counting can be varied on the more modern of these instruments (Passo and Kessler, 1993), as high energy β events can also give rise to pulses with long tails. In these instances the use of a 75 ns cut off causes not only a reduction in background, but a significant loss of counting efficiency as well, caused by the rejection of sample derived events. By increasing the time before the PSA commences, counting efficiency can be restored, although at the expense of increasing the background again. A compromise position can usually be found, for example by maximizing the figure of merit (E^2/B - where E is efficiency and B

is background) (Cook and Anderson, 1993; Passo and Kessler, 1993).

An alternative approach to background reduction by PSA makes use of the fact that all PMT anode pulses are made up of a prompt and a delayed component (Laustriat, 1968) (see section 1.3.1 for a more detailed discussion of their derivation). Background events have a greater delayed component (presumably due either to the effect of after-pulses or the fact that some background pulses are the result of higher energy events) and so can be electronically discriminated from the shorter β pulses derived from the sample radioactivity (Burns and Steiner, 1991). While all β events have a delayed component, the proportion varies with event energy, more energetic events giving rise to larger delayed components. However, the contribution of the delayed component is reduced significantly by the quenching effect of oxygen. Hence, most low energy β emitters, in the presence of oxygen, will give rise to the short pulses mentioned.

The use of PSA makes sample composition crucial to the performance of the system. The fact that the presence of dissolved oxygen sharpens PMT anode pulses increases the chance of discriminating valid cocktail derived events from unquenchable background events. Therefore, use of nitrogen or argon purged samples can reduce the detection efficiency of the counter when background reduction by PSA is employed (Cook and Anderson, 1992). In addition, the use of fluors which increase pulse widths or reduce after-pulsing has the same effect (Cook and Anderson, 1992). Therefore, it is necessary to carefully optimize cocktail composition whenever PSA is used. This is exemplified by the contrasting data given by Cook and Anderson (1992) and Polach *et al.* (1988). The two groups were able to achieve comparable background rates, but the former group obtained approximately 20% higher counting efficiencies for ^{14}C than the latter, by using a suitable secondary fluor, which sharpened the pulses.

1.2.3 Liquid scintillation samples

The following section is concerned with the LS sample, by which is meant the vial and its

contents in a state to be counted. Analyte and cocktail composition and vial type can have an effect on many aspects of LSS, such as quenching, background and counting efficiency. Therefore, it is vital to fully appreciate how different components of the sample will affect the final result, if accurate data are to be obtained.

1.2.3.1 *The sample*

Generally, material to be analysed by LS is dissolved in either an aqueous or organic medium prior to mixing with the cocktail. This allows the analyte to form a homogeneous mixture with the cocktail, in order to benefit fully from the 4π counting geometry that LS offers. However, in some instances, the analyte may be supported on an inert material, such as a filter paper (*e.g.* Long *et al.*, 1976) or a stainless steel planchette, as for ^{241}Pu analysis (*e.g.* Cook and Anderson, 1991; Ryan *et al.*, 1993). In these cases, the counting geometry is reduced to 2π , but LS still retains a sufficiently high counting efficiency to be a suitable method for analysis of low energy β emitters. The suspension of particulate material in a cocktail has also been used for some applications, particularly when an insoluble substance is to be analysed, or when significant time savings can be made by not dissolving the material, as in the case of soil (Adu and Oades, 1974). Suspension is achieved through the addition of some gelling agent to a "home-made" cocktail, such as a thixotropic powder (*e.g.* Helf, 1958) or a non-ionic surfactant (*e.g.* Kobayashi and Maudsley, 1974), or by the use of one of the more modern gel cocktails, such as Insta-Gel®, which contain non-ionic surfactants (*e.g.* Buzinny *et al.*, 1993). The analysis of particulate material in this way is subject to self absorption effects and light scattering. Problems can also arise due to partial solubility of the analyte, with the dissolved and solid phases giving rise to individual counting efficiencies, but used carefully it can be a valuable technique, facilitating sample preparation.

1.2.3.2 *The vial*

The material to be counted and the cocktail are contained in a vial. The composition and size

of the vial will both influence background, counting efficiency and the shape of the energy spectrum. Over the years, many different vial types and sizes have been investigated - primarily by researchers in the field of radiocarbon dating, in an effort to date older material. The earliest commercial LS counters were designed to accept 5 dram (20 ml) vials (Packard, 1958), and this has become the international standard for all LS instruments (Polach, 1992). Many laboratories are now using standard 7 ml vials, which can either be loaded directly into the counter, or be converted to fit the 20 ml vial size with a special holder. These vials have the economic advantage of costing less, due to their smaller size, and have implications in the reduction of background as discussed below. Very small (< 1 ml) vials are also available (Kaihola *et al.*, 1992), but these are designed for more specialized applications, such as the radiocarbon dating of very small samples.

It has been found that background can be reduced by using smaller vials (Horrocks, 1985). This feature could be due to one of two effects: (i) the smaller vial has less material and, hence, less inherent radioactivity (primarily ^{40}K and the natural decay series radionuclides); or (ii) the reduced mass of the smaller vial provides fewer atoms for cosmic background to interact with and, hence, produce scintillations. Horrocks (1985) found that the background reduction occurs in empty vials (35.08 cpm for empty 20 ml Pyrex vials and 22.85 cpm for empty 7 ml Pyrex vials), implying that the source is primarily Cerenkov radiation, caused either by cosmic radiations or by ^{40}K . If a low background is required, it is advantageous to use a small vial, within the restrictions of the quantity of cocktail needed to keep the analyte dissolved. However, as background is also directly related to cocktail volume (Horrocks, 1985), efforts should be made to keep it to a minimum.

In addition to producing lower background, small vials can give higher counting efficiencies for low energy β emitters such as ^3H (Elliott, 1984). Counting efficiency is influenced by the sample geometry and the reduced diameter of the 7 ml vials results in a more favourable geometry compared to 20 ml vials. However, the same does not hold true for higher energy particles, as the total energy

of the particle may not be fully dissipated in the cocktail.

The most commonly available LS vials are made of glass or plastic. Glass vials are usually made of low potassium borosilicate glass (in order to minimize background due to ^{40}K). Plastic vials are made of either high density polyethylene or polypropylene. Some highly specialized, ultra low background vials are available commercially, including those made of Teflon (Polach *et al.*, 1983b) and quartz (Polach, 1992), but these are expensive and are not, therefore, suitable for routine analysis. Synthetic silica vials have also been developed recently (Hogg and Noakes, 1992; Hogg, 1993). These vials are similar in performance to Teflon vials, but as they are easier to manufacture should be less expensive. In an attempt to reduce still further the costs associated with LSS, Simonnet *et al.* (1981) designed small plastic bags for use with scintillator impregnated filter papers. These are then placed in a vial, which can be reused as the bags are impermeable to the cocktail.

Plastic vials have an advantage of generating lower backgrounds than glass (Elliott, 1984). Horrocks (1985) found a 50% reduction in background by use of plastic vials compared to Pyrex within the ^{14}C counting window (0-156 keV). It has been suggested that the lower background of these vials is due simply to their smaller mass (Painter, 1974), but the absence of natural radioactivity must also play a part (Kaihola, 1993). Momoshima *et al.* (1983) found that background was indirectly proportional to mass for Teflon vials and attributed this effect to variations in wall thickness. Thicker walls absorb a greater percentage of photons before they reach the PMTs, reducing both the counting efficiency of the sample and the background count rate. Translucent vials also bring about a reduction in crosstalk between the PMTs, which results in fewer background events being seen in coincidence by the PMTs (section 1.2.2.2), a significant factor in the low background of non-glass vials (Polach, 1992). Plastic vials have been shown to perform better than glass, in terms of the E^2/B figure of merit (Polach *et al.*, 1988), for samples containing ^3H (304 for 20 ml polyethylene, compared to 196 for 20 ml low potassium borosilicate glass) (Elliott, 1984). The difference in these figures is due to the lower

background of the plastic vials (10.5 cpm compared to 16.0 cpm), as the efficiencies are virtually identical (56.5% and 56.0%, for plastic and glass respectively).

Plastic vials have one further advantage over glass - namely higher light transmission to the PMTs, which can result in improved resolution. This property is due to their matt surfaces, which reduces the probability of light being either reflected back into the vial, where it is subject to further quenching, or trapped within the vial wall by repeated reflections (Painter, 1974). Similar effects can be induced in glass vials by etching the surface (Yu *et al.*, 1990), but this has to be done by the laboratory staff, as etched vials are not commercially available. Improving the light transmission can also increase counting efficiency, however, the data for plastic vials are contradictory. Only small effects are seen - some with greater efficiencies than the corresponding glass vial (Rapkin and Gibbs, 1965) and some with lower (Elliott, 1984). This conflicting evidence may be due to the type of vial used. Some plastic vials have shiny walls, while others are more matt. The reflectivity of the vial's surfaces will affect light transmission for plastic as much as glass.

Despite their advantages, plastic vials have the significant disadvantage of being permeable to many common LS solvents, including xylene and toluene (Painter, 1974). Thus, they are unsuitable for any application which requires sample stability over more than a day. This permeability can be reduced by using Teflon-lined plastic vials and the use of a modern solvent (section 1.2.3.3), but some sample loss still occurs.

1.2.3.3 *The cocktail*

The LS cocktail or liquid scintillator is made up of several components, as described earlier. Although LS spectrometers are designed for use with liquid scintillators, solid scintillators (yttrium silicate) have been used recently in place of the traditional cocktail (Wunderly, 1993; Yang, 1993) in order to avoid the problem of disposal of liquid, organic radioactive waste. They have also been shown to be of use in the analysis of α emitting nuclides. Melttable plastic scintillators, into which a filter or

other solid sample is incorporated, are also being introduced for the same reasons (Suontausta *et al.*, 1993; Thomson, 1993). However, these alternatives are not widely used at present and the discussion will focus on liquid cocktails.

The solvent provides a medium in which to dissolve the sample and fluors, and acts as an energy transfer agent between the ionizing radiation and the fluors. LSS has higher counting efficiencies than many other radiometric techniques, due to the intimate mixing of the radionuclide and the solvent. This mixing allows a high energy transfer efficiency and 4π geometry. For unquenched samples, modern cocktails allow counting efficiencies of greater than 60% for ^3H and greater than 90% for β emitters with E_{max} greater than or equal to that of ^{14}C (ter Wiel and Hegge, 1991). Alpha particles are detected with approximately 100% efficiency (Horrocks, 1974).

A good solvent will have π molecular orbitals of the correct energy spacing to transfer energy efficiently to the fluors, and yet be transparent to the fluor emissions. It will also be compatible with the other cocktail components in terms of solubility. Early in the history of LS, Kallmann and Furst (1951) and Hayes *et al.* (1955b) did extensive surveys of possible scintillator solvents. Both groups compared the energy transfer efficiency of each potential solvent to that of toluene by comparing PMT anode pulse heights, using an external γ emitting source and a single PMT. The rate of energy transfer is proportional to the relative pulse height (RPH) (Hayes *et al.*, 1955a). The best solvents found in these studies are still in common use and include toluene and isomers of xylene. A mixture of dioxane and naphthalene (Bray's solution), which is miscible with water (Bray, 1960), was also commonly used for aqueous samples until the advent of surfactant incorporation (Kobayashi and Maudsley, 1974).

More recently, much interest has been generated in modern "safe" cocktails. The traditional solvents are hazardous compounds (Table 1.1), which need to be used in a fume cupboard and present disposal problems. Often, the cost of disposing of scintillation vials and cocktails is a

significant proportion of the purchase price (Klein and Gershey, 1990), and is determined as much by the hazard rating of the cocktail as by the amount of radioactivity in the vial. Hence, the current trend is towards the use of less hazardous materials.

Table 1.1: Safety and performance data for some LS solvents.

Solvent	RPH ^a	Flash point ^a	Long term exposure limit ^c
Di-isopropylnaphthalene (DIN)	114	152°C	n.a. ^d
Naphthalene	--	78°C ^b	10 ppm
Phenyl- <i>o</i> -xylylethane (PXE)	114	150°C	n.a. ^d
Pseudocumene	112	50°C	25 ppm
Toluene	100	5°C	50 ppm
<i>p</i> -Xylene	110	30°C	100 ppm
<i>o</i> -Xylene	98	29°C	100 ppm
<i>m</i> -Xylene	107	25°C	100 ppm

a Relative pulse height, from Passo and Kessler (1992).

b From Aldrich (1992).

c From Health and Safety Executive (1992).

d Not assigned, from ter Wiel and Hegge (1991).

The first deviation from the traditional scintillation solvents came with the introduction of 1,2,4-trimethylbenzene (pseudocumene) in the late 1970s (Nibeck *et al.*, 1980). While this compound is more toxic than toluene (Health and Safety Executive, 1992), it has a higher flash point, making it a less hazardous material in terms of storage and transport. This was followed in the 1980s by linear polyalkylbenzenes, di-isopropylnaphthalene (DIN) and phenyl-*o*-xylylethane (PXE) (Thomson, 1991). It should be noted, however, that alkylbenzenes had been indicated as efficient solvents 20 years previously by Hayes *et al.* (1955*b*). These modern solvents have advantages in terms of equivalent or greater counting efficiencies (Spate and Langhorst, 1986; Elliott and van Mourik, 1987; Klein and

Gershey, 1990) and, perhaps more significantly, in terms of safety and disposal. They have high flash points and low toxicity (Health and Safety Executive, 1992; Passo and Kessler, 1992), enabling cocktails to be dispensed in the open laboratory. In addition, many modern cocktails are marketed as being biodegradable and drain disposal, subject to local regulations, is often allowed. There is conflicting evidence as to whether or not the manufacturers are fully justified in labelling these cocktails as biodegradable (Klein and Gershey, 1990; Thomson, 1991), particularly in the case of DIN, but there is no doubt that they are more pleasant to work with and many laboratories are switching to them for purely economic reasons (Spate and Langhorst, 1986). DIN-based cocktails have only one major disadvantage when compared with traditional cocktails, which is an instability in the presence of air. Over a period of time (approximately three months), samples tend to turn yellow and their counting characteristics are degraded. However, this is not usually a problem, except when long term stability is required, as in the case of calibration standards.

Surfactants allow homogeneous mixing of aqueous and organic phases *via* micelle production (Atkins, 1986). One end of a surfactant molecule is hydrophilic, while the other is hydrophobic. A micelle is a group of surfactant molecules, in this case with their hydrophilic ends pointing inwards. Thus, water can be dispersed in an organic medium, within the micelle. The sizes and shapes of the micelles are dependent on the surfactant type, as defined by the hydrophilic group. For example, non-ionic surfactants can form much larger micelles than equivalent ionic surfactants (Atkins, 1986) and, hence, the type and concentration used in a cocktail can affect the sample holding capacity and the cocktail's performance under various conditions.

Some cocktails which contain non-ionic surfactants, *e.g.* Insta-Gel®, are designed to form a gel with certain sample:cocktail ratios. Small samples form a true homogeneous mixture, but as the sample volume is increased, the mixture becomes heterogeneous and is no longer suitable for counting. Still larger samples form a homogeneous gel with the cocktail, and this can be counted by

LSS (Fujii *et al.*, 1989). Non-ionic surfactants have been used alone, as a complete scintillation cocktail, for samples containing high concentrations of inorganic salts (Reed, 1984).

The fluors emit photons of light at the correct wavelength to be detected by the PMTs. Light transmitting properties, peak fluorescence wavelength, decay time of the light emission, resistance to quenching and physical and chemical properties are all important considerations in selecting a fluor. As with the solvents, most of the common fluors in use today are those that were identified by Hayes *et al.* (1952, 1955a, 1956), such as 2,5-diphenyloxazole (PPO), 1,4-di-[2-(5-phenyloxazolyl)]-benzene (POPOP), and dimethyl-POPOP, in studies of RPHs. Another fluor, *p*-terphenyl was also commonly used at this time (Hayes *et al.*, 1956), but has fallen from favour owing to its low solubility in common LS solvents (Wunderly and Kauffman, 1990). It was found at an early stage that performance can be improved by using two different fluors, rather than a single one (Kallmann and Furst, 1951), for reasons which are discussed below.

Physico-chemical properties are perhaps the most important consideration in choosing a fluor. The scintillation efficiency of a cocktail varies with fluor concentration, increasing to a maximum, before starting to decrease due to self-quenching (Hayes *et al.*, 1955a). Therefore, it is important that a fluor should be sufficiently soluble to attain this optimum concentration, and not be prone to self-quenching at low concentrations. The use of two fluors can help alleviate this problem. A high concentration of primary fluor (3-10 g l⁻¹) is enhanced by a much smaller concentration (< 1 g l⁻¹) of a secondary fluor. The secondary fluor often has better scintillation characteristics, but self-quenching, solubility and often cost may prohibit its use as a primary fluor (Wunderly and Kauffman, 1990). Fluors that colour the cocktail are also undesirable, as this can cause colour quenching (section 1.2.2.1). In some instances, chemical reactions have been observed between fluors and strong acids or bases (McEvoy *et al.*, 1972). This is the case with butyl-PBD (Fujii *et al.*, 1989) which reacts with solubilizing agents, forming a strongly-quenching, yellow compound. Thus, butyl-PBD, despite being the more

efficient fluor, is less widely used than PPO.

Light transmission is an indicator of how much of the emitted light reaches the PMTs, without being reabsorbed by the cocktail and, hence, exposed to a greater probability of being lost to competing processes (see below). Emission spectra are of higher wavelengths than the corresponding absorption spectra, due to the Stokes shift (Berlman, 1971), but the degree of overlap between the two determines how much of the emitted light is reabsorbed by the fluor. By shifting the wavelength of the emission still further by use of a second fluor, this absorption becomes negligible. The fluorescent yield, Φ , is a measure of light transmission (equation 1.9) (Horrocks, 1974)

$$\Phi = \frac{\textit{number of photons emitted}}{\textit{number of excited molecules}} \quad (1.9)$$

A quench resistant cocktail will maintain a high fluorescent yield, even in the presence of quenching agents, and secondary fluors can enhance this resistance.

The final benefit of using a secondary fluor is in order to match the emission spectra more closely with the PMT response. PMTs are chosen that have a maximum response for wavelengths of approximately 420 nm, and primary fluors emit photons with wavelengths in the range 300-425 nm (Fig. 1.2). The secondary fluors absorb and re-emit these photons at longer wavelengths (370-420 nm). Originally, glass-faced PMTs had a very narrow response range, necessitating the use of secondary scintillants (Wunderly and Kauffman, 1990). However, while modern bi-alkali PMTs are able to detect the photons emitted by the primary fluor, secondary fluors are still used for the reasons mentioned above.

The decay time (τ) of a fluor determines the length of the photon pulse (Birks, 1964) and is controlled by variables such as the formation of excited complexes and dimers. Sterically hindered fluors, which are unable to form stable dimers or be approached by solvent molecules, have shorter decay times and are less prone to internal quenching (Birks and Aladekomo, 1963). Traditional β

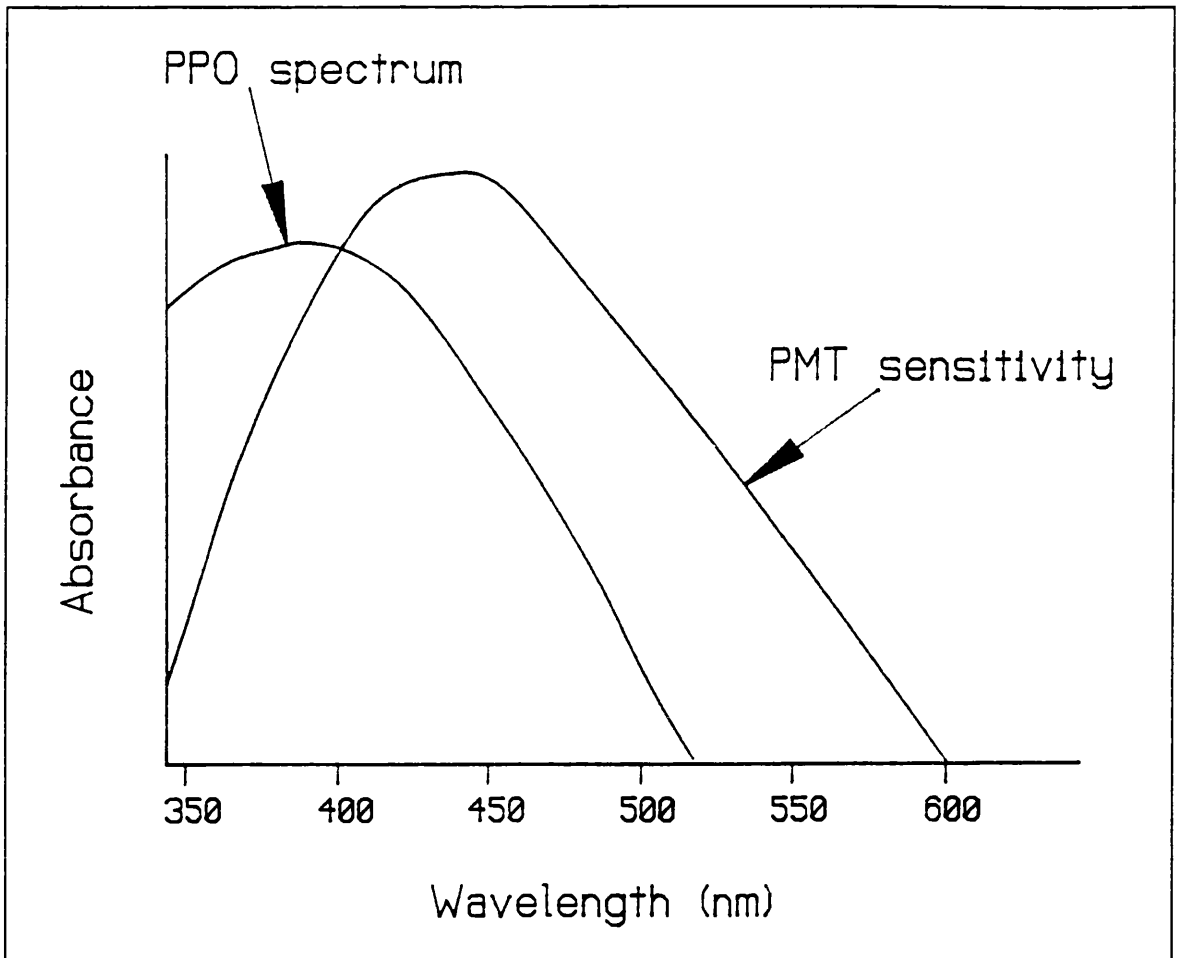


Figure 1.2: The spectrum of PPO compared to the sensitivity of a typical PMT (after Kessler, 1989).

counting requires very short decay times (*i.e.* < 2 ns) in order that the individual pulses remain distinct from each other (Kessler, 1989). At the other extreme, the modern, single PMT counters, used for flat-bed, multi-sample counting (Effertz *et al.*, 1993), require the use of a fluor with a long decay constant, such as dimethylantracene (DMA), in order to discriminate effectively against PMT noise by PSA. α/β separation LSS lies between these two points, requiring fluors with significantly different decay times when excited by α and β particles (section 2.3.1). In addition, the decay time is an indicator of how quench resistant a fluor will be. The more quickly a photon is emitted, the lower the probability of a competing process occurring (Dyer, 1974).

The scintillation cocktail emits light as a result of the radioactive decay of the sample. As ionizing radiation is emitted from the radionuclide, it gives up its energy to the surrounding matter (in

this case the LS cocktail) by electrostatic interactions (Friedlander *et al.*, 1981). The solvent, being the major component of the cocktail, absorbs the energy by ionization and the excitation of its electrons, but only excitation of π -electrons contributes to the scintillation process. Ionization causes the production of secondary electrons (δ rays), which go on to cause further excitation (Brooks, 1979). Although it is the solvent that absorbs the majority of the excitation energy, it is the fluors that emit the photons that are detected by the PMTs (Kallmann and Furst, 1958). Therefore, this energy must be transferred to the fluors. Figure 1.3 illustrates the energy transfer processes occurring in a simple binary solution containing a solvent (X) and a solute (primary fluor) (Y). LS cocktails are usually ternary solutions, composed of a solvent, primary fluor and secondary fluor (Z). However, the processes are essentially the same, with energy now also being transferred from Y to Z.

Excitation by ionizing radiation causes higher excited states to become occupied (*e.g.* S_2 , S_3 , etc.) (process (i)). These electrons then rapidly lose energy *via* non-radiative internal conversion (process (ii)) to the lowest excited singlet, S_1 . Several processes can then occur: intersystem crossing to the lowest excited triplet state, T_1 (process (xii)); non-radiative transfer to another X molecule (process (vi)) or a Y molecule (process (viii)); internal quenching (process (iv)); or the emission of a photon (process (iii)). Photons emitted by X molecules are of the wrong wavelength to be detected by the PMTs, but can be absorbed by another X molecule (process (v)), by a Y molecule (process (vii)) or be lost to the system (process (ix)). Similar processes take place until the energy is absorbed by a Z molecule and emitted as a photon, which can then be detected.

Some of these processes will now be discussed in more detail. Energy transfer to the fluors (Y and Z) can be either radiative or non-radiative, the relative importance of which varies with their concentration (Birks and Kuchela, 1961) (Fig. 1.4). It has been shown that the non-radiative transfer of excitation energy (process (viii)) to Y and Z occurs by dipole-dipole interaction over several molecular diameters, rather than by collision, with the excited X molecule coming into range of Y by

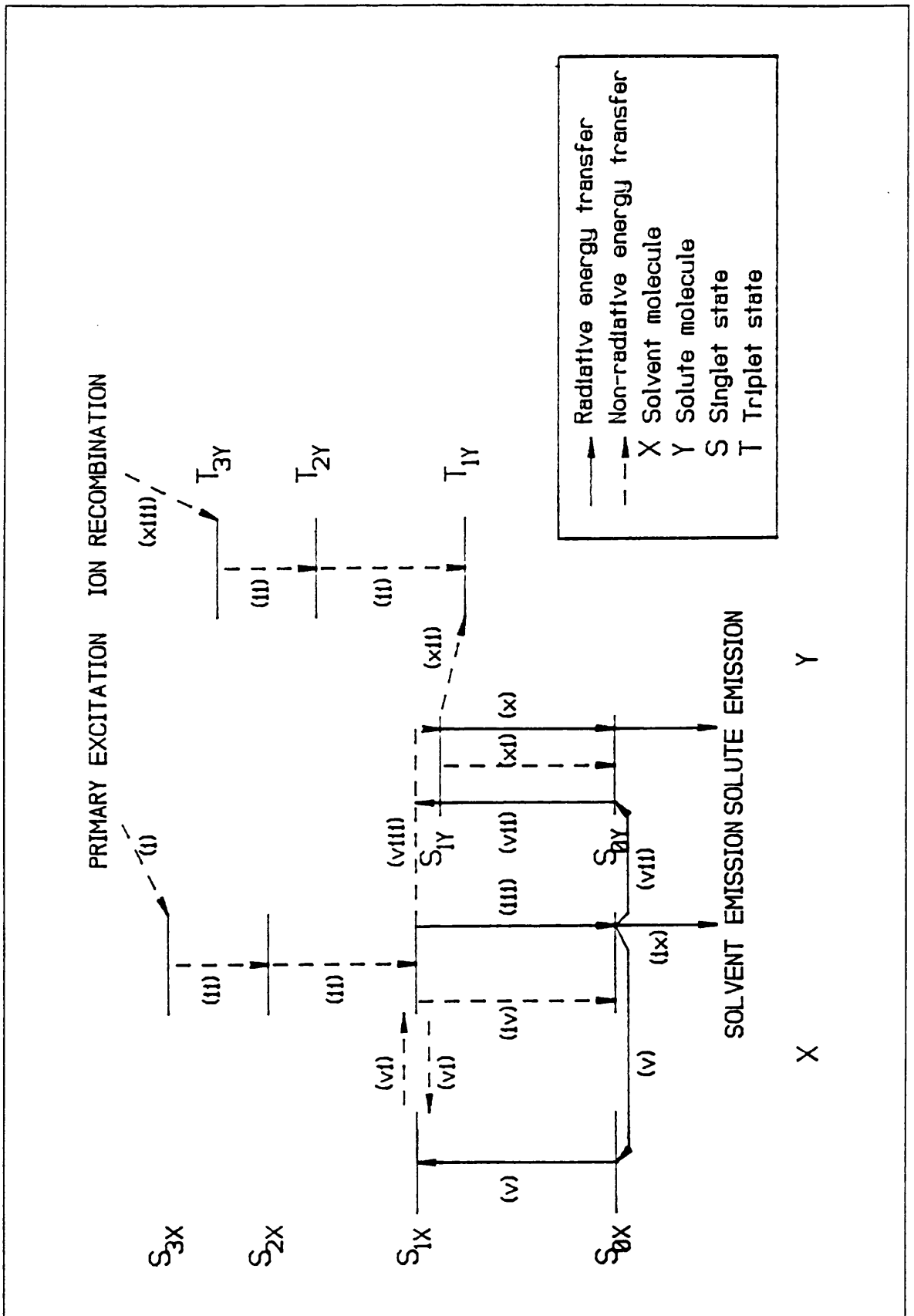


Figure 1.3: Energy transfer in a liquid binary solution. Numbered arrows are energy transfer processes and are referred to in the text.

a combination of thermal diffusion and migration of excitation energy by exchange or multipole-multipole interactions (Birks, 1964). Once the excitation energy has been absorbed by Y or Z, similar processes occur until the emission of a detectable photon.

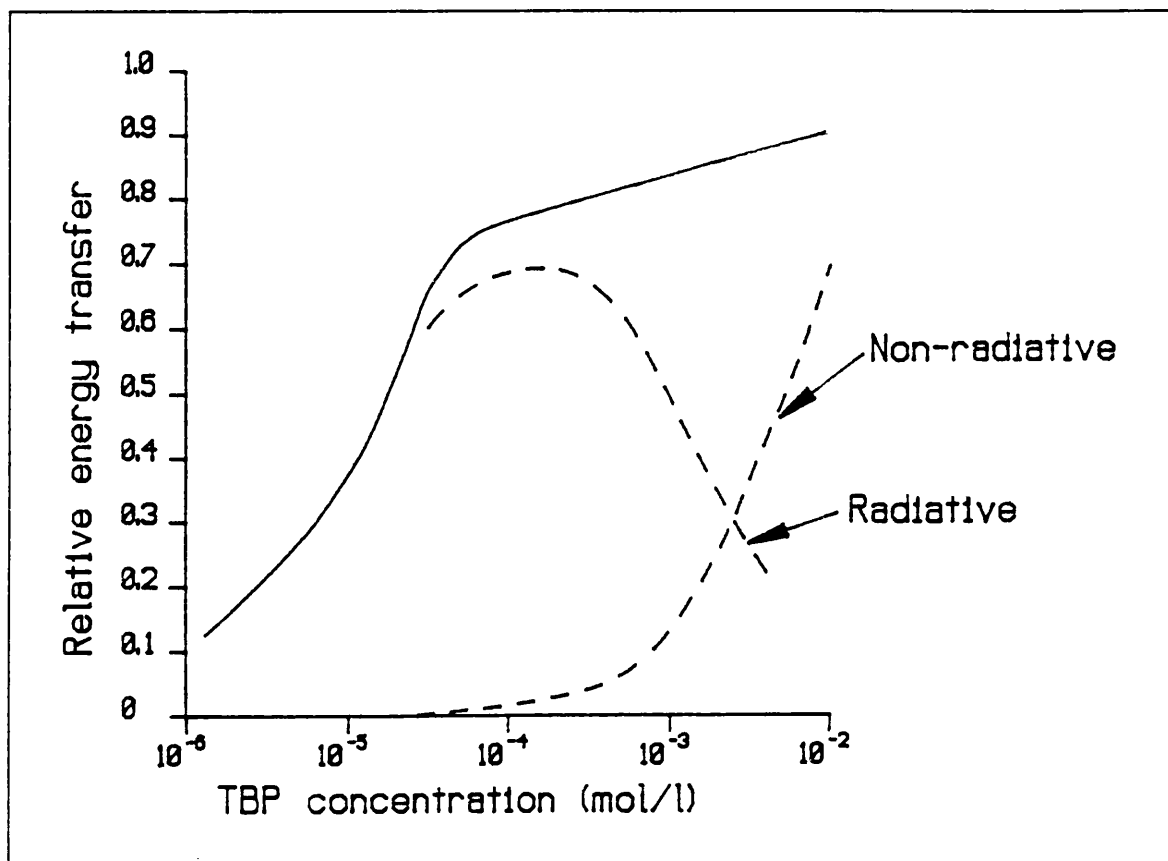


Figure 1.4: Schematic diagram of the relative contributions of radiative and non-radiative energy transfer between fluors (after Birks and Kuchela, 1961).

Excited triplet states may become occupied either via ion recombination (process (xiii)) or via non-radiative, intersystem crossing from excited singlet states (process (xii)). Primary excitation cannot cause excited triplet states to become occupied, as this is a spin-forbidden process (Birks, 1964). Statistically, ion recombination causes triplet and singlet states to be occupied in the ratio 3:1 (Laustriat, 1968). Excited triplet states rapidly decay to the lowest excited state, T_1 , by internal conversion. Triplet states cannot directly lose their energy radiatively, *i.e.* by phosphorescence, as this is a forbidden process (Brooks, 1979). Neither can they transfer energy back to the singlet states by internal conversion, as triplet states have lower energies than their corresponding singlet states

(Birks, 1970). Instead, they undergo a process called triplet annihilation, whereby two excited triplets collide to produce an excited singlet, a molecule in the ground state and a photon. This process will be discussed in more detail in section 1.3.1.

An efficient liquid scintillator will have high energy transfer rates between X and Y, and Y and Z. Productive processes, *i.e.* those that result in photons which can be detected by the PMTs, should have sufficiently high rates to be able to compete with wasteful processes. The overall efficiency of a scintillator can be described by equation 1.10 (Birks, 1964),

$$S_Z = PC \frac{E_{pZ}}{E_{1X}} f_{XY} f_{YZ} q_{0Z} \quad (1.10)$$

where S_Z is the overall fluorescence efficiency of Z; P is the efficiency of the primary excitation of π -electrons, relative to ionization and excitation of non- π electrons; C is the efficiency of internal conversion; E_{pZ} is the mean energy of the emitted photon; E_{1X} is the mean excitation energy; f_{XY} is the energy transfer efficiency from X to Y; f_{YZ} is the energy transfer efficiency from Y to Z; and q_{0Z} is the fluorescence quantum efficiency of Z. A cocktail consisting of toluene, PPO and POPOP gives rise to a typical fluorescence or scintillator efficiency of 0.052 (Horrocks, 1974). This should not be confused with the detection or counting efficiency for the system. While individual fluor molecules have a low probability of producing a photon, each decay event results in a sufficiently large number of excitations for high detection efficiencies to be reached.

1.3 ALPHA / BETA SEPARATION LSS

It had been recognized as early as the 1950s that LSC could be used to assay α emitters (Basson and Steyn, 1954). The technique has many advantages over traditional α counting methods, such as approximately 100% counting efficiency and a lack of self-absorption effects. However, there is considerable overlap in the spectra produced by α and β emitters, despite the relatively large

differences in energy between the two types of decay. In addition, the relatively poor resolution and variable background afforded by LSS have meant that, in the past, it was not generally regarded as a method suitable for determining α activity. PSD was first suggested as a means of detecting neutron events against a γ background by Brooks (1956, 1958), after the recognition that different modes of nuclear decay give rise to characteristic scintillation decay times. It was the application of PSD technology to LS counting that led to the development of α/β separation LSS (Thorngate *et al.*, 1974; McKlveen and Johnson, 1975). The next section explains the differences between pulse shapes, before the discussion turns to the means of distinguishing between different types of ionizing radiations and the LS spectrometers that have been designed to carry out this procedure.

1.3.1 Pulse shape characteristics

In 1956, Wright observed significant differences between the scintillation decay times of organic crystals excited by α particles and electrons. When anthracene was excited by γ photons (*i.e.* Compton electrons) and α particles, the resulting scintillations had mean durations of 31 ns and 53 ns respectively. Upon mathematical analysis, the scintillation pulses were observed to comprise two components: a short, initial surge of fluorescence, constituting only a small fraction of the total pulse and a longer, non-exponential portion, which formed the tail of the pulse. Wright's analysis of these pulse shapes led him to the conclusion that they were the result of two processes: an initial, rapid emission by molecules that avoided immediate ionization quenching; followed by migration within the crystal of excitation energy allowing recombination of ions, with the resultant excited molecules producing the slower emission. He surmised that α particles gave rise to longer scintillation decay times as a result of their greater specific ionization and, hence, the greater concentration of ionization quench centres.

Several other researchers found similar pulse shapes for the scintillation decay of other organic crystals and liquid solutions upon irradiation with γ photons, x-rays, neutrons and α particles

(e.g. Brooks, 1958; Owen, 1958; Bollinger and Thomas, 1961). Each experiment added to the available data, with the result that Wright's theory was quickly rejected. Alternative theories that were proposed included the formation of meta-stable excited states and formation of long-lived pairs of excited molecules (Horrocks, 1970). Finally, Parker and Hatchard (1962a and 1962b) proposed a mechanism for the production of a two component scintillation pulse, which is currently accepted as the most accurate explanation of this phenomenon. This mechanism has been described theoretically by King and Voltz (1966) and is summarized below.

The scintillation pulse comprises a prompt and a delayed component. The prompt component is the result of a fast, exponential decay process, with a decay time similar to that of the fluorescence decay time (when excitation is the result of photostimulation), which led to the conclusion that it is due to the fluorescent emission from S_{1Z} (King and Voltz, 1966). This process (reaction 1.11) has since been observed to take less than 8 ns (Brooks, 1979).



The delayed component was finally attributed to the decay of excited triplet states, T_{1Z} , which cannot lose their excitation energy radiatively (section 1.2.3.3), but must interact with another excited triplet, in the process of triplet annihilation (Brooks, 1979) (reaction 1.12).



This non-exponential process results in the delayed component, which has a lifetime of greater than 300 ns. Triplet annihilation relies on the physical approach of two molecules in the excited state, either by diffusion or the transfer of energy from molecule to molecule, as previously described in section 1.2.3.3. King and Voltz (1966) suggested that after an initial period of rapid bimolecular annihilation, the kinetics of the delayed component would be principally controlled by diffusion. This theory was supported by experimental data from a number of sources. The fact that the decay of excited triplets

relies on a diffusion controlled process causes the retardation in the emission of those photons that comprise the delayed component.

The longer scintillation decay times of α particle induced pulses than γ or β induced pulses, stems from a greater proportion of the fluorescence occurring in the delayed component (Horrocks, 1970). This can be attributed to the greater specific ionization of α particles, which results in a greater concentration of ionized molecules along their tracks. Remembering that ion recombination favours triplet formation, with a ratio of 3:1, over singlet formation (section 1.2.3.3), it follows that the greater number of molecules in the excited triplet state will result in a larger delayed component.

1.3.2 Scintillation response

It has been previously stated that pulse height (equivalent to scintillation response, L) is proportional to the energy of the ionizing particle or photon, E (section 1.2.2). Therefore, it would be expected that the peaks due to, for example, ^{36}Cl ($E_{\text{max}} = 714 \text{ keV}$) and ^{241}Am ($E_{\alpha} = 5.486 \text{ MeV}$ (86%), 5.443 MeV (12.7%)) would be well separated in a combined energy spectrum. However, this is not the case, as can be seen by Figure 1.5. Although L is directly proportional to E for electrons, making dL/dE (the scintillation or fluorescence efficiency) constant, this relationship breaks down for particles with different specific energy loss (Birks, 1951a and 1951b). According to Horrocks (1976b), the scintillation efficiency of electrons is approximately 10 times greater than that of α particles, however, the exact ratio depends on the scintillator (Berlman *et al.*, 1963; Czirr, 1963).

Birks (1951a) proposed a simple model relating specific fluorescence (dL/dr - the number of photons emitted, L , per unit path length, r) to dE/dr (specific energy loss) (equation 1.13)

$$\frac{dL}{dr} = \frac{A \left(\frac{dE}{dr} \right)}{1 + kB \left(\frac{dE}{dr} \right)} \quad (1.13)$$

where A , B and k are constants dependent on the scintillator. This equation implies that at low dE/dr ,

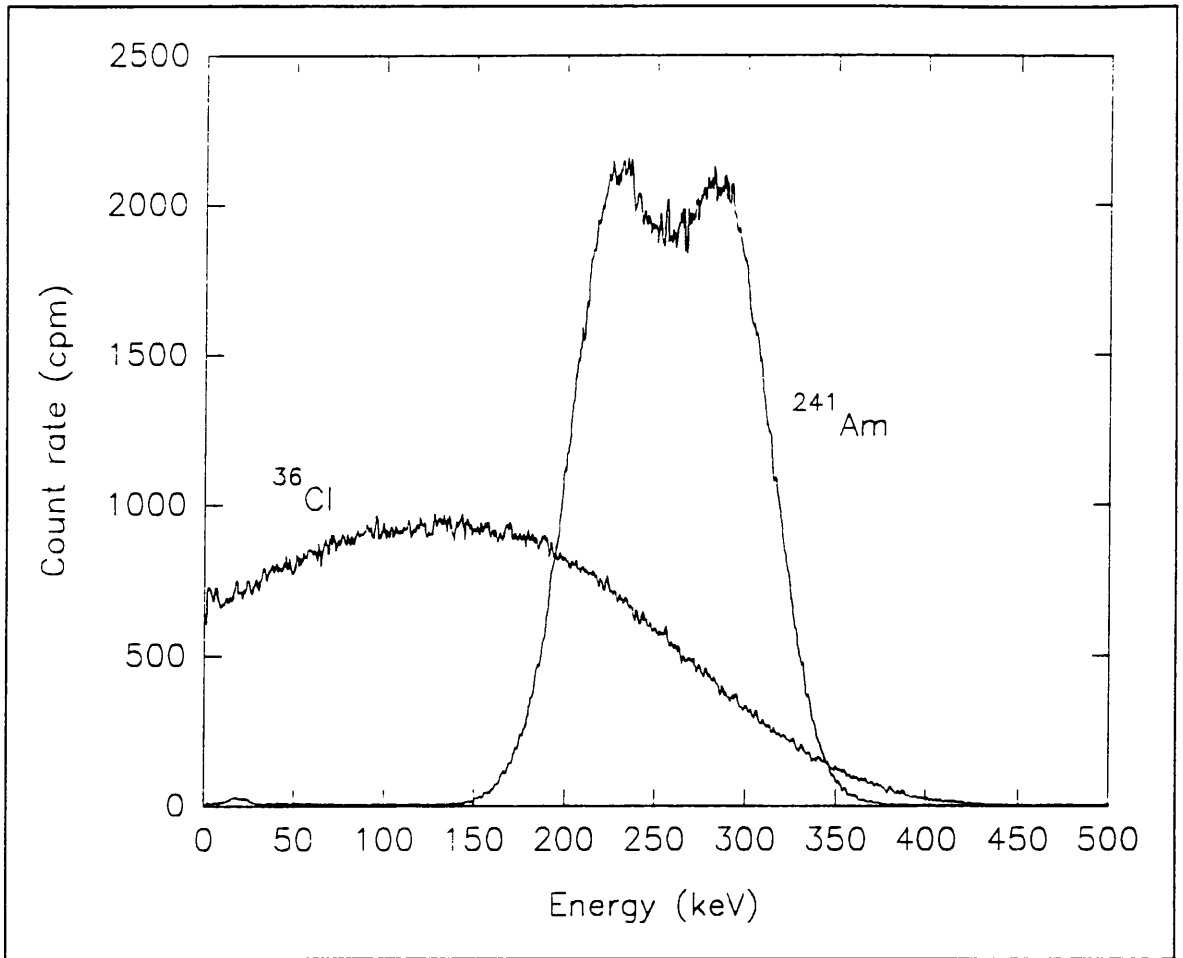


Figure 1.5: Liquid scintillation spectra of ^{241}Am and ^{36}Cl .

dL/dr becomes equal to $A(dE/dr)$, *i.e.* particle energy is proportional to pulse height, whereas at high dE/dr , dL/dr is equivalent to A/kB , a constant. This model was tested using anthracene crystals stimulated by electrons, α particles and protons of varying energies. The theory appeared to agree well with the experimental data (from a number of sources) and Birks proposed that the difference in scintillation response was the result of ionization quenching (section 1.2.2.1). However, one part of the data set produced disagreement with the predictions of the model. Hopkins (1951) had shown that the scintillation response for electrons was linear with energy above 125 keV, but not below. Several attempts were made at refining Birks' model in order to correct for this failing, but they were based on the same assumptions and were all tested with anthracene systems (Brooks, 1979). This behaviour of low energy electrons had not shown up in the anthracene studies and was attributed to the surface

quenching effects that these crystals are prone to as a result of radiation damage (Birks, 1974).

Voltz *et al.* (1966) took a somewhat different approach to the problem of theoretically defining the specific luminescence or fluorescence caused by different incident particles. Rather than simply considering the effect of high ionization densities on the prompt component of the scintillation pulse, they looked at the prompt and the delayed components separately, considered the effect of quenching on molecules excited by secondary electrons or δ rays and, perhaps most significantly, included a term dependent on the charge of the incident particle. As a result they formulated two equations, one for particles of low specific energy loss, such as electrons, and the other for heavy particles with higher specific energy loss. These equations predict that the specific luminescence should reach a maximum when plotted against particle energy (for α particles this maximum occurs at ~ 5 MeV) and that particles of differing charges produce different response curves. Experiments with thin films of plastic scintillators (Voltz *et al.*, 1966) and single, organic crystals and liquid solutions (Voltz *et al.*, 1968) have confirmed these predictions.

1.3.3 Pulse shape discrimination

Soon after the discovery that different types of ionizing radiation result in scintillation pulses of differing lengths, Brooks (1956, 1958) realized that this feature could be usefully exploited in neutron spectrometry, which suffers from a high γ background. By electronically timing each pulse, it was possible to determine if it was due to either a neutron interaction or a γ event. Horrocks (1963) showed that it was possible to discriminate between α and electron derived pulses with both organic crystal and liquid scintillators. Plastic scintillators produced some difference in the delayed component of the pulses, but to a lesser degree, making them less suitable for practical applications.

There are several ways to time and separate different pulses electronically, which collectively are called PSD. An effective PSD circuit will be applicable to all types of ionizing radiation and function at a wide range of scintillation intensities (Bollinger and Thomas, 1961). Two approaches that have

been employed are the determination of the relative intensities of the prompt and delayed component (Daehnick and Sherr, 1961), and the constant fraction method, whereby the time taken for the pulse to reach some predetermined fraction of the total intensity is recorded (Bollinger and Thomas, 1961). Various other systems have been described by Owen (1962). However, the zero-crossing method of PSD, first introduced by Alexander and Goulding (1961) and later refined by Rousch *et al.* (1964), has been widely favoured to the present day, owing to its relative insensitivity to a wide range of pulse amplitudes. This system has been successfully applied in neutron spectrometry by liquid scintillation (Perkins and Scott, 1979) and is the technique employed in the LS spectrometers used in this study.

The zero-crossing method of PSD works as follows: after the pulse has been slowed, it is doubly differentiated to produce a new curve. This curve will cross zero at a point related to the duration of the original pulse. Different types of ionizing radiation will produce characteristic zero-crossing times (Rousch *et al.*, 1964). In its application to internal LS, the zero-crossing point is compared to an operator defined time or pulse decay discriminator (TD or PDD) setting. Pulses which cross zero before the PDD are classified as β events, and those

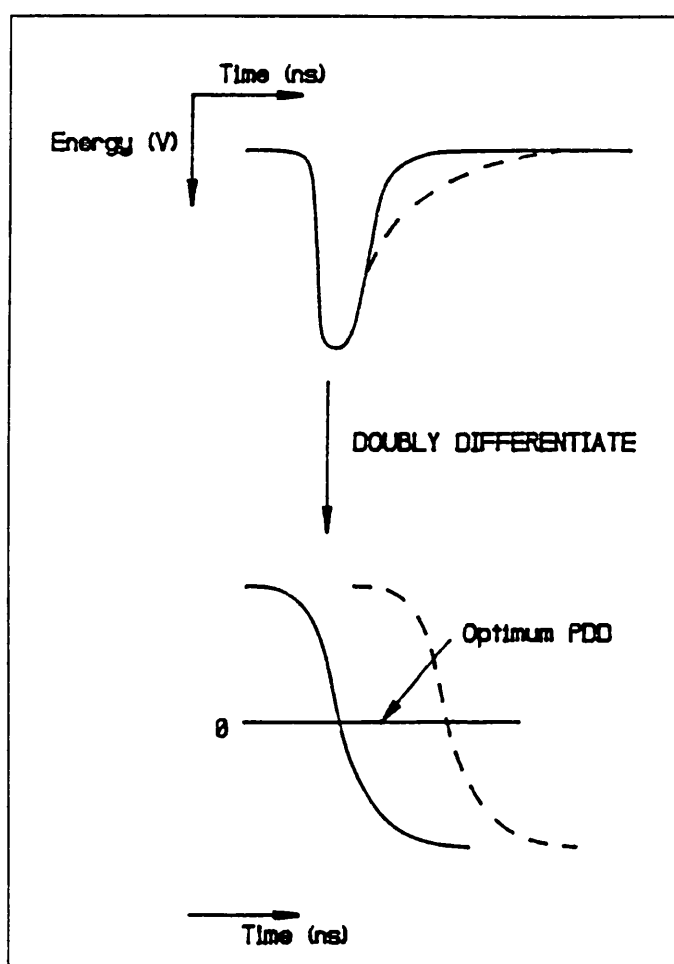


Figure 1.6: Schematic representation of the zero-crossing method of pulse shape discrimination.

after the PDD as α events (Figure 1.6). By systematically varying the PDD it is possible to find the

optimum setting at which the majority of events are correctly classified.

1.3.4 Pulse shape discrimination applied to LSS

While PSD was being intensively used and investigated in the field of neutron spectrometry, very little attention was paid to the possibility of the simultaneous determination of α and β activity by internal LSS (other than some work by Horrocks (*e.g.* 1970)) until the mid 1970s. At this point it was realized that the combination of PSD with LSS could prove to be a powerful technique for the assay of α emitting radionuclides (Thorngate *et al.*, 1974). Until the introduction of PSD, LS could not be used to assay α activity separately from β activity. Not only did α and β spectra overlap in a mixed sample, but the α spectrum had a high background, poor energy resolution and variable pulse heights, making nuclide identification difficult. PSD enabled the problem of the spectral overlap to be solved by separating α and β events into different MCAs, at the same time reducing the α background, as background events tend to be allocated to the β MCA. Improved detector design has resulted in better energy resolution and novel sample preparation techniques can eliminate variable pulse heights.

Thorngate *et al.* (1974) were able to reduce the background across the ^{239}Pu spectrum from 1 cpm to approximately 0.01 cpm by use of a combination of PSD and extractive scintillators (section 1.3.4.1). They attributed this background to three sources: (i) β and γ emitting nuclides in the sample (this cannot be avoided sometimes, when, for example, the nuclide of interest has a series of rapidly ingrowing daughters with different modes of decay, such as ^{222}Rn); (ii) the inherent activity present in the materials used in the construction of the detector; and (iii) cosmic and external γ activity. PSD is particularly useful in eliminating background due to the first cause and also for other γ derived background. It is less useful for discriminating against Cerenkov radiation, which can also give rise to pulses with an apparently long decay time due to the after-pulses that occur (section 1.2.2.2).

Several workers in this field had designed experimental instruments to count α emitting nuclides by LS (*e.g.* Horrocks, 1963 and 1964*b*), however, McKlveen, McDowell and co-workers were

the first to make serious efforts to optimize the system and develop a technique suitable for routine analyses. McKlveen (1974, 1976) and McKlveen and Johnson (1975) compared the suitability of, then, modern β LS counters with an experimental counter with a single PMT and PSD circuitry for α counting. They considered two factors in the separation of α from β events. Firstly, the degree of energy resolution attainable (*i.e.* both the minimizing of spectral overlap and the resolution between α peaks) and secondly, the degree of pulse shape resolution that was possible.

1.3.4.1 Energy resolution

Fluctuations in the height of pulses produced at the PMT anode, which are derived from events of the same energy, cause a broadening of the energy spectrum and a reduction in energy resolution. These variations can be due to a number of factors, including non-uniform emission of photons by the scintillator, non-uniform collection of photons and emission of photoelectrons by the photocathode and irregularities in the multiplication process in the PMT (Horrocks, 1964*b*). If fluctuations in photon production were the sole cause of these variations, monoenergetic α particles would produce a spectrum with a Gaussian distribution. An investigation of the spectral distribution of a number of α emitters showed that this was not the case, implicating the other factors mentioned (Horrocks, 1964*b*).

As these fluctuations are more significant when the pulse height is smaller (Horrocks, 1974), it is important to increase the number of photons reaching the photocathode, if the best resolution is to be attained. This can be achieved in a number of ways. Firstly, a scintillator could be chosen that produces the maximum number of photons per eV of excitation energy. However, this course of action has been rejected by some researchers, wanting to work within the constraints of the scintillation efficiencies of known compounds (McKlveen and McDowell, 1976). Secondly, light collection can be optimized and, finally, quenching, which results in the reduction of light output, can be minimized (McKlveen and McDowell, 1976). Not only can increasing the light output improve the energy

resolution, but it can also increase the separation efficiency of α from β events (Horrocks, 1974).

The problem of optimizing light collection was approached by comparing the pulse height and pulse shape resolution attainable with different types and shapes of light guide (McKlveen and McDowell, 1976; Thorngate and Christian, 1977). These groups found that the two parameters were not necessarily at a maximum in the same detector configurations, but this was solved by using a combined response. The optimum combined response was found to be for a hemispherical sample chamber coated with a reflective paint, coupled to a single PMT. A two PMT system gave a poorer overall response, despite having a better pulse height resolution. McKlveen and McDowell (1976) advocated the use of silicone oil to optically couple the sample to the PMT, in order to minimize reflections due to the change in refractive index as the photons pass from the sample holder into air and then into the photocathode. A sample holder immersed in silicone oil can create problems when changing samples and, therefore, Thorngate and Christian (1977) investigated the effect of using water as a coupling agent. Although the refractive index of distilled water, at 1.3, is lower than that of silicone oil (1.5), it produced a 22% better overall response. Despite this result, silicone oil is used in the PERALS® (Photon Electron Rejecting Alpha Liquid Scintillation) spectrometer, which was the first commercially produced α LS spectrometer and is based on the design described above (McDowell and McDowell, 1993).

The method commonly employed for quench reduction in this situation is the use of extraction agents. By carefully choosing an appropriate extractor, usually a long-chain, aliphatic amine, a high degree of specificity can be gained, with the added advantage of improving nuclide identification. McDowell and his co-workers at the Oak Ridge National Laboratory pioneered the use of extractants for use with liquid scintillators and coined the phrase extractive scintillators, whereby the extraction agent is contained in the LS cocktail. The nuclide of interest can be taken into the organic phase by equilibrating the aqueous sample with the extractive scintillator, leaving the aqueous phase containing

most of the quenching agents and sometimes interfering nuclides as well. The aqueous phase can then be removed prior to counting. Methods have been developed for the use of thorium (Bouwer *et al.*, 1979), uranium (Abuzeida *et al.*, 1987), radium (Burnett and Tai, 1992) and polonium (Case and McDowell, 1982) -specific extractive scintillators, amongst others.

In addition to these experiments, the effects of cocktail volume on pulse height resolution have also been investigated. Horrocks (1964*b*) examined the RPH and the line width (the full width of the peak at half its maximum height divided by the value of the pulse height at the peak maximum) as a function of both cross-sectional area and cocktail depth, for vials placed directly on the photocathode of a PMT. He found that pulse height was reduced by increasing the height of scintillator in the vial, due to the increased probability of reabsorption of photons before they reach the PMT. Line width was at a minimum (energy resolution, therefore, at a maximum) for an intermediate height of cocktail (between 0.2 and 0.6 cm). This was attributed to incomplete absorption of energy from the α particles in small volumes and longer path lengths at greater volumes, increasing the probability of disruptive reflections occurring. The effects of cross-sectional area could not be assessed due to the non-uniformity of the photocathode, making comparisons between vials impossible. McKlveen and McDowell (1976) reported that the optimum cocktail volume with their system was found to be 1 ml, in a 10 ml culture tube, for similar reasons.

1.3.4.2 Pulse shape resolution

Early PSD circuits that were used in conjunction with LS instrumentation were simply adapted from those used in neutron spectrometry (Thorngate, 1978). McKlveen and McDowell (1976) compared the resolution attainable with the zero crossing method and the constant fraction method of PSD (section 1.3.3), and found that the former gave superior results. The circuitry used by Thorngate and Christian (1977) was deemed to be too complex and expensive to be used in anything other than an experimental instrument. This led to the adaptation by Thorngate (1978) of the circuits

used by Rousch *et al.* (1964). The separation of α from β and γ events requires less complex PSD circuits than does neutron spectrometry, due to the smaller range of pulse heights encountered. This simplified zero-crossing method circuit developed by Thorngate was adopted for the commercial PERALS® instrument. This system was later updated by Carrasco and McKlveen (1985) with modern electronics, to examine the rise time of the different pulses.

It is not only the TD setting or the electronic method of PSD that affect the efficiency of event separation. Various factors, such as the timing characteristics of the scintillator, can play a crucial role in the rate of misclassification. For example, Horrocks (1970) stated that liquid scintillators containing dissolved oxygen cannot be used for PSD purposes. Oxygen has been shown to reduce the mean lifetime of triplet states (Laustriat, 1968), thus affecting the rate of triplet annihilation. All the research on the PERALS® spectrometer used de-oxygenated samples and their use is recommended with the system (McDowell and McDowell, 1993). However, Cross and McBeth (1976) found that PSD could be performed satisfactorily on an air-saturated, dioxane-based scintillator. A more detailed analysis of the different factors that need to be considered and their effects on α/β separation is found in Chapter 2.

1.3.4.3 α/β separation liquid scintillation spectrometers

Two different approaches to the determination of α activity by LSS have been taken. The first approach regarded LSS as an alternative to conventional α spectroscopy. Therefore, in order to simultaneously assay multiple α emitters, energy resolution must be at an optimum and instruments designed for β counting will not be the best solution. The PERALS® system was formulated on this basis, with McKlveen and McDowell (1976) quickly recognizing the inadequacies of traditional β LS instrumentation for this purpose. The other approach saw the problem being less of finding a new method of α spectrometry, but of developing an instrument capable of the simultaneous assay of both α and β emitters. A traditional β LS spectrometer could be successfully adapted for this purpose, with

the inclusion of PSD circuitry. These two approaches are, to a certain extent, mutually exclusive, although some features, such as sample preparation, are compatible with both instrument types. McDowell and McDowell (1994) have extensively reviewed the counting characteristics of all the commercially available α and α/β LS spectrometers.

The PERALS® spectrometer has excellent energy resolution (Table 1.2), resulting from the design of the light collection system. As this system is superior, in this respect, to conventional β LS spectrometers, this degree of energy resolution cannot be matched by them, although Yu *et al.* (1990) have improved resolution to 290 keV by the use of either etched glass or plastic vials and extractive scintillators. However, the instrument has a single PMT (and hence no coincidence circuitry) and no passive shielding so the high background in the β spectrum makes it unsuitable for β analysis, especially for those β emitters with a low E_{\max} . Therefore, the simultaneous assay of both α and β emitters is better done using one of the other instruments, with the advantage of automatic sample changing facilities, which are useful when short count times are to be employed.

Table 1.2: A comparison of different LS spectrometers and their performance with respect to α analysis. Data taken from McDowell and McDowell (1994).

Instrument	Background over α spectrum (4-8 MeV)	Energy resolution (FWHM ^a)	Light coupling	Number of PMTs	PSD	LLD ^b (cpm/ml)
Conventional β LS counter	1-10 cpm	900 keV-1 MeV	No	2	No	5
α/β separation LS spectrometer	0.1-1 cpm	600-900 keV	No	2	Yes	0.05-1 ^c
PERALS® spectrometer	0.001-0.01 cpm	~ 250 keV	Yes	1	Yes	0.001

a Full width at half the peak maximum.

b Lower limit of detection; based on a 2 ml sample, where LLD = background / sample volume.

c These figures are based on either 100% α counting efficiency, but 40% contribution from the β spectrum, or 60% α counting efficiency and < 1% contribution from the β spectrum. This may not be an accurate reflection of the true detection limits of these spectrometers (see Chapter 2).

α/β LS spectrometers can be used in one of two ways. Either the sample can be prepared as for straightforward β counting (*i.e.* mix the analyte and cocktail together in a vial to form a homogeneous mixture) or one of the extractive scintillators developed by McDowell can be employed, depending on the requirements of the analysis. There are three basic restrictions when using these instruments for α/β separation, namely the identity of the nuclide should be known (either through the use of an extractive scintillator or by other prior chemistry), quenching should be constant for all samples and standards and, obviously, the activity should be above the minimum detectable activity (McDowell and McDowell, 1994). Typical values quoted in the literature for detection limits for α emitters range between 0.20 mBq (Yu *et al.*, 1992) and 5.3 mBq (Saarinen and Suksi, 1993).

Two methods of PSD have been adopted for the α/β separation LS spectrometers. The first integrates the charge contained in the tail of the pulse and compares this value with the charge of the entire pulse (L. Kaihola, 1994, personal communication). This method is insensitive to differences in the amplitude of pulses. This information is then used as either the "R"-value (the ratio of the tail to the whole pulse) (McDowell and McDowell, 1994), which is a TD setting, or the Pulse Shape Analyser (PSA) discriminator setting, which is based on a combination of both pulse height and pulse shape data (L. Kaihola, 1994, personal communication). This method gives a better degree of event separation than PSD alone, as β pulses of a similar length to α pulses tend to be of higher energy. The PERALS® instrument also allows combination of the two parameters, as both time and energy spectra are stored by the instrument, using the Datamap® system. This has been shown to be useful in separating α from β/γ events in low activity samples (Kopp and Kopp, 1991). An alternative method, as described in section 1.3.3, is the zero crossing method of PSD, which relies solely on pulse shape information. A description of the limitations and abilities of this type of instrument can be found in Chapter 2.

1.4 URANIUM SERIES RADIONUCLIDES IN THE MARINE ENVIRONMENT

Consideration now turns from the instrumentation that was used in this study, to the field for which novel methods have been developed. Firstly, the sources and distribution of naturally occurring radionuclides are discussed, before turning to radioactive disequilibrium and its potential uses in oceanographic studies.

1.4.1 Geochemistry and Distribution

There are three types of naturally occurring radionuclide: primordial radionuclides, *e.g.* those that have been present since the formation of the Earth; the shorter lived progeny of primordial radionuclides and cosmogenically produced radionuclides, such as ^{14}C (Libes, 1992). The latter are the result of spallation reactions in the atmosphere, whereby high energy cosmic rays cause the fragmentation of atmospheric nuclei, with the side effect of neutron production. These neutrons are then able, after some attenuation by collisions, to be captured by a nucleus. Thus, ^{14}C is derived from ^{14}N (reaction 1.14)



and ^7Be is derived from ^7B (Faure, 1986). While cosmogenic radionuclides are also important tools in the study of natural processes, they will not be discussed to the same extent as natural decay series radionuclides, which are the main focus of this work.

The radionuclides present since the formation of the Earth, approximately 4.6×10^9 years ago (Friedlander *et al.*, 1981), have, by definition, half-lives of the order of 10^9 years or greater. They include the isotopes of uranium, ^{238}U and ^{235}U , and ^{40}K (an important contributor to instrumental background). ^{238}U , ^{235}U and ^{232}Th decay to produce further radioactive nuclides, giving rise to the natural decay series. These are called the uranium, actinium and thorium series respectively (Figure 1.7). It is surmised that another decay series headed by ^{237}Np once also existed in nature, however,

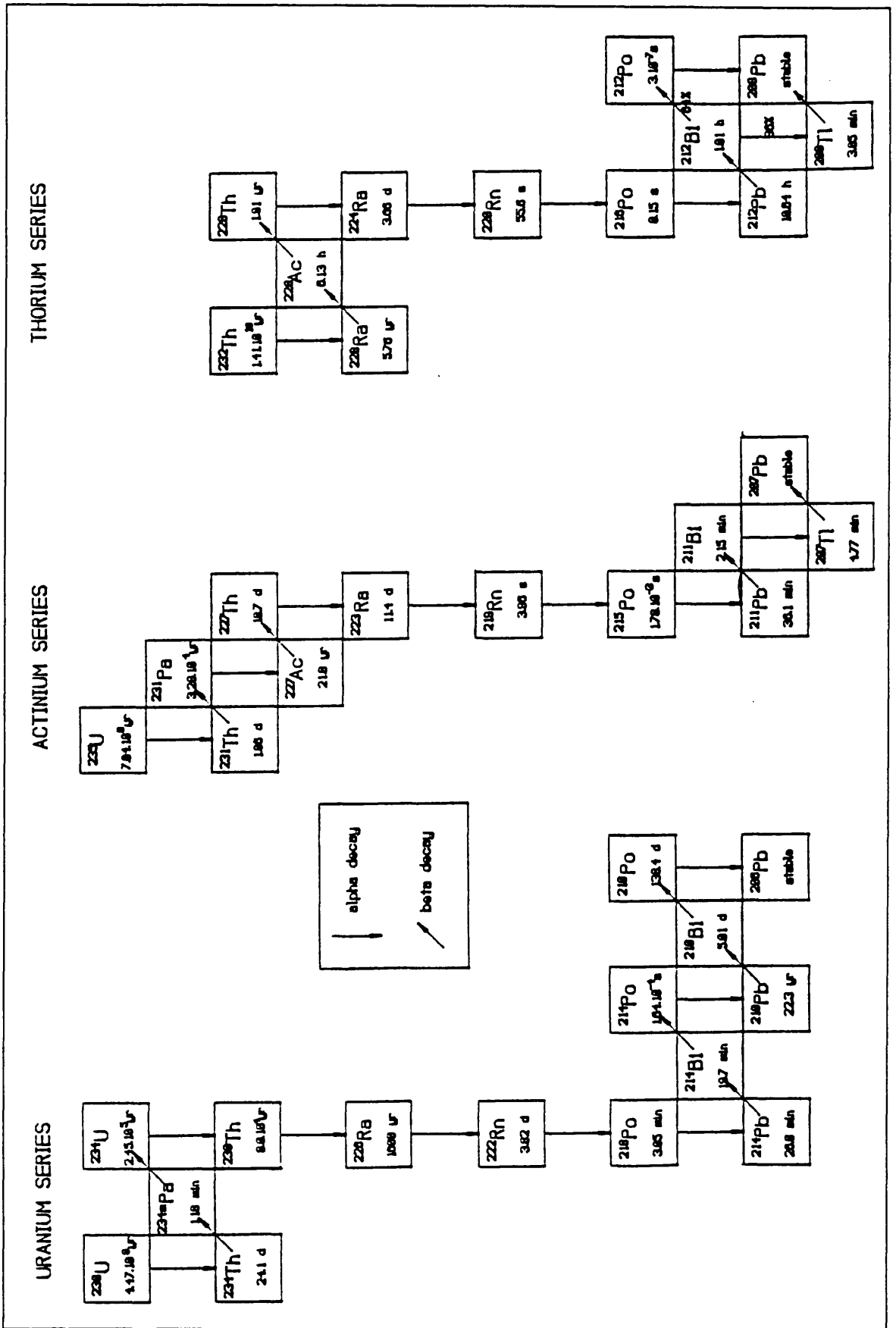


Figure 1.7: The natural decay series (major branching schemes).

the relatively short half-life of ^{237}Np (2.14×10^6 y) means that it has completely decayed away over the lifetime of the Earth (Friedlander *et al.*, 1981). The radionuclides studied here all belong to the uranium series, *i.e.* with ^{238}U as the parent. Therefore, the following discussion will use these radionuclides as examples, although other naturally occurring and anthropogenic radionuclides can also be used for similar work.

Uranium and thorium are mainly found in silica-rich, granitic rocks. They principally occur in accessory minerals, either as a major or minor constituent, such as uraninite, thorianite (oxides), some silicates and some phosphates (Faure, 1986). Weathering by wind and water causes the eventual dissolution and, hence, dispersal throughout the environment of the parent nuclides and all subsequent daughters. Uranium is present in nature in the +4 and +6 oxidation states, the latter forming the stable $\text{UO}_2(\text{CO}_3)_3^{4-}$ ion in oxidizing, aqueous environments with $\text{pH} \geq 6$ (Langmuir, 1978). As a result, uranium exhibits conservative behaviour (*i.e.* it is soluble and mobile) in most surface waters, but becomes insoluble under reducing conditions, such as occur in an anoxic sediment. Thorium, on the other hand, exists only in the +4 state, which results in extremely low solubility in water (Faure, 1986). However, while thorium is generally insoluble, it does not usually occur in nature at sufficiently high concentrations to reach its solubility limit, *i.e.* form a precipitate. Instead, thorium is extremely particle reactive, due to its instability in the dissolved phase, and will react with an available surface, which in the marine environment is usually a particle of biogenic or terrigenous origin.

The part of the environment that is of concern in this study is the ocean. There are essentially five mechanisms of supply of natural decay series radionuclides to the ocean. In brief, these are dissolved uranium and radium in river waters, particulate material from rivers, desorption of radium and radon from sediments, *in-situ* production by radioactive decay, which is particularly important for the short lived nuclides, and atmospheric supply, which is a major source of ^{210}Pb , the longest lived

decay product of the noble gas ^{222}Rn (Cochran, 1992).

Removal can also occur by several mechanisms, radioactive decay being the most obvious of these. Settling and suspended particles, including both terrigenous and biogenic material, can sorb radionuclides onto their surfaces, in particular the more particle reactive elements, such as thorium. Sorption has been defined as including adsorption, absorption, surface precipitation and, sometimes, coagulation of colloidal particles with their sorbed metals (Honeyman and Santschi, 1989). Even at concentrations well below the theoretical solubility limit, these elements will not readily maintain a dissolved state, as they are not sufficiently stabilized by the surrounding water molecules. However, as the concentration is not sufficiently high for an insoluble precipitate to form, the ions will stabilize themselves by sorbing onto any available surface.

Oxidation can cause the formation of insoluble hydroxides, which can remove radionuclides by co-precipitation type reactions. Iron and manganese oxyhydroxides, which occur ubiquitously in the near-surface oxidizing environment and are also produced in high concentrations in areas of hydrothermal activity, are particularly effective at this process. Often, the formation of oxides occurs on a surface, and thus is included as a sorption process. Finally, marine organisms may inadvertently take up radionuclides, along with the nutrients phosphate and nitrate, and incorporate them into tissue or hard parts (Broecker *et al.*, 1973). The boundaries between these various mechanisms are vague and often several processes are co-existent, but they can be collectively described as scavenging (Cochran, 1992).

Estimates can be made of the inventory of natural uranium in the world's oceans, for example Sarin *et al.* (1990) have estimated that the average ^{238}U concentration in river water is $0.27 \mu\text{g l}^{-1}$, implying a total flux to the world's oceans *via* this route of $0.85 \times 10^{10} \text{ g y}^{-1}$. ^{238}U and ^{235}U are not fractionated during dissolution and, hence, are present at a constant ratio of 137.88:1 (Cochran, 1992). However, the ratio of ^{234}U to ^{238}U varies as a result of the preferential dissolution of the former,

possibly due to recoil during the α decay of ^{238}U or to lattice defects resulting from the passage of the α particle (Fleischer, 1980). A recent estimate of the $^{234}\text{U}/^{238}\text{U}$ activity ratio for the open ocean is 1.1444 ± 0.002 (2σ) derived from both Atlantic and Pacific samples (Chen *et al.*, 1986).

Uranium in the open ocean exhibits conservative behaviour and, thus, the concentration varies linearly with salinity. Ku *et al.* (1977) found the uranium concentration of 35‰ salinity seawater to be $3.3 \pm 0.2 \mu\text{g l}^{-1}$ and the uranium/salinity ratio to be $(9.34 \pm 0.56) \times 10^{-8} \text{ g g}^{-1}$. More recently, Chen *et al.* (1986) obtained ^{238}U concentrations of between 3.162 and 3.281 $\mu\text{g kg}^{-1}$ for 35‰ salinity seawater. The variability in these data is greater than expected, but may be due to adsorption onto sample container walls (Cochran, 1992). Taking the data from Ku *et al.* (1977) it is possible to calculate the mean uranium inventory and the mean residence time of uranium in the ocean to be $4.5 \times 10^{15} \text{ g}$ and $4.5 \times 10^5 \text{ y}$ respectively (Cochran, 1992).

Although uranium is soluble in seawater, the same is not true of most of the other radionuclides in the natural decay series. As a result, a state of disequilibrium often exists between parent and daughter radionuclides, and this can be used as a tool in oceanographic studies. The state of radioactive disequilibrium and its causes are now further discussed.

1.4.2 Radioactive Disequilibrium

Before considering the concept of radioactive disequilibrium, it is necessary first to understand the equilibrium situation. In the case where a radioactive species has a daughter which is also radioactive, the number of atoms of the daughter present is governed by the number of atoms of the parent (equation 1.15 (Friedlander *et al.*, 1981)).

$$N_d = \frac{\lambda_p}{\lambda_d - \lambda_p} N_p^0 (e^{-\lambda_p t} - e^{-\lambda_d t}) + N_d^0 e^{-\lambda_d t} \quad (1.15)$$

where N_d is the number of atoms of the daughter at time, t ; λ_p and λ_d are the decay constants of the parent and daughter respectively; and N_p^0 and N_d^0 are the number of atoms of the parent and

daughter at time = 0. This relationship can be simplified in two instances. The first results in the state of transient equilibrium. When $\lambda_p < \lambda_d$ and t becomes sufficiently large, $N_d^0 e^{-\lambda(d)t}$ tends to zero and $e^{-\lambda(d)t}$ becomes negligible relative to $e^{-\lambda(p)t}$. Thus, the activities of parent and daughter can be expressed as a ratio (equation 1.16)

$$\frac{A_p}{A_d} = \frac{(\lambda_d - \lambda_p)}{\lambda_d} \quad (1.16)$$

where A_p and A_d are the activities (*i.e.* the rate of change of the number of atoms, dN/dt) of the parent and daughter respectively. The other special case occurs when $\lambda_p \ll \lambda_d$ and the activity of the parent is effectively a constant with respect to the activity of the daughter. This situation leads to a state of secular equilibrium, in which equation 1.16 can be further simplified to equation 1.17.

$$\frac{A_p}{A_d} = 1 \quad (1.17)$$

The distribution of naturally occurring radionuclides in the environment is controlled by the geochemistry of each element, so there is often a state of disequilibrium in the natural decay series radionuclides as supplied to the oceans, a notable example of which has already been mentioned, the case of ^{234}U and ^{238}U . Despite this, there are many parent-daughter pairs in the natural decay series that fulfil the conditions for secular equilibrium, owing to the short half-life of the daughter nuclide. It could be expected that rapid ingrowth of the daughter product would compensate for differences in supply mechanisms that might occur. Indeed, the basis for disequilibrium studies is the assumption that the sole input of the daughter is the decay of the parent (Broecker and Peng, 1982). However, these radioactive elements are subject to further disequilibrium. Scavenging processes are important in creating disequilibria. For example, as previously mentioned, the activity of ^{238}U ($t_{1/2} = 4.468 \times 10^9$ y) in the world's oceans is dependent only upon salinity. However, its daughter, ^{234}Th ($t_{1/2} = 24.10$ d), is highly particle reactive and will be removed from solution in the presence of any particulate material.

Thus, parent and daughter do not occur in secular equilibrium in the dissolved phase of particle rich nearshore or surface ocean water, although this state is readily attained in particle free water. For example, at mid depths in the deep ocean the particle load is very small, which allows ^{234}Th in solution to reach equilibrium with its parent (Bacon and Rutgers van der Loeff, 1989).

1.4.3 Marine tracer studies

The degree of radioactive disequilibrium in the oceans between parent and daughter (as given by the activity ratio) is usually dependent on the concentration of particulate material in the water column and on the rate of removal of the particulate matter. By determining the distribution of the daughter between the dissolved and particulate phases, and the use of mathematical models, information on residence times and rates of removal can be derived. Radionuclides have three advantages with regard to kinetic studies. Firstly, it is often simpler to detect the radioactive decay that is occurring, than the nuclide itself. Secondly, for short-lived nuclides, it is possible to define the input into the system (decay of the parent) accurately (Broecker *et al.*, 1973). Finally, and perhaps most importantly, radioactive decay provides a means for determining the time-scale of a process. Thus, natural decay series radionuclides are not only of interest in themselves, but are used to mimic the behaviour of other reactive species in the water column, such as other reactive metals (Santschi *et al.*, 1980) and nutrients (Broecker *et al.*, 1973).

Within the uranium series there are several radionuclide pairs that usually do not occur at equilibrium. These include $^{234}\text{Th}/^{238}\text{U}$, $^{230}\text{Th}/^{234}\text{U}$, $^{210}\text{Pb}/^{226}\text{Ra}$, and $^{210}\text{Po}/^{210}\text{Pb}$, with the more particle reactive species first in each case. These disequilibria all have different characteristics which make them suitable for a variety of different studies. The most significant difference between parent-daughter pairs is the half-life of the daughter (Fig. 1.7), the relevance of which is discussed below. Radionuclide disequilibrium studies play an important role in the study of ocean dynamics. Some examples of applications involving thorium isotopes are used to illustrate the following section, which discusses the

use of models to develop an understanding of the kinetics of scavenging processes, although it should be emphasized that these models could be applied to other disequilibria. A more detailed discussion of the disequilibrium studied in this work (*i.e.* $^{234}\text{Th}/^{238}\text{U}$) and its applications can be found in section 3.2.

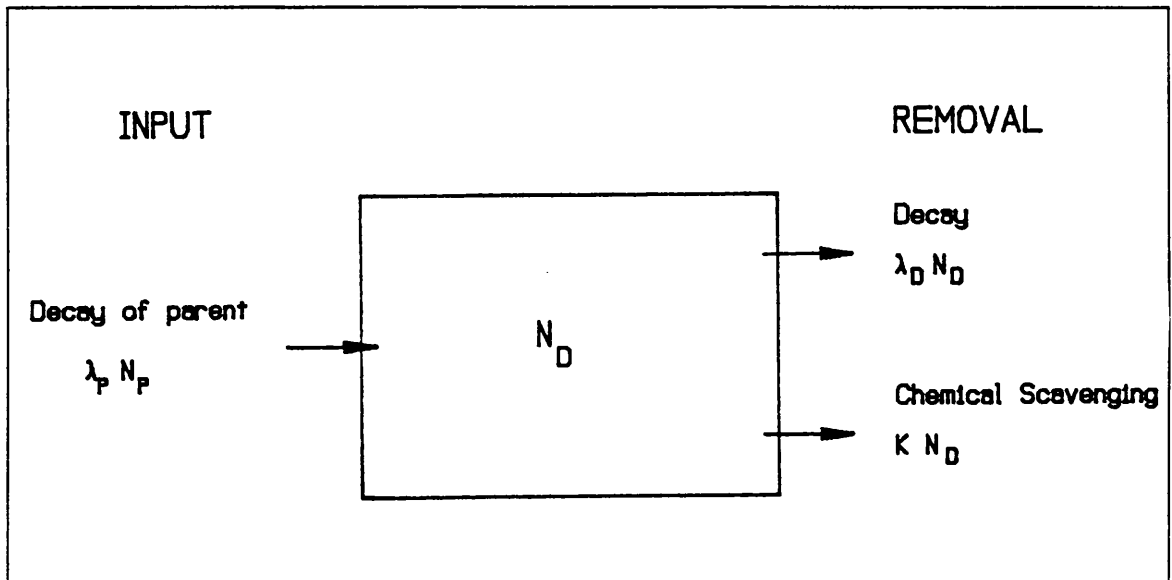


Figure 1.8: Simple box model (after Cochran, 1992).

The simplest models that can be applied to these data are box models that assume no horizontal transport and, thus, are only strictly applicable to the open ocean situation. Even there, simple box models are often only used when there is little data or when the system is homogeneous (Cochran, 1992). Equation 1.18 and Figure 1.8 (Cochran, 1992) illustrate a box model with first order kinetics, where a steady state is assumed in order to derive a residence time and rate of removal for the daughter nuclide.

$$\lambda_p N_p = \lambda_d N_d + k N_d \quad (1.18)$$

where k is the rate constant for removal processes other than radioactive decay and the remaining terms are the same as in previous definitions. Substituting activities into equation 1.18 leads to equation 1.19.

$$J = A_p \lambda_d - A_d \lambda_d \quad (1.19)$$

where J is the rate of scavenging and is equivalent to kA_d . This equation can also be expressed as equation 1.20.

$$\frac{\partial A_d}{\partial t} = A_p \lambda_d - A_d \lambda_d - J = 0 \quad (1.20)$$

where $\partial A_d / \partial t$ is the rate of change of the activity of the daughter nuclide (assumed to be zero for the steady-state calculation). The rate of removal of suspended particulate material by dissolution, settling, *etc.* can also be found in the same way. Residence times are simply given by the activity of the daughter divided by the rate of removal (Coale and Bruland, 1985). One problem with such a simple model is the assumption that scavenging is a non-reversible process. Moore and Hunter (1985) have shown this assumption to be incorrect for thorium isotopes and the same is probably true for other radionuclides.

Despite its shortcomings, this type of model has been used successfully to model euphotic zone production rates (Coale and Bruland, 1985 and 1987) and to predict the behaviour of reactive pollutants, such as lead, mercury and chromium (III) (Santschi *et al.*, 1980). However, the use of the steady-state assumption, while necessary in some instances due to a lack of data, can produce misleading results, especially when applied to a dynamic situation, such as a phytoplankton bloom. If more than one data set is available, which differ only in the time of collection, it is possible to integrate equation 1.20 with respect to time, and, using an approximation, produce equation 1.21 (Buesseler *et al.*, 1992a)

$$k = \lambda_d \left[A_p - \frac{(A_{d(1)} + A_{d(2)})}{2} \right] - \left[\frac{(A_{d(2)} - A_{d(1)})}{t_2 - t_1} \right] \quad (1.21)$$

where $A_{d(1)}$ and $A_{d(2)}$ are the activities of the daughter at times t_1 and t_2 respectively. This non-steady

state version has been applied by Buesseler *et al.* (1992a) to a time-series study of a phytoplankton bloom event.

More complex models can be developed if more data are available to show small scale differences in activity, especially if other parameters are known, such as temperature, salinity or the distributions of other radionuclides. Two other examples of kinetic models (from Cochran (1992)) are discussed below.

In reality, supply and removal terms are not restricted to those mentioned above. Often there is significant mixing of the water column, by advection and diffusion, and this will affect the disequilibrium position. If the rate of mixing can be determined, a one-dimensional model can be developed which takes this into account (equation 1.22).

$$\frac{\partial N}{\partial t} = K \frac{\partial^2 N}{\partial z^2} + w \frac{\partial N}{\partial z} - \lambda N + J + P \quad (1.22)$$

where $\partial N/\partial t$ is the rate of change of the number of atoms of the daughter, usually assumed to be zero (the steady-state situation); K is the eddy diffusion coefficient; z is a linear distance, such as depth; w is the advection velocity; J is the removal term (equivalent to kN) and P is the input by radioactive decay by the parent. K/w can be determined by salinity or temperature determinations.

A multi-isotope approach can be readily undertaken with the thorium isotopes ^{234}Th , ^{230}Th and ^{228}Th ($t_{1/2} = 24.10$ d, 8.0×10^4 y and 1.9131 y respectively). The different half-lives of these isotopes provide a means of examining various parts of a system independently, and comparing data to evaluate its validity. One such model attempts to describe the scavenging process, and is illustrated by Figure 1.9 and equations 1.23, 1.24 and 1.25 (Cochran, 1992).

$$\frac{dA_D}{dt} = P + k_{-1}A_s - (\lambda + k_1)A_D = 0 \quad (1.23)$$

$$\frac{dA_s}{dt} = k_1 A_D + \beta_{-2} A_L - (\lambda + k_{-1} + \beta_2) A_s = 0 \quad (1.24)$$

$$\frac{dA_L}{dt} = \beta_2 A_s - (\lambda + \beta_{-2}) A_L - \omega \frac{dA_L}{dz} = 0 \quad (1.25)$$

where A_D , A_s and A_L are the activities of the thorium isotope of concern in the dissolved, suspended particle and large particle phases respectively; k_1 and k_{-1} are the adsorption and desorption rate constants; β_2 and β_{-2} are the aggregation and disaggregation rate constants; ω is the sinking rate of large particles and remaining terms have been defined previously.

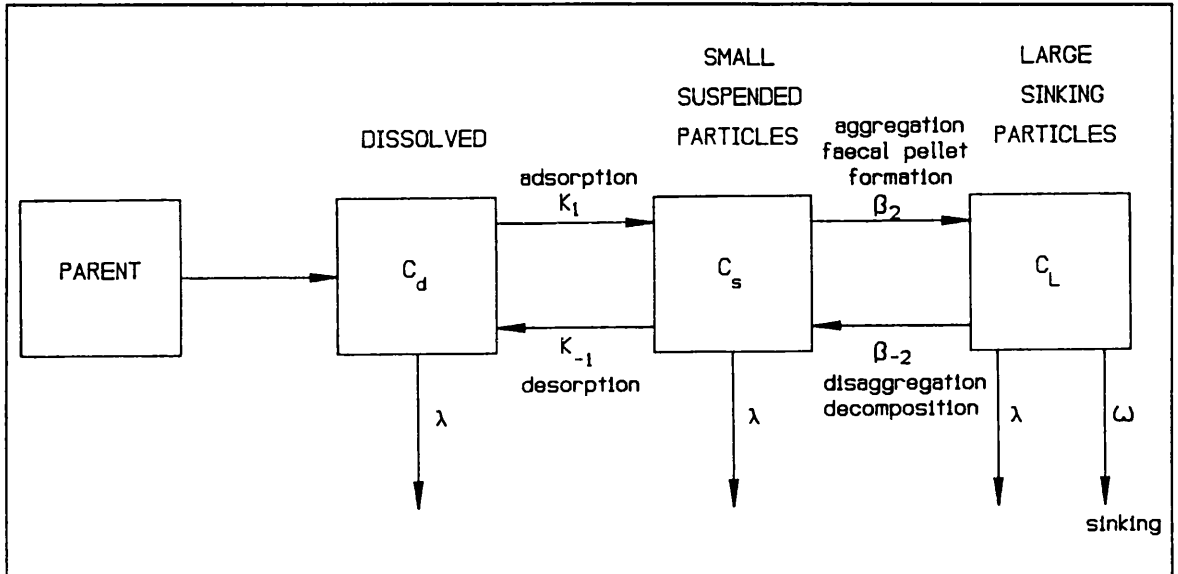


Figure 1.9: Partitioned box model for radionuclide scavenging (after Cochran, 1992).

In the case of ^{230}Th , equations 1.23-1.25 can be simplified as λ is small relative to the other rate constants (equations 1.26, 1.27 and 1.28) (Cochran, 1992).

$$A_L = \frac{P}{\omega} Z \quad (1.26)$$

$$A_s = \frac{\beta_{-2}}{\beta_2} \frac{P}{\omega} Z + \frac{P}{\beta_2} \quad (1.27)$$

$$A_D = \frac{k_{-1} \beta_{-2} P}{k_1 \beta_2 \omega} Z + \frac{\beta_2 + k_{-1} P}{k_1 \beta_2} P \quad (1.28)$$

It is possible to determine all the rate constants in either case. P/ω is the gradient of ^{230}Th in sinking particles with depth (as found in sediment traps). β_2 is determined by taking the value of C_s at the surface, and likewise k_1 is found, yielding values for k_{-1} and β_{-2} by calculation.

This model is based on the assumptions that thorium is supplied in the dissolved phase by radioactive decay of the parent (also in solution), and that small particles are suspended in the water column. Thorium can be sorbed onto small particles and then either desorbed or the particles are transformed into larger sinking particles by aggregation. Alternatively, if the small particles are consumed by a larger organism, faecal pellets can also be formed which constitute large, sinking particles. These larger particles can be removed from the system by sinking, or be returned to the small particle pool by disaggregation or decomposition processes. A more realistic model would also need to include remineralization terms, whereby both large and small particles can decompose, returning adsorbed thorium to the dissolved phase (Clegg and Whitfield, 1990). In addition, the role of colloidal material is now also considered to be significant in scavenging processes and should be included (Honeyman and Santschi, 1989; Baskaran *et al.*, 1992).

This type of approach has been taken by Cochran *et al.* (1993) to examine data from the JGOFS (Joint Geochemical Ocean Flux Survey) North Atlantic Bloom Experiment. Two thorium isotopes were used - ^{234}Th and ^{228}Th . Thus, two sets of rate constants were generated and could be compared. The data show reasonably good correlation between the two isotopes. The largest difference is for the β_2 and β_{-2} terms, but this has been accounted for, in that these terms rely heavily on figures calculated from sediment trap data, which have been shown to be unreliable in the surface ocean by detailed comparison with ^{234}Th data (Buesseler, 1991).

The choice of parent-daughter pair in environmental kinetic studies of natural decay series

disequilibrium is governed by their half-lives and the system to be studied. The residence or turn-over time of the system should be of the same order of magnitude as the half-life of the daughter nuclide. For example, the low sedimentation rates of the deep ocean are measured using $^{230}\text{Th}/^{234}\text{U}$ disequilibrium ($t_{1/2}[^{230}\text{Th}] = 7.54 \times 10^4 \text{ y}$), whereas in the coastal environment sedimentation rates are much higher and it is more appropriate to use $^{234}\text{Th}/^{238}\text{U}$ disequilibrium ($t_{1/2}[^{234}\text{Th}] = 24.10 \text{ d}$). The arguments for this can be understood by referring back to equation 1.19. Both k and λ_d should be expressed in the same units (for examples days^{-1} or years^{-1}). If either the rate constant or the decay constant becomes either very large or very small, large errors will be introduced into the calculations. Another facet of this argument is the value of the activity ratio of parent and daughter. For example, the use of $^{234}\text{Th}/^{238}\text{U}$ disequilibrium is best suited to waters with rapid rates of removal, such as coastal waters. A typical activity ratio for these nuclides in coastal waters is 0.6 (Broecker and Peng, 1982). However, in the deep ocean, particles are formed and sink only slowly, allowing ^{234}Th to almost attain equilibrium with its parent, giving an activity ratio of approximately one (Broecker and Peng, 1982). The ideal activity ratio should neither be too close to one or too close to zero to cause problems in measuring it accurately (Libes, 1992). McKee *et al.* (1984) suggest that processes with a timescale of up to five times the half-life of the daughter nuclide can be followed using the disequilibrium situation.

1.5 AIMS

The aims of this work are two fold. Firstly, to increase the understanding of the instrumentation in use. α/β separation LSS, while becoming a popular analytical technique, has been poorly characterized in the past, in terms of both instrument optimization and factors influencing separation efficiency. This work attempts to define those aspects of the sample which influence α/β separation and to understand why these factors have the effects they do.

Secondly, to develop methodology to use α/β LSS to its best advantage in the field of marine tracer studies. Marine tracer studies using natural decay series radionuclides depend on having analytical techniques which can be readily transferred to the ship-board environment, especially for short lived nuclides, and it is with this in mind that LSS has been examined as a potential tool. Reduced sample sizes and reliability of instrumentation are only two of the possible benefits for these methods. Small scale studies have also been undertaken, in which the methods have been applied to oceanographic situations, in order to demonstrate their feasibility.

CHAPTER 2: OPTIMIZATION OF COUNTING CONDITIONS AND COCKTAIL DEVELOPMENT FOR ALPHA/BETA LSS

2.1 INTRODUCTION

As described in Chapter 1, the use of PSD within commercial LS instrumentation has become widespread over the past 10 years. Many applications for α/β separation LSS have also been documented and put into routine use (*e.g.* uranium in water, Venso *et al.*, 1993; radium in rocks, Saarinen and Suksi, 1992; plutonium in soils, Yu *et al.*, 1992). While it is taken for granted that many aspects of the sample preparation and composition affect the performance of standard LS procedures, such as quench correction and counting efficiency determination, it is only slowly being recognized that features of modern instruments which depend on the electronic analysis of PMT anode pulses are highly dependent on the sample composition (*e.g.* Cook and Anderson, 1992).

McKlveen and McDowell (1976) documented a thorough investigation into the effects of sample composition and geometry on energy resolution and PSD for the PERALS® system (section 1.3.4). However, some of the features used for this optimization, such as the sample holder, are exclusive to the PERALS® spectrometer and the findings cannot be transferred easily to other α/β LS spectrometers. In addition, some features of the PERALS® system represent a compromise between pulse shape and pulse height resolution. Finally, PERALS® requires the use of extractive scintillators and, although these cocktails can be used with other α/β LS spectrometers, to do so is not always desirable. Therefore, as the conditions that promote efficient PSD and the effects of sample and cocktail composition on PMT anode pulse shapes were not well understood for α/β LS spectrometers, an initial study of these areas was first undertaken with respect to the development of aqueous accepting cocktails, in order that the most efficient system could be used in later applications of the α/β LSS technique.

applications of the α/β LSS technique.

2.1.1 The effect of cocktail composition

Many aspects of the sample composition and geometry that could affect either pulse height or pulse shape resolution have been thoroughly investigated by McDowell and co-workers in developing the PERALS® spectrometer (section 1.3.4). This has led to a highly specialized methodology for the analysis of α emitters, which is effective but, in some respects, restrictive in its scope. This procedure consists of extracting the nuclide of interest into a scintillation cocktail, which is then purged with an oxygen-free gas before counting. McDowell's extractive scintillators (section 1.3.4.1) employ toluene as a solvent and use naphthalene as an energy transfer agent (see below for a discussion of the mechanism) (McDowell *et al.*, 1974; Bouwer *et al.*, 1979; McDowell and McDowell, 1994).

However, the use of extractive scintillators is not always appropriate. For example, gross α/β analysis could be hindered by the nuclide specificity of an extractive scintillator as a range of nuclides is of interest (*e.g.* Salonen, 1993a), the identity of which may not be known in advance. The use of an extractant can also add to the complexity of sample preparation, as a very specific chemical composition for the analyte, in terms of both pH and salt concentrations, is required for the extraction procedure to work efficiently (McDowell and McDowell, 1994). In some cases, water analysis can be performed simply by mixing an aliquot of water directly with an aqueous accepting cocktail (*e.g.* Salonen, 1993b). Despite this, much of the early work on the modern, commercial instruments used for α/β separation has focused on extractive scintillators (*e.g.* Yang *et al.*, 1991).

At the start of the present work, in 1991, a limited number of studies had been published on the effects of cocktail composition on PSD. Kaihola and Oikari (1991) recommended the addition of naphthalene to a traditional cocktail or the use of a cocktail based on a naphthalene derivative solvent (Optiphase HiSafe™). However, this paper provided no explanation for the choice of solvent, other

than the fact that this cocktail provided similar PSD properties to those of naphthalene. In a comparison of the energy resolution attainable with different scintillators, McDowell *et al.* (1974) showed that 2-ethylnaphthalene produced similar peak-to-valley ratios for "natural" uranium to toluene + 20% w/v naphthalene, but did not document the differences in pulse shape resolution.

In choosing fluors for extractive scintillators, McDowell *et al.* (1974) compared their energy resolution or light output properties. They found that the use of a secondary fluor is unnecessary for α LS, as quenching does not cause a significant loss of counts from the α spectrum. PBBO (2-(4'-biphenyl)-6-phenylbenzoxazole) and butyl-PBD were the most effective of the fluors studied at producing light and, hence, have been used in all subsequent formulations (McDowell and McDowell, 1994). Yang *et al.* (1991) found that PPO was the best choice of fluor for α/β separation purposes with an extractive scintillator, once economic considerations had been taken into account (PPO is the primary fluor used in the majority of commercial LS cocktails and, hence, is widely available). Neither Yang *et al.* (1991) nor Kaihola and Oikari (1991) had attempted to look at anything other than the overall α/β separation properties of these cocktails. Therefore, it was decided to undertake a systematic study of all the cocktail components, and to attempt to derive an understanding of the processes that lead to PMT anode pulse shape differences, with the aim of developing an ideal aqueous accepting cocktail for α/β separation purposes.

The PSD afforded by traditional LS cocktails, such as those based on xylene or toluene, is generally poor, but has been shown to be enhanced by the addition of 20% naphthalene (Oikari *et al.*, 1987; Yang *et al.*, 1991). Naphthalene improves α/β separation by acting as an intermediate in the energy transfer process between the solvent and the fluor (Brooks, 1979; McDowell, 1986) (reactions 2.1 and 2.2).





where S_{0N} , S_{1N} and T_{1N} are the ground, first excited singlet and first excited triplet states of naphthalene respectively, and the remaining terms are the corresponding electronic states for the solvent (X) and the primary fluor (Y). This more energetically favourable route increases the production efficiency of excited fluor molecules. The production of fluor triplet states is especially enhanced, as energy transfer to triplet states, being a non-radiative process, relies on physical approach and so is affected by the concentration of both the fluors and the intermediate, naphthalene, in the cocktail (section 1.2.3.3). Assuming a constant proportion of triplet states is produced by each type of event, the more triplet states that are produced overall, the greater the resolution between the pulses will be. In other words, increasing the production of triplet states has the effect of stretching α pulses relative to β pulses. Even so, in a comparison with an optimized extractive scintillator (with toluene as the solvent and 20% naphthalene), Yang *et al.* (1991) found that Insta-GeI® + 20% naphthalene gave the poorer pulse shape resolution.

The ability of naphthalene to act as an intermediate in this way, results from the extensive delocalization of its π electrons. Thus, it could be assumed that, where aromaticity is maintained, naphthalene derivatives, such as DIN, will have the same effect on PSD as naphthalene itself. In section 1.2.3.3, the merits of modern LS solvents, such as DIN, in terms of safety, disposal and performance for β counting, were discussed. Given these advantages over both the traditional solvents and naphthalene, and the possibility that DIN could enhance α/β separation, the potential existed to develop a new aqueous accepting cocktail that could give equivalent or even better separation of events and at the same time be safer to handle. Therefore, the initial part of this work focused on the effects on PSD of DIN relative to those of naphthalene.

The role of surfactants was examined, as this area had not been discussed in the literature and is important in developing an aqueous accepting cocktail. This initial study also compared two

secondary fluors, namely *bis*-MSB (*p-bis*-(*o*-methylstyryl)-benzene) and DMA. As DMA has three conjugated benzene rings and is known to stretch PMT anode pulses even more than naphthalene (Effertz *et al.*, 1993), it could possibly enhance the separation of events still further.

During the period within which this work was being carried out, other groups investigated cocktails and solvents for their α/β separation properties. Prichard *et al.* (1992) compared cocktails containing no surfactants for ^{222}Rn analysis. They found that a solvent base containing a 50:50 mixture of DIN and PXE produced the best separation of events, relative to DIN alone and PXE alone. In a similar study of aqueous immiscible cocktails, Spaulding and Noakes (1993) compared a mineral oil scintillator and cocktails based on DIN or a mixture of DIN and PXE. In this case, the DIN based cocktail was found to be preferable to the DIN/PXE mixture, as it produced a lower background and a longer plateau region, in which α counting efficiency was constant. Salonen (1993*b*) compared three aqueous accepting cocktails, again for ^{222}Rn analysis, namely Optiphase HiSafe™ 3 (DIN based), Ultima Gold™ XR (DIN based) and Lumagel®-Safe (a gel-forming cocktail based on diarylalkanes). The DIN based cocktails were found to produce the best limits of detection for this method. McDowell and McDowell (1994) suggested that some naphthalene derivatives could be used as alternative energy transfer agents to naphthalene, rather than substituting the primary solvent for a naphthalene derivative, but provide no data to support this hypothesis.

Having developed an optimized cocktail for α/β separation (section 2.3.1), it was felt that further investigation of the effects of fluors on pulse shapes was merited. Any organic molecule that contains an aromatic structure will produce fluorescence when excited, in this case by ionizing radiation, owing to the delocalized nature of its electrons. However, not all of these potential fluors will be suitable for LSS. The ideal fluor should be colourless (coloration of the cocktail leads to quenching), should not react chemically with the sample or other cocktail constituents, and should be reasonably quench resistant (section 1.2.3.3). Beyond this, there are many subtle differences in molecular

structure that can bring about much larger differences in scintillation properties.

Wolff *et al.* (1993) demonstrated that DMA is able to form excited complexes (exciplexes) with DIN, which results in an increase in the decay time of the excited molecules. The ability of a molecule to form these complexes is dependent on the presence of substituents, which may either hinder or encourage the process (Birks and Aladekomo, 1963). The decay of the excited fluor could have a bearing on α/β separation efficiency, as this factor is related to the duration of the scintillation pulse. In this work, a number of different fluors are compared that could be potentially useful for α/β separation LSS and an attempt is made to define any structural features, in particular specific substituent groups, that bring about enhanced performance.

2.1.2 The effects of quenching

Impurities in an LS sample, or the sample itself, can result in a reduction in counting efficiency and a shift in the energy spectrum to lower energies, principally by the processes of chemical and colour quenching. Consequently, various techniques for determining the degree of quenching in a sample have been developed, in order to correct for its effects, as described in section 1.2.2.1. McKlveen and McDowell (1976) noted that quenching by chloroform reduces α/β separation efficiency and variations in quenching between samples caused problems, both in terms of nuclide identification, due to the spectral shift, and variable α/β separation. Extractive scintillators were adopted as a means of resolving these problems, however, with the focus of the present work being on aqueous accepting cocktails, some quenching is inevitable and its effects on PSD need to be quantified.

Rundt (1991), in a study of β counting efficiencies, observed that quenching agents produce different effects according to their energy levels in comparison to those of the solvent. "Electron scavengers", such as oxygen and carbon tetrachloride, reduce the delayed component of the scintillation pulse, while the prompt component is largely unaffected (Birks, 1970). Other quenching agents, such as acetone, are able to interact with excited singlet states, and thus affect both the

prompt and the delayed component. McDowell and McDowell (1994) suggested that the relatively long lifetime of triplet states makes them inherently more vulnerable to quenching than excited singlets. It therefore seems likely that quenching and pulse shape are interdependent, with implications for PSD.

Despite the possibility that quenching can affect pulse shapes, there have been relatively few mentions in the literature of the effects of quenching on α/β separation using aqueous accepting cocktails. Sanchez-Cabeza *et al.* (1993) studied the effects of quenching by carbon tetrachloride on the separation of α from β events, and found that increasing quench results in increased misclassification. In addition, Parus *et al.* (1993) and Yang (1993) observed that changes in quenching could bring about anomalous changes in counting efficiency (*i.e.* the apparent β counting efficiency increasing as quench increases), which are effectively attributable to changes in the rate of misclassification. Grau Carles and Grau Malonda (1994) found that at the high quench levels attainable with gel-forming cocktails, which have large sample holding capacities, α/β separation could not be achieved to the level required (*i.e.* an α spectrum with minimal spill from the β spectrum). Finally, Yang (1994) attempted to derive a relationship between quenching and α/β separation. Although this study produced data for tSIE and misclassification which clearly lie on a single line, no mention is made of the quenching agent used or the causes of this relationship.

Despite the evidence that variable quenching causes variations in the degree of misclassification, and the fact that it is difficult to obtain uniform quenching throughout a batch of real samples, the majority of studies that utilize α/β LSS pay little attention to this potential source of error. Therefore, it was decided to look systematically at the ways in which quenching could affect PSD. For β emitters, the amount of delayed component in the scintillation pulse is dependent on event energy (higher energy β events giving rise to pulses that are longer in duration) (Passo and Kessler, 1993). Therefore, as quenching can affect the delayed component (Rundt, 1991), a number of β emitters of variable E_{max} were considered. Although Yang (1994) found no differences in separation efficiency

when comparing the β emitters $^{90}\text{Sr}/^{90}\text{Y}$, ^{137}Cs and $^{152,154}\text{Eu}$, it is possible that the ability of the instrument to differentiate between pulse types is dependent on the E_{max} of the β emitter. Both the effect on the optimum PDD setting and on the degree of misclassification at a given PDD were considered. The latter is the more important factor in the case of variations in quench within a batch of samples. In light of the work by both Rundt (1991) and Hiller *et al.* (1994) it was considered necessary to compare the effects of a number of different quenching agents, as the integrity of pulse shapes is not necessarily maintained under a variety of quenching conditions.

Horrocks (1970) noted that the presence of oxygen suppressed the delayed component of a scintillation pulse and, hence, the use of oxygen-free cocktails for α/β separation was seen as essential for the PERALS® system (McKlveen and McDowell, 1976). However, the work of Cook and Anderson (1992) found that nitrogen purging reduced the efficiency of the electronic background reduction feature of their instrument, as it increased the delayed component of the ^{14}C pulses at the PMT anode, making them less distinguishable from background pulses. The same could be true for α/β separation, in which the β emitter generally has a higher E_{max} than ^{14}C . Therefore, an investigation was carried out into the effects of oxygen on α/β separation.

2.1.3 Other factors

Other aspects of the sample have also been investigated for both the PERALS® spectrometer and for conventional LS spectrometers with PSD capabilities, with regard principally to enhancing α/α resolution. McKlveen and McDowell (1976) and Horrocks (1964*b*) compared various geometries and cocktail volumes, but the principal concern in both cases was the optimisation of energy resolution (section 1.3.4.1). Small sample volumes approximating a spherical geometry were found to give optimum performance in this respect.

Polyethylene vials and etched glass vials have both been found to enhance energy resolution relative to standard glass vials (Yu *et al.*, 1990; Kaihola and Oikari, 1991). However, Yang *et al.* (1991)

reported that PSD is poorer with polyethylene vials than with glass. Many studies employing α/β separation LSS have used Teflon (*e.g.* Yu *et al.*, 1992), Teflon-coated polyethylene (*e.g.* Saarinen and Suksi, 1993) or polyethylene (*e.g.* Ryan *et al.*, 1993) vials, rather than glass or etched glass. Salonen (1993*b*) compared different types of vial and found that, for ^{222}Rn analysis, Teflon-coated polyethylene vials produced the optimum limit of detection. In all cases, it appears that the benefits of these opaque vials, with respect to both background reduction and energy resolution enhancement, have outweighed any disadvantages for α/β separation.

The applications of interest in this study do not require good energy resolution between α peaks, but good separation of α and β events into their respective MCAs. Hence, a comparison of the effect of vial type, vial volume and cocktail volume was undertaken, with respect to α/β separation efficiency.

2.2 EXPERIMENTAL

The instruments used in this work were the Packard Tri-Carb® 2250 CA with an additional α/β separation facility, and the Packard Tri-Carb® 2550 TR/AB. These instruments both have the ability to discriminate between α and β events on the basis of their different PMT anode pulse shapes, by applying pulse decay analysis (PDA) circuitry before the event is allocated to the MCA channel. The instruments have two MCAs - one for " β " events and the other for " α " events. Events that have energies < 30 keV or > 1000 keV are automatically assigned to the β MCA. These values were preset by the manufacturers in order to reduce misclassification, as no α emitter should produce events in these regions of the spectrum, even under conditions of extreme quenching. Several different 2550 TR/AB instruments were used, which have been designated as (a), (b) and (c). Counters (a) and (b) are, in fact, the same instrument, but the PMTs were replaced and, consequently, have been differentiated in the text, and are temperature controlled to 16°C , both by a refrigeration unit attached

to the instrument and by an air-conditioning system in the laboratory, as is the 2250 CA α/β . Counter (c) had no temperature control of any kind.

Both the 2550 and 2250 instruments also have a low-level option which reduces the background by further PSA. However, in the 2250 CA α/β this PSA is applied to all pulses and, consequently, it reduces the α counting efficiency considerably and was not used. The more advanced instrument (2550 TR/AB) applies the low-level option only to events already allocated to the β MCA and, hence, the α counting efficiency is not affected. This aspect of the instrument was not investigated at a general level, but was studied with respect to the method developed for ^{234}Th analysis (section 3.3.2).

A standard sample composition was used throughout this work, unless otherwise stated, in order to investigate individual components of the system selectively. This consisted of a 20 ml low potassium glass vial, containing 10 g of cocktail and 0.4 ml loading, which consisted of 0.2 ml ^{238}Pu spike (in 0.5M nitric acid) + 0.2ml 0.1M hydrochloric acid (α sample), 0.2 ml $^{90}\text{Sr}/^{90}\text{Y}$ spike (in 0.1M hydrochloric acid) + 0.2 ml 0.5M nitric acid (β sample) or 0.1M hydrochloric acid + 0.2 ml 0.5M nitric acid (background sample). Comparisons were made using sets of samples consisting of a pure α emitter, a pure β emitter and a background sample. $^{90}\text{Sr}/^{90}\text{Y}$ was the β emitter of choice for all the experiments described here, as the high E_{max} of ^{90}Y (2950 keV) implies that this nuclide will be more difficult for the instrument to distinguish from an α emitter, due to its longer PMT anode pulses, than one of a lower energy. The work described below led to the development and commercial production of the cocktail Ultima Gold™ AB, which was used for all subsequent experiments.

The QIP used throughout this work is the tSIE. For early work, using the 2250 CA α/β , this was determined at the start of each count as defined by the instrument (*i.e.* the external standard is placed next to the vial and the sample counted until a preset number of counts has been recorded). In later work, using the 2550 TR/AB instruments, samples were counted separately to obtain the tSIE.

In this case, each sample was counted four times, during which the external standard was unshielded for 15 s, and the average tSIE found.

2.2.1 Determination of the optimum PDD setting

The separation efficiency was determined by finding the optimum PDD setting, and determining the degree of misclassification of events at that point. This was achieved by counting the α and β samples at a series of PDD settings and deriving a cross-over plot. This was carried out in one of two ways. The 2550 TR/AB is able to produce a cross-over plot automatically, and this feature was used on some occasions. In other experiments, and for the 2250 CA α/β , the cross-over plot was determined manually. The basic principles were the same for both the instrumental and the manual determinations, but there are some differences which are discussed below.

2.2.1.1 Manual determination

For the manual determination, a background sample was counted alongside the α and β standards for each setting. At each PDD, the misclassification of α and β events (% spills) were calculated as follows: a window was chosen that encompassed the α peak by examination of the α sample spectrum. The count rate in the α window of both the α and β MCAs was found for the α sample and the background sample. As ^{238}Pu is a pure α emitter, any counts found in the β MCA in excess of the background will be the result of misclassification. Hence, the following equation (2.3) could be applied

$$\% \text{ spill}_{\beta} = \frac{\text{cpm}_{\alpha(\beta)} - B_{\alpha(\beta)}}{(\text{cpm}_{\alpha(\beta)} - B_{\alpha(\beta)}) + (\text{cpm}_{\alpha(\alpha)} - B_{\alpha(\alpha)})} \times 100\% \quad (2.3)$$

where $\% \text{ spill}_{\beta}$ is the misclassification of α events into the β MCA; $\text{cpm}_{\alpha(\beta)}$ is the count rate recorded in the α window of the β MCA for the α sample; $B_{\alpha(\beta)}$ is the equivalent count rate for the background sample; and $\text{cpm}_{\alpha(\alpha)}$ and $B_{\alpha(\alpha)}$ are the equivalent count rates for the α MCA. The misclassification into the α MCA is calculated in the same way using the region of the MCA incorporating the β spectrum,

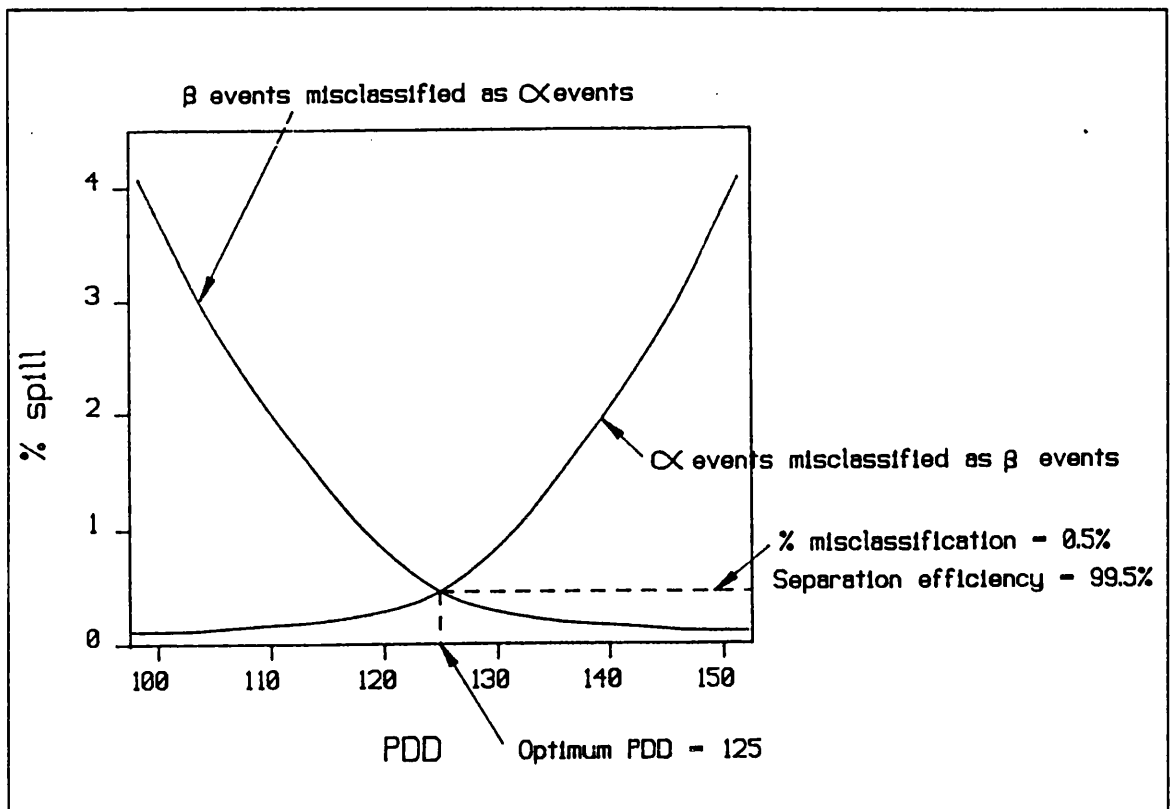


Figure 2.1: Schematic representation of a cross-over plot.

and the two sets of data are plotted against PDD. An example of this type of plot is given in Figure 2.1.

For an ideal system, the point at which the two curves cross is the point at which the least total misclassification occurs, giving both the optimum PDD and the minimum % spill at that point. However, as the PDD is a whole number, the cross-over point will not always give the optimum PDD. In other cases, the two curves are not symmetrical, producing the same effect. Addition of the two lines to produce a total misclassification curve allows the determination of the optimum PDD, which is at the minimum of this curve. Unless the optimum PDD occurs precisely at the cross-over point, the $\% \text{ spill}_\beta$ and $\% \text{ spill}_\alpha$ will not be equal. Therefore, the mean of these two numbers has been used and defined as the $\% \text{ spill}_m$. Although a total spill curve allows the minimum misclassification to be determined more easily, the traditional cross-over plot is more readily interpreted visually and is the conventional method of presenting this type of data. It is therefore used throughout the present work.

Ideally, the cross-over plot should be produced with the maximum number of points, in order to obtain the most accurate curve. However, as this is a time consuming process, especially if good counting statistics are to be achieved, this is not usually possible, and so the resolution of the data is reduced. In these cases, a best-fit line should be derived and plotted at a greater resolution than simple interpolation between points would allow, as this can give rise to an overestimation of the % spill and cause significant skewing in the optimum PDD (Fig. 2.2).

In order to determine the most useful approximation for this type of data, a set of standards

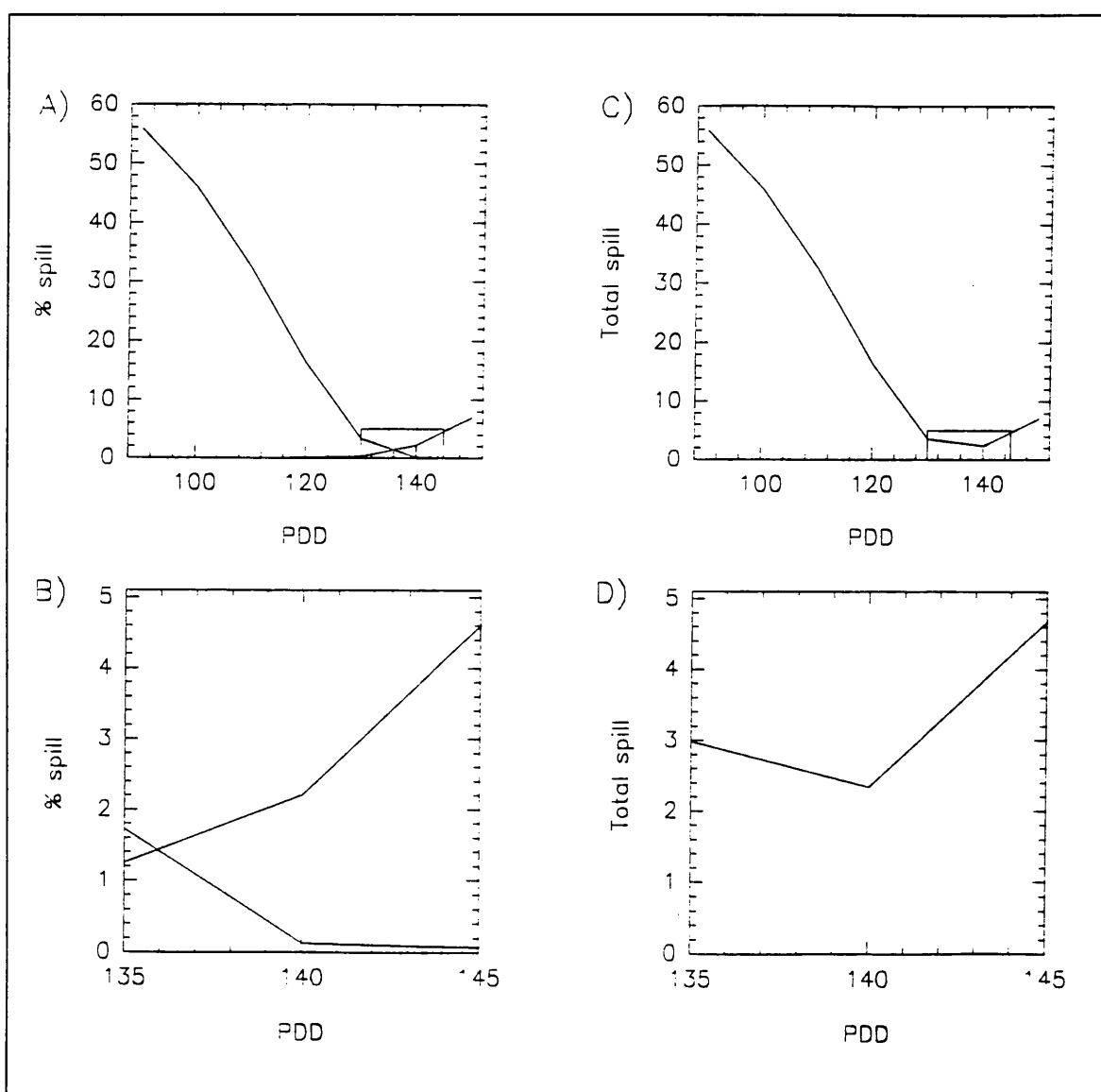


Figure 2.2: Cross-over (A and B) and total spill (C and D) plots showing skewing of the apparent optimum PDD. B is a detail of A and D of C.

(^{241}Am , ^{36}Cl and a background in Insta-Gel® XF + 20% naphthalene, with approximately 50,000 dpm activity per vial) were counted at one PDD unit intervals over the range 100-120, and also at 90, 95, 125 and 130, for 10 min at each setting. It was found that a 5th order polynomial, of the form given in equation 2.4, best fitted the data, in a comparison of 2nd - 5th order polynomials (Fig. 2.3).

$$y = ax^5 + bx^4 + cx^3 + dx^2 + ex + f \quad (2.4)$$

Although a 5th order polynomial may not completely describe the data in all cases, it appears to be a reasonable approximation within the bounds of this study.

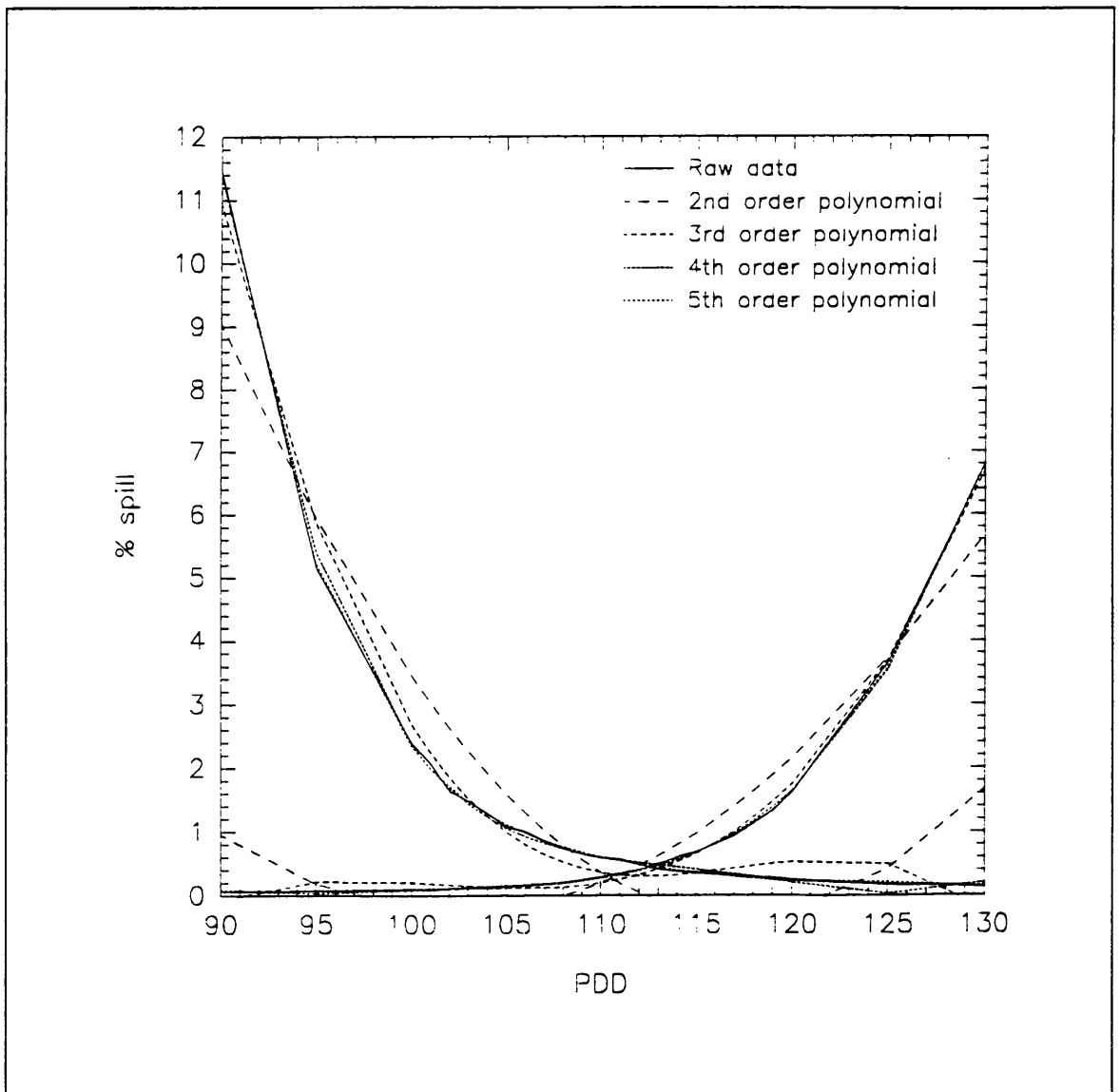


Figure 2.3: The ability of different polynomials to model cross-over plots.

The optimum PDD and % spill_m were determined by examining the total spill curve for this data set. The resolution of the data was then reduced firstly to five PDD units and then 10 PDD units and a 5th order polynomial was fitted to these points using curve-fitting software. Using the equations derived, intermediate points (at intervals of one PDD unit) were calculated. The total spill plots, so determined, were compared to the original data set and found to be in good agreement (Fig 2.4). However, for some real samples the data were of sufficiently low quality to prevent this procedure from working (Fig 2.5). In these cases, a spline curve was used, generated automatically by the curve fitting program (Sigma Plot, Jandel Scientific). In general, the agreement between the fitted curve and the simple joining of points with a straight line is high, providing the optimum PDD is centrally placed and data points have been determined at a minimum of 5 PDD unit intervals. Therefore, the curve fitting procedure was only used for those samples which produced skewed total spill plots.

2.2.1.2 Instrumental determination

The 2550 TR/AB has the capability of automatically calculating the misclassification and producing a cross-over plot. However, it utilizes the full 0-2000 keV range of the MCA (excluding those regions mentioned above) and does not take into account the contribution of the background. This causes an increase in the apparent misclassification into the β MCA (% spill _{β}) and cannot be avoided by simply increasing the activity of the samples, as there will always be a point at which the misclassification of events is low compared to the contribution of the background. This effect is illustrated by Table 2.1 and Figure 2.6. While this facility is useful for scanning a large number of different samples, it cannot provide the fine detail required when comparing small effects.

2.2.2 Cocktail development and optimization

Two groups of cocktails were studied in this experiment. Firstly, commercially available cocktails were examined, both with and without the addition of 20% w/w naphthalene (the saturation point for most LS solvents and the concentration recommended by Yang *et al.* (1991)). A range of

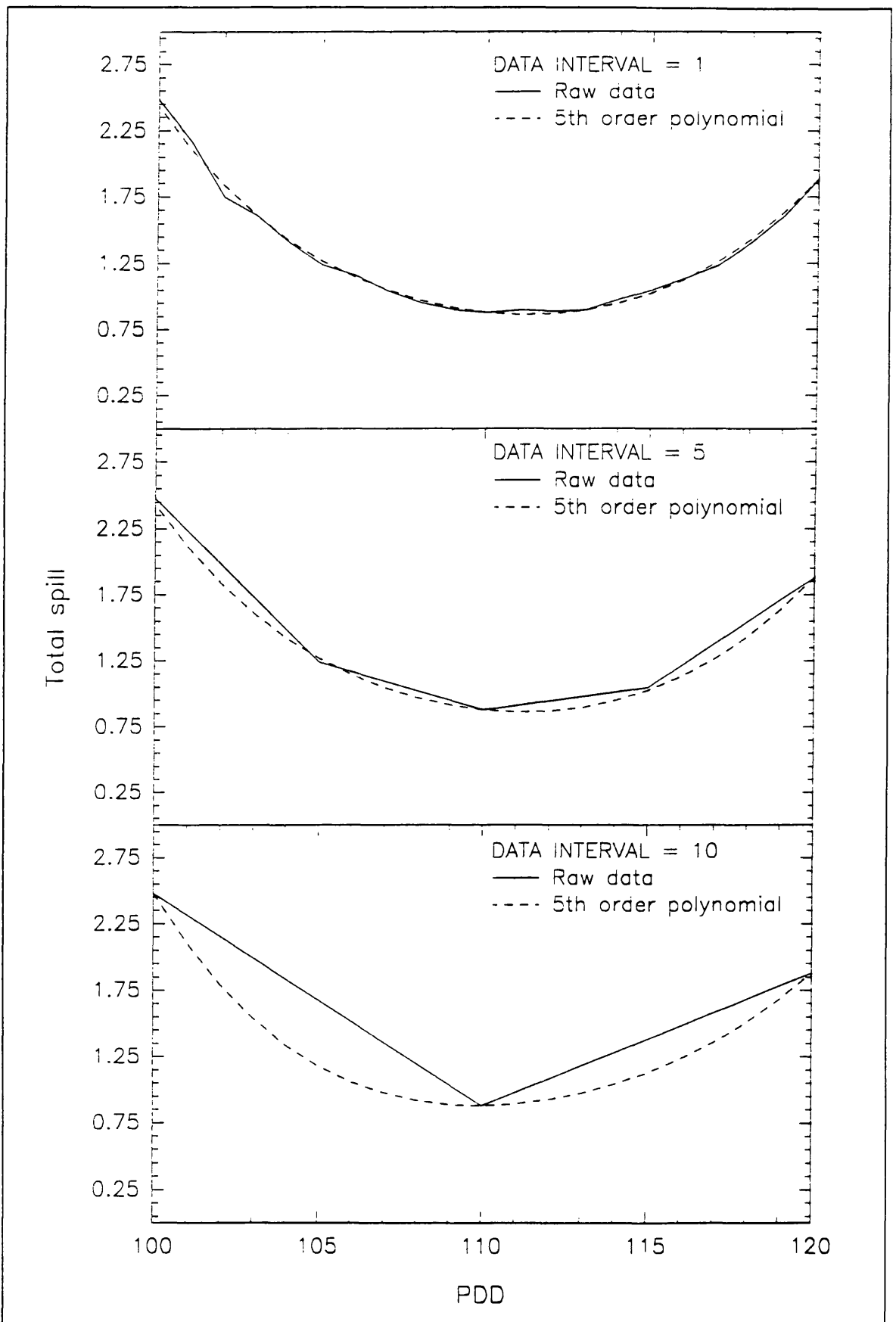


Figure 2.4: 5th order polynomial fitted to data of varying resolution.

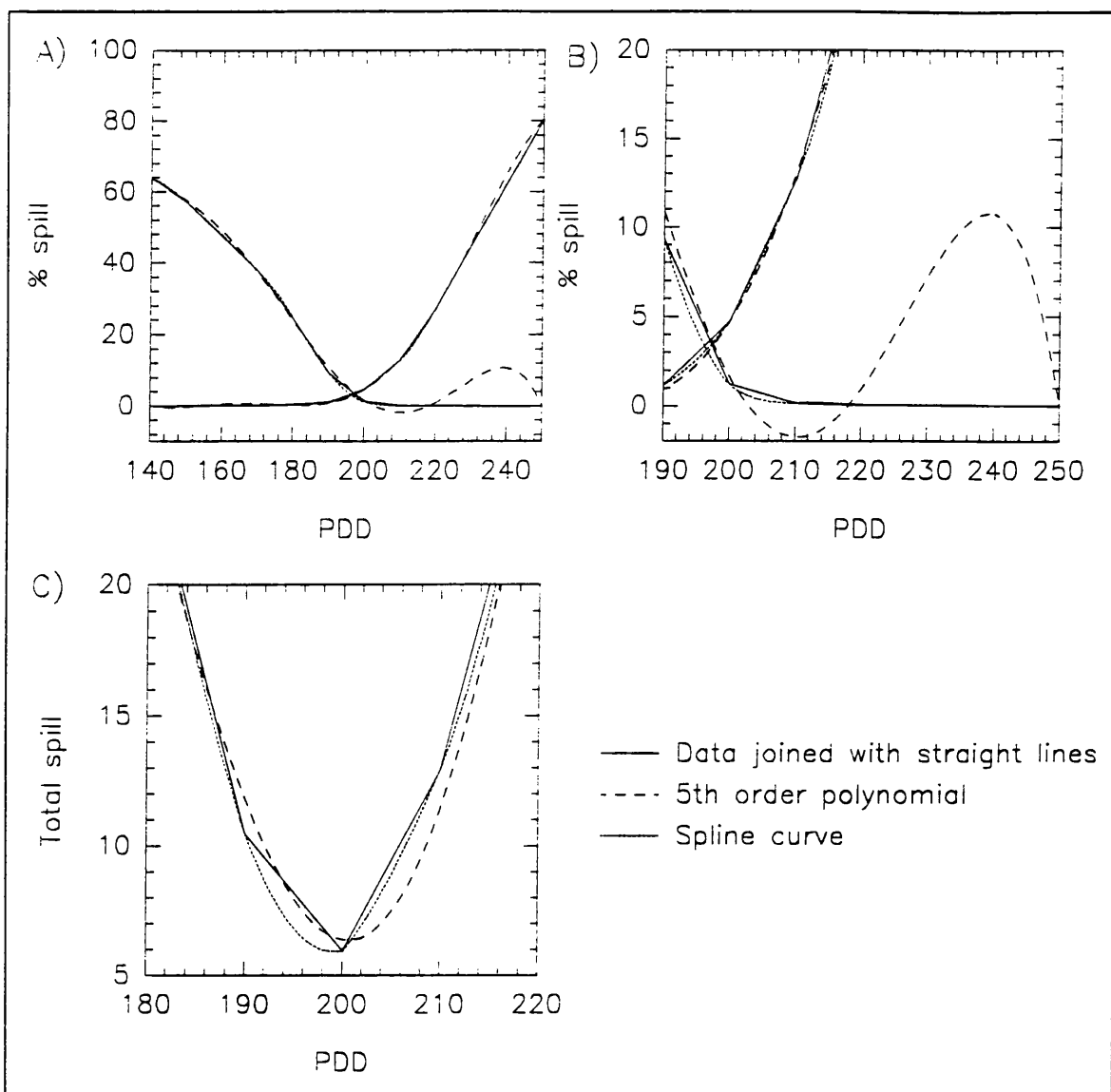


Figure 2.5: Cross-over (A and B) and total spill (C) plots for cocktail 08. B is a detail of A.

experimental cocktails was then made up, in which each cocktail differed from either a commercial cocktail or another experimental cocktail in only one component. In this manner, it was possible to assess individually the effects of solvent type, surfactant type and concentration and fluor type on separation efficiency using the 2250 CA α/β . In this experiment, the cocktail mass was 15 g (~ 15 ml) and the sample loading 0.4 ml, with the exceptions of Ultima Gold™, when only 0.2 ml sample loadings were used, and Pico Fluor™ LLT + 20% naphthalene, when 15 ml volumes of cocktail were used. The differences in cocktail densities were regarded as being sufficiently low to justify the use of cocktail masses rather than volumes, since masses are more easily and accurately determined for

Table 2.1: Comparison of % spills for open and narrow windows, with and without background subtraction, for ^{238}Pu and $^{90}\text{Sr}/^{90}\text{Y}$ in Ultima Gold™ AB. The samples were counted for 10 min at each setting using the Tri-Carb® 2550 TR/AB (b).

A) Misclassification of α events.						
0 - 2000 keV						
PDD	$\text{cpm}_{(\alpha)}^a$	$\text{cpm}_{(\beta)}^b$	$B_{(\alpha)}^c$	$B_{(\beta)}^d$	% spill $_{\beta}$ no subtraction	% spill $_{\beta}$ subtracting background
115	3188.80	50.70	1.40	38.80	1.57	0.37
120	3191.10	52.80	1.00	40.20	1.63	0.39
125	3183.60	79.00	0.90	40.50	2.42	1.20
130	3120.80	125.50	1.00	41.90	3.87	2.61
135	3033.20	206.10	0.10	40.10	6.36	5.19
180 - 390 keV						
PDD	$\text{cpm}_{(\alpha)}^a$	$\text{cpm}_{(\beta)}^b$	$B_{(\alpha)}^c$	$B_{(\beta)}^d$	% spill $_{\beta}$ no subtraction	% spill $_{\beta}$ subtracting background
115	3173.50	8.10	0.20	2.90	0.25	0.16
120	3171.80	12.20	0.10	4.00	0.38	0.26
125	3164.10	32.70	0.20	4.20	1.02	0.89
130	3106.10	82.50	0.20	3.10	2.59	2.49
135	3018.40	159.20	0.00	3.70	5.01	4.90
B) Misclassification of β events.						
0 - 2000 keV						
PDD	$\text{cpm}_{(\beta)}^b$	$\text{cpm}_{(\alpha)}^a$	$B_{(\beta)}^d$	$B_{(\alpha)}^c$	% spill $_{\alpha}$ no subtraction	% spill $_{\alpha}$ subtracting background
115	1822.80	82.10	38.80	1.40	4.31	4.50
120	1871.60	42.80	40.20	1.00	2.24	2.23
125	1880.60	21.20	40.50	0.90	1.11	1.09
130	1933.30	11.90	41.90	1.00	0.61	0.57
135	1912.00	7.70	40.10	0.10	0.40	0.40
0 - 1300 keV						
PDD	$\text{cpm}_{(\beta)}^b$	$\text{cpm}_{(\alpha)}^a$	$B_{(\beta)}^d$	$B_{(\alpha)}^c$	% spill $_{\alpha}$ no subtraction	% spill $_{\alpha}$ subtracting background
115	1818.10	82.10	36.20	1.40	4.50	4.33
120	1864.50	42.80	37.80	1.00	2.24	2.24
125	1872.90	21.20	38.40	0.90	1.12	1.09
130	1926.30	11.90	39.70	1.00	0.61	0.57
135	1905.60	7.70	37.30	0.10	0.40	0.41

- a Count rate in the α MCA.
- b Count rate in the β MCA.
- c Background count rate in the α MCA.
- d Background count rate in the β MCA.

the viscous solvents in these cocktails. The α emitter was ^{238}Pu and the β emitter $^{90}\text{Sr}/^{90}\text{Y}$, with activities of ~ 2000 dpm per vial.

The effect of secondary fluors on α/β separation was then examined further by substituting the secondary fluor in Ultima Gold™ AB (*i.e.* bis-MSB) with a number of different secondary fluors. At this point, some additional solvents were studied in order to understand the exact role of the solvent and fluors in combination with one another. This second part of the experiment was carried out using the standard sample composition, and the same α and β emitters as above, but with the 2550 TR/AB (b) instrument. The automatic option was used initially to screen the samples, and then the ones that

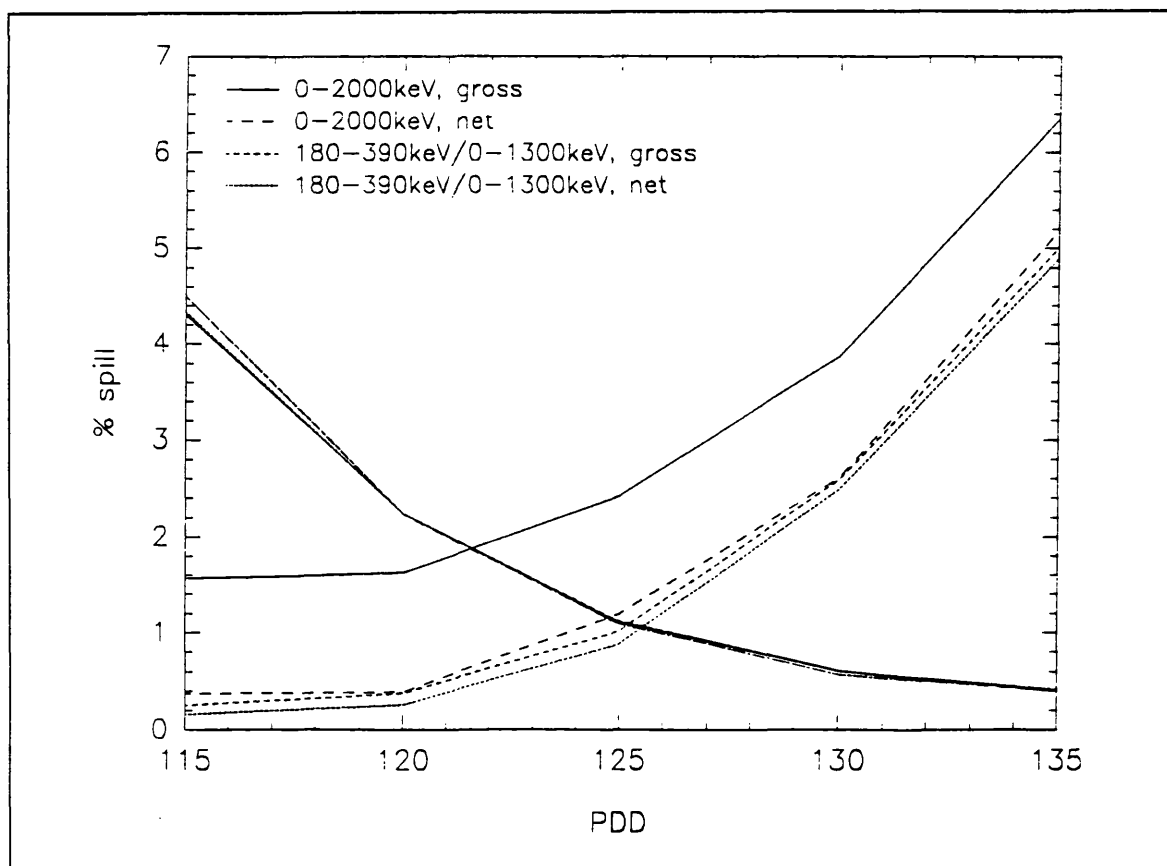


Figure 2.6: The effect on the % spill of using open and narrow windows, with and without background subtraction.

gave the lowest misclassification were counted again and the cross-overs were calculated manually, due to the problems discussed above. The tSIE of each cocktail was measured and, as the samples were of identical compositions, the tSIE was not regarded as a measure of the quenching caused by the sample, but of the quenching caused by the cocktail components (section 1.2.2.1), in other words, the efficiency with which the cocktail produces light, as suggested by McKlveen (1976).

For both parts of the experiment, PMT anode pulse shapes were recorded for certain cocktails that were of particular interest, by connecting one PMT anode of a counter (a 2550 TR/AB for the first set and a test-bed counter for the second) to a digitizing oscilloscope (Hewlett Packard 54111D). The oscilloscope was set to calculate the average of 64 pulses. The pulse shapes derived from the initial set of cocktails were obtained using ^{241}Am and ^{36}Cl . The cocktails that varied in the secondary fluor component were compared using ^{238}Pu and $^{90}\text{Sr}/^{90}\text{Y}$.

2.2.3 Quenching

Two aspects of quenching were studied: quenching by chemical agents added to the vial and that caused by dissolved oxygen. The effect of nitromethane quenching on a variety of β emitters was examined. The α emitter used was ^{210}Po and the β emitters were $^{90}\text{Sr}/^{90}\text{Y}$ ($E_{\text{max}} = 546$ keV and 2950 keV, respectively); ^{32}P ($E_{\text{max}} = 1710$ keV); ^{36}Cl ($E_{\text{max}} = 714$ keV); ^{99}Tc ($E_{\text{max}} = 292$ keV); ^{14}C ($E_{\text{max}} = 156$ keV) and ^3H ($E_{\text{max}} = 18.6$ keV). In each case, the sample loading was 0.6 ml dilute acid (0.2 ml 0.5M hydrochloric acid, 0.2 ml 0.1M hydrochloric acid + 0.2 ml distilled water) in 15 ml cocktail, and the activities $\sim 20,000$ dpm per vial. The samples were progressively quenched by the addition of small volumes of nitromethane, typically 20 μl , allowing the assumption to be made that changes in geometry were negligible. The cross-over plot was recorded for each pair of samples at each level of quenching, using the automatic instrumental option of the 2550 TR/AB (c). The level of quenching was determined by the tSIE parameter. The misclassification of events was also determined with the PDD kept constant for each quenching level, in order to simulate the effect of different degrees of

quenching within a batch of samples. PMT anode pulse shapes were measured for ^{210}Po and $^{90}\text{Sr}/^{90}\text{Y}$ quenched with 0, 35 and 100 μl nitromethane. The tSIEs were also determined for these samples.

The effect of different quenching agents was examined by comparing the optimum PDD and separation efficiency for four sets of samples, using the 2550 TR/AB (b). The quenching agents were nitromethane, carbon tetrachloride, acetone and 9M hydrochloric acid. Equal volumes of the quenching agents result in widely differing tSIEs. Therefore, a quenching mixture was made up for each, consisting of cocktail and acid, in the same ratio as the samples, and a volume of the quenching agent, such that a 0.5 ml addition of any of the mixtures resulted in approximately the same change in tSIE. The cross-over plot was determined for each pair without quenching, and then with progressive 0.5 ml additions of a quenching mixture, to a total of 2 ml (1.5 ml for the 9M hydrochloric acid as this was the maximum capacity of the cocktail). Samples were also made up with the same tSIE as the unquenched vials, but with a total volume of 12 ml, and the optimum PDD and % spill_m were found in order to check that the change in volume had not affected them. The first and last cross-over determinations for each quenching agent and the cross-over for the geometry check were determined manually, as described above. Intermediate points were determined instrumentally. This section was carried out on duplicate sets of samples.

Although DIN based cocktails have a limited capacity for the absorption of oxygen compared to cocktails based on traditional solvents (Prichard *et al.*, 1992), it was felt necessary to examine the effects of dissolved oxygen. Six sets of samples (α , β and background) were made up in 20 ml flame-sealable ampoules. Two sets were sealed with no additional processing. The remaining sets were either purged with oxygen or oxygen-free nitrogen for approximately 15 s, before sealing.

2.2.4 Other factors

The remaining factors possibly affecting PSD that were studied are cocktail volume, vial type (glass or polyethylene) and vial size. The 2550 TR/AB (b) was used for all these determinations. The

vials used in this experiment were 20 ml and 7 ml low potassium glass, 20 ml low diffusion polyethylene and 7 ml HDPE (high density polyethylene). The low diffusion polyethylene vials are coated with Teflon and have a matt surface, whereas the HDPE vials have a shiny, reflective surface. The samples in the 7 ml vials consisted of 5 ml cocktail with 0.2 ml loading. The 20 ml vials were made up with either 5 ml cocktail plus 0.2 ml loading or 10 ml cocktail plus 0.4 ml loading. The cross-overs were determined manually. All measurements were done on duplicate sets of vials. In the case of the plastic vials, all the measurements were made within 24 hrs, as diffusion of the cocktail into the vial wall with DIN based cocktails has been noted previously (G. T. Cook, 1992, personal communication).

2.3 RESULTS AND DISCUSSION

2.3.1 Cocktail optimization

Table 2.2 summarizes the composition and performance of each of the experimental and commercial cocktails initially examined. The first aspects of cocktail composition to be discussed are surfactant type and concentration. The impact of increasing surfactant concentration can be seen with two sets of cocktails: the Ultima Gold™ (DIN based) and the Pico-Fluor™ (pseudocumene based with 20% naphthalene) cocktails. In these groups, the degree of misclassification at the optimum PDD decreases with decreasing surfactant concentration. The experimental 07 group of cocktails would also be expected to show this trend. However, the % spill_{m,s} for 07, 07A and 07B are too close to discriminate between them with any degree of confidence. The cocktails that give the most efficient separation (<0.2% spill_{m,s}) are those with the lowest surfactant concentration (*i.e.* Pico-Fluor™ 15 + 20% naphthalene and cocktail 07D). Figure 2.7 shows that while higher surfactant concentrations tend to produce higher % spill_{m,s}, a cocktail with a relatively high surfactant concentration may still produce efficient α/β separation (*e.g.* cocktail 07 contains 30-40% nonionic surfactant and yet the

Table 2.2: Cross-over characteristics and composition of the cocktails studied. N = naphthalene. Measurements were made using a Packard Tri-Carb® 2250 α/β . The α emitter was ^{235}Pu , and the β emitter $^{90}\text{Sr}/^{90}\text{Y}$. The curve fitting procedure was used in all cases, unless stated otherwise.

Cocktail	Optimum PDD	% spill _m	tSIE	Solvent	Primary fluor	Secondary fluor	Surfactant
Insta-Gel® ^a	107	4.6	498	60-69% xylene	PPO	bis-MSB	30-40% nonionic
Insta-Gel® + 20% N	132	0.30	561	40-55% xylene	PPO	bis-MSB	25-32% nonionic
Insta-Gel® XF + 20% N	130	0.46	-- ^b	48-55% pseudocumene	PPO	bis-MSB	25-32% nonionic
Pico Fluor™ LLT ^a	97	8.8	455	70-75% pseudocumene	PPO	bis-MSB	25-30% nonionic/anionic
Pico-Fluor™ 40 + 20% N	114	1.33	483	45-55% pseudocumene	PPO	bis-MSB	25-35% anionic
Pico-Fluor™ LLT + 20% N	117	0.73	499	56-60% pseudocumene	PPO	bis-MSB	20-24% nonionic/anionic
Pico-Fluor™ 15 + 20% N	115	0.15	586	64-69% pseudocumene	PPO	bis-MSB	11-16% anionic
Hlonic Fluor™	94	9.0	440	65-70% pseudocumene	PPO	bis-MSB	30-35% anionic/nonionic
Ultima Gold™ ^a	124	0.36	545	65-70% DIN	PPO	bis-MSB	30-35% nonionic/anionic
Ultima Gold™ XR	120	1.63	476	55-60% DIN	PPO	bis-MSB	40-45% nonionic/anionic
MicroScint™ 40	149	3.7	411	55-60% DIN	PPO	DMA	40-45% nonionic/anionic
01M	137	0.85	505	55-65% DIN	PPO	bis-MSB	35-45% nonionic/anionic
02M ^a	200	3.1	426	55-65% DIN	PPO	DMA	35-45% nonionic/anionic
05 ^a	144	1.45	468	60-70% Actrel™	PPO	bis-MSB	30-40% nonionic
06 ^a	212	4.25	404	60-70% Actrel™	PPO	DMA	30-40% nonionic
08 ^a	199	2.95	458	60-70% DIN	PPO	DMA	30-40% nonionic
07 ^a	135	0.30	569	60-70% DIN	PPO	bis-MSB	30-40% nonionic
07A	135	0.34	575	66-75% DIN	PPO	bis-MSB	25-34% nonionic
07B	132	0.36	-- ^b	78-83% DIN	PPO	bis-MSB	17-22% nonionic
07D	137	0.13	-- ^b	90% DIN	PPO	bis-MSB	10% nonionic
09	163	0.49	-- ^b	44-52% PXE + 20% N	PPO	bis-MSB	28-36% nonionic
10	161	0.28	-- ^b	44-52% PXE + 20% DIN	PPO	bis-MSB	28-36% nonionic

^a Curve fitting procedure did not work, spline used to obtain data instead.

^b Not determined.

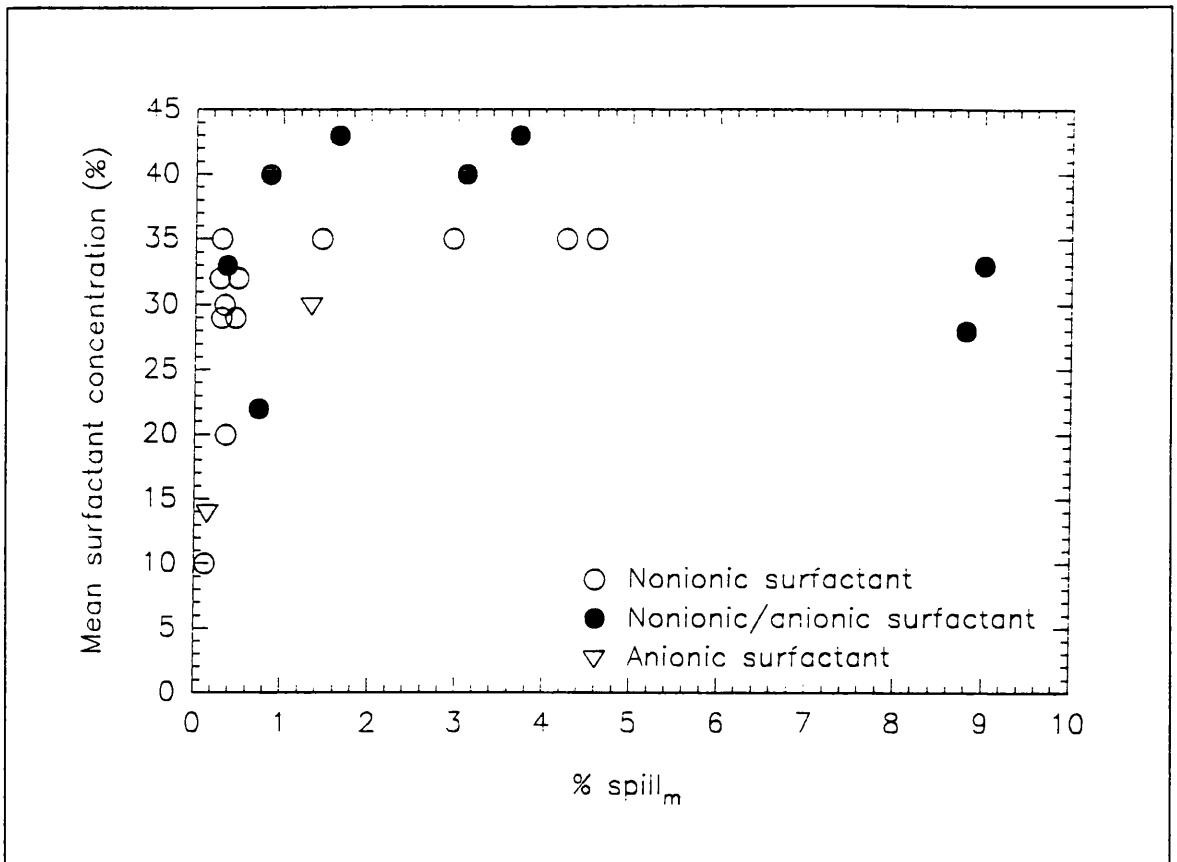


Figure 2.7: The relationship between surfactant concentration and % spill_m.

misclassification at the optimum PDD is only 0.3%).

Figure 2.8 shows the relationship between tSIE and % spill_m at the optimum PDD of all the cocktails studied in this work. As two different sample loadings were used, the two sets of data cannot be compared with each other. However, both sets show similar correlations between the degree of self-quenching and the separation efficiency they produce. Those cocktails which produce light most efficiently are the best for α/β separation, which agrees with McDowell's suggestion that quenching adversely affects PSD (McDowell and McDowell, 1994). Figure 2.9 indicates that there is a relationship between tSIE of the cocktail and surfactant concentration, with the lowest tSIEs (*i.e.* the highest degree of quenching) being produced by those cocktails with the highest surfactant concentrations, particularly for nonionic/anionic mixtures and anionic surfactants. While nonionic surfactants show a slight trend, it is significantly less marked than for the other groups. This relationship between tSIE

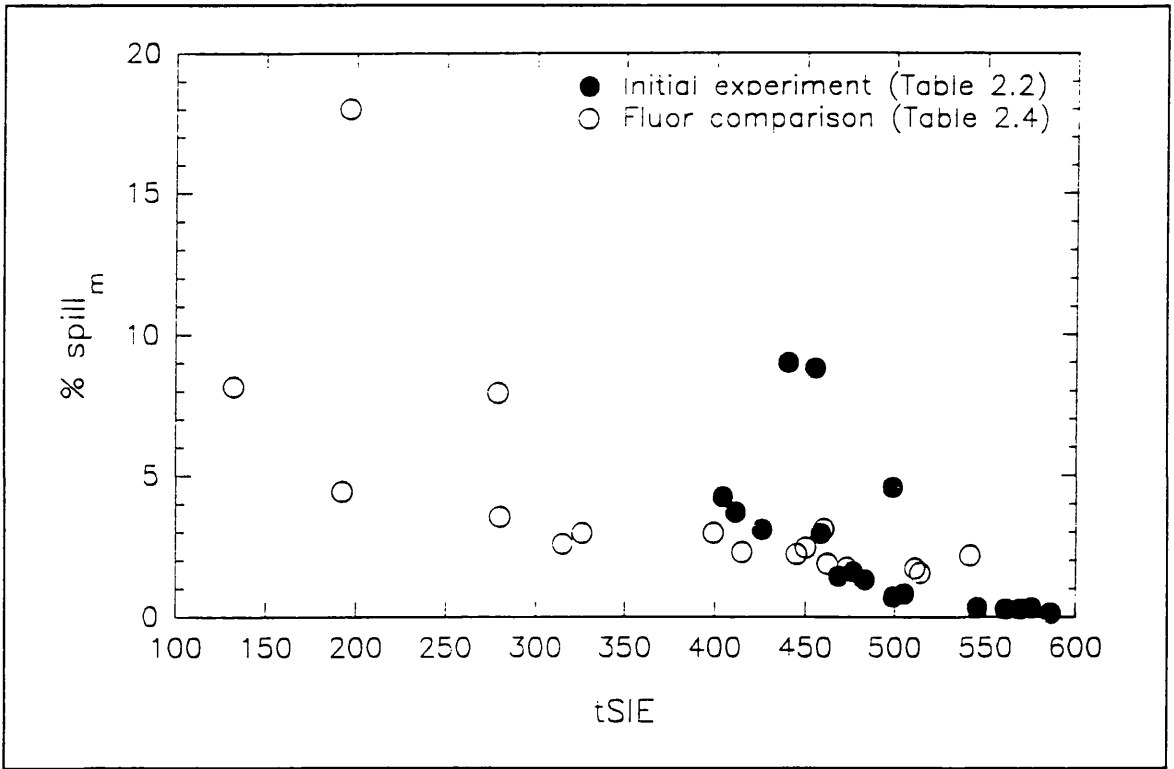


Figure 2.8: The relationship between $\% \text{ spill}_m$ and tSIE.

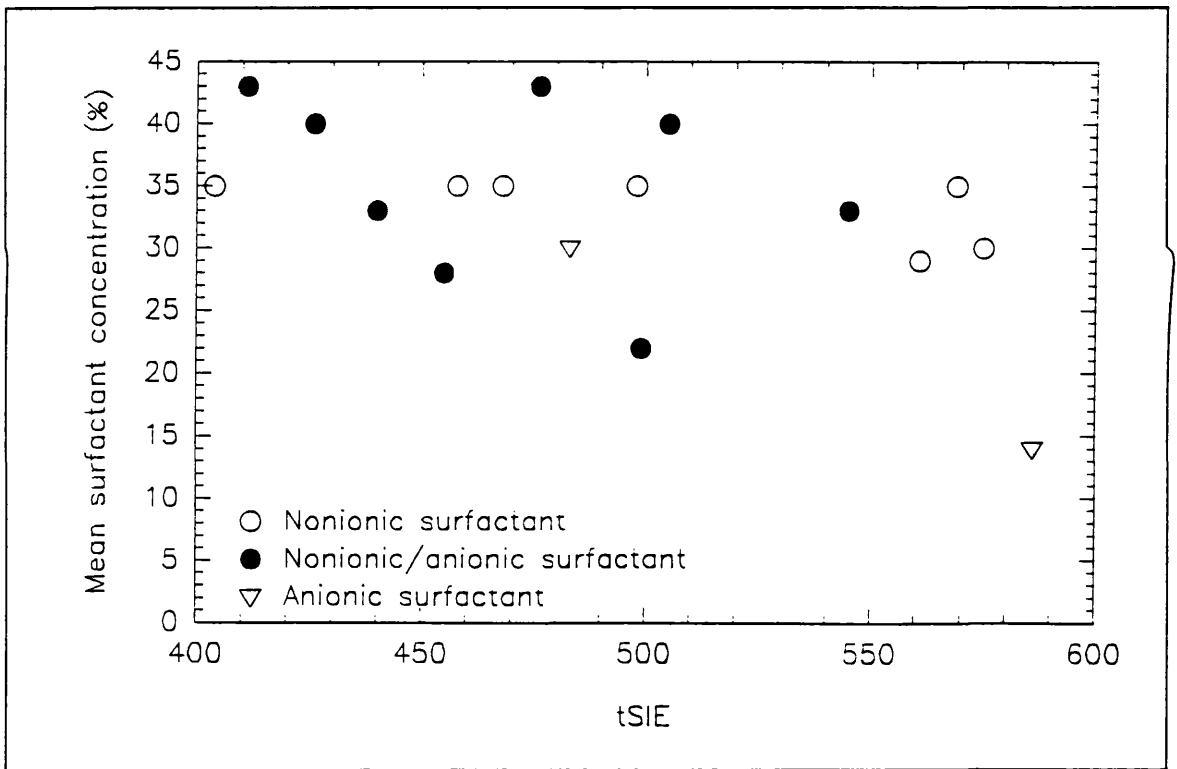


Figure 2.9: The relationship between surfactant concentration and tSIE.

and surfactant concentration implies that it is the surfactant that is causing the quenching, which in turn may contribute to the reduction in separation efficiency.

When Figures 2.7, 2.8 and 2.9 are considered together some overall conclusions can be made. Surfactants contribute significantly to the reduction in light output of a cocktail and it is implied that to obtain an extremely high degree of α/β separation, it is necessary to use a cocktail with a small surfactant concentration and, hence, a low sample-holding capacity (< 0.5 ml water). However, this defeats the purpose of using an aqueous accepting cocktail, as in many situations it is not possible to use such a small sample volume, and still maintain a reasonable limit of detection. Therefore, a compromise must be made between sample size and separation efficiency. This problem may be circumvented, to a certain extent, by the use of different surfactant types. Although none of the surfactants studied here inherently provides better α/β separation, nonionic surfactants can be used in higher concentrations without serious degradation of α/β separation performance, allowing higher sample holding capacities to be achieved. Ultima Gold™ and cocktail 07 are identical in composition, except for the type of surfactant used. Although the difference in separation efficiency between the two cocktails is small (0.33% and 0.3% respectively), the nonionic surfactant used in cocktail 07 allows a larger sample holding capacity (Table 2.3).

Comparing cocktails with and without the addition of 20% naphthalene confirms the results of Yang *et al.* (1991). For example, Insta-Gel® alone gives a % spill_m of 4.6% at the optimum PDD, but the addition of naphthalene reduces this to 0.30%. This benefit applies to several solvent systems, including xylene (Insta-Gel®) and pseudocumene (Pico Fluor™ LLT). The improvement observed in the presence of naphthalene is also seen with DIN based cocktails, as expected. Comparing cocktails 09 and 10 (Table 2.2) shows that the addition of 20% DIN to PXE gives 0.28% misclassification at the optimum PDD, as opposed to 0.49% with 20% naphthalene, which confirms the suggestion of McDowell and McDowell (1994) that naphthalene derivatives can be used effectively as a substitute

Table 2.3: Water and mineral acid holding capacities of the DIN based cocktails (ml uptake per 10 ml cocktail). Data are from J. Thomson (personal communication, 1992).

Cocktail	H ₂ O	1M HCl	2M HCl	1M HNO ₃	2M HNO ₃	1M H ₂ SO ₄	2M H ₂ SO ₄
Ultima Gold™	3.5	0.25	0.10	0.70	0.30	0.10	Nil
Ultima Gold™ XR	10.0	2.00	0.90	3.00	1.75	0.40	0.10
07	10.0	5.50	2.25	3.25	2.25	6.50	4.00
07A	10.0	2.00	1.25	1.75	1.50	2.50	1.50
07B	2.25	1.25	1.00	1.25	1.00	1.50	1.00
07D	0.50	0.40	0.30	0.40	0.30	0.40	0.30

for naphthalene. DIN alone as the primary solvent also gives comparable results to other solvents with the addition of naphthalene. For example, cocktail 07A (DIN based) and Pico-Fluor™ 40 + 20% naphthalene (pseudocumene based) have similar surfactant concentrations, allowing the solvent to be compared directly. These cocktails give % spill_ms of 0.34% and 1.33% respectively.

Based on the conclusions of Yang *et al.* (1991), PPO was the only primary fluor used in this study, however, an initial comparison was made between the secondary fluors *bis*-MSB and DMA. The latter was expected to bring about some degree of improvement in the α/β separation, due to its noted pulse stretching effect. However, the opposite was found to be true. Table 2.2 shows four pairs of cocktails identical in composition except for the secondary fluor (namely Ultima Gold™ XR and MicroScint™ 40, cocktails 01M and 02M, cocktails 05 and 06 and cocktails 07 and 08). In every case, the DMA containing cocktail shows a marked degradation in performance. For example, cocktail 01M (*bis*-MSB) produces 0.85% spill_m at the optimum PDD, whereas cocktail 02M (DMA) produces 3.1%. This can be understood by examining the PMT anode pulse shapes produced by cocktails 07 and 08 (Fig. 2.10). The former cocktail gives rise to α and β pulses that are distinctly different from each other. The α pulse is much broader than the β pulse, with a significant delayed component. However,

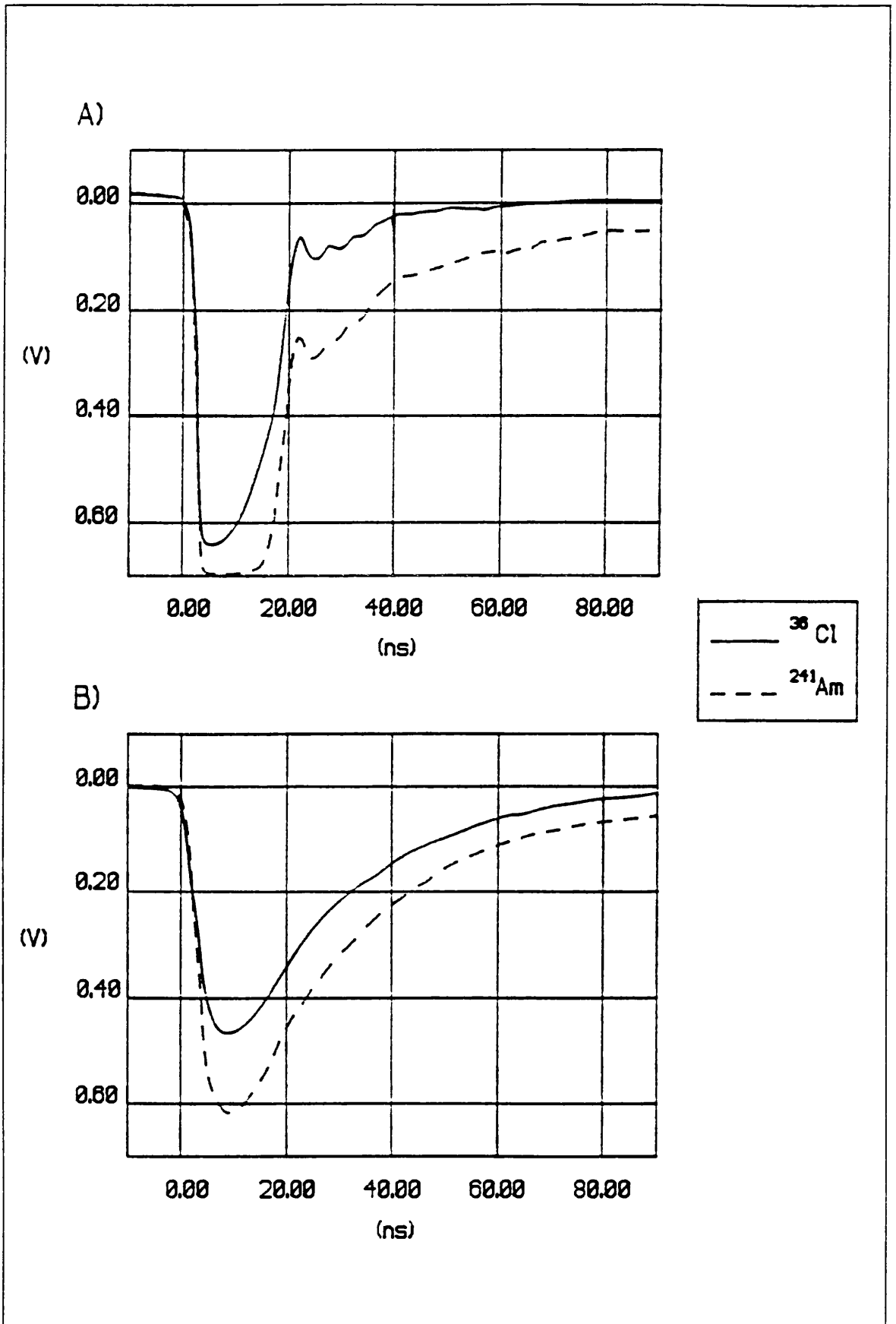


Figure 2.10: PMT anode pulse shapes for A) cocktail 07 and B) cocktail 08.

both types of pulse produced by cocktail 08 are much broader and less distinct from each other. This suggests that while naphthalene or DIN enhances separation by principally stretching the α pulses, DMA stretches both types of pulse making it harder for the instrument to distinguish between them.

Given the limited nature of this first experiment, in terms of the effects of fluors, a more extensive comparison was carried out. Again, the primary fluor was restricted to PPO, but the secondary fluor was varied between those illustrated in Figure 2.11. Table 2.4 gives the results from the instrumental determinations of the cross-over plots, and the manual determinations of a selection (two series with structurally related fluors, F-H and I-K, and those that performed similarly to Ultima Gold™ AB). The table is ordered such that fluors with similar structures are adjacent.

It can be seen that the optimum PDDs in Table 2.4 agree closely between the methods of determination. However, the % spill_ms are much higher for the former, as would be expected from the data shown in Table 2.1, accountable for by the contribution of the background to the activity in the β MCA. One point that should be taken into consideration when examining these data is the different values for the % spill_m found for Ultima Gold™ AB with the 2550 TR/AB (b) (1.47%) and for cocktail 07A with the 2250 CA α/β (0.34%). These cocktails have the same formulation, indicating that this difference is instrument related. Significant differences have also been noted between instruments of the same series. This was confirmed by determining the cross-over for the same set of samples in the 2250 CA α/β , 2550 TR/AB (a) and 2550 TR/AB (b) instruments using open windows and no background subtraction. The results are given in Table 2.5 and Figure 2.12. Comparisons between instruments (b) and (c) are made in section 2.3.2, but these data cannot be directly related to each other as the same samples were not analysed. As the only difference between instruments (a) and (b) is the PMTs, it is implied that poor selection of the PMTs can cause a difference in PMT anode pulse shapes, with a resultant degradation in α/β separation efficiency. The data in Table 2.5 and Figure 2.12 show differences between % spill _{α} dependent on the E_{max} of the β emitter. This effect is

Table 2.4 Comparison of the α/β separation efficiency of $^{90}\text{Sr}/^{90}\text{Y}$ and ^{238}Pu in cocktails differing only in the secondary fluor, with an Ultima Gold™ AB (UGAB) base. Data were determined using the Packard Tri-Carb® 2550 TR/AB (b).

Cocktail	Secondary fluor	tSIE	Instrument determination		Manual determination	
			% spill _m	Optimum PDD	% spill _m	Optimum PDD
UGAB	<i>bis</i> -MSB	541	2.19	124	1.47	126
A	acenaphthene	450	2.46	122	1.71	125
B	fluoranthene	196	18.01	246	-- ^a	-- ^a
C	3-phenylfluoranthene	279	7.91	223	-- ^a	-- ^a
D	phenanthrene	399	2.98	129	-- ^a	-- ^a
E	2-methylphenanthrene	326	2.98	126	-- ^a	-- ^a
F	POPOP	514	1.58	122	0.79	125
G	dimethyl-POPOP	511	1.74	122	0.89	125
H	α -NOPON ^b	415	2.30	123	1.56	125
I	anthracene	192	4.45	108	3.58	110
J	DMA	460	3.12	197	2.34	197
K	DPA ^c	473	1.75	158	1.19	160
L	<i>trans,trans</i> -1,4-diphenyl-1,3-butadiene	280	3.54	105	-- ^a	-- ^a
M	7-diethylamino-4-methylcoumarin	462	1.89	127	1.24	130
N	1,3,5-triphenylbenzene	445	2.24	122	1.55	125
O	2-(2-hydroxyphenyl)-benzoxazole	315	2.60	116	-- ^a	-- ^a
P	3-hydroxyflavone	132	8.17	95	-- ^a	-- ^a
Q	triphenylene	426	-- ^d	-- ^d	-- ^a	-- ^a

^a Not determined.

^b 1,4-*bis*-[2-(5- α -naphthyloxazolyl)]-benzene.

^c 9,10-diphenylanthracene.

^d The cross-over point for this formulation lies below the range of the instrument, *i.e.* the optimum PDD < 0. There is significant misclassification of α events even at this low PDD, which implies that the delayed component of the PMT anode pulses is absent for this fluor.

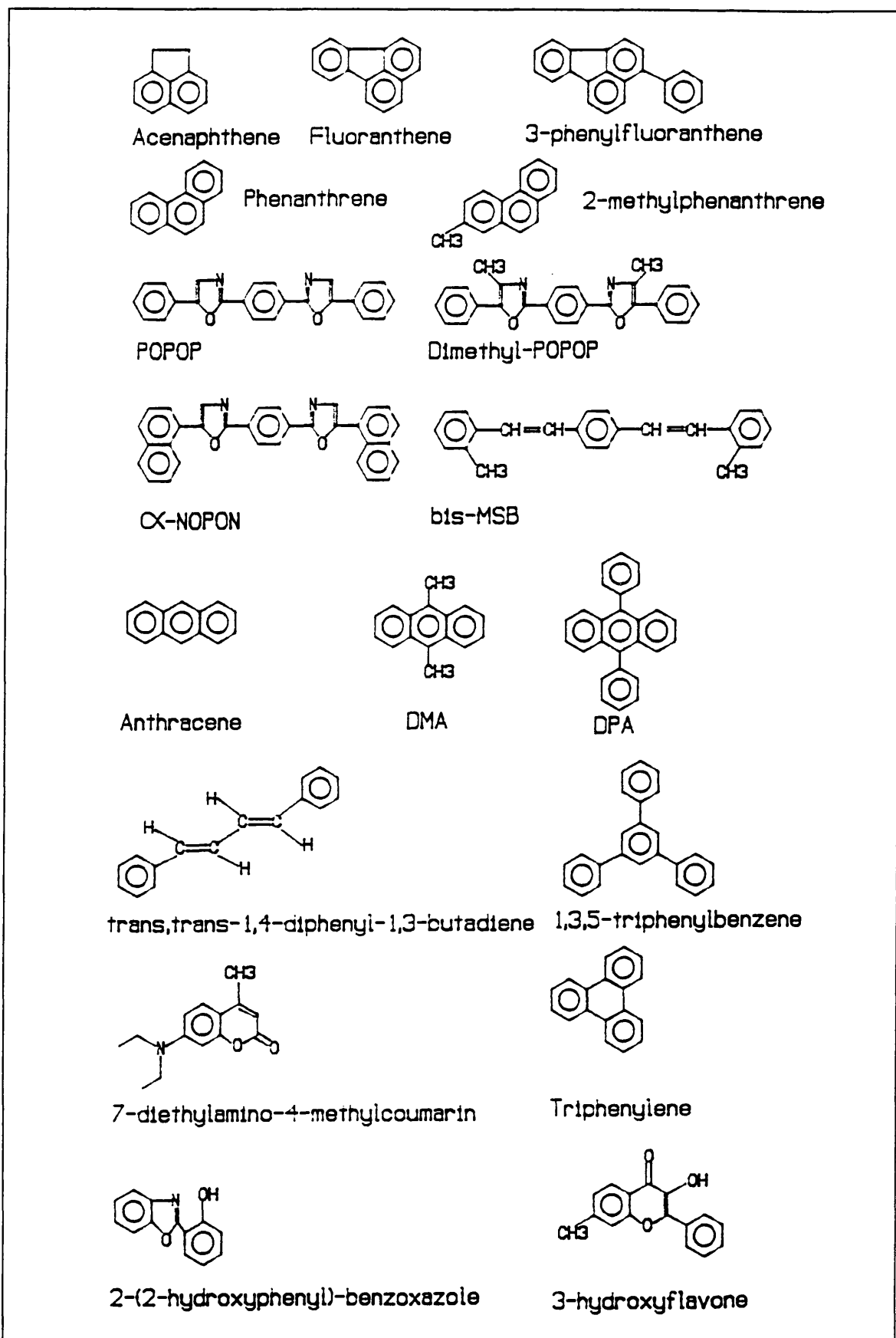


Figure 2.11: Molecular structures for the fluors studied.

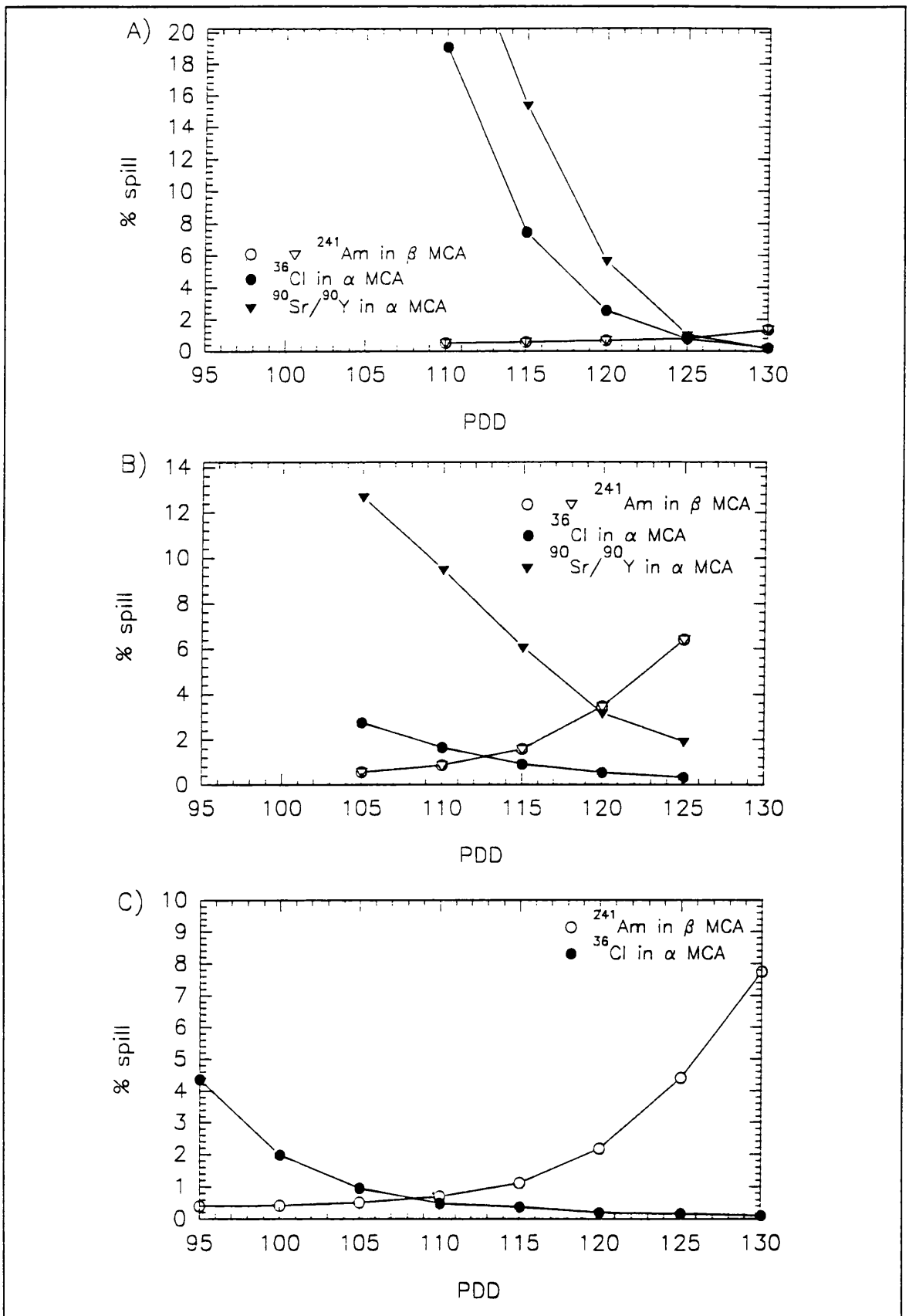


Figure 2.12: Comparison of different instruments with samples in Insta-Gel® XF + 20% naphthalene. A) 2250 CA α/β , B) 2550 TR/AB (a) and C) 2550 TR/AB (b).

discussed further in section 2.3.2, but it should be noted at this point that the degree of difference is highly dependent on the instrument used for the measurements. It is important to stress that caution should be exercised when comparing data produced by different instruments, not only within the confines of this study, but also data published in the literature. In addition, the PDD can only be compared between data sets obtained using the same instrument. It is not an absolute scale, being adjusted by the manufacturer to produce good α/β separation in the mid-region of the scale (0-250 units).

Table 2.5: Comparison of the 2250 CA α/β , the 2550 TR/AB (a) and the 2550 TR/AB (b), using ^{241}Am and $^{90}\text{Sr}/^{90}\text{Y}$ or ^{36}Cl in Insta-Gel® XF + 20% naphthalene.

Instrument	β emitter	% spill _m	Optimum PDD
2250 CA α/β	^{36}Cl	0.65	127
	$^{90}\text{Sr}/^{90}\text{Y}$	0.63	127
2550 TR/AB (a)	^{36}Cl	1.25	112
	$^{90}\text{Sr}/^{90}\text{Y}$	3.32	120
2550 TR/AB (b)	^{36}Cl	0.61	108

Figure 2.13 shows the relationship between the optimum PDD and the misclassification at that point, for all the cocktails described in Tables 2.2 and 2.4. The majority of the cocktails which allow the most efficient separation of α and β events have their optimum PDD within the range 120-160 PDD units. Figure 2.14 illustrates the PMT anode pulse shapes for three experimental cocktails (J, L and M) which give rise to high, low and intermediate optimum PDDs respectively. The duration of the PMT anode pulses correlates with the optimum PDD, suggesting that this parameter can be used as an indicator of pulse duration. Therefore, the data in Figure 2.13 imply that there is an optimum PMT anode pulse length for effective PSD. However, there is considerable spread in the data,

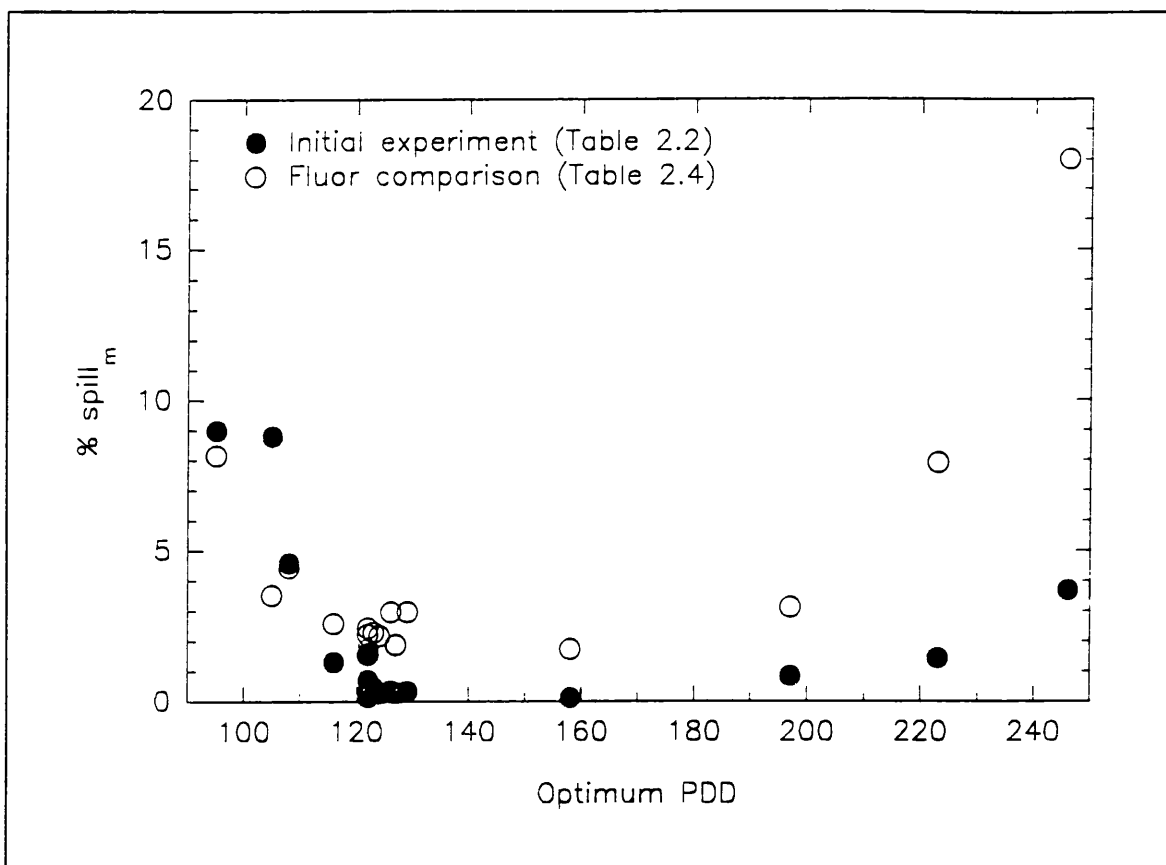


Figure 2.13: The relationship between % spill_m and optimum PDD.

indicating that this is not a simple, direct relationship, but that other factors are involved in optimising PSD.

The % spill_m at the optimum PDD also appears to be related to the tSIE, or the light output, of the cocktail, as shown in Figure 2.8. Self-quenching and pulse duration are sometimes interdependent, as demonstrated by Birks and Aladekomo (1963), who suggested that a fluor with a short decay time might be less prone to self-quenching effects. This adds to the complexity of analysing the data in Table 2.4, as small structural changes in the fluor can result in the tSIE, the optimum PDD and the % spill_m all differing widely, as can be seen for cocktails B and C, F-H and I-K, the latter two series being illustrated in more detail in Figure 2.15. Again, quenching is not the sole parameter affecting PSD. Figure 2.16 illustrates the relationship between tSIE, % spill_m and optimum PDD. Despite considering two variables, the data show considerable spread indicating that a further

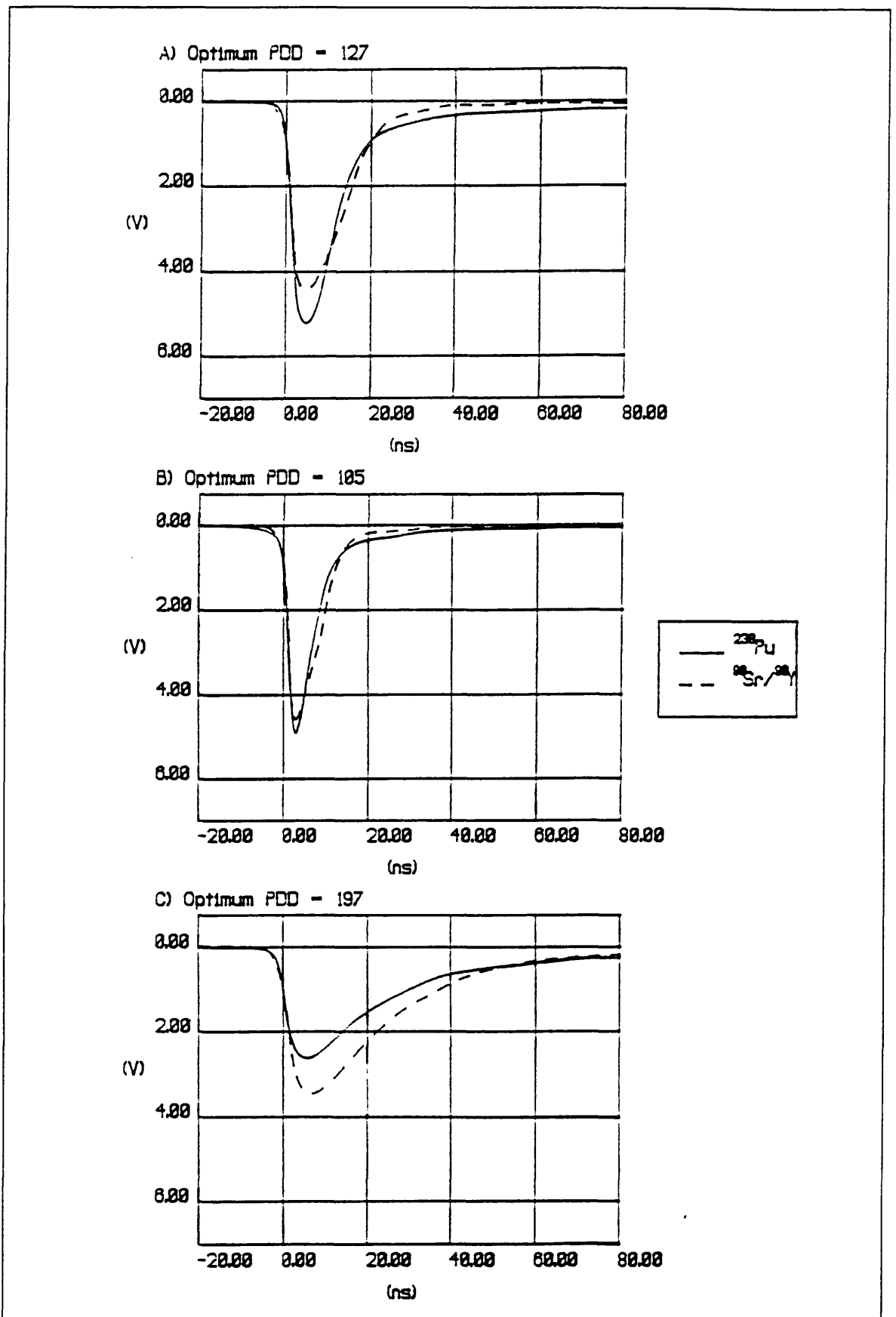


Figure 2.14: PMT anode pulse shapes for: A) cocktail M, B) cocktail L and C) cocktail J.

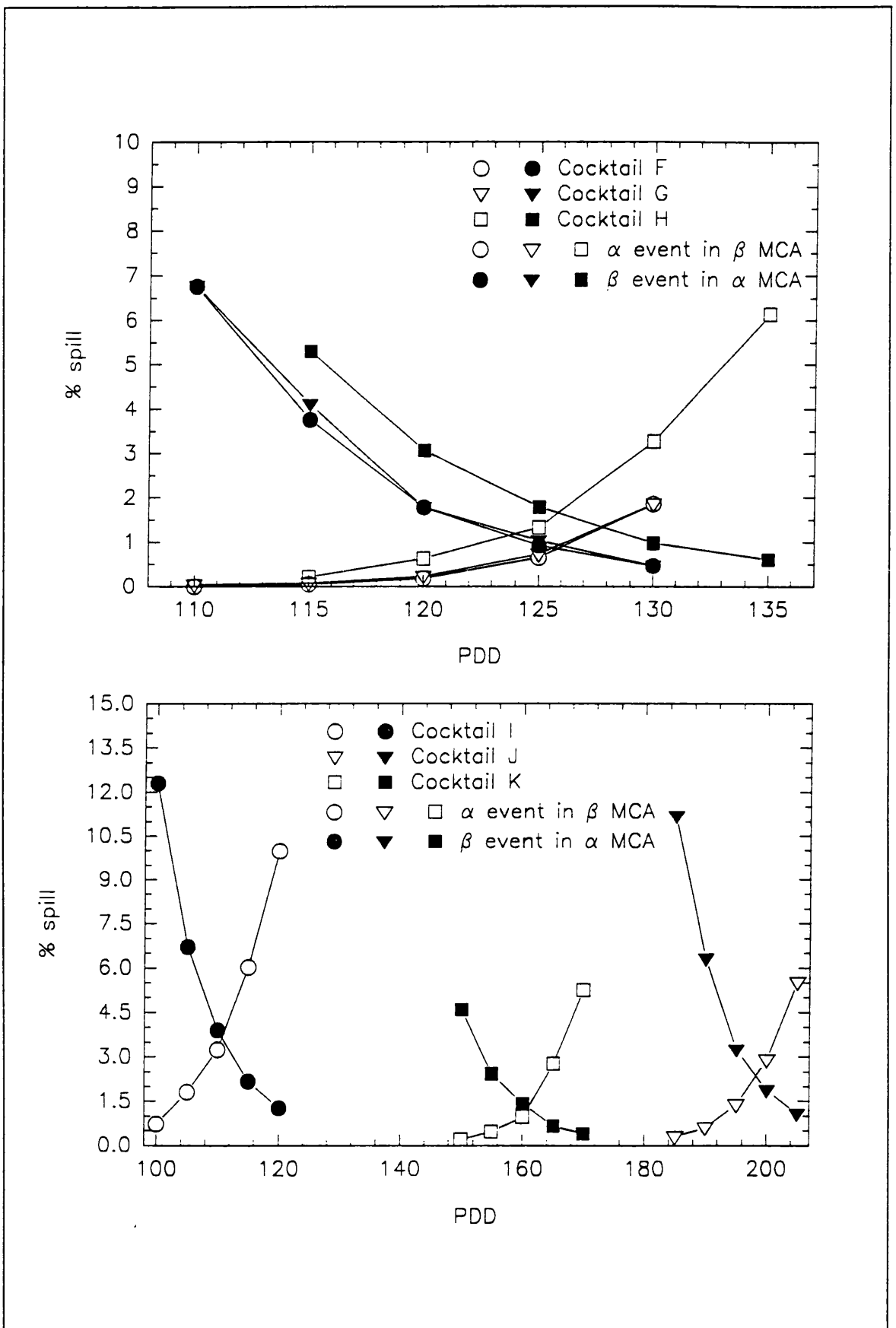


Figure 2.15: The effect on optimum PDD and % spill of two groups of secondary fluors.

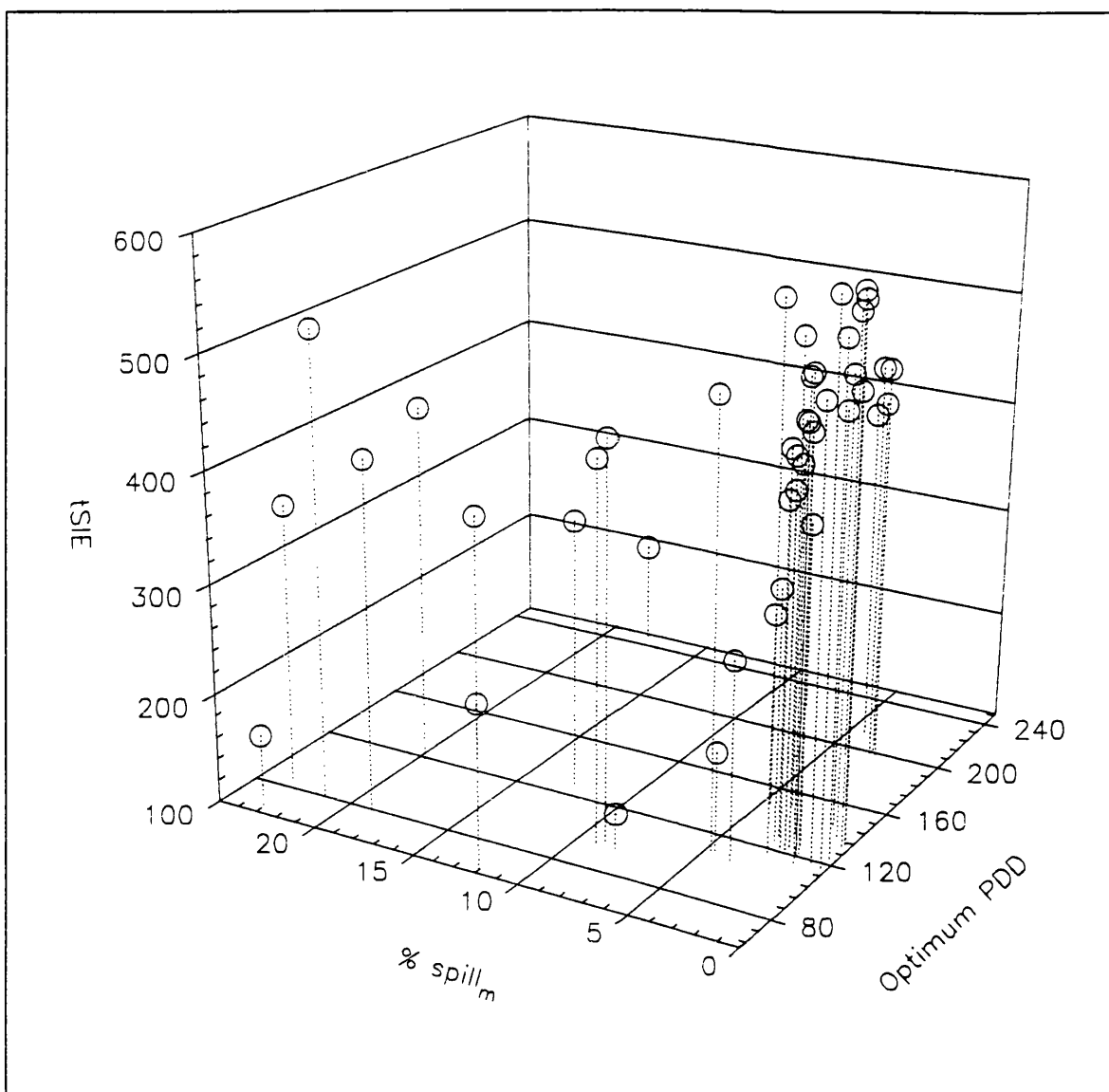


Figure 2.16: The relationship between tSIE, % spill_m and optimum PDD.

parameter is required to describe the effect fully. The effects of quenching will be discussed further in section 2.3.2.

In order to compare effectively the fluors used in this experiment, it is necessary to restrict comparisons to groups that have the same tSIE or the same PDD, as this will eliminate one of the variables. However, this process complicates the comparison of molecular structure. The following pairs of cocktails have tSIEs within 4 units of each other, allowing a comparison of PDD and % spill_m: cocktails B and I (tSIE = 196 and 192); C and L (tSIE = 279 and 280); F and G (tSIE = 514 and 511) and J and M (tSIE = 460 and 462). These comparisons show that the pulse duration and the tSIE are

not wholly interdependent on one another, as both the optimum PDD and the % spill_m vary significantly within pairs. In all cases, there is less misclassification for the cocktail that has the lower optimum PDD and is closer to the optimum region of PDDs.

Cocktails F (POPOP) and G (dimethyl-POPOP) are interesting, as they have similar tSIEs, the same optimum PDD and the secondary fluors have similar molecular structures. The methyl groups in dimethyl-POPOP have little effect on the separation efficiency, unlike those in DMA (cocktail J). A comparison can also be made between cocktails A (acenaphthene) and N (1,3,5-triphenylbenzene), where A has the higher rate of misclassification, despite similar tSIEs and optimum PDDs. Therefore, pulse duration and quenching are not the only factors involved in determining the separation efficiency. The ability of the instrument to differentiate between the two types of pulse is also important. This is controlled by the relative proportions of the delayed component in α and β pulses, which implies that a fluor that has readily occupied triplet states might give better separation efficiency.

Looking at the series of cocktails, I-K, some further comments can be made. It has been suggested that the presence of the methyl substituents in DMA encourages the formation of excited dimers (excimers) and exciplexes (Birks and Aladekomo, 1963; Wolff *et al.*, 1993). This would explain the dramatic lengthening of the PMT anode pulses relative to anthracene (cocktail I), as indicated by the optimum PDDs, if the exciplex is relatively stable, only losing its excitation energy when it dissociates. However, the suggestion that short decay times reduce the probability of quenching (Birks and Aladekomo, 1963) has not been supported in this instance. With cocktail K (DPA), the trend has been reversed, with a lower optimum PDD, but higher tSIE. The % spill_m is again lower, as would be expected from this intermediate pulse duration. However, the cause of these changes is obscure. The lower optimum PDD suggests that fewer exciplexes have formed with this fluor than with DMA, perhaps due to the larger size of the phenyl groups, which may cause steric hindrance and interfere

with the approach of excited molecules.

From Table 2.4, it can be seen that four fluors have resulted in better α/β separation than *bis*-MSB, however, it may not be advantageous to use these, as other aspects of cocktail performance are also important. Of the fluors studied, it can be seen that *bis*-MSB has the highest light output, as measured by the tSIE, and is least prone to self-quenching at these concentrations, with only POPOP and dimethyl-POPOP approaching it. As a high tSIE is desirable for α/β separation, as well as for producing an efficient cocktail, these two fluors would be the only viable alternatives to the Ultima Gold™ AB formulation. However, it should be noted that a high light output cocktail is probably not as critical for α/β separation as it is for ^3H determinations, for example, when a drop in light output can result in a serious loss in counting efficiency. It is of interest to note that these fluors are among those identified as useful for β LSC in early studies (section 1.2.3.3).

The effect of the solvent in conjunction with the fluor was then considered, as the energy transfer between the two will affect the pulse shape. Reducing the duration of PMT anode pulses, by combining a fast solvent, such as pseudocumene, with a slow fluor, such as DMA, was considered. However, it can be seen (Table 2.6) that while the optimum PDD is lower in all cases, bringing it into the most efficient range in the case of DMA, the separation efficiency has been consistently degraded. This effect cannot be wholly attributed to changes in tSIE, as in many cocktails there is insufficient difference between the fast solvent base and the DIN base to bring about the large changes in % spill_m (e.g. cocktail I and S (tSIE = 196 and 165); L and W (tSIE = 280 and 247) and Ultima Gold™ AB and Y (tSIE = 541 and 519)). Indeed, for cocktail U there is an increase in tSIE relative to cocktail K (both DPA), and yet U has the higher % spill_m. This indicates that it is necessary to use a slow solvent, such as DIN, in combination with a fluor of intermediate decay time. The slow decay of the solvent is necessary for a sufficient number of triplet states to become occupied, while a slow fluor simply results in pulses that are long in duration and similar for both α and β events. Reducing the

decay time of the solvent reduces the delayed component, by reducing the time available for energy transfer to the fluors, thereby reducing the separation efficiency.

Table 2.6: The effect of varying solvent on the α/β separation properties of various secondary fluors. The data were determined for $^{90}\text{Sr}/^{90}\text{Y}$ and ^{238}Pu using the 2550 TR/AB (b).

Cocktail	Solvent	Secondary fluor	% spill _m	Optimum PDD	tSIE
R	pseudocumene	DMA	17.60	127	331
S	pseudocumene	anthracene	23.14	65	165
T	pseudocumene	DPA	19.49	117	429
U	benzyl toluene	DPA	4.58	147	550
V	dodecyl benzene	DPA	12.66	127	345
W	pseudocumene	<i>trans,trans</i> -1,4-diphenyl-1,3-butadiene	12.04	63	247
X	pseudocumene	7-diethylamino-4-methylcoumarin	23.53	85	354
Y	pseudocumene	<i>bis</i> -MSB	21.25	79	519
Z	pseudocumene	DIN	18.71	78	418

2.3.2 Quenching

Table 2.7 shows the effect of nitromethane quenching on the optimum PDD and misclassification for the β emitters used in this study. The optimum PDD is highest for β emitters with the highest E_{max} for all levels of quenching and the % spill_m is highest for these higher energy nuclides. These instruments are supposed to allow for differences in the β energy, but as the duration of the β pulses increases with increasing energy, it is not unexpected that a higher PDD is required to differentiate higher energy β pulses from α pulses effectively. However, the degree of difference is likely to be exaggerated. The % spill_m obtained with this instrument for $^{90}\text{Sr}/^{90}\text{Y}$ is higher than for the 2550 TR/AB (b) (*e.g.* compare Tables 2.7 and 2.8). It is unlikely that this effect is caused by the

Table 2.7: Changes in optimum PDD and % spill_m for various β emitters with increasing quench by nitromethane. The α emitter in all cases is ²¹⁰Po and data were collected using the 2550 TR/AB (c). The % spill_m and optimum PDD were determined instrumentally.

β emitter	tSIE ^a	% spill _m	Optimum PDD
⁹⁰ Sr/ ⁹⁰ Y	506	7.16	155
	364	4.02	144
	279	2.43	135
	224	2.24	129
	183	4.14	114
³² P	509	7.52	155
	359	2.69	139
	279	1.75	132
	224	2.15	128
	183	4.04	115
³⁶ Cl	507	2.32	144
	356	1.75	131
	279	1.63	127
	223	1.81	125
	182	2.59	104
⁹⁹ Tc	512	1.78	142
	367	1.29	122
	291	1.62	112
	234	1.00	112
	191	1.46	71
¹⁴ C	509	1.61	124
	365	1.31	99
	284	0.71	80
	224	0.87	66
	183	-- ^b	-- ^b
³ H	506	-- ^b	-- ^b

^a Mean tSIE for α and β emitter.

^b Range too high, *i.e.* the optimum PDD is below the range of the instrument.

different α emitters used, as spectral differences are small. The experiment to obtain the data in Table 2.7 was curtailed as the instrument ceased to function, due to a failure in the electronics. Therefore, while these data reflect a real trend (see Table 2.5), the absolute magnitude is probably over-estimated.

^3H and ^{14}C , at the highest quench level, do not have an optimum PDD within the range of the instrument. In both cases, there was less than 2 % misclassification of α and β events. Although these instances do not produce overlapping α and β spectra, the use of PSD could still be useful. For example, ^{241}Pu (β emitter, $E_{\text{max}} = 20.8$ keV) has a similar spectrum to ^3H . Yet its simultaneous determination with $^{239,240}\text{Pu}$ (α emitters) is enhanced by the use of PSD, which reduces the background in the α spectrum (Yu *et al.*, 1992). As the purpose of PSD, in this case, is background reduction, a higher PDD could be used effectively.

For each β emitter there appears to be an optimum degree of quenching in terms of separation efficiency. Figure 2.17 shows this for $^{90}\text{Sr}/^{90}\text{Y}$, where the optimum quench results in approximately one third of the % spill_m of the least quenched sample. The higher energy β emitters give rise to a smooth decrease and then increase in the degree of misclassification as quench increases (Fig. 2.17B). Some of the data for the lower energy nuclides do not fit this pattern, although the overall trend is the same. These anomalies are caused by the influence of the background on the spills, which was discussed in section 2.3.1.

Figure 2.18 illustrates the cause of these changes in misclassification with nitromethane quenching. As the tSIE decreases, both the α and the β pulses become shorter in duration. Thus, the optimum PDD for separation will decrease. However, the β pulses appear to decrease in duration more quickly than the α pulses (Fig. 2.18B), resulting in a larger difference in shape between the pulse types than at lower levels of quenching, allowing more efficient separation. This is consistent with nitromethane quenching the excited triplet states and, as a smaller proportion of the total β pulse

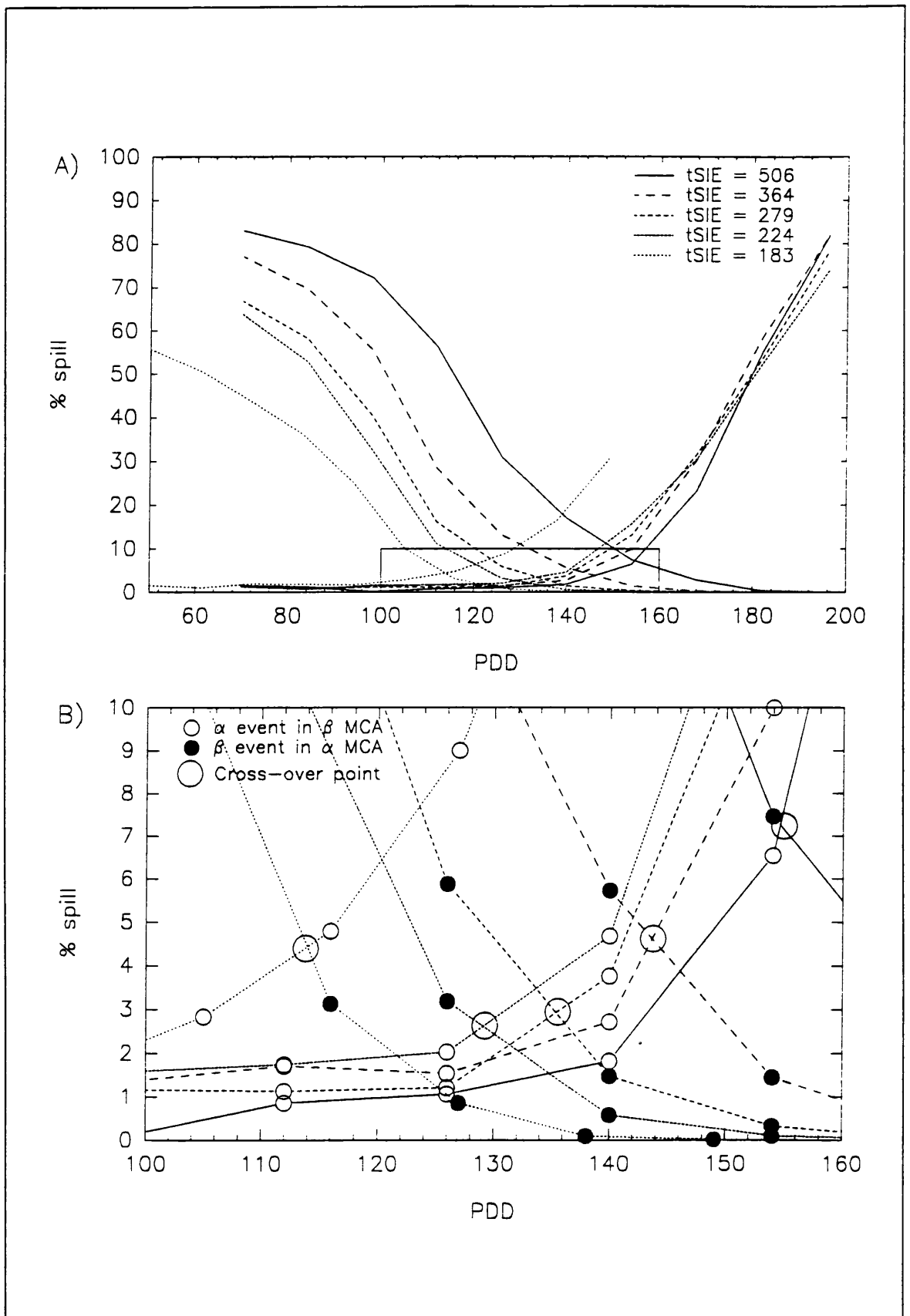


Figure 2.17: $^{90}\text{Sr}/^{90}\text{Y}$ and ^{210}Po cross-over plots with increasing quenching by nitromethane. B) is a detail of A).

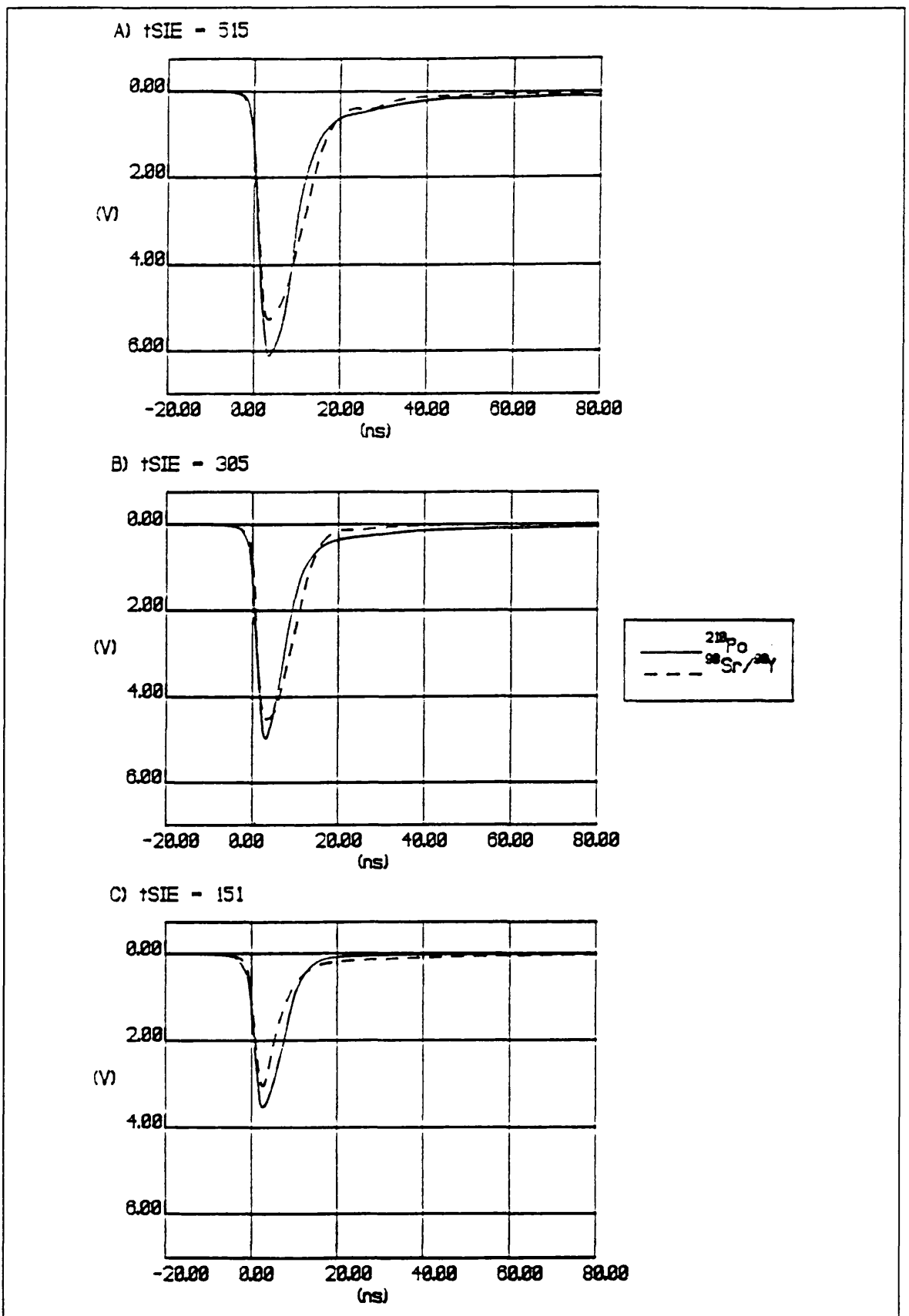


Figure 2.18: PMT anode pulse shapes with increasing nitromethane quench. A) no added CH_3NO_2 , B) 35 μl and C) 100 μl CH_3NO_2 .

is in the delayed component, there is a greater impact on length for β pulses. At very high levels of quenching, both types of pulse are significantly shorter, resulting in an increase in misclassification again.

The effect of quenching by nitromethane on the degree of misclassification at constant PDD is illustrated in Figure 2.19. In all cases, increasing quench increases the misclassification of β events, but decreases the misclassification of α events, as would be expected from Figure 2.17. The effects of quenching are most significant for the higher energy β emitters, but again it should be emphasized that the magnitude of this effect is larger than would normally be expected. This is opposite to the effect of quenching on counting efficiency, which has a greater impact on low energy β emitters. Chemical quenching reduces the number of photons that are produced by the scintillator, moving the energy spectrum to lower energies. For low energy β emitters, this process can result in reduced counting efficiency, as a significant proportion of their scintillation events produce an insufficient number of photons for a coincident event to be detected. Quenching affects α/β separation because of its impact on the shapes of PMT anode pulses. As low energy β events already have a lower degree of misclassification, nitromethane quenching will have very little effect in comparison to that on higher energy events. The effect on the misclassification of α events is dependent on the PDD at which the sample is counted. For a high PDD, nitromethane quenching rapidly increases the % spill _{β} , as α events are reduced to a shorter duration than the PDD. The converse is true for lower PDDs, as the initial misclassification is low. This effect is illustrated in Figure 2.20, which shows that the same increase in quenching causes a larger increase in misclassification for the higher PDD than for the lower.

Table 2.8 shows the optimum PDD and % spill_m for the different quenching agents at a number of tSIEs. Again, comparison of the instrumental and manual determinations of the data shows good agreement for the optimum PDDs both between the two determination methods and between

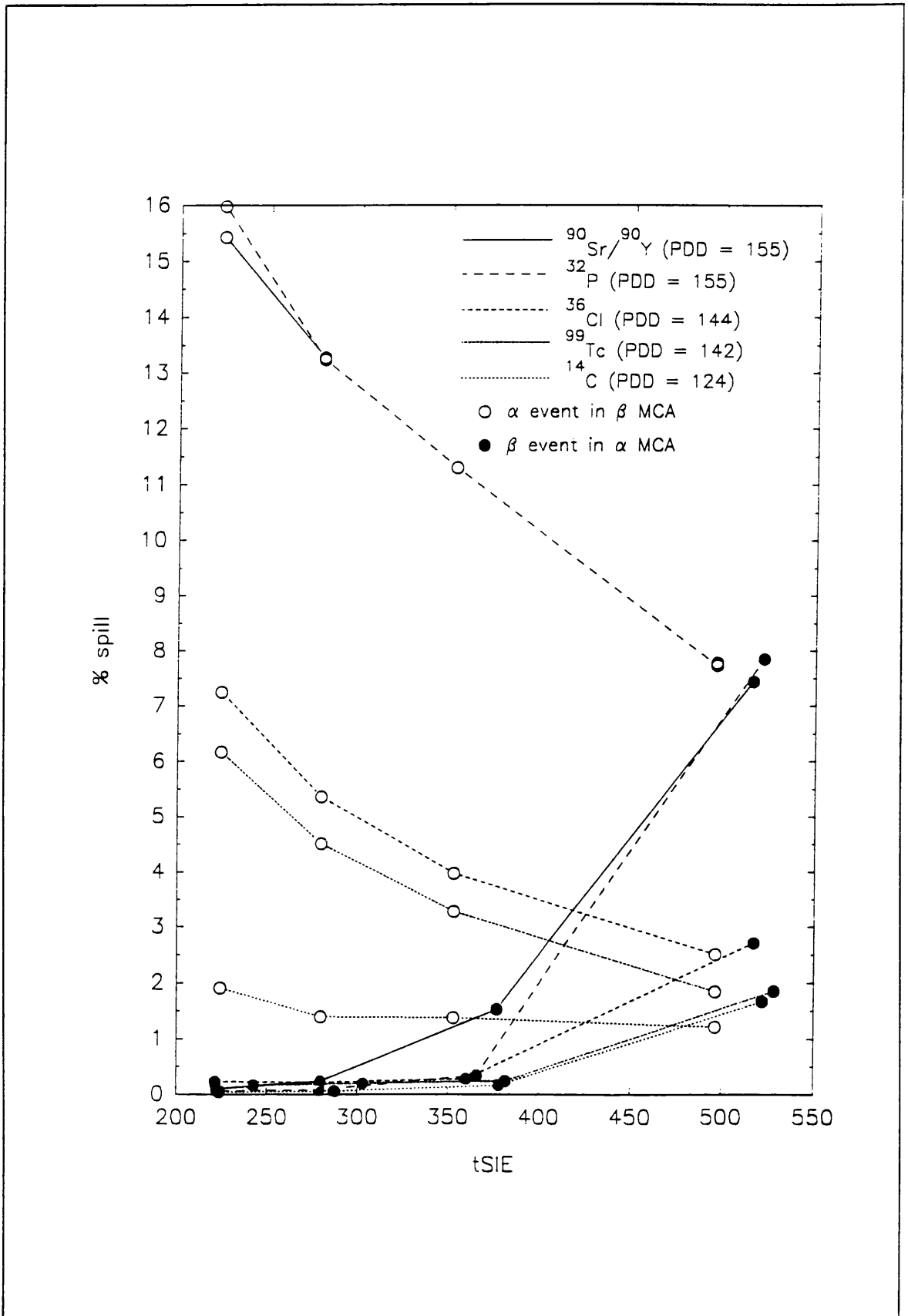


Figure 2.19: The change in % spill with increasing nitromethane quench at constant PDD for a range of β emitters.

Table 2.8: Change in optimum PDD and misclassification with quenching for various quenching agents, based on both the instrument and manual determinations of the misclassification for ^{238}Pu and $^{90}\text{Sr}/^{90}\text{Y}$ using the 2550 TR/AB (b). Values in brackets are duplicate samples.

Quench agent	tSIE	Instrument determination		Manual determination	
		% spill _m	Optimum PDD	% spill _m	Optimum PDD
Nitromethane	547 (544)	1.64 (1.54)	126 (125)	0.98 (1.06)	125 (125)
	458 (456)	0.57 (0.52)	116 (118)	-- ^a	-- ^a
	419 (413)	0.37 (0.49)	112 (112)	-- ^a	-- ^a
	384 (378)	0.62 (0.49)	108 (108)	-- ^a	-- ^a
	354 (345)	0.79 (0.75)	106 (107)	0.50 (0.52)	110 (110)
Acetone	544 (545)	1.65 (1.72)	125 (124)	1.04 (1.01)	125 (125)
	451 (447)	1.82 (2.02)	122 (122)	-- ^a	-- ^a
	401 (408)	1.62 (1.85)	122 (122)	-- ^a	-- ^a
	373 (369)	1.98 (1.81)	121 (121)	(1.02)	(120)
	346 (-- ^a)	1.94 (-- ^a)	121 (-- ^a)	1.02	120
Carbon tetrachloride	542 (543)	1.86 (1.85)	125 (125)	0.95 (1.14)	125 (125)
	450 (446)	1.22 (2.10)	112 (112)	-- ^a	-- ^a
	395 (394)	2.41 (2.06)	102 (103)	-- ^a	-- ^a
	359 (354)	2.98 (2.38)	99 (100)	-- ^a	-- ^a
	328 (324)	3.36 (3.31)	98 (98)	1.86 (1.77)	95 (100)
9M hydrochloric acid	546 (545)	1.81 (2.25)	126 (125)	0.97 (1.02)	125 (125)
	436 (439)	2.34 (2.51)	100 (100)	-- ^a	-- ^a
	402 (401)	2.80 (2.59)	99 (100)	-- ^a	-- ^a
	377 (375)	2.68 (2.70)	100 (101)	1.69 (1.72)	100 (100)
None - 12 ml geometry	530 (525)	2.09 (1.97)	123 (124)	1.13 (0.94)	125 (125)

a Not determined.

duplicate samples, but % spill_ms are significantly lower for the manual determinations. In most cases, these data show better agreement between duplicates than the instrumentally derived data. The four "unquenched" samples show good agreement, as does the "unquenched" 12 ml geometry sample. Therefore, small changes in the sample geometry appear to have little effect on PSD. This will be

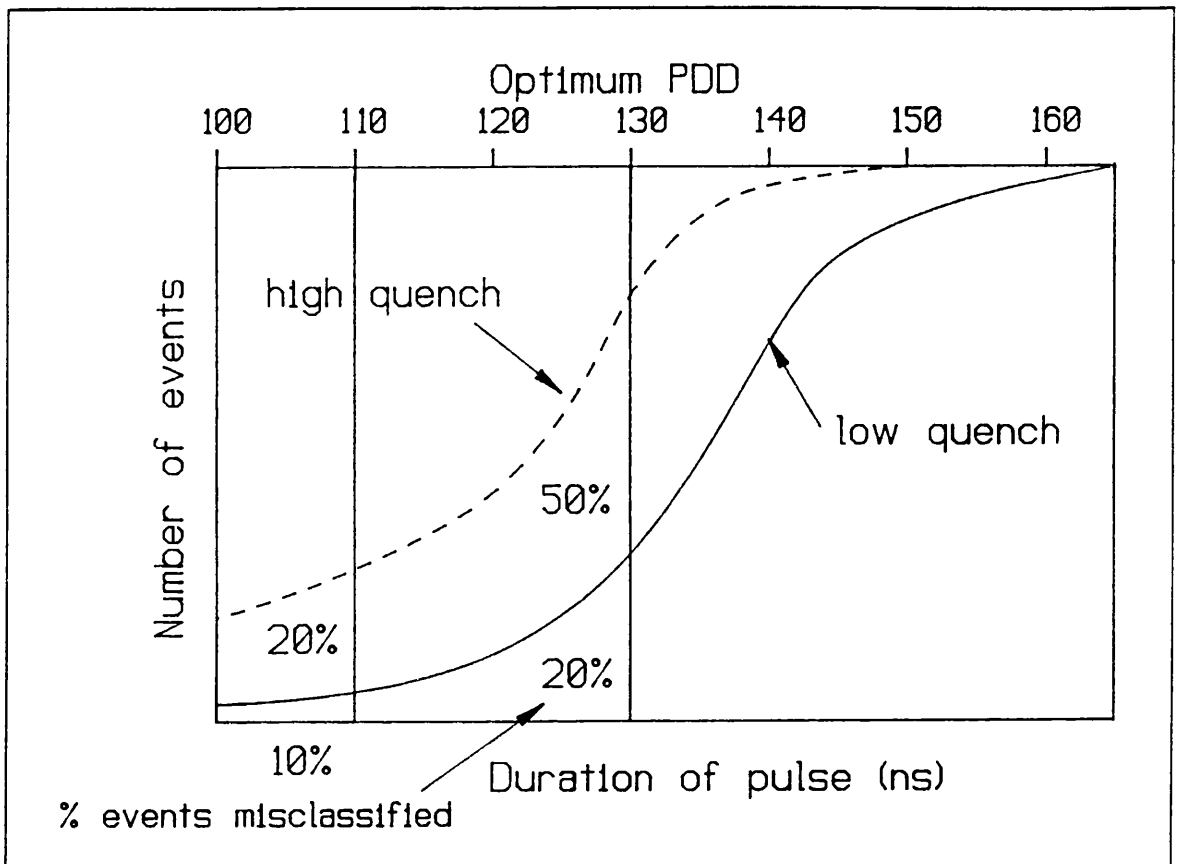


Figure 2.20: Schematic of the effect of quenching on the misclassification of α events.

discussed further in section 2.3.3. The data also indicate a good degree of instrument stability over the counting period.

The differences between the four quenching agents are illustrated by Figure 2.21. Three different types of behaviour can be seen. Firstly, nitromethane has reduced pulse lengths and the % spill at the optimum PDD (Fig. 2.21A), as was found in the first part of this experiment. Carbon tetrachloride (Fig. 2.21C) and hydrochloric acid (Fig. 2.21D) also have reduced pulse lengths, as indicated by the lower optimum PDDs, but in both cases the % spill_m has increased. Acetone has a small effect on pulse lengths (Fig. 2.21B), but the misclassification has remained approximately the same. Rundt (1991) grouped nitromethane and carbon tetrachloride together, in terms of their quenching effects, in a separate group from acetone. While nitromethane and carbon tetrachloride behave differently here, they are displaying different aspects of the same effect. Table 2.7 shows that

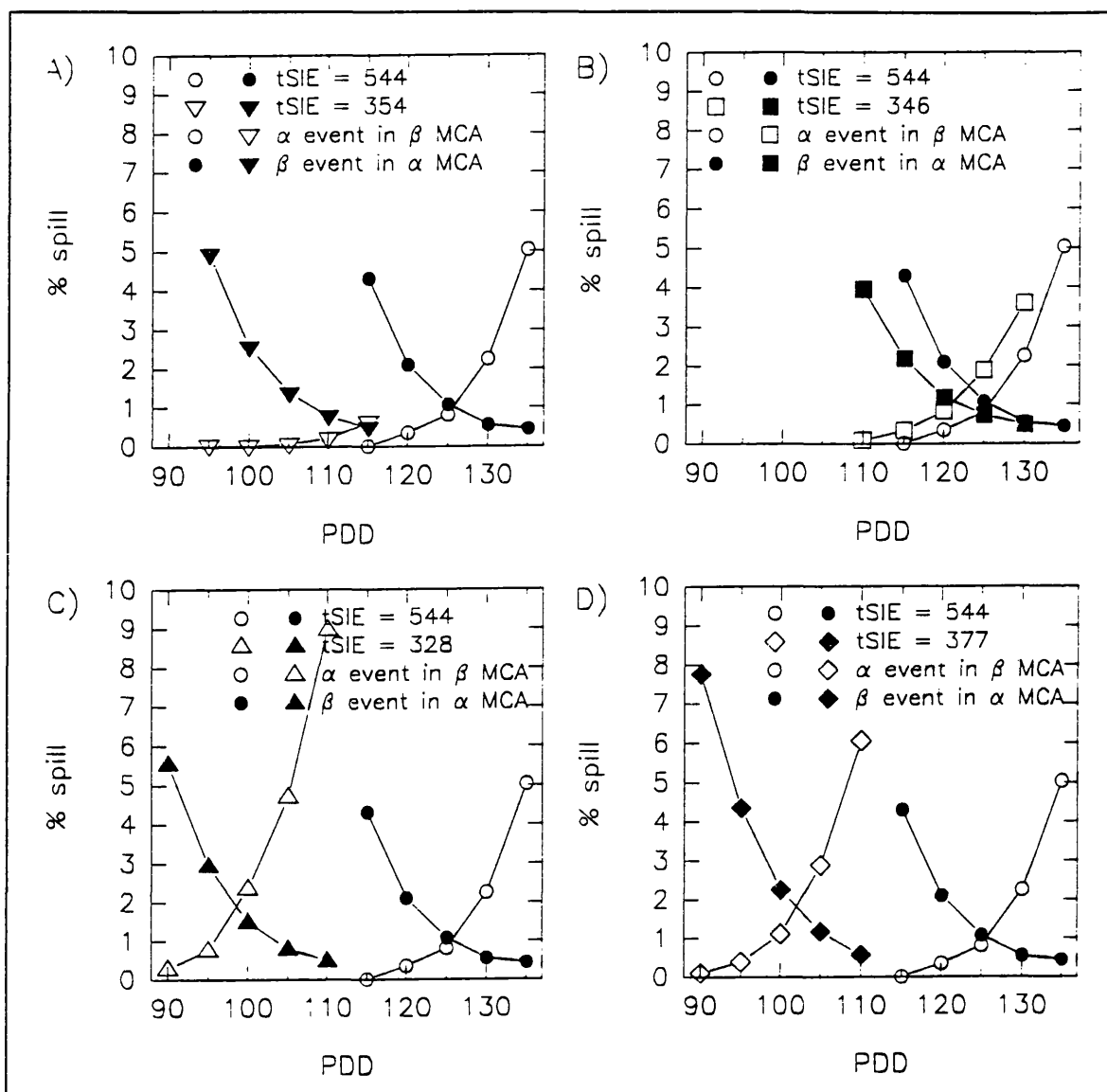


Figure 2.21: The effect on the optimum PDD and % spill of various quenching agents. A) nitromethane, B) acetone, C) carbon tetrachloride and D) 9M hydrochloric acid.

if this experiment had been continued, the final cross-over for nitromethane would have had a higher % spill_m. Thus, both have caused a decrease in misclassification before an increase. However, it remains that the same change in tSIE has had a markedly different effect for all four quenching agents. In practical terms, this means that if a quench calibration is to be carried out for an α/β LSS analytical procedure, it is critical to use a quenching agent that will behave in the same way as impurities in the sample. Carbon tetrachloride and nitromethane, which are commonly used to prepare quench standards, should be avoided in the majority of cases.

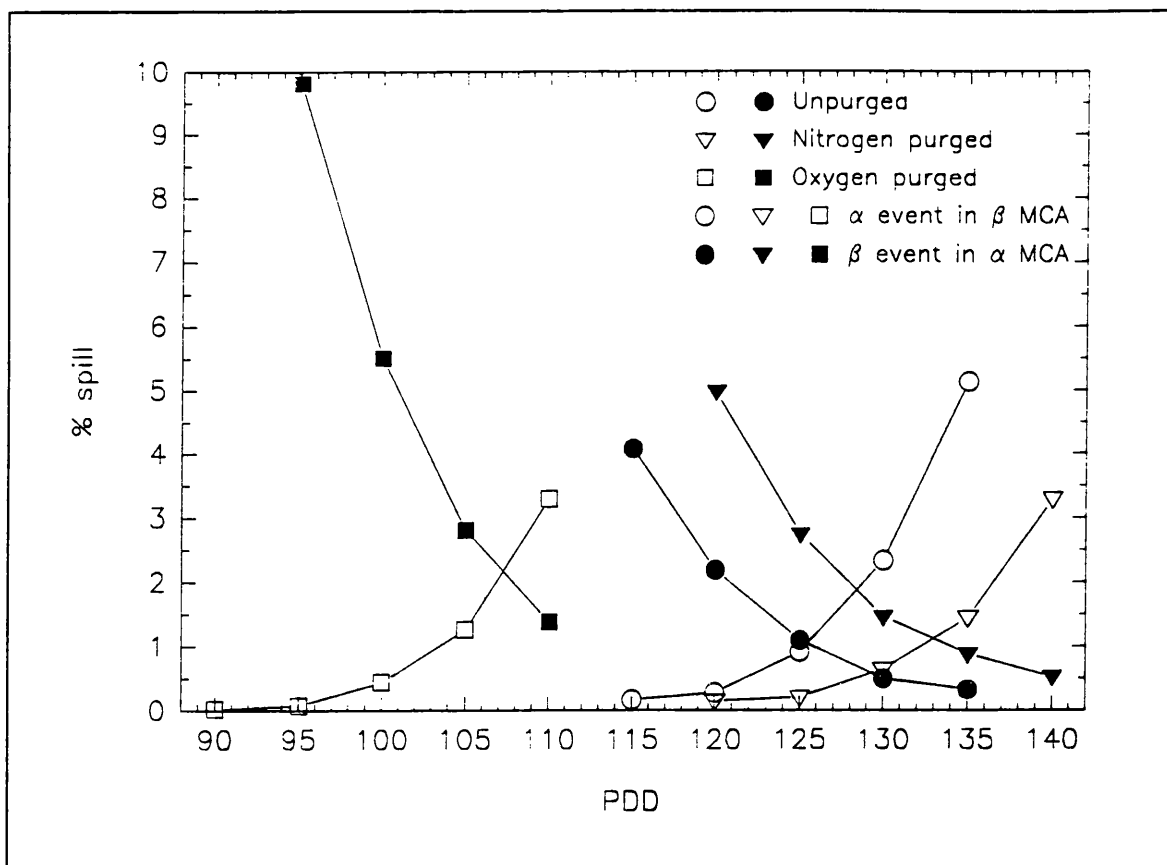


Figure 2.22: The effect on optimum PDD and % spill of purging Ultima Gold™ AB.

Table 2.9 and Figure 2.22 show the effect on α/β separation of purging with oxygen and nitrogen. As would be expected, oxygen has reduced the optimum PDD, indicating shorter PMT pulses. The degree of misclassification has also increased as would be expected, as oxygen is known to act on triplet states in the same way as nitromethane (Birks, 1970). The results from the nitrogen purging, however, do not follow the expected pattern. McKlveen and McDowell (1976) showed that purging extractive scintillators with nitrogen causes a significant improvement in PSD. This is not the case here with Ultima Gold™ AB as, although the nitrogen purging has caused an increase in pulse length, there has been little effect on misclassification. The reason for this difference is likely to be the different solubilities of oxygen in the solvents. Extractive scintillators generally use toluene as a solvent base, which dissolves oxygen far more readily than does DIN (Prichard *et al.*, 1992). Therefore, the two types of cocktail do not start from a common point and the effects of purging cannot be directly

Table 2.9: The effect of purging Ultima Gold™ AB with oxygen and nitrogen on α/β separation. The α emitter is ^{238}Pu and the β emitter $^{90}\text{Sr}/^{90}\text{Y}$. The data were determined using the 2550 TR/AB (b). Values in brackets are for duplicate samples.

Sample	Purging agent	tSIE	% spill _m	Optimum PDD
P1	none	528 (542)	1.02 (1.07)	125 (125)
P2	nitrogen	579 (579)	1.06 (1.03)	130 (130)
P3	oxygen	448 (451)	2.05 (1.92)	105 (105)

compared. The presence of a small amount of oxygen is probably beneficial to PSD, as it will suppress the delayed component of the β emitter more than that of the α emitter, as was seen with nitromethane (Fig. 2.18).

2.3.3 Other factors

The effect of different vial types and volumes on PSD can be seen in Table 2.10 and Figure 2.23. Glass vials, both 7 and 20 ml, produce better separation of events than the two types of plastic vial. This confirms the observations of Yang *et al.* (1991). The reason for this difference is unclear, but it may be the result of some distortion of the PMT anode pulse shapes. It should be noted, however, that the use of a plastic adapter with a 7 ml glass vial causes no change in either the % spill or the optimum PDD. This indicates that the effect on PMT anode pulse shapes may be the result of an interaction between the cocktail and the plastic. Cocktail volume and geometry appear to have little effect on separation efficiency (Table 2.10 and Fig. 2.24). When the data for the 12 ml geometry samples are taken into account as well, it seems that once the very small volumes recommended by McKlveen and McDowell (1976) are exceeded, increasing the volume does not degrade performance significantly. 7 ml glass vials appear to have marginally higher % spill_ms than 20 ml glass vials with the same volume of cocktail. However, the difference (0.2%) is not large and may not be significant.

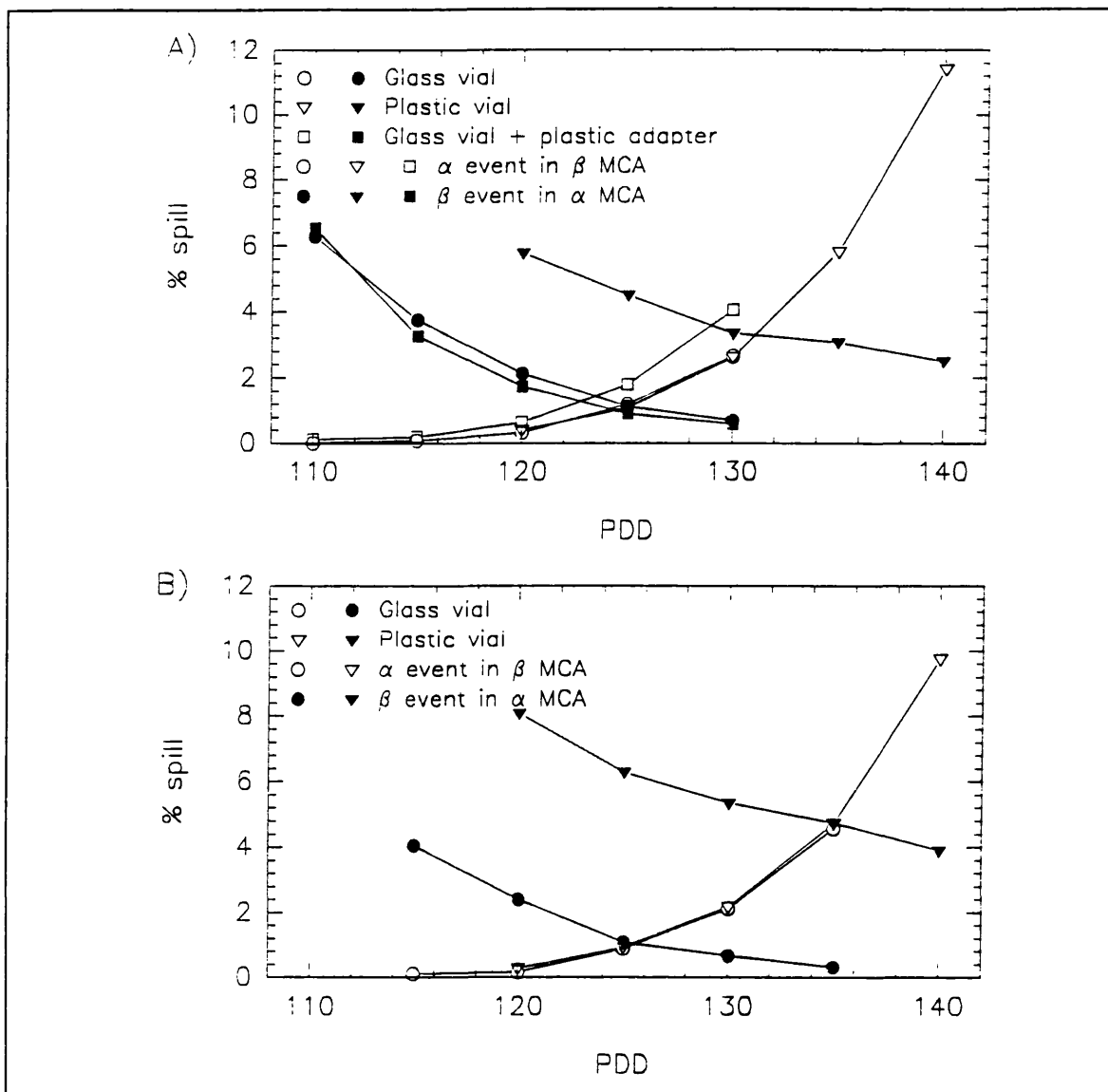


Figure 2.23: The effect of vial type on optimum PDD and % spill. A) 7 ml vials + 5 ml cocktail, B) 20 ml vials + 10 ml cocktail.

Table 2.10: The effect of varying cocktail volume, vial type and vial volume on α/β separation. Measurements were made using ^{238}Pu and $^{90}\text{Sr}/^{90}\text{Y}$ with the 2550 TR/AB (b). Values in brackets are for duplicate samples.

Sample	Cocktail volume (ml)	Vial volume (ml)	Vial type	% spill _m	Optimum PDD	tSIE
V1	10	20	glass	0.99 (1.00)	125 (125)	553 (548)
V2	5	20	glass	0.92 (1.01)	125 (125)	542 (543)
V3	10	20	polyethylene	3.61 (3.50)	125 (125)	556 (571)
V4	5	7	glass	1.17 (1.12)	125 (124)	480 (477)
V5	5	7	polypropylene	2.80 (2.94)	125 (125)	543 (547)
V6	5	7	glass + plastic vial holder	1.20 (1.14)	120 (120)	439 (442)

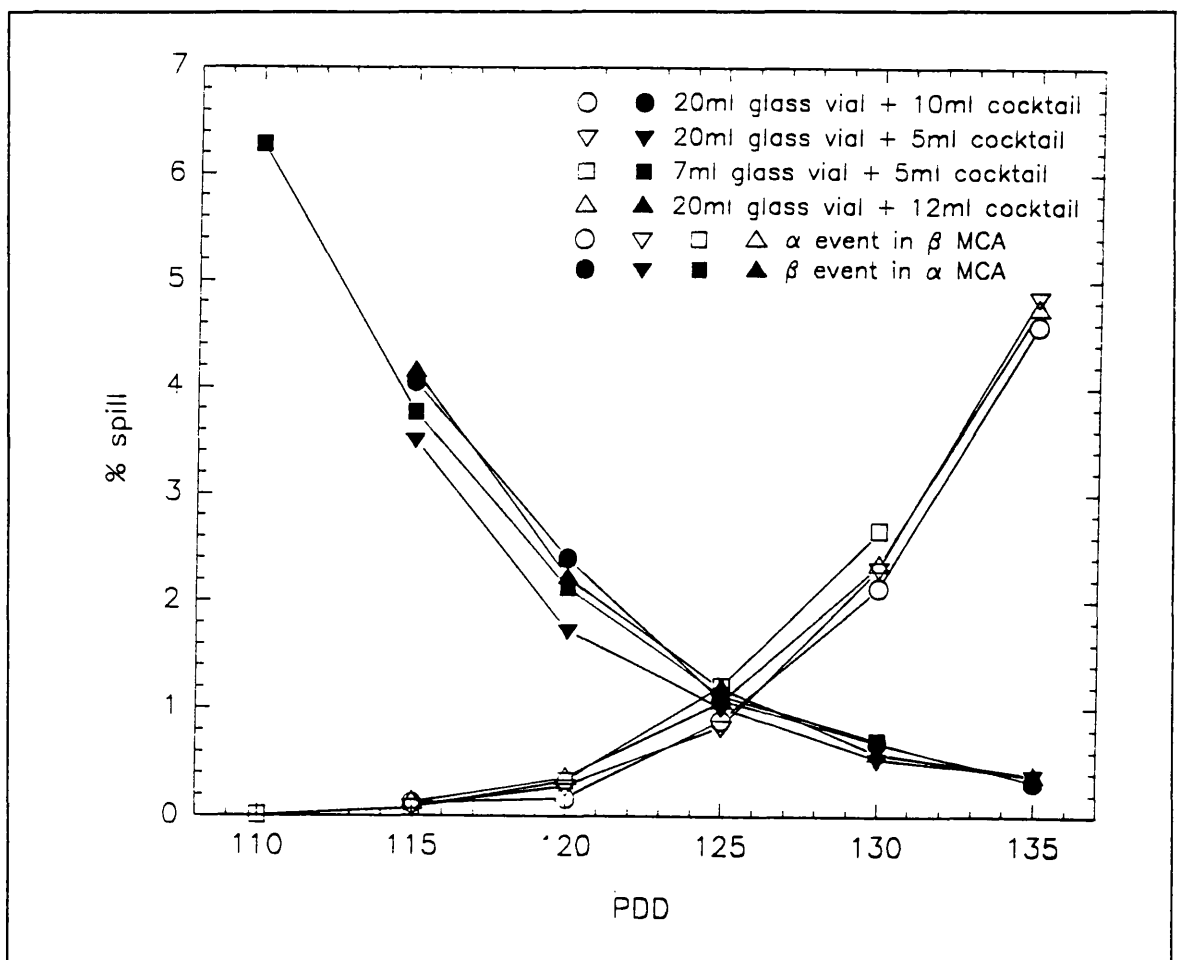


Figure 2.24: The effect of cocktail volume and size on optimum PDD and % spill.

2.4 CONCLUSIONS

PMT anode pulse shapes and hence PSD are highly dependent on cocktail composition and quenching. Even small changes in the composition of a cocktail can bring about large differences in the separation efficiency, as a result of changes to pulse shapes and changes in the light output of the cocktail. Generally, cocktails which produce pulses of an intermediate duration and those with the highest light outputs give rise to the most efficient separation of events. The use of a slow solvent, such as DIN, is essential, however, in order to enhance the differences between pulse types. It was not possible to define any structural features of fluors that have useful properties, in terms of α/β separation, within the bounds of this work. Nonionic surfactants are the most appropriate, as high sample holding capacities can be achieved without sacrificing separation efficiency. Ultima Gold™ AB is an optimum formulation, but could possibly be improved by the use of POPOP or dimethyl-POPOP instead of *bis*-MSB as the secondary fluor.

Quenching had variable effects on separation efficiency, depending on the quenching agent used. However, as misclassification can vary significantly with quenching if the samples are counted at the same PDD, it is extremely important to examine the effects of quenching over the range encountered within batches of samples and to prepare standards with the same tSIE. In doing this it is necessary to choose a quenching agent that mimics the behaviour of any quenching impurities present in the sample. As a result, the quenching agents that are usually used to generate quench correction curves, nitromethane and carbon tetrachloride, are probably not the best choice for any study of quenching involving PSD, in relation to real samples.

The energy of the β emitter used may have an effect on separation efficiency, and therefore it is desirable to calibrate the PDD using the same β emitter as is present in the real sample. This could present problems when the nuclides of interest rapidly attain secular equilibrium, for example ^{222}Rn and its progeny. In these instances it may not be possible to separate the nuclides of interest

into α and β emitters for use as standards to determine the optimum PDD, and alternative means need to be sought. Spaulding and Noakes (1993) used ^{222}Rn in equilibrium with its progeny as a single standard sample, but instead of determining the optimum PDD in terms of a cross-over plot and minimum misclassification, defined the optimum PDD by examining a curve of α counting efficiency. The optimum was at the point which gave 300% efficiency (^{222}Rn , ^{218}Po and ^{214}Po), misclassification of β events leading to greater than 300% efficiency and misclassification of α events causing a reduction in counting efficiency.

Purging Ultima Gold™ AB with nitrogen does not improve separation efficiency, as DIN does not dissolve oxygen well. Glass vials produce better separation than plastic vials, possibly due to an interaction between the cocktail and the plastic vials. On the other hand, neither vial nor cocktail volume appear to have a significant effect. However, once the effect of quenching on counting efficiency is considered, it is desirable to use identical sample preparation techniques to prepare both standards and samples.

All types of LSS require samples and standards to be prepared in similar ways, but this is particularly the case when PSD is used. The chemical composition of standards and samples in particular affects α/β separation, and variations should be kept to a minimum. Vial type and size have less impact on separation efficiency, but are significant in determining both the background and counting efficiency.

CHAPTER 3: DEVELOPMENT OF AN α/β LIQUID SCINTILLATION SPECTROMETRY METHOD FOR ^{234}Th ANALYSIS

3.1 INTRODUCTION

Chapter 1 (section 1.4) outlined the theoretical and chemical basis for the use of natural decay series disequilibria as tracers of marine processes. As stated in section 1.4.1, uranium forms a soluble, uranyl carbonate complex in an oxic, marine environment, whereas thorium is highly particle reactive. This difference leads to the creation of disequilibrium between parent and daughter pairs. The disequilibrium between ^{234}U and its daughter ^{230}Th has been used for many years to study sedimentation processes in the deep ocean (*e.g.* Anderson *et al.*, 1983) and hydrothermal activity (*e.g.* Shimmield and Price, 1988). However, the relatively long half-life of ^{230}Th (7.54×10^4 y) means that it can only be used to study processes that occur over thousands of years.

Bhat *et al.* (1969) demonstrated the use of the $^{234}\text{Th}/^{238}\text{U}$ disequilibrium for examining settling velocities of particles in the water column. This early work was relatively crude in comparison with more recent studies; for example, no attempt was made to differentiate between the dissolved and particulate phases. However, it led the way for more detailed studies which have grown in complexity as the understanding of marine systems has increased. More recently, there has been an increasing level of interest in the use of the $^{234}\text{Th}/^{238}\text{U}$ disequilibrium to study processes with short time-scales (up to 100 days), in particular with relevance to carbon cycling in the oceans (*e.g.* Buesseler *et al.*, 1992a) and the mechanisms of scavenging (*e.g.* Niven and Moore, 1988).

It is the $^{234}\text{Th}/^{238}\text{U}$ disequilibrium that is of particular interest in the present work. The analytical methods currently in use and their problems are now discussed (section 3.2), followed by a section on method development for LSS (section 3.3). A more detailed discussion of the various applications for $^{234}\text{Th}/^{238}\text{U}$ disequilibrium can be found in Chapter 4, along with specific applications carried out in

the present work, employing the method discussed in the current chapter.

3.2 ANALYTICAL METHODS

3.2.1 Current methods of analysis

The analysis of ^{234}Th is highly influenced by its half-life and the concentration at which it is present in the marine environment. The maximum activity that can occur in seawater is 2.5 dpm l^{-1} - the activity of ^{238}U in the open ocean at 35‰ salinity, unless redissolution of settling particles is occurring, therefore necessitating the use of a reasonably sensitive counting technique. ^{234}Th decays by the emission of a low energy β particle ($E_{\text{max}} = 190 \text{ keV}$) and produces γ photons at 63 keV (probability 3.8%), 92.78 keV (probability 2.69%) and 92.35 keV (probability 2.72%) (Fig. 3.1). Its daughter, $^{234\text{m}}\text{Pa}$ ($t_{1/2} = 1.17 \text{ min}$) occurs in secular equilibrium with its parent, within the time frame of most analytical procedures. As $^{234\text{m}}\text{Pa}$ decays by the emission of a high energy β particle ($E_{\text{max}} = 2.33 \text{ MeV}$), it can also be used to determine the ^{234}Th activity of a sample.

The complicating factor is the half-life of ^{234}Th ($t_{1/2} = 24.1 \text{ d}$), which means that the analysis must be completed within a few weeks of sampling, depending on sample size, if the activity is to remain above the limit of detection. As oceanographic cruises can often last much longer than this, the analytical procedure should ideally be applicable to the ship-board environment. This creates a number of problems related to the motion of the vessel and the restricted facilities available onboard even scientific ships. Therefore, the most appropriate analytical techniques will be rapid, simple and will not involve excessive chemical manipulation. Thus, two methods are commonly used to determine the activity of ^{234}Th in marine samples, namely *via* the γ emission (γ spectrometry) or *via* the β emission of either $^{234\text{m}}\text{Pa}$ or both ^{234}Th and $^{234\text{m}}\text{Pa}$ combined (gas proportional counting). These methods and the problems associated with them are discussed below, before turning to the possibility of using LSS.

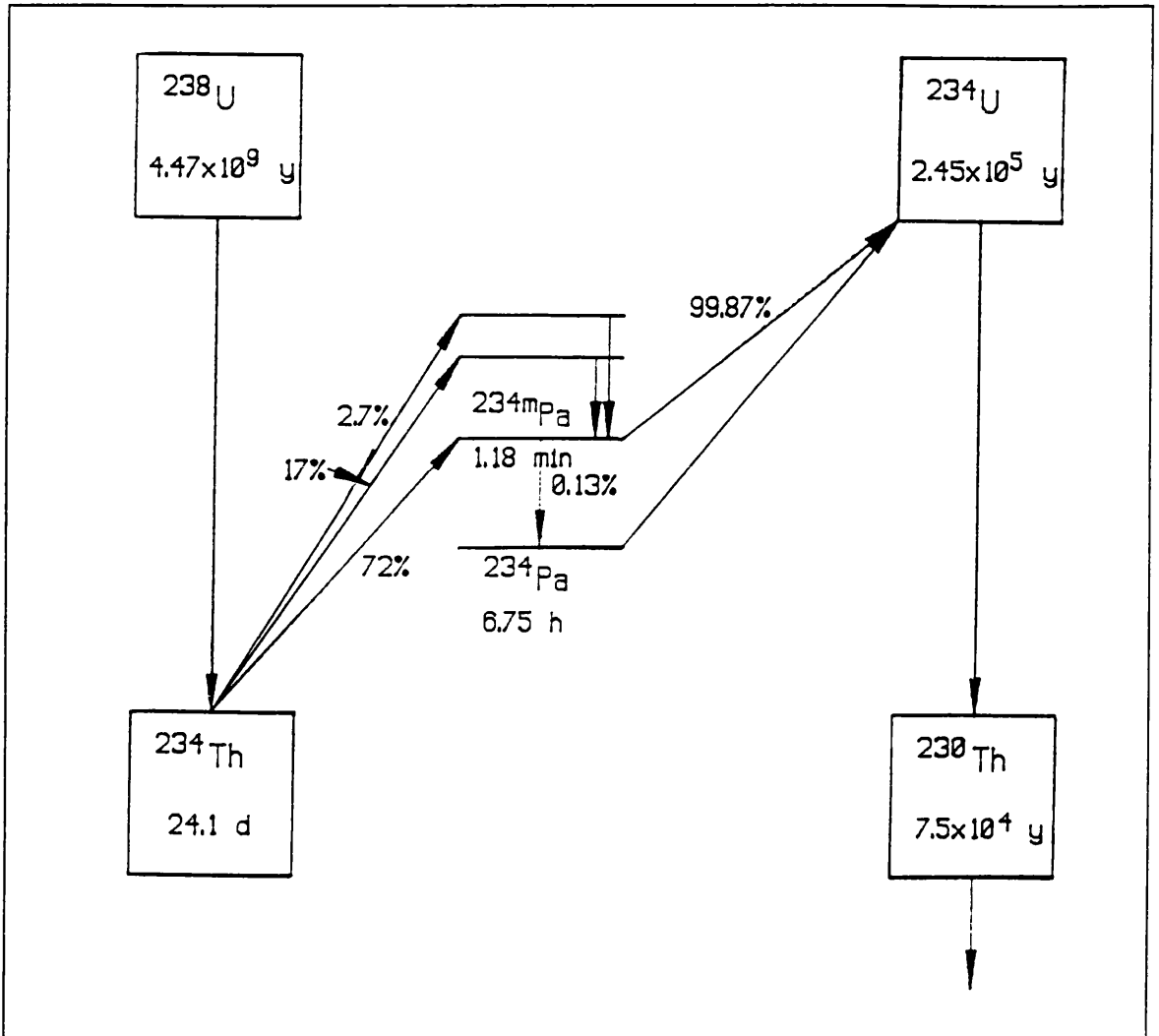


Figure 3.1: Schematic of the principal decay schemes of ^{234}Th , $^{234\text{m}}\text{Pa}$ and ^{234}Pa .

3.2.1.1 Gamma spectrometry

^{234}Th emits low intensity γ photons at 63 keV and 93 keV (the two emissions mentioned above are detected as a single peak at 93 keV). However, the low intensity combined with the low detection efficiency of most γ spectroscopy systems (Buesseler *et al.* (1992b) quote a γ detection efficiency of 16% at the 63 keV peak for their germanium detector) results in the requirement for large sample volumes, typically of the order of 1000-4000 l. The collection of such a large sample by traditional means (*e.g.* with wire-operated bottles, such as the Niskin bottle) is complex and time-consuming, however, workers at Woods Hole Oceanographic Institute and the State University of New York have developed a rapid means of sampling thorium isotopes from large volumes of seawater (Buesseler

et al., 1992b). This method consists of an *in-situ* pump, which forces seawater through a pre-filter and then sequentially through two manganese dioxide cartridges at between 4 and 8 l min⁻¹, allowing the sampling of more than 3000 l in 8 hours. Finally, the water passes through a flow meter, which allows the accurate determination of the quantity sampled.

Manganese dioxide impregnated fibres were originally developed as a means of scavenging radium from seawater samples (Moore and Reid, 1973; Moore, 1976). The original preparation technique consisted of reacting acrylic fibre with sodium hydroxide before soaking it in manganese chloride and then again in sodium hydroxide. Manganese hydroxide was deposited on the fibre, which was then oxidized by exposure to air to manganese dioxide (Moore and Reid, 1973). However, this method produced a precipitate that was poorly bound to the fibre, creating problems during sampling. Therefore, the preparation method was changed to soaking the acrylic fibre in a potassium permanganate solution, which rapidly oxidized the fibre, depositing manganese dioxide that is more tightly bound (Moore, 1976). From using loose fibre packed into columns (Reid *et al.*, 1979), the technique was developed to using fibre wound round an inert polypropylene core. Livingston and Cochran (1987) adapted it further for use with the actinide elements by replacing acrylic with inert polypropylene fibres, which have a lower blank contribution. Again, manganese dioxide was deposited through the use of a potassium permanganate solution.

In a study of marine samples, Livingston and Cochran (1987) found that the collection efficiency for thorium with these cartridges was between 69 and 93%, averaging 84%. The efficiencies can be found by comparing the activities on the two cartridges (equation 3.1)

$$\text{Efficiency} = 1 - \frac{A_b}{A_a} \quad (3.1)$$

where A_b is the activity on the second cartridge and A_a is the activity on the first. This equation assumes that the collection efficiency of each cartridge is the same, within error, and that none of the

thorium initially deposited on the first cartridge is subsequently leached off and redeposited on the second. The validity of these assumptions is discussed in section 4.3.2, based on experimental evidence gained during this work.

The chemistry required to determine the activity of ^{234}Th collected on manganese dioxide cartridges is minimal. Although the cartridges can be analysed by γ spectrometry with no further processing, it has been found that the γ detection efficiency for this geometry is very poor ($< 1\%$) and Buesseler *et al.* (1992b) therefore investigated two further geometries. The first involves melting the cartridge for 8 h at 185°C in a 600 ml beaker, which produces a disc of diameter 8 cm and height 4 cm, increasing the γ detection efficiency to 5.3% (using the 63 keV peak), but the reproducibility, found by spiking cartridges with known activity solutions, was poor, with relative errors of up to $\pm 15\%$. The reproducibility was further improved (to $< \pm 5\%$) by ashing the samples for 24 h at 450°C . The γ detection efficiency increased to 16.1% for the 63 keV peak. Modern high-purity germanium γ spectrometers are sufficiently rugged for use in the field, including at sea and, thus, the counting can be performed during a cruise, fulfilling the criteria outlined above. In addition, further radiochemical analyses can be performed on the ashed sample for other thorium isotopes, such as ^{228}Th , which have insufficient activities to be detected in smaller volumes. One problem with this method is that only simple particulate and dissolved fractions can be analysed. If more detailed size fractionation is required, the analysis has to be performed by an alternative technique (Moran and Buesseler, 1993).

3.2.1.2 Gas proportional counting

Gas proportional counting, with various types of instrument, has been the traditional method for the determination of ^{234}Th in seawater and sediments. The sample volume required is constrained by the detection efficiency and the background of the instrument in use, some typical examples employed being 30 l (Coale and Bruland, 1987), 50 l (Tanaka *et al.*, 1983) and 100 l (Kershaw and Young, 1988). Typical detectors used are gas flow counters with anti-coincidence shielding (Coale and

Bruland, 1987) and low-background GM counters (Tanaka *et al.*, 1983), the former being the more common. The sample activity is determined either *via* the emission of ^{234m}Pa , by shielding the sample with aluminium foil (*e.g.* Moran and Buesseler, 1993) or by recording all the available β counts ($^{234}\text{Th} + ^{234m}\text{Pa}$) (*e.g.* Coale and Bruland, 1987). As gas proportional counting techniques provide little spectroscopic information, many workers repeatedly count the sample over several half-lives to check that the recorded counts are not derived from a β emitting impurity (*e.g.* Bacon and Rutgers van der Loeff, 1989).

Whichever detector is used, the sample requires pre-concentration and purification in order to prepare a near-weightless source that contains neither radioactive impurities nor substantial quantities of other impurities that could result in self-absorption. Therefore, it is necessary to employ a chemical yield tracer if the activity of ^{234}Th is to be determined with any degree of accuracy. Unfortunately, no β emitting isotope of thorium exists with a sufficiently long half-life to be of use as a yield tracer. Hence, ^{230}Th , ^{228}Th or occasionally ^{232}Th (Tanaka *et al.*, 1983) or ^{229}Th (Martin and Sayles, 1987), all α emitters, are used. ^{229}Th is an artificial isotope of thorium with a half-life of 7.3×10^3 y, whereas ^{230}Th ($t_{1/2} = 7.54 \times 10^4$ y), ^{228}Th ($t_{1/2} = 1.9131$ y) and ^{232}Th ($t_{1/2} = 1.41 \times 10^{10}$ y) are naturally occurring. ^{230}Th is perhaps the most commonly used yield tracer for ^{234}Th analysis, as it can be readily prepared from natural uranium that is in equilibrium with its progeny (*e.g.* Mirza, 1978). A combined ^{232}U - ^{228}Th spike, that is in equilibrium, is used when both uranium and ^{234}Th are to be analysed (*e.g.* Kershaw and Young, 1988). However, this spike suffers the problem that it has a chain of rapidly ingrowing α and β emitting progeny (Fig. 1.7), requiring the sample to be counted within a few hours of separation. In addition, ^{228}Th may be present at sufficient concentrations in the sample to require a separate unspiked sample to be analysed in order to obtain an accurate estimation of the yield (Aller and DeMaster, 1984).

There are two main problems with this analytical procedure. The first is the chemistry required

to purify the sample. This must be rigorous in order to obtain a sufficiently pure sample that will yield a well-resolved spectrum. The second is the use of the α emitting yield tracer, which has to be counted separately, either by α -spectrometry using, for example, a silicon surface-barrier detector, (*e.g.* Kershaw and Young, 1988; Moran and Buesseler, 1993) or by using the same gas flow counter used for the detection of the β emissions (*e.g.* Matsumoto, 1975; Bacon and Rutgers van der Loeff, 1989). Either method requires two counts that need to be independently calibrated for detection efficiency (Aller and DeMaster, 1984). With low detection efficiencies for both α and β counting, a total counting period of 48 h is not unrealistic (no figures were found in the literature, so this value was estimated on the basis of a 24 h count for β emissions and the same for α emissions), and more would be required if the sample is counted several times. In none of the literature examined was evidence found of the full procedure being carried out on board a ship.

A summary of the chemical procedures typically used for gas proportional counting is now given, but examples of specific details are given in section 3.3.3, so that they may be compared with the similar techniques adopted for use with LSS.

After filtration (which should take place as soon after sampling as is reasonably achievable, in order that the condition of disequilibrium is maintained) the sample is acidified, spiked with a yield tracer and an iron (III) carrier is added. The sample is then thoroughly mixed and left in order that the spike and the ^{234}Th reach isotopic equilibrium. The pH of the sample is then raised to precipitate iron (III) hydroxide, which co-precipitates thorium and uranium. The precipitate is removed and dissolved and the sample is passed through a sequence of ion-exchange columns, usually anion exchange in some combination of the chloride (which retains uranium) and nitrate (which retains thorium) forms. It is essential to separate the ^{234}Th from any ^{238}U present in the sample as quickly as possible, as ^{234}Th is constantly growing in, requiring the use of a correction factor. Finally, the counting source is prepared either by electrodeposition onto a silver (*e.g.* Tanaka *et al.*, 1983), platinum (*e.g.* Coale and

Bruland, 1987) or stainless steel (*e.g.* Moran and Buesseler, 1993) planchette or by extraction into a solvent such as TTA (thenoyltrifluoroacetone), followed by evaporation onto a stainless steel planchette (*e.g.* McKee *et al.*, 1984). Most reported procedures allow the purification to the stage of the uranium separation to be performed at sea, with the remaining part of the analysis being carried out in the laboratory. Examples of the full analytical procedure employed by two groups are given in Figure 3.2.

3.2.1.3 ^{238}U analysis

To establish the degree of disequilibrium, it is not only necessary to know the concentration of the daughter nuclide, but also the parent. The activity of ^{238}U can be determined in a number of ways. As discussed in section 1.4.1, uranium exhibits conservative behaviour in seawater. Therefore, in water column studies where no anthropogenic source of uranium is present, the activity of ^{238}U can be derived from the relationship with salinity established by Chen *et al.* (1986) (equation 3.2)

$$A_{U-238} \text{ (dpm l}^{-1}\text{)} = 0.06905 \times \text{salinity (\%o)} \quad (3.2)$$

This method has been adopted by Coale and Bruland (1987) and Moran and Buesseler (1993), for example. The uranium activity present in suspended sediments or in seafloor sediments must be found by conventional radiochemical methods, such as purification by ion-exchange, followed by α spectrometry. This method has been adopted by Aller and DeMaster (1984), for example, and for seawater analysis by Kershaw and Young (1988). Alternatively, the possibility exists to obtain the ^{238}U activity in seawater by inductively coupled plasma-mass spectrometry (ICP-MS) (J. Toole, personal communication, 1994) or other mass spectrometric techniques (*e.g.* Chen *et al.*, 1986), although these methods have not been adopted for ^{234}Th disequilibrium studies, probably due to their limited availability and complexity relative to salinity measurements.

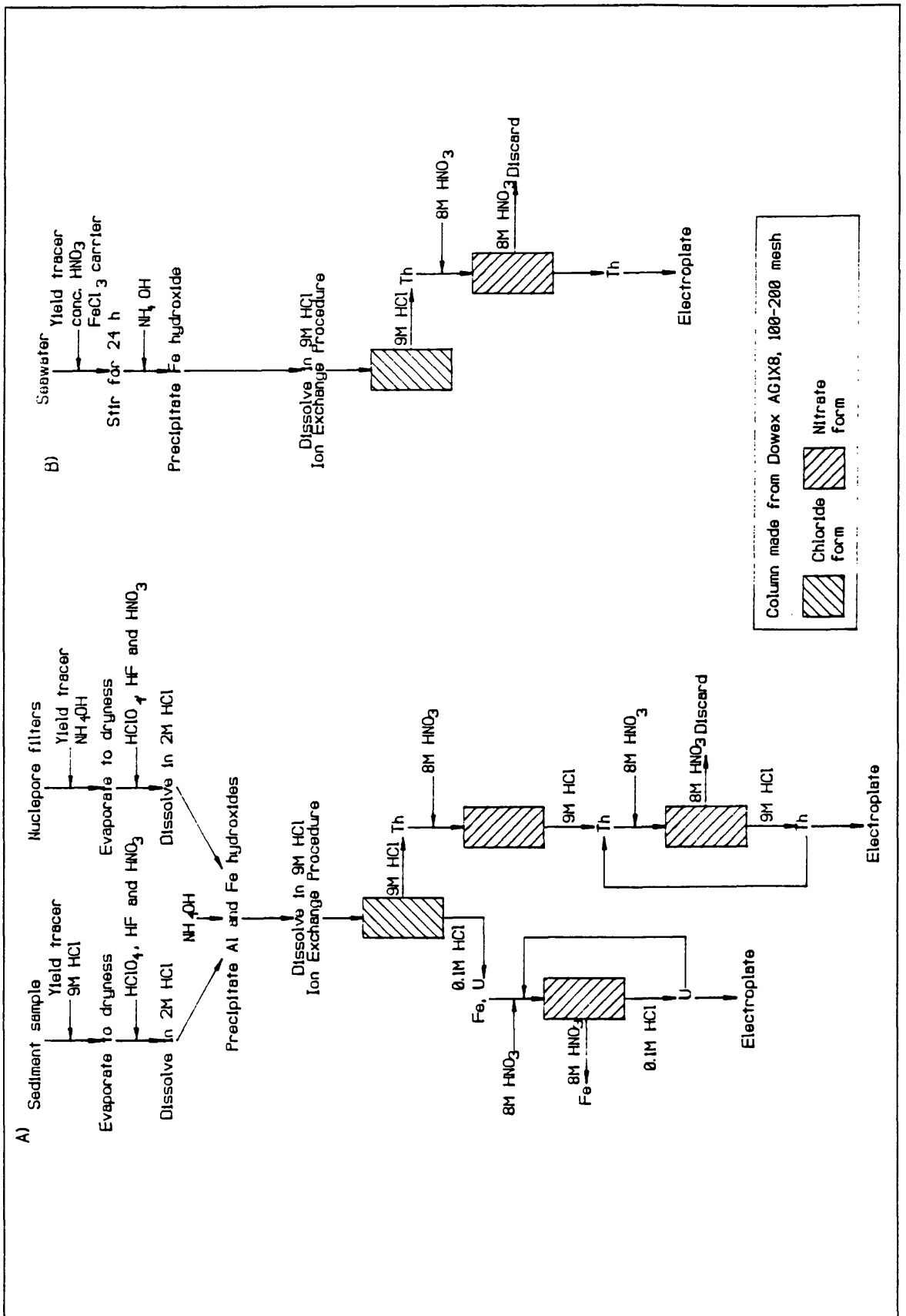


Figure 3.2: Typical procedures employed for ^{234}Th analysis of A) sediment (Aller and DeMaster, 1984) and B) seawater (Moran and Buesseler, 1993).

3.2.2 LSS as an alternative method

LS is a technique suitable for the analysis of both α and β emitters (section 1.3). It has much higher detection efficiencies for both α and β emitters than either α -spectrometry or gas proportional counting techniques, thus creating the possibility that the analysis could be performed on a smaller volume with shorter counting times being employed. Sample handling could become simpler and electrodeposition and manganese dioxide cartridges are avoided.

LSS has been employed in laboratory studies of thorium behaviour using either ^{234}Th (Niven and Moore, 1988) or ^{228}Th (Honeyman and Santschi, 1989), but in both cases these were restricted to artificial samples that needed no chemical purification prior to counting. Bouwer *et al.* (1979) and McDowell *et al.* (1980) reported the development of a technique for assaying ^{230}Th in phosphatic materials by LSS, using solvent extraction and the PERALS® spectrometer. In this procedure, the analyte is first dissolved and uranium and thorium are extracted together into TOPO (trioctyl phosphine oxide). Uranium is then extracted from the mixture with an Adogen 364 (a tertiary amine) extractive scintillator, leaving the thorium, which is extracted using a nonyldecylamine extractive scintillator. These extractive scintillators have since been marketed as URAEX® and THOREX® (McDowell and McDowell, 1994). This method cannot be directly applied to the analysis of ^{234}Th in seawater, partly because of the different sample matrix and partly because the PERALS® instrument rejects all β activity, although the use of an extractive scintillator, rather than an aqueous accepting cocktail, is feasible in a conventional LS spectrometer (section 3.3.3.3).

Anderson *et al.* (1991) demonstrated that LSS could be applied to the simultaneous determination of ^{234}Th in seawater with ^{230}Th as a yield tracer. This method was based on similar preparative chemistry to that which is employed for gas proportional counting, but sample volumes were reduced to 20 l and the counting time was limited to 300 min. The only problem with this technique was the overlapping spectra of $^{234\text{m}}\text{Pa}$ and ^{230}Th (Fig. 3.3), which had to be resolved using

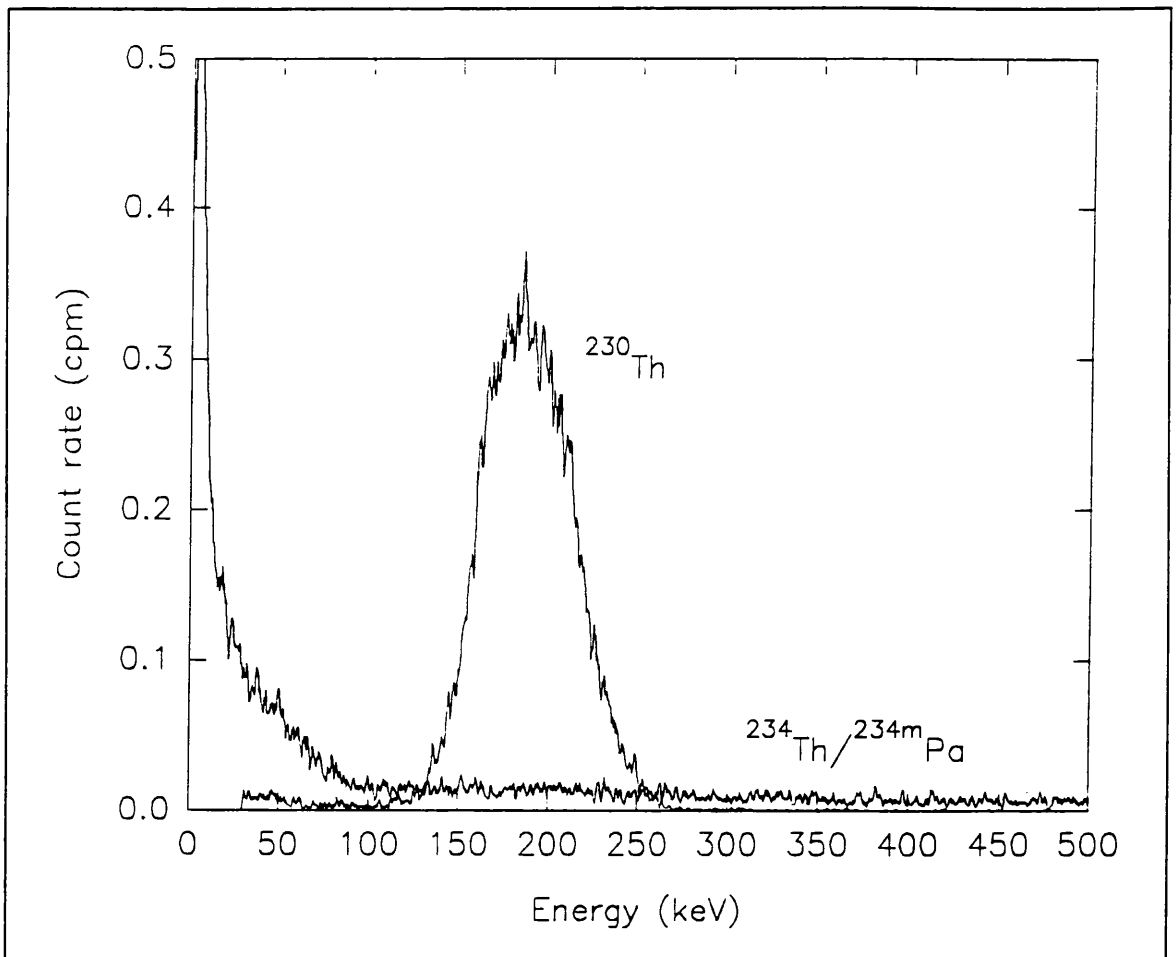


Figure 3.3: Spectrum from a seawater sample counted in the 2550 TR/AB (b) showing the ^{230}Th peak and the underlying $^{234}\text{Th}/^{234\text{m}}\text{Pa}$ continuum.

mathematical techniques. The procedure was successfully applied to a study of phytoplankton production by Cook *et al.* (in preparation) and LS spectrometers have been taken to sea successfully (Queirazza *et al.*, 1991). α/β LSS could solve the problem of overlapping spectra by separating the counts derived from $^{234}\text{Th} + ^{234\text{m}}\text{Pa}$ and ^{230}Th into two MCAs and, therefore, this was the approach taken in the present work.

3.3 DEVELOPMENT OF AN α/β LSS METHOD FOR ^{234}Th IN MARINE SAMPLES

The chemical separation procedure employed in this method has been adapted from that routinely used at the Scottish Universities Research and Reactor Centre (SURRC) for thorium analysis of rocks and fresh-water by α -spectrometry (MacKenzie *et al.*, 1994), which is based on that of Bacon

and Rosholt (1982). Method development covered two principal areas, namely optimization of the instrument and optimization of the chemical separation for the alternative sample matrices - seawater and marine particulate matter (the final counting source preparation was developed from the method used by Anderson *et al.* (1991)). It was necessary to prepare relatively high activity sources of ^{230}Th and ^{238}U (in equilibrium with ^{234}Th) for use in method development and as a yield tracer and for efficiency calibrations respectively, and this is also described.

3.3.1 Preparation of ^{234}Th and ^{230}Th spikes

A small quantity of uraninite (~ 0.5 g) was placed in a Teflon beaker with 20 ml of a 50:50 mixture of concentrated nitric and hydrochloric acids. The mixture was heated gently on a hotplate in order to effect dissolution. The resulting solution was counted on a germanium detector, to ascertain that the uranium series nuclides were in equilibrium to at least ^{230}Th and that there was an insignificant activity of ^{232}Th present. The solution was then separated into uranium and thorium fractions by anion exchange as described below (Fig. 3.4).

The solution was heated to near dryness and ~ 20 ml 9M hydrochloric acid was added. This procedure was repeated twice more, with increasing volumes of hydrochloric acid being added on each occasion, to ensure that there were no nitrate ions present. The remaining solution was taken up in 100 ml 9M hydrochloric acid, in preparation for adding to the first column. The solution was then split into two batches, each treated identically. The column consisted of Bio-Rad AG 1-X8 100-200 mesh (1 cm diameter x 10 cm length) converted to the chloride form by preconditioning with 50 ml 1M hydrochloric acid followed by 50 ml 9M hydrochloric acid. The uranium solution was added to the top of the column, and the eluent, together with 3 x 20 ml 9M hydrochloric acid washes, was collected in a beaker - this solution contained the thorium fraction, as ThCl_4 , being a neutral species, is not retained by the resin. The uranium, which was initially retained by the column, was eluted with 3 x 25 ml 1M hydrochloric acid, and this solution was then taken to dryness, redissolved in 50 ml 9M

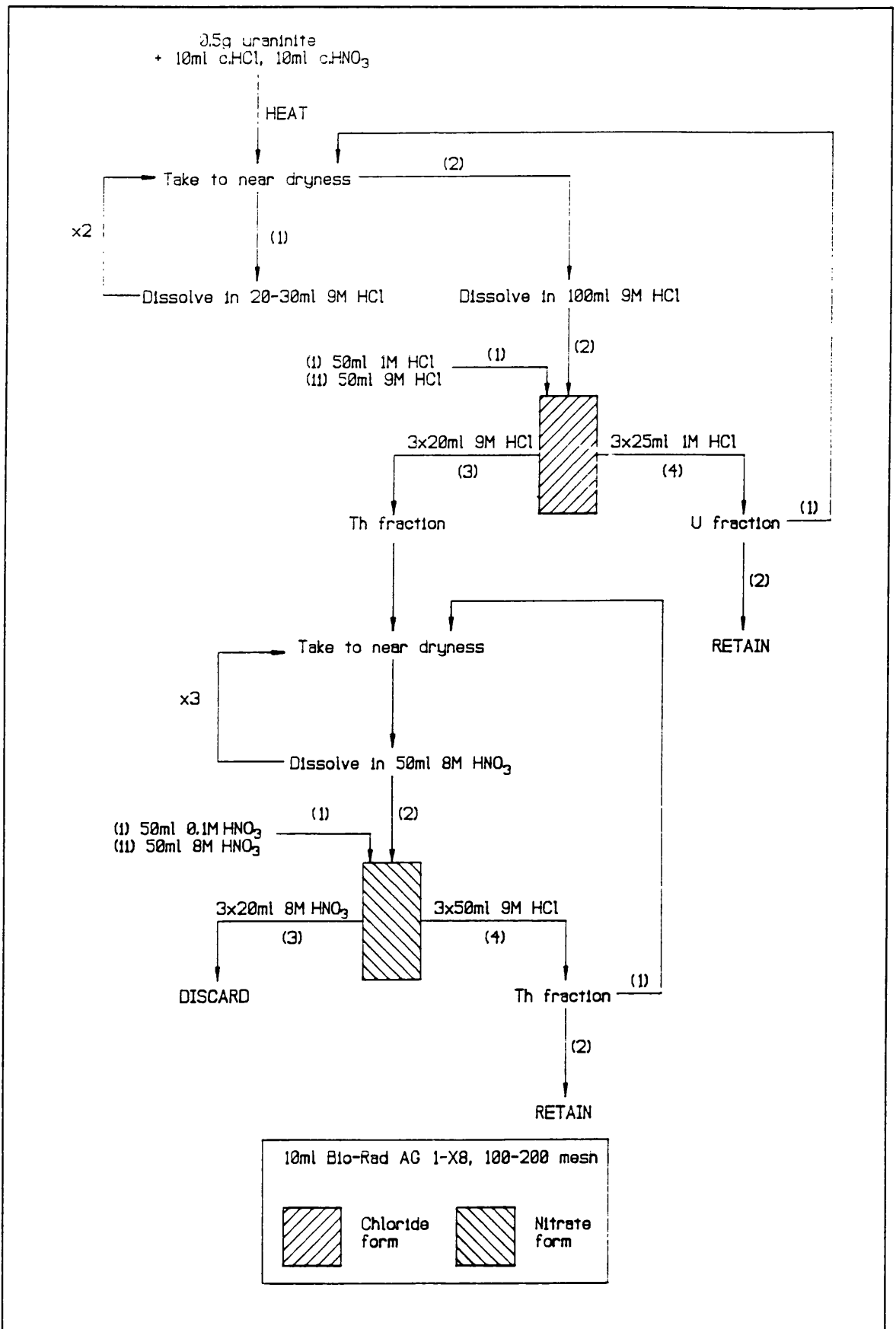


Figure 3.4: Separation procedure employed for spike preparation.

hydrochloric acid and passed through another column in the chloride form. The 9M hydrochloric acid eluent from this column was discarded and the uranium again eluted with 1M hydrochloric acid. The two batches of purified uranium solution were combined and taken to near dryness. The solution was made up to 50 ml with 9M hydrochloric acid and set aside.

In order to convert the thorium fraction to the nitrate form, it was repeatedly taken to near dryness (three times) and taken up in 50 ml 8M nitric acid. The second column was identical to the first, except that it had been preconditioned with 50 ml 0.1M nitric acid followed by 50 ml 8M nitric acid. The thorium solution was added to the column, which, in the nitrate form, retains the thorium. It was then washed with 3 x 20 ml 8M nitric acid and the eluent, together with these washings, was discarded. The thorium was then eluted with 3 x 50 ml 0.1M hydrochloric acid and the solution was converted to the nitrate form, in preparation for a second nitrate form column. A 0.1 ml aliquot of this solution was then counted by LS with no α/β separation for 10 min to estimate the recovery of ^{230}Th . It was found to be low (~ 70 cpm gross), so the procedure was adapted for the second batch of the spike solution by eluting the thorium from the nitrate column with 9M hydrochloric acid.

The uranium fraction consisted of ^{238}U and ^{234}U , with a small quantity of ^{235}U . The thorium fraction comprised ^{230}Th , together with any naturally occurring, short lived thorium isotopes that were present in the ore, including ^{234}Th . By ageing these solutions for approximately one year, ^{234}Th grows towards secular equilibrium in the uranium solution (after 1 y, 99.997% of equilibrium is reached) and decays away from the thorium solution (with the other isotopes), leaving a pure ^{230}Th spike (Figure 3.5 illustrates the decay and ingrowth of ^{234}Th over time). Small concentrations of ^{231}Th will also grow into the uranium solution (supported by ^{235}U), but interference from this nuclide ($t_{1/2} = 1.06$ d) can be avoided by allowing freshly separated ^{234}Th to decay for at least four days before counting.

The aged uranium solution was used to provide ^{234}Th spikes. A dilution was made up containing ~ 50 dpm ml^{-1} ^{238}U , which was characterized by ICP-MS (53.82 ± 0.001 dpm ml^{-1}), to be

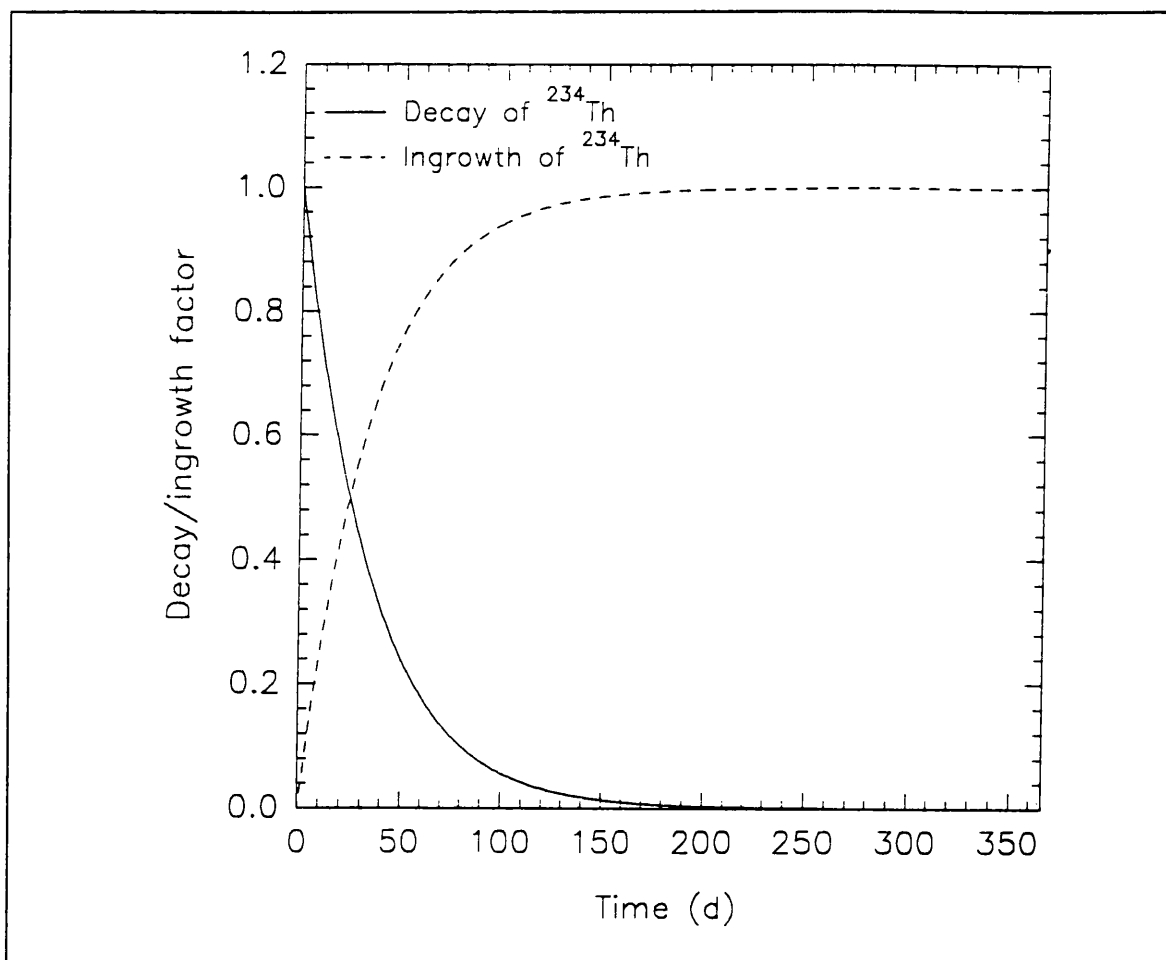


Figure 3.5: Decay and ingrowth of ^{234}Th in an unsupported and a supported situation respectively.

used for counting efficiency calibrations. The high activity uranium solution ($\sim 50,000$ dpm ^{238}U) was used for determining the optimum PDD, by passing the entire solution through a chloride column as described above. The eluted thorium is passed through a nitrate column and the uranium is eluted from the chloride column, taken to dryness and redissolved in 9M hydrochloric acid in preparation for its next use. Although a year is required for the solution to reach near equilibrium, sufficient ^{234}Th grows in for the solution to be reused after approximately one half-life (50% equilibrium, $\sim 25,000$ dpm). A working solution of the ^{230}Th spike was made up containing ~ 50 dpm ml^{-1} for spiking samples and method development.

3.3.2 Optimization of instrumental parameters

Some initial method development work was performed using both the Packard Tri-Carb® 2250

CA α/β and the 2550 TR/AB (a) instruments (section 2.2). However, the bulk of the analyses and most of the marine samples were analysed using the 2550 TR/AB (b). Three types of instrumental parameter have been examined and optimized, namely the PDD setting, the low-level count mode (LLCM) with the delay-before-burst (DBB) feature and the counting windows. The instrumental option was used to determine the optimum PDD (section 2.2.1.2) for the 2550 TR/AB (a) (Fig. 3.6) and again when the PMTs were changed (2550 TR/AB (b)) using high activity spikes of ^{234}Th and ^{230}Th (~ 25,000 dpm per vial). These were prepared by separating ^{234}Th from the uranium stock solution as described in section 3.3.1 and by passing 5 ml of the ^{230}Th stock solution, made up to 10 ml 8M nitric acid, through a nitrate column to remove interference from decay products. These solutions were taken to

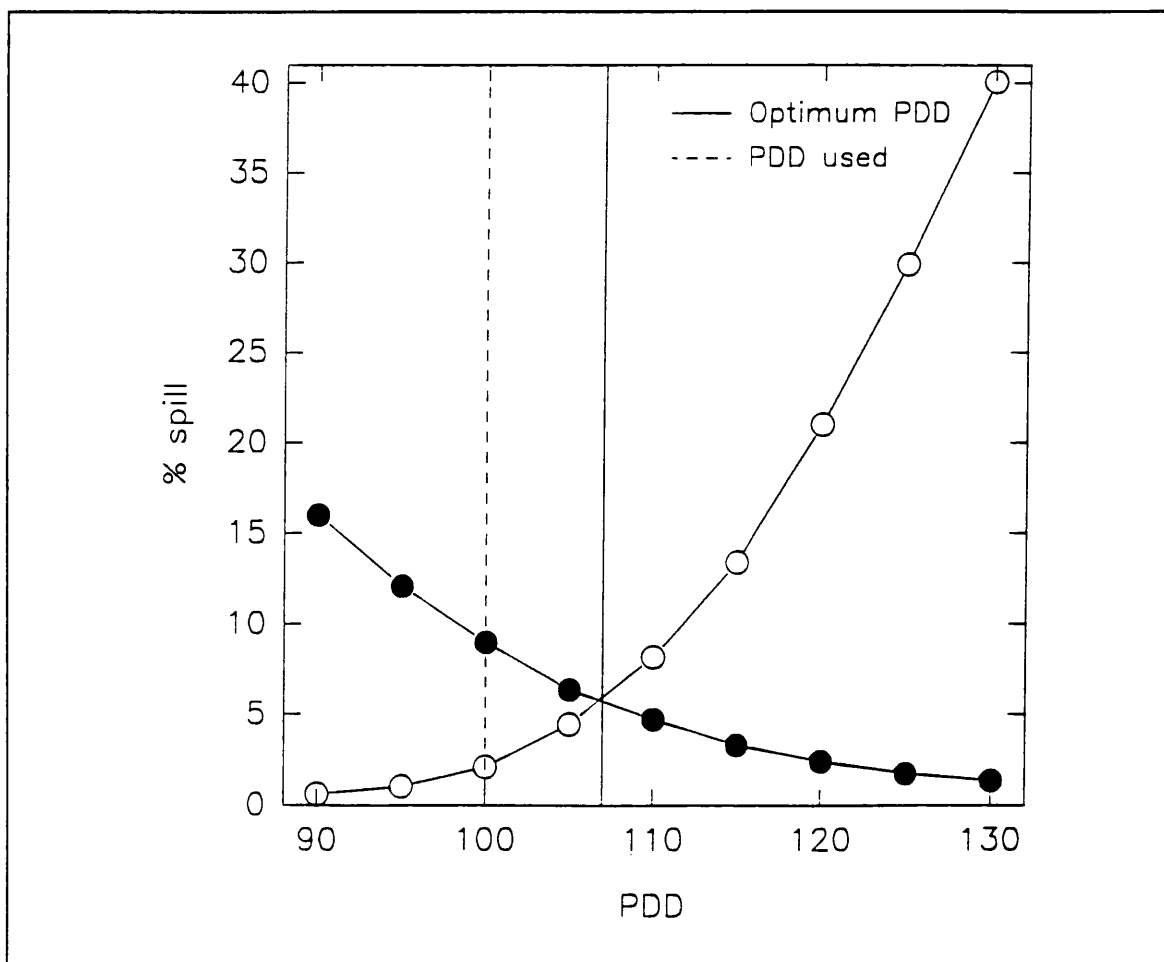


Figure 3.6: Instrumentally determined cross-over plot for ^{234}Th and ^{230}Th , showing the optimum PDD and the PDD employed, using the 2550 TR/AB (b).

dryness in the vial (7 ml glass) and treated as for samples (dissolved in 0.5 ml 0.1M hydrochloric acid and 4.91 g cocktail (Ultima Gold™ AB) added). For the 2550 TR/AB (a), although the optimum PDD was 107, the setting used for counting samples was 100, to minimize misclassification of α events without significantly increasing β misclassification into the α region of interest. Similarly, 110 was the setting used for the 2550 TR/AB (b) although the optimum PDD was 113. At this setting (PDD = 110), β misclassification into the α window (120-280 keV) was 0.13% and α misclassification into the β window (0-120 keV) was 0.08% of the total counts (0-2000 keV). These figures, which are based on net count rates, are lower than those given in Table 3.10, which are based on gross count rates. These % spills were deemed to be negligible for the activities seen in 10 l samples (25 dpm ^{234}Th and 50 dpm ^{230}Th maximum) and were assumed to be zero in all subsequent calculations.

The low-level option of this counter starts examining PMT anode pulses for after-pulsing after an initial period of 75 ns. As $^{234\text{m}}\text{Pa}$ is a high energy β emitter and, hence, will have relatively long PMT anode pulses with the delayed component often exceeding 75 ns, the use of the low-level option could cause a significant loss in counting efficiency (due to classifying β pulses as background), unless programmable DBB is employed to extend this period (section 1.2.2.2). High activity ^{234}Th and ^{230}Th spikes were again prepared as described above and these were counted for 30 min using the 2550 TR/AB (b) in the normal count mode (NCM) and the LLCM with no DBB, and then increasing the DBB in increments of 100 ns, with PDD=110. Alongside the high activity samples, a background sample was counted at the same settings, but for 400 min. Using the Replay™ feature of the counter, the spectra were processed to find the count rate in several regions of interest, namely that covering the α peak (120-280 keV) and the β counting region (0-120 keV), but also reducing this second window in increments of 2 keV, as the largest part of the background occurs in the first 10 keV of the spectrum, the final β counting window examined being 18-120 keV. The ^{234}Th data were decay corrected to the time of separation and the relative E^2/B figure of merit was calculated for each point.

The results from this experiment are shown in Table 3.1 and Figure 3.7. The maximum E^2/B value occurred with a window of 12-120 keV and DBB = 700 ns. A broad plateau occurs around this point extending down to a window of 6-120 keV, up to the upper limit and out to DBB = 300 ns for the 10-120 keV window. The E^2/B value falls off from DBB = 700 to DBB = 800 ns, indicating that LL/800 ns, chosen for the analysis of samples in early work (section 3.3.3.1, Table 3.6) may not have been the optimum setting. However, a maximum E^2/B figure of merit does not necessarily give rise to the lowest errors, as is discussed later (section 3.3.4).

3.3.3 Optimization of chemical separation procedure

Figure 3.8 illustrates the main features of the final, optimized analytical scheme developed in this work. The method described employs a 10 l seawater sample, although for some sample types with high particle fluxes, such as in an estuarine environment, it is preferable to increase this to 20 l in order to ensure that there is sufficient ^{234}Th present to exceed the limit of detection and to reduce errors due to counting statistics (section 3.3.4). This increase in volume has very little impact on the difficulty of the method, especially once the iron (III) hydroxide precipitation step is passed. To compensate for the larger volume additions of concentrated hydrochloric acid in the initial acidification step, iron (III) carrier and ammonium hydroxide are increased proportionally, all other steps remaining the same. Two periods of method development were undertaken, with sample numbers from each prefixed either T1 or T2.

Immediately after sampling, the sample was filtered, then acidified, spiked and an iron carrier was added (Fig. 3.8). Filtration was performed by one of two methods, the former being preferable with smaller sample sizes. The first method (Fig 3.9A) filters 10 l seawater in ~ 2 h by creating a vacuum in the receiving vessel, while the second (Fig 3.9B) can filter 20 l in ~ 20 min, using a diaphragm pump powered by compressed air. The most significant difference, in terms of the analysis, is that the first apparatus uses 9 cm diameter filters (0.2 μm cellulose nitrate membrane filters),

Table 3.1: Optimization of the E^2/B figure of merit for ^{234}Th using the normal count mode (NCM) and the low-level count mode (LLCM) of the 2550 TR/AB (b) with increasing delay-before-burst (DBB) in ns.

Window	Count mode	NCM	LL on	LL/100 ns	LL/200 ns	LL/300 ns	LL/400 ns	LL/500 ns	LL/600 ns	LL/700 ns	LL/800 ns
0-120 keV	Count rate (cpm)	28516.0	11617.3	16405.1	20236.9	22618.6	23936.2	25091.4	25457.4	25836.2	26095.7
	Background	20.86	5.76	6.79	8.15	9.10	9.69	10.23	10.52	10.93	11.29
	Relative efficiency	1	0.407	0.575	0.710	0.793	0.839	0.880	0.893	0.906	0.915
	E^2/B	479	288	487	619	691	726	757	758	751	742
2-120 keV	Count rate (cpm)	27785.5	11014.4	15789.1	19593.2	21971.9	23279.6	24328.5	24754.8	25140.6	25381.7
	Background	18.30	4.41	5.41	6.71	7.54	7.97	8.55	8.86	9.19	9.58
	Relative efficiency	0.974	0.386	0.554	0.687	0.771	0.816	0.853	0.868	0.882	0.890
	E^2/B	518	338	567	703	788	835	851	850	846	827
4-120 keV	Count rate (cpm)	26143.9	9915.1	14631.1	18318.7	20642.7	21921.1	22826.5	14166.4	23700.4	23892.6
	Background	14.27	3.18	4.16	5.26	5.99	6.36	6.78	7.02	7.30	7.47
	Relative efficiency	0.917	0.348	0.513	0.642	0.724	0.769	0.800	0.817	0.831	0.838
	E^2/B	589	380	633	784	875	930	944	951	946	940
6-120 keV	Count rate (cpm)	24606.6	9000.8	13612.3	17154.1	19418.7	20652.8	21427.6	21945.1	22334.0	22497.8
	Background	11.37	2.34	3.20	4.07	4.82	5.07	5.47	5.65	5.84	6.00
	Relative efficiency	0.863	0.316	0.477	0.602	0.681	0.724	0.751	0.770	0.783	0.789
	E^2/B	655	427	711	890	962	1034	1031	1049	1050	1038
8-120 keV	Count rate (cpm)	23210.8	8241.6	12757.6	16124.0	18316.9	19493.2	20183.2	20721.0	21088.7	21247.2
	Background	9.53	1.74	2.57	3.32	4.10	4.22	4.61	4.75	4.93	5.10
	Relative efficiency	0.814	0.289	0.447	0.565	0.642	0.684	0.708	0.727	0.740	0.745
	E^2/B	695	480	777	962	1005	1109	1087	1113	1111	1088

10-120 keV	Count rate (cpm)	21941.2	7609.1	12011.3	15198.0	17312.1	18437.6	19052.9	19594.7	19938.7	20093.6
	Background	8.21	1.39	2.19	2.89	3.63	3.74	4.02	4.20	4.34	4.49
	Relative efficiency	0.769	0.267	0.421	0.533	0.607	0.647	0.668	0.687	0.699	0.705
	E ² /B	720	513	809	983	1015	1119	1110	1124	1126	1107
12-120 keV	Count rate (cpm)	20775.0	7066.9	11356.5	13558.5	15330.0	15879.4	18011.4	18556.1	18864.5	19021.3
	Background	7.18	1.17	1.98	2.58	3.25	3.43	3.69	3.83	3.86	4.09
	Relative efficiency	0.729	0.248	0.398	0.475	0.538	0.557	0.632	0.651	0.662	0.667
	E ² /B	740	526	800	875	891	905	1082	1107	1135	1088
14-120 keV	Count rate (cpm)	19671.6	6610.4	10771.9	13608.4	15541.2	16557.2	17024.9	17585.0	17865.5	18014.4
	Background	6.45	1.04	1.82	2.38	2.98	3.20	3.39	3.51	3.59	3.80
	Relative efficiency	0.690	0.232	0.378	0.477	0.545	0.581	0.597	0.617	0.627	0.632
	E ² /B	738	518	785	956	997	1055	1051	1085	1095	1051
16-120 keV	Count rate (cpm)	18616.4	6194.7	10236.6	12889.7	14725.5	15686.8	16106.7	16663.0	16948.4	17074.6
	Background	5.89	0.93	1.73	2.21	2.79	2.99	3.20	3.27	3.34	3.54
	Relative efficiency	0.653	0.217	0.359	0.452	0.516	0.550	0.565	0.584	0.594	0.599
	E ² /B	724	506	745	924	943	1012	998	1043	1056	1014
18-120 keV	Count rate (cpm)	17633.7	5759.6	9686.5	12182.3	13950.0	14865.2	15221.3	15782.7	16050.9	16163.9
	Background	5.44	0.84	1.61	2.05	2.60	2.82	3.02	3.08	3.13	3.32
	Relative efficiency	0.618	0.202	0.340	0.427	0.489	0.521	0.534	0.553	0.563	0.567
	E ² /B	702	486	718	889	920	963	944	993	1013	968

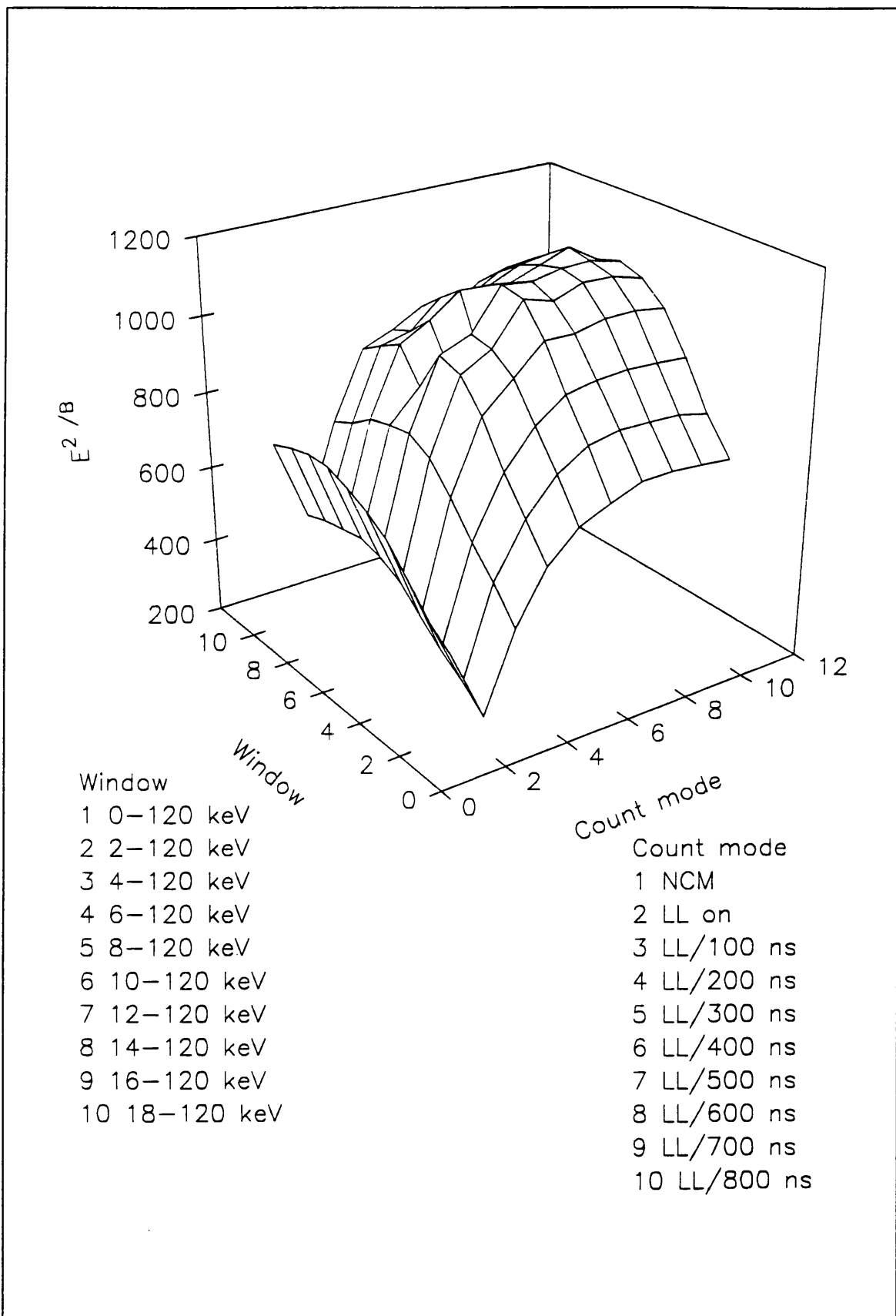


Figure 3.7: Optimization of the β counting window and low-level option for ^{234}Th using the 2550 TR/AB (b).

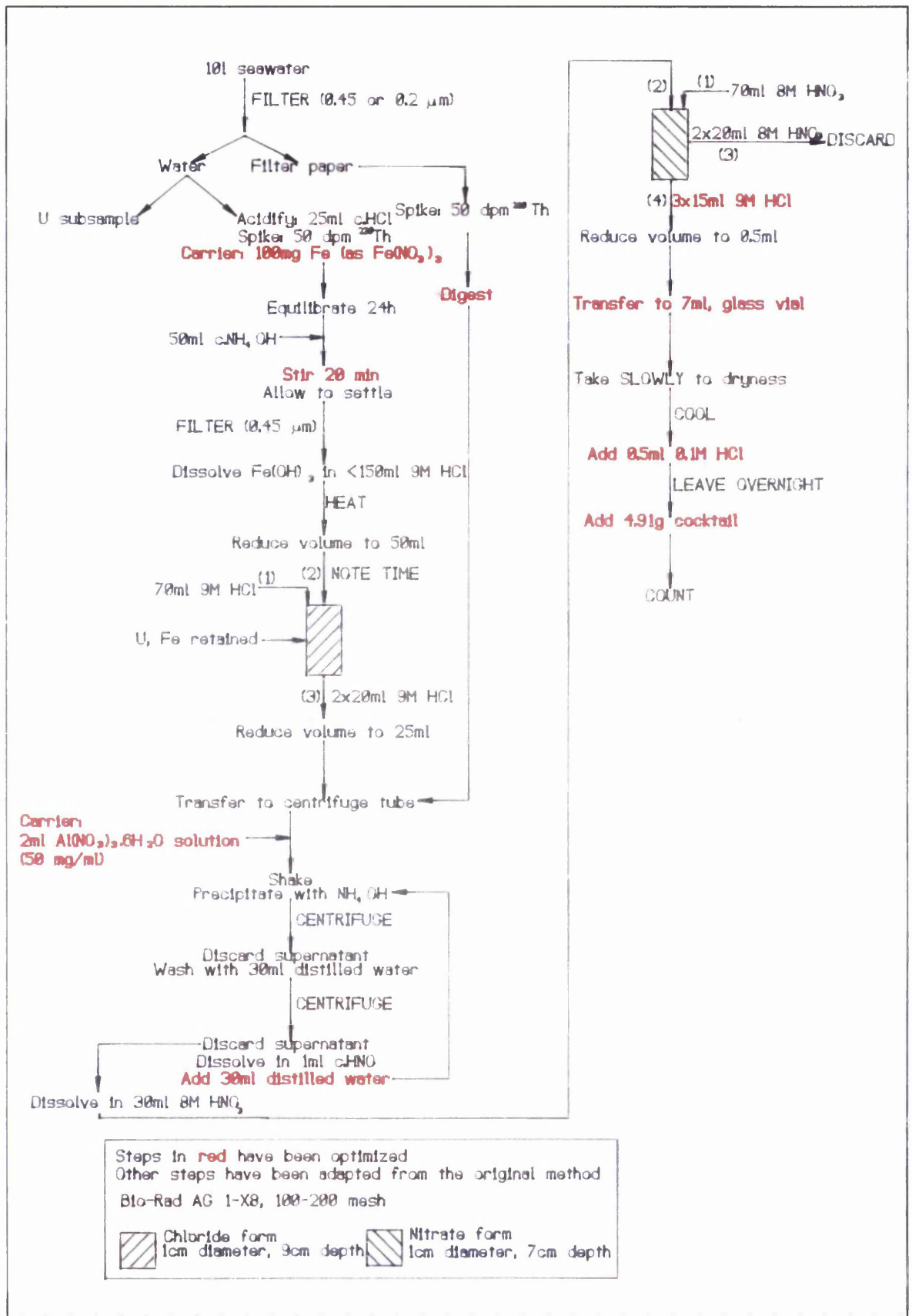


Figure 3.8: The separation procedure developed and employed in the present work for the determination of ²³⁴Th in seawater and marine particulate material.

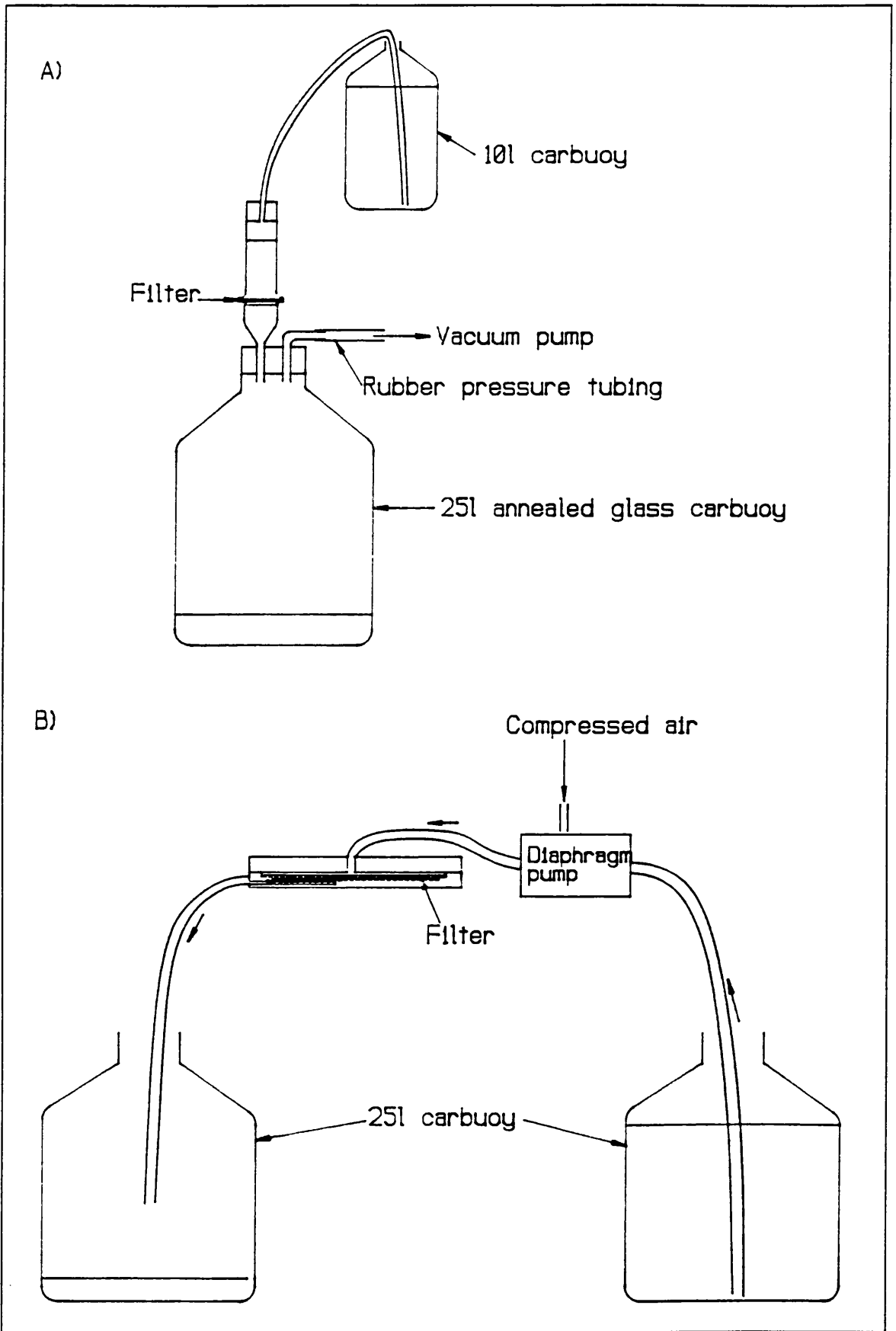


Figure 3.9: The two types of filtration apparatus employed in the present work.

whereas the second uses 293 mm diameter filters of the same type, which are significantly more expensive and more difficult to digest due to their larger size (section 3.3.3.2). The wet filter was then folded and sealed in a labelled plastic bag for later analysis.

3.3.3.1 Dissolved ^{234}Th analysis

The iron carrier was purified by solvent extraction, prior to addition, to minimize interferences by uranium and thorium. The purification was performed by dissolving 11 g $\text{Fe}(\text{NO}_3)_3 \cdot 9\text{H}_2\text{O}$ in 50 ml 9M hydrochloric acid. The iron was then extracted into 3 x 50 ml DIPE (di-isopropyl ether). The aqueous phase was discarded and the iron back-extracted into 150 ml 1.2M hydrochloric acid, from which any traces of DIPE were removed by gentle heating. This solution contained $\sim 10 \text{ mg Fe ml}^{-1}$.

Wei and Hung (1993) determined that the minimum time needed for the equilibration of the yield tracer and ^{234}Th in the dissolved fraction ($< 0.45 \mu\text{m}$) is four hours, if the sample is continuously stirred for this period. This experiment was carried out on 5 l aliquots, so the possibility remains that larger samples could require longer equilibration periods. In consensus with previously published work, which employed larger sample volumes (*e.g.* Bacon and Rutgers van der Loeff, 1989) (Table 3.2), the sample was thoroughly stirred, for $\sim 1 \text{ min}$, upon addition of the spike and then left, without additional stirring, for a 24 h equilibration period. After this time, ammonium hydroxide was added, to precipitate iron (III) hydroxide, which is known to co-precipitate thorium and, to a certain extent, uranium. The amount of uranium that is scavenged is controlled by the concentration of iron carrier that is used (Tanaka *et al.*, 1983) and, therefore, some workers have minimized the quantity of iron added to samples to reduce ingrowth from ^{238}U . Kershaw and Young (1988), for example, reported only 1-2% recovery of ^{238}U with an addition of 0.1 mg Fe l^{-1} (Table 3.2). However, if small concentrations of iron are used, the recovery of thorium will also be reduced, unless compensated for by long periods of stirring and settling. Bacon and Rutgers van der Loeff (1989) and Moran and Buesseler (1993) reported collection of the iron (III) hydroxide precipitate by centrifugation, which is the probable reason

for their use of long settling periods (Table 3.2). Kershaw and Young (1988) separated their precipitate by filtering through a 0.22 μm membrane filter and leaching with 9M hydrochloric acid. This was the procedure adopted here, either filtering through GF/A papers using a Buchner apparatus or using 0.45 μm filters with the apparatus illustrated in Figure 3.9B.

Table 3.2: Comparison of a selection of reported details of spike equilibration and iron (III) hydroxide precipitation procedures.

Reference	Sample volume (l)	Spike equilibration		Iron (III) hydroxide precipitation	
		Time allowed	Stirring?	Added iron	Time allowed
Matsumoto (1975)	40-50	" a few hours"	no	500 mg Fe	-- ^a
Tanaka <i>et al.</i> (1983)	50	6 h	yes	100 mg Fe	-- ^a
McKee <i>et al.</i> (1984)	20-40	24 h	no	-- ^a	-- ^a
Coale and Bruland (1987)	30	-- ^a	-- ^a	-- ^a	-- ^a
Kershaw and Young (1988)	99	-- ^a	-- ^a	10 mg Fe (as FeCl ₃)	-- ^a
Bacon and Rutgers van der Loeff (1989)	20	≥ 24 h	no	250 mg Fe	12-24 h no stirring
Anderson <i>et al.</i> (1991) ^b	20	-- ^a	-- ^a	100 mg Fe (as FeCl ₃)	2 h stirring ~ 12 h settling
Moran and Buessler (1993)	< 70	24 h	yes	90 mg Fe (as FeCl ₃)	12 h no stirring

^a Not reported.

^b Liquid scintillation method. All others are gas proportional counting methods.

As the iron (III) hydroxide precipitate was to be collected by filtration, not requiring long settling periods, it was decided to optimize recovery of thorium and to separate ²³⁴Th from ²³⁸U as quickly as

possible to minimize ingrowth. Therefore, four 10 l coastal seawater samples (samples T2/7-T2/10) that had previously been filtered, acidified, spiked and equilibrated were compared with different additions of iron carrier and different stirring periods. After processing in the normal manner, the samples were counted in the 2550 TR/AB (b) for 30 min at PDD=110 in the LLCM with DBB=800 ns. The different procedures used and the results obtained are summarized in Table 3.3. Yields were determined by the method outlined in section 3.3.4 for marine samples.

Table 3.3: The effect of added iron concentration and stirring times on the recovery of ^{230}Th from 10 l seawater samples. Errors are quoted at the 1σ level of confidence.

Sample	Iron added	Stirring period	Yield (%)
T2/7	50 mg	20 min	69.9 ± 2.3
T2/8	100 mg	20 min	94.6 ± 2.7
T2/9	200 mg	20 min	93.0 ± 2.7
T2/10	100 mg	2 h	97.5 ± 2.8

It was found that doubling the quantity of iron added to 100 mg resulted in an increase in the yield of 25%. However, further increases in either iron concentration or stirring time did not result in significant increases in yield. Therefore, it was decided to adopt the procedure used for sample T2/8 for all further analyses, which is equivalent to the concentrations employed by Matsumoto (1975) and Bacon and Rutgers van der Loeff (1989). The resulting precipitate was leached from the paper using not more than 150 ml 9M hydrochloric acid. This upper limit was used to restrict the amount of time spent reducing the volume of acid before adding it to the first ion-exchange column (Fig 3.8).

After washing the thorium through the chloride form column (Fig. 3.8), the sample is in ~ 90 ml 9M hydrochloric acid. All the chloride ions have to be removed from the solution before passing the sample through the nitrate form column, as the resin is now required to retain thorium. Several

different methods have been used for this conversion step, including taking the sample to dryness and redissolving in nitric acid (*e.g.* Moran and Buessler, 1993) and taking the sample to near dryness and adding 3-4 times the volume of nitric acid (*e.g.* Anderson and Fleer, 1982). Taking the sample to dryness was not seen as desirable, as the particle reactivity of thorium means that it can readily adsorb to surfaces if no acid is present, with potential reduction in yields and contamination of glassware. The method of Anderson and Fleer (1982) was tried unsuccessfully in preliminary work on this method. Even with several repeated volume reductions, the potential for chloride ions to remain in solution is present, with an associated loss of thorium, and this method also increases the time taken relative to the method adopted.

MacKenzie *et al.* (1994) used an aluminium hydroxide precipitation to convert the system to the nitrate form. In this method, 100 mg Al^{3+} are added to the sample and aluminium hydroxide is precipitated with ammonium hydroxide. The precipitate is then centrifuged, washed with distilled water, recentrifuged and dissolved in nitric acid (A. M. Whitton, personal communication, 1992). The quantity of aluminium and the number of precipitation steps that are needed were examined by spiking 90 ml aliquots of 9M hydrochloric acid with 1 ml ^{230}Th working solution. These samples (T1/1-T1/4) were then reduced in volume to ~ 30 ml and varying amounts of aluminium (as $\text{Al}(\text{NO}_3)_3$ dissolved in 1M nitric acid) were added (10-100 mg Al^{3+} per sample). The samples were then treated as for the method outlined above, passed through nitrate columns and vialled. They were each counted in the NCM (with no α/β separation) on the 2250 CA α/β for 100 min.

A further experiment was performed on the aluminium hydroxide precipitation step using two samples (T1/23 and T1/24), which consisted of 10 l demineralized water spiked with 1 ml ^{230}Th working solution. Each was treated as illustrated in Figure 3.8, but with 100 mg Al^{3+} being added to each. One was precipitated once before adding to the nitrate column and the other was precipitated, dissolved and reprecipitated. These samples were counted on the 2550 TR/AB (a) for 10 min in the

NCM (with no α/β separation). The results from both these experiments are given in Table 3.4.

Table 3.4: Effect of varying aluminium concentration and number of precipitations on the recovery of ^{230}Th from spiked solutions. Errors are quoted at the 1σ level of confidence.

Sample	Aluminium added	No. precipitations	Net α count rate (cpm)	Yield (%)
T1/1	10 mg	1	42.6 ± 0.7	83.0 ± 1.6
T1/2	20 mg	1	31.4 ± 0.6	61.2 ± 1.3
T1/3	40 mg	1	44.3 ± 0.7	86.4 ± 1.6
T1/4	100 mg	1	9.1 ± 0.4	17.7 ± 0.7
T1/23	100 mg	1	22.8 ± 1.6	44.4 ± 3.1
T1/24	100 mg	2	30.4 ± 1.8	59.3 ± 3.6

It can be seen that even 10 mg Al^{3+} produces an $\sim 80\%$ yield. Samples T1/3 and T1/4 went to dryness during the volume reduction step and it is possible that these yields are low because of this error. Still, it can be concluded that ~ 10 mg Al^{3+} per sample is sufficient to obtain reasonable recovery of the thorium. Furthermore, samples T1/23 and T1/24 show that performing the precipitation twice does not reduce the recovery, but might improve it due to more thorough removal of the chloride ions. The concentration of aluminium carrier added to seawater samples was 8.4 mg Al^{3+} per sample (this concentration was chosen for convenience, as 100 mg $\text{Al}(\text{NO}_3)_3 \cdot 6\text{H}_2\text{O}$ is equivalent to 8.4 mg Al^{3+}). A centrifugation time/speed of 1.5 min at 5000 rpm is sufficient to separate the precipitate (R. Anderson, personal communication, 1992).

The second ion-exchange column was converted to the nitrate form by preconditioning with 8M nitric acid, allowing it to retain thorium, which could then be eluted by washing with either 9M hydrochloric (*e.g.* Anderson and Fleer, 1982) or 0.1M nitric acid (*e.g.* Bacon and Rosholt, 1982). However, when the spikes were prepared, eluting with 0.1M nitric acid appeared to result in a low

recovery of thorium (section 3.3.1). The effectiveness of 9M hydrochloric acid and 0.1M nitric acid as eluents for thorium was compared by spiking 2 x 50 ml 8M nitric acid with 1 ml ^{230}Th working solution and adding each to a nitrate form column. Each column was washed with 3 x 20 ml 8M nitric acid before the thorium was eluted with 3 x 50 ml of the appropriate acid. The samples (T1/A and T1/5) were then vialled and counted in the 2250 CA α/β in the NCM (no α/β separation) for 200 min. This comparison showed that 9M hydrochloric acid resulted in approximately twice the recovery of thorium as obtained using 0.1M nitric acid (Table 3.5).

An alternative eluent for thorium is 1.2M hydrochloric acid (A. M. Whitton, personal communication, 1992) and this was also compared to 9M hydrochloric acid. In this experiment, a 0.1 ml aliquot of the high activity ^{230}Th spike (~ 500 dpm) was added to 50 ml 8M nitric acid and passed through a nitrate form column. Each fraction of acid was collected separately as it came off the column (*i.e.* the 50 ml 8M nitric acid that had contained the spike, 3 x 20 ml 8M nitric acid washings and 3 x 50 ml eluent acid) (samples T1/8-T1/21) and was vialled and counted as above for 100 min or in the 2550 TR/AB (a) in the NCM (no α/β separation) for 10 min. Table 3.5 shows that while 9M hydrochloric acid and 1.2M hydrochloric acid are equally effective for the elution of thorium, more is eluted in the first 50 ml with the 9M strength. As the aim was to reduce column washings to a minimum, 9M hydrochloric acid was adopted for subsequent work and the volume used for eluting thorium reduced to 3 x 15 ml.

After the nitrate form column, the sample was prepared for counting. It is at this point that the method is substantially different from those using other β counting techniques. Anderson *et al.* (1991), in their LS method, took the sample to dryness in a 7 ml low potassium glass vial, redissolved the sample in 0.5 ml 1M hydrochloric acid and added 5 g Hionic FluorTM cocktail before counting. As this method did not use α/β separation, the choice of cocktail, vial and quantity of acid employed were affected by different factors. The sample preparation procedure employed in the present work is

Table 3.5: Comparison of the effect of different elution acids on thorium recovery from nitrate form columns. Errors are quoted at the 1 σ level of confidence.

Sample	Eluent	Volume (ml)	Net α count rate (cpm)	Yield (%)	% total net α count rate ^a
T1/A	0.1M HNO ₃	150	17.9 \pm 0.3	34.9 \pm 0.7	-- ^b
T1/5	9M HCl	150	34.6 \pm 0.4	67.4 \pm 1.1	-- ^b
T1/8	8M HNO ₃	50	19.3 \pm 0.5	-- ^b	4.5 \pm 0.1
T1/10	8M HNO ₃	20	2.8 \pm 0.2	-- ^b	0.7 \pm 0.1
T1/12	8M HNO ₃	20	0.9 \pm 0.5	-- ^b	0.2 \pm 0.1
T1/14	8M HNO ₃	20	1.3 \pm 0.2	-- ^b	0.3 \pm 0.05
T1/16	9M HCl	50	391.9 \pm 2.0	-- ^b	91.6 \pm 0.7
T1/18	9M HCl	50	9.2 \pm 0.3	-- ^b	2.2 \pm 0.1
T1/20	9M HCl	50	2.4 \pm 0.2	-- ^b	0.6 \pm 0.1
T1/9	8M HNO ₃	50	9.1 \pm 1.1	-- ^b	1.9 \pm 0.2
T1/11	8M HNO ₃	20	1.2 \pm 0.6	-- ^b	0.2 \pm 0.1
T1/13	8M HNO ₃	20	0.6 \pm 0.2	-- ^b	0.1 \pm 0.04
T1/15	8M HNO ₃	20	1.3 \pm 0.6	-- ^b	0.3 \pm 0.1
T1/17	1.2M HCl	50	412.4 \pm 2.0	-- ^b	84.2 \pm 0.6
T1/19	1.2M HCl	50	54.9 \pm 0.8	-- ^b	11.2 \pm 0.2
T1/21	1.2M HCl	50	10.5 \pm 0.4	-- ^b	2.1 \pm 0.1

- a The net ²³⁰Th count rate for each fraction determined as a percentage of the total ²³⁰Th count rate eluted from the column.
- b Not determined.

discussed below before turning to the experiments that were used to determine the choice of vial type and acid strength for dissolution of the sample. The choice of cocktail was based on the work described in section 2.3.1.

Following Anderson *et al.* (1991), the sample was reduced in volume to ~ 1 ml and transferred, with 8M nitric acid washes of less than 1 ml, to a 7 ml low potassium glass vial. The sample was then slowly taken to complete dryness on a hotplate. At this stage, a white residue was

left in the vial, probably composed principally of aluminium salts. On occasions, this residue was observed to contain a slight brown coloration, due to the presence of some unoxidized organic material. When such samples are prepared for counting, a yellow coloration persists, with resulting colour quenching. This problem was avoided by examining each vial, and redissolving any coloured residues with 8M nitric acid and taking the sample back to dryness. This procedure removed any impurity that was causing the coloration and allowed the method to proceed as usual. In taking samples to dryness in the vial, care was taken that dryness was only just reached, with the vial being removed from the heat as soon as the last acid had evaporated to ensure later dissolution.

Once the vial had cooled, 0.5 ml 0.1M hydrochloric acid was added and the vial left to stand overnight before the addition of cocktail. On occasion, samples failed to dissolve fully under these conditions, and so stronger acid (9M hydrochloric acid) was used to effect dissolution of the sample before taking it to dryness again. This usually resolved the problem, which was often the result of the sample being left to dry for too long. Samples were left to cool before the acid was added so that no evaporative losses occur prior to addition of the cocktail, with the aim of minimizing variations in quenching.

The cocktail used for initial method development was the experimental cocktail 07A (section 2.3.1), but this was later replaced with the commercial formulation Ultima Gold™ AB. As with the method of Anderson *et al.* (1991), 5 ml cocktail were used, as this is the maximum quantity of cocktail readily usable in a 7 ml vial. This quantity of cocktail was weighed out (4.91 g) as this can be done more quickly and accurately than by dispensing it volumetrically.

The choice of counting vial was considered, in relation to both the degree of α/β separation that could be achieved and background reduction. Glass vials have the advantage that the sample could be taken to dryness in the vial and redissolved with no transferring steps and associated losses. The method considered for use with plastic vials involved taking the sample to dryness in a 7 ml glass

vial (these having smaller surface areas than the smallest available beakers), redissolving and transferring an aliquot quantitatively to a plastic vial before adding cocktail. Plastic vials have the advantage of lower backgrounds, but suffer from reactions with the cocktail over time (section 1.2.3.2) and do not give as good α/β separation as glass vials (section 2.3.3). Glass and plastic vials were compared for both efficiency and background using the 2550 TR/AB (b) instrument (Table 3.6), and the E^2/B figure of merit found for the β count rate. Although the plastic vials had lower backgrounds in the NCM, this did not compensate for their other disadvantages. Once the background reduction features of the 2550 TR/AB were taken into account, *i.e.* the LLCM and DBB, plastic vials lost even this advantage over glass when comparing the figures of merit. This experiment led to the adoption of the LLCM with DBB = 800 ns as the preferred count mode, before this feature was investigated more thoroughly (section 3.3.2), and 7 ml vials were used rather than 20 ml vials due to their lower background (section 1.2.3.2).

The optimized β counting window referred to in Table 3.6, and also later in the text, was found using a computer program developed at the SURRC. This program employs the general method outlined below: a "spike" sample and a "background" sample are counted under the required counting conditions and the spectra are saved. The program is then able to use these spectra to find the window that gives the highest value for the E^2/B figure of merit, by looking at all the possible upper and lower limits for regions of interest. The background sample consisted of 0.5ml 0.1M hydrochloric acid and 4.91 g cocktail and the spike sample was 1 ml ^{230}Th working solution (the same ~ 50 dpm ml^{-1} solution as used for spiking the samples) taken to dryness in a vial and prepared for counting in the same way as the background sample. These are referred to as "backgrounds" and "spikes" from now onwards.

As quenching had previously been found to adversely affect α/β separation efficiency (section 2.3.2), the amount of acid that was required to redissolve the sample in the vial was examined. Three

Table 3.6: Comparison of the background and efficiency obtainable with 7 ml glass and plastic vials for ^{234}Th , using the low-level count mode (LL) with delay-before-burst (in ns) of the 2550 TR/AB (b).

Glass						
Count mode	0-2000 keV	0-120 keV	Optimized window			
	Background (cpm)	Background (cpm)	Window (keV)	Background (cpm)	Relative efficiency	E^2/B
NCM ^a	24.38	19.25	16-108.5	4.87	51.0	534
LL/500 ns ^b	13.77	9.98	12.0-79.5	2.86	48.0	804
LL/600 ns ^b	14.38	10.26	11.5-86.5	3.32	50.2	758
LL/700 ns ^b	15.34	11.10	12.0-79.5	3.36	48.8	712
LL/800 ns ^b	15.32	11.09	13.0-83.0	3.02	48.4	777
Plastic						
Count mode	0-2000 keV	0-150 keV	Optimized window			
	Background (cpm)	Background (cpm)	Window	Background (cpm)	Relative efficiency	E^2/B
NCM ^a	17.55	15.18	17.5-139.5	4.92	53.1	574
LL/500 ns ^b	14.33	11.34	15.5-102.0	3.675	48.4	637
LL/600 ns ^b	14.32	11.14	12.5-149.5	4.97	56.4	641
LL/700 ns ^b	13.77	10.77	13.5-149.0	4.47	55.7	694
LL/800 ns ^b	14.43	11.13	14.0-144.5	4.65	55.0	652

a Normal count mode.

b Low-level count mode with delay-before-burst in ns.

different strengths of hydrochloric acid were compared, namely 0.1M, 0.5M and 1M, redissolving 0.1ml aliquots of the ^{230}Th spike (~ 500 dpm) that had been taken to dryness in separate vials. The samples were counted in the NCM of the 2250 CA α/β , with no α/β separation. The dissolution ability of each acid was compared by examining both the yield and the shape of the α peak (Table 3.7). If the nuclide is not fully dissolved and in homogeneous contact with the cocktail, the α spectrum is broadened (McDowell and McDowell, 1994). The results given in Table 3.7 show that there was no

significant increase in recovery with the 1M acid and the α peak was found entirely within the 120-350 keV window for all three acid strengths. Therefore, the 0.1M acid was used as it resulted in the highest tSIE.

Table 3.7: Comparison of the effectiveness of different hydrochloric acid strengths in redissolving ^{230}Th spike solutions taken to dryness in 7 ml glass vials.

Acid strength	tSIE	Count rate (cpm) (0-2000 keV)	Count rate (cpm) (120-350 keV)	% count rate in α window
0.1M	566	575	535	93.0
0.5M	543	574	534	93.0
1M	544	580	541	93.3

3.3.3.2 Suspended particulate ^{234}Th analysis

The wet filter paper was placed in a beaker and carefully spiked with 1 ml ^{230}Th working solution. It was then left to dry at room temperature overnight, covered with a watch glass. Two methods for the dissolution of membrane filters, together with any suspended particulate material they contain, were examined, along with small variations within each procedure. Many of the published methods involve the use of perchloric acid (*e.g.* Anderson and Flear, 1982), which could not be used in this laboratory for safety reasons.

The first method was based on ashing the filter, in a beaker, at 450°C overnight and then dissolving the residue. Based on the method of Anderson and Flear (1982), the residues were initially soaked in concentrated ammonium hydroxide and taken to dryness before oxidizing agents were added. Combinations of concentrated nitric acid, hydrogen peroxide and concentrated hydrochloric acid were used. Table 3.8 uses data from the analysis of the particulate (P) fraction of some duplicate estuarine samples (AR1 and 2P, LG1 and 2P, HB1 and 2P) collected at various locations in the Firth

of Clyde and associated sea lochs (Fig. 3.10) (see section 4.3.1 for the exact collection procedure and an interpretation of the data). Examination of the yields showed that the combination of hydrogen peroxide and nitric acid was generally more effective than nitric acid alone (Table 3.8), but hydrochloric acid still needed to be added on some occasions, when the residues were more stubborn.

Table 3.8: Comparison of recovery of thorium from filter papers treated in various ways. Errors are quoted at the 1σ level of confidence.

Sample	Treatment	Net α count rate (cpm)	Yield (%)
T2/1	ashed, no cover	15.85 ± 0.73	30.3 ± 1.5
T2/2	ashed, with cover	26.55 ± 0.94	50.7 ± 1.9
AR1P	HNO ₃	26.07 ± 0.36	48.0 ± 0.9
AR2P	HNO ₃	26.75 ± 0.37	49.2 ± 0.9
LG1P	HNO ₃	33.58 ± 0.41	61.8 ± 1.1
LG2P	HNO ₃ + H ₂ O ₂	35.37 ± 0.42	65.1 ± 1.1
HB1P	HNO ₃ + H ₂ O ₂	42.00 ± 0.46	77.3 ± 1.3
HB2P	HNO ₃ + H ₂ O ₂	42.59 ± 0.46	78.3 ± 1.3

In some cases, the residue did not appear to dissolve completely, but the recovery of thorium still appeared to be reasonably high. Furthermore, an experiment which consisted of spiking two blank filter papers and ashing them, with (sample T2/2) and without a cover (sample T2/1), and analysing the residue showed that the resulting yield can be very low, even though the residue dissolved readily (Table 3.8). Together, these results imply that ashing filters is a step that should be avoided if possible. A potential problem with this approach is that hydrofluoric acid was not used, with the possibility of not dissolving siliceous material, resulting in erroneous yield determinations.

Therefore, an alternative method was examined, using a microwave digestion system. For this method, the unspiked filter paper was placed in a 160 ml Teflon digestion vessel and then spiked as

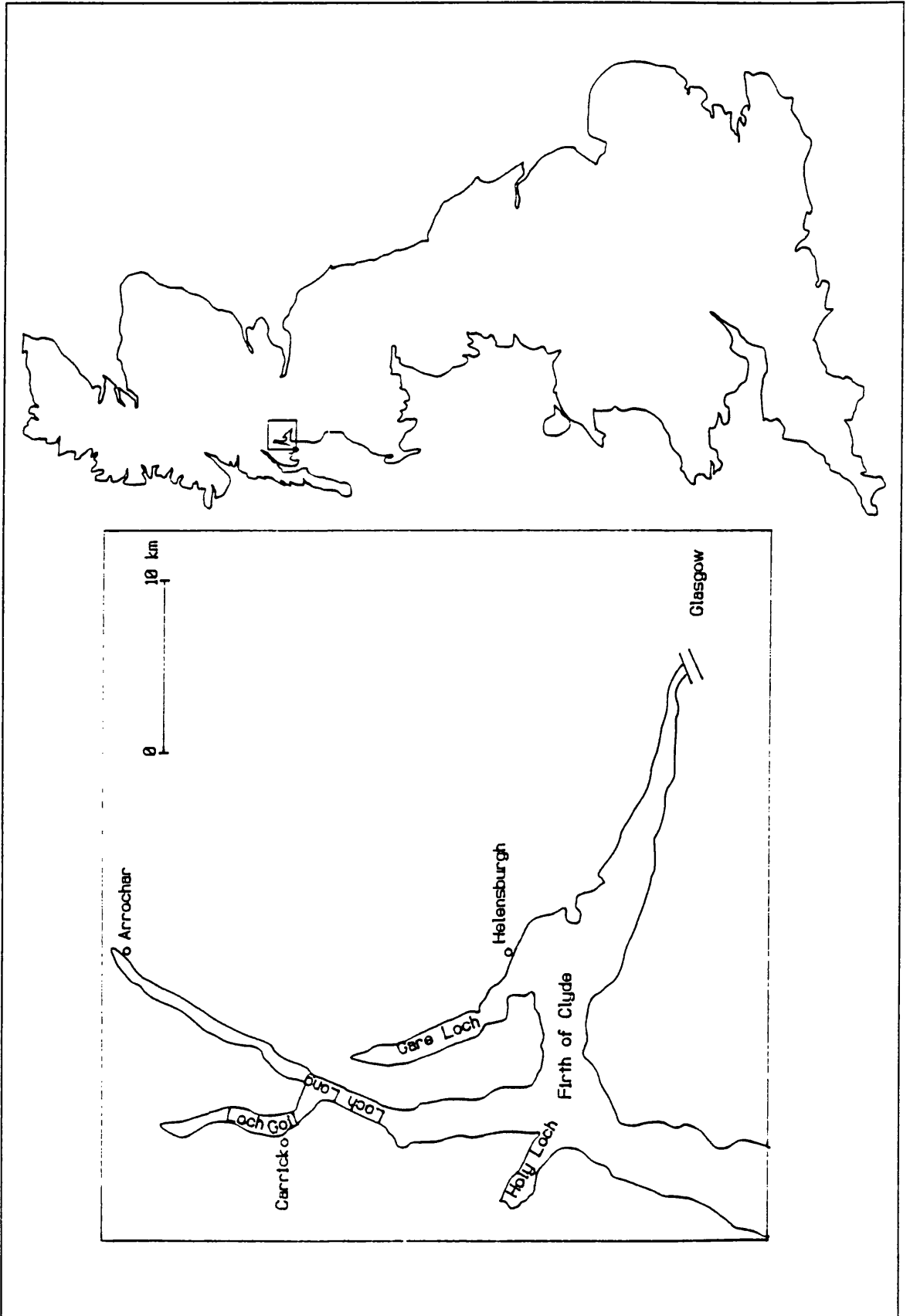


Figure 3.10: Sampling locations for samples HB (Helensburgh), AR (Arrochar) and LG (Carrick).

above. 5 ml concentrated nitric acid, 1 ml hydrogen peroxide and 1-2 ml hydrofluoric acid were added to the filter and the container capped and placed in the holder for microwaving. A torque of 23 Nm was applied to the lid of each vessel (the holder takes six samples at a time) to seal it. The samples were then digested in a step programme (1 min at 250 W, unpulsed; 2 min 0 W; 5 min 250 W, unpulsed; 5 min 400 W; 5 min 600 W) twice, with cooling between each programme. After the second digestion programme, the microwave was left venting overnight to allow the samples to cool thoroughly before opening the container.

The samples were transferred to Teflon beakers, with distilled water rinses, and the volume reduced on a hotplate. The walls of the beaker were rinsed down with 8M nitric acid and the sample taken to near dryness, before taking up in 30 ml 8M nitric acid. Unfortunately, it was not possible to assess the yields obtained by this method as the batch of samples analysed in this way were spiked with a solution that contained insufficient activity to allow a yield determination. However, the solutions obtained appeared to be clearer than on previous occasions and smaller quantities of acid were used, which helps minimize potential reagent contamination. The disadvantage of this technique is the limitation of sample sizes - there is danger of an explosive reaction if an attempt is made to digest more than 0.5 g organic material. Therefore, only the smaller filter paper sizes could be analysed by this method, the 293 mm diameter papers needing to be ashed or simply dissolved by heating in Teflon beakers with the same combination of acids.

After digestion, the filter paper samples were taken up in 30 ml 8M nitric acid and followed the same analytical procedure as the aqueous phase from the beginning of the aluminium hydroxide precipitation, although, in some cases, the quantity of aluminium added to the samples needed to be increased to 12.6 mg Al^{3+} to obtain sufficient precipitate.

3.3.3.3 Extractive scintillators

The method described in Figure 3.8 is still too complex for performing completely onboard

ship. Therefore, the possibility of using an extractive scintillator was examined, with the aim of replacing the second ion-exchange column and reducing the need to boil off large quantities of acid. The extractive scintillator tested was THOREX®, which requires the sample to be in the sulphate form at pH 2. Therefore, an initial experiment (performed in duplicate) consisted of taking 1 ml 0.05M sulphuric acid and 1 ml ²³⁰Th working solution to dryness together and transferring the residue to a 20 ml glass vial with 3 x 2 ml portions 0.1M sodium sulphate solution. The pH was adjusted to 2 with sulphuric acid and 1.5 ml THOREX® were added, with the weight of the vial and its contents being measured before and after the addition. The mixture was then shaken thoroughly to ensure equilibration of thorium and the phases were allowed to separate. As much of the organic phase as possible was then transferred to a 7 ml glass vial and weighed. The samples (TH/A and TH/B) were counted in the 2550 TR/AB (b) in the LLCM, DBB = 800 ns, PDD = 110 for 30 min. Table 3.9 shows that the yields from this experiment were rather low, but this could be accounted for by the quantity of the organic phase that could be transferred. This proportion could be increased by using a more suitable equilibration vessel, so a further experiment was performed to take the method a step further.

Table 3.9: The recovery of ²³⁰Th from spiked solutions using the extractive scintillator THOREX®. Errors are quoted at the 1σ level of confidence.

Sample	Mass added (g)	Mass transferred (g)	Net α count rate (cpm)	Yield (%)	Relative yield ^a (%)
TH/A	1.3256	0.4676	12.3 ± 0.7	23.4 ± 1.3	66.3
TH/B	1.3593	0.7673	29.4 ± 1.0	56.2 ± 2.0	99.5

^a Yield multiplied by the percentage of THOREX® transferred.

Four samples were made up, consisting of 1 ml ²³⁰Th working solution and 2 ml aluminium carrier solution (4.2 mg Al³⁺ ml⁻¹ - either aluminium nitrate or sulphate) made up to 30 ml with distilled

water. The aluminium hydroxide precipitation was then carried out as usual (Fig. 3.8) and the resulting precipitate dissolved in a minimum volume of 8M nitric acid. The solution was then transferred to a 7 ml glass vial containing 1 ml 0.05M sulphuric acid, with distilled water rinses, and taken to near dryness. Then, 4 ml 0.1M sodium sulphate and 1 ml 0.05M sulphuric acid were added to the vials to dissolve the residue, convert the solution to the sulphate form and attain the correct pH. Although the vials were left overnight it was not possible to dissolve the residue. More sulphuric acid was added, but the residue remained insoluble. This would be the step at which the use of THOREX® would be a beneficial variation of the procedure, so it did not seem to be worthwhile to pursue this alternative method, as additional interfering ions would be present in marine samples, which would only serve to further reduce yields and complicate the extraction method.

3.3.3.4 Manganese dioxide columns

Another attempt was made to circumvent some of the more laborious and complex parts of the procedure, in particular the reduction of large volumes of acid, by passing the filtered and spiked, but not acidified, sample through a manganese dioxide column as an alternative to the iron (III) hydroxide precipitation. The ^{230}Th spike could be used to accurately assess the adsorption of thorium onto the manganese dioxide, which could then be dissolved in a small quantity of acid (< 10 ml). The analysis could then proceed as normal, but using micro-columns and substantially reduced quantities of acid. In this way, only a final volume reduction would be needed at the vialing stage, making the analysis faster and more compatible with the ship-board environment.

The manganese dioxide was prepared by mixing 250 ml 5M manganese chloride with 250 ml 6M sodium hydroxide in a beaker to form a manganese hydroxide precipitate. This mixture was left to stand, with occasional stirring, until the precipitate had dried and partially oxidized. It was then ground in a pestle and mortar and passed through 150 μm and 45 μm sieves, the middle portion being retained. To make up the column, the powder was slurried with distilled water to remove the

finer and loaded to a 5 cm depth (column diameter = 1 cm), and this was then attached to the base of a 10 l reservoir (Fig. 3.11). The column was primed with distilled water until the water ran clear and then a sample was placed in the reservoir. Although the sample ran through the column at a sufficiently high rate for the first few hours, it soon became blocked, perhaps due to the solid phase gradually absorbing water and swelling. Therefore, it was concluded that while this variation on the method had potential, some kind of support was needed for the manganese dioxide, such as the acrylic fibre used in manganese dioxide cartridges (section 3.2.2.1).

3.3.3.5 The effect of variable quenching

In Chapter 2 it was noted that quenching plays an important role in the efficiency of α/β separation LSS (section 2.3.2). When the first batch of marine samples was analysed by this method (section 4.3.1.3), it was found that the tSIE varied by up to 40 units, despite rigorous sample preparation procedures. Therefore, the effect of quenching was studied, over the range of tSIE found in these samples, *i.e.* 430-390, on the counting efficiency of ^{234}Th and ^{230}Th within the windows used. This parameter was used, in addition to the % spill, as changes in the degree of misclassification will appear as changes in counting efficiency, on top of those changes brought about by shifts in the energy spectrum.

In section 2.3.2, it was shown that the effect of quenching on α/β separation is dependent on the quenching agent used. However, with environmental samples it is difficult to identify the chemical that is causing variations in quenching within a batch. Therefore, nitromethane was chosen as the quenching agent in this experiment, with the knowledge that it might not bring about the same effect as the quenching agent in the marine samples, but hypothesizing that its effects would be more pronounced. In addition, the range of tSIEs covered was small and the effects of quenching were examined again by manipulating the counting windows for the marine samples (section 4.3.1.3) to see if any change in the results could be brought about. Nitromethane quenching would be expected to

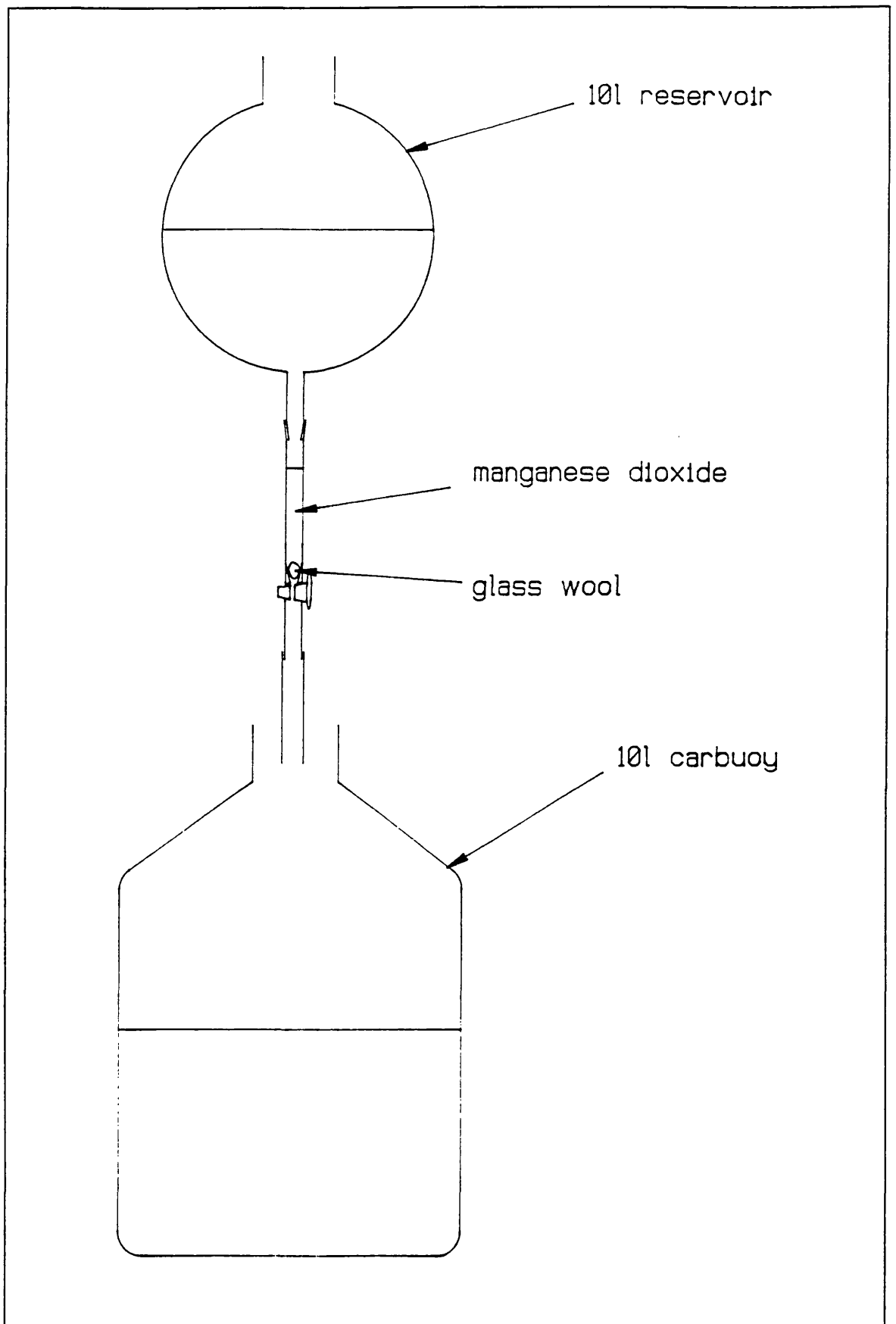


Figure 3.11: Manganese dioxide column apparatus.

cause an increase in % spill_β, but a decrease in % spill_α, causing β counting efficiencies to apparently increase as tSIEs decrease. However, the trends shown in section 2.3.2 were for tSIE changes of several hundred units, whereas the differences here are of a much smaller magnitude. Therefore, it was possible for the β counting efficiency to be constant over the small quenching range experienced with the samples, avoiding the need for any quench correction.

High activity ²³⁴Th and ²³⁰Th spike samples (~ 20,000 dpm) were made up as previously described, and prepared for counting in the same manner as marine samples. A quenching mixture was made up, which consisted of 2% nitromethane in 4.91 g cocktail and 0.5 ml 0.1M hydrochloric acid. This solution was then added to the high activity samples in 20 μl aliquots, each bringing about a change of ~ 5 tSIE units, from a starting point of 432 tSIE units.

The samples were counted for 5 min in the 2550 TR/AB (b), with no quenching agent added, at PDD = 110 in both the NCM and the LLCM with DBB = 800 ns, with two β windows - an open window of 0-120 keV and an optimized window of 13-83 keV. An aliquot of the quenching mixture was added and the samples were shaken thoroughly and allowed to equilibrate for 2 min. The tSIEs were then determined and the samples were recounted in both the count modes described above. This procedure was repeated until 220 μl of the quenching mixture had been added. The % spill_β used in Table 3.10 was defined to be the % of ²³⁰Th counts in the α window that appeared in the β window and *vice versa* for the % spill_α.

The results from this study are given in Table 3.10 and Figure 3.12. The range of tSIEs covered extends beyond the range found with the samples, but only the points that fall within the range are illustrated in Figure 3.12. The trend in tSIEs for the first three samples (0, 20 and 40 μl added quench) is of interest, as each value is greater than the last, contrary to expectation. This effect could be due to insufficient cooling prior to the start of the experiment, however, from the third point onwards the trend is as expected, indicating that a constant temperature had been reached. When

Table 3.10: The effect of quenching on ^{234}Th and ^{230}Th counting efficiencies, using the 2550 TR/AB (b) in the normal (NCM) and low-level (LL/800 ns) count modes with open (0-120 keV) and optimized (13-83 keV) windows. Errors are quoted at the 1σ level of confidence. All ^{234}Th activities have been decay corrected to time of separation.

A) Open window, NCM							
Addition of quench (μl)	tSIE ^a	^{234}Th (0-120 keV)			^{230}Th (110-280 keV)		
		cpm _{$\beta(\beta)$} ^b	cpm _{$\alpha(\alpha)$} ^c	% spill _{α}	cpm _{$\alpha(\alpha)$} ^c	cpm _{$\beta(\beta)$} ^b	% spill _{β}
0	432	18626 ± 61	22.4	0.12	25432 ± 71	40.6	0.16
20	439	18712 ± 61	30.6	0.16	25477 ± 71	57.2	0.23
40	436	18738 ± 61	31.8	0.17	25453 ± 71	56.2	0.22
60	423	18904 ± 62	27.2	0.14	25412 ± 71	61.8	0.24
80	419	18859 ± 61	24.4	0.13	25485 ± 71	52.0	0.20
100	414	18972 ± 62	25.4	0.13	25205 ± 71	65.0	0.26
120	408	18923 ± 62	24.0	0.13	25205 ± 71	68.8	0.27
140	401	19074 ± 62	26.2	0.14	25307 ± 71	74.4	0.29
160	397	19134 ± 62	26.0	0.14	25221 ± 71	80.8	0.32
180	394	19061 ± 62	21.4	0.11	25222 ± 71	81.0	0.32
200	389	18881 ± 62	24.0	0.13	25176 ± 71	80.0	0.32
220	382	19037 ± 62	20.8	0.11	25147 ± 71	80.6	0.32

B) Open window, LL/800 ns							
Addition of quench (μl)	tSIE ^a	^{234}Th (0-120 keV)			^{230}Th (110-280 keV)		
		cpm _{$\beta(\beta)$} ^b	cpm _{$\alpha(\alpha)$} ^c	% spill _{α}	cpm _{$\alpha(\alpha)$} ^c	cpm _{$\beta(\beta)$} ^b	% spill _{β}
0	432	17535 ± 59	39.6	0.23	25370 ± 71	24.0	0.10
20	439	17479 ± 59	30.2	0.17	25459 ± 71	24.6	0.10
40	436	17399 ± 59	31.2	0.18	25310 ± 71	36.2	0.14
60	423	17555 ± 59	25.2	0.14	25408 ± 71	36.4	0.14
80	419	17536 ± 59	25.0	0.14	25453 ± 71	34.0	0.13
100	414	17625 ± 59	23.4	0.13	25415 ± 71	42.8	0.17
120	408	17594 ± 59	25.0	0.14	25260 ± 71	44.8	0.18
140	401	17594 ± 59	28.2	0.16	25397 ± 71	47.8	0.19
160	397	17636 ± 59	23.6	0.13	25238 ± 71	51.6	0.20
180	394	17595 ± 59	25.0	0.14	25347 ± 71	55.6	0.22
200	389	17633 ± 59	22.2	0.13	25304 ± 71	60.6	0.24
220	382	17718 ± 60	26.8	0.15	25276 ± 71	57.0	0.23

C) Optimized window, NCM							
Addition of quench (μ l)	tSIE	^{234}Th (13-83 keV)			^{230}Th (120-280 keV)		
		cpm $_{\beta(B)}$ ^b	cpm $_{\alpha(\alpha)}$ ^c	% spill $_{\alpha}$	cpm $_{\alpha(\alpha)}$ ^c	cpm $_{\beta(B)}$ ^b	% spill $_{\beta}$
0	432	12907 \pm 51	21.0	0.16	25423 \pm 71	19.2	0.08
20	439	12970 \pm 51	27.6	0.21	25460 \pm 71	23.8	0.09
40	436	12973 \pm 51	28.2	0.22	25437 \pm 71	25.2	0.10
60	423	12982 \pm 51	24.4	0.19	25397 \pm 71	23.2	0.09
80	419	12962 \pm 51	21.4	0.17	25470 \pm 71	18.8	0.07
100	414	12981 \pm 51	22.2	0.17	25187 \pm 71	25.4	0.10
120	408	12924 \pm 51	21.6	0.17	25181 \pm 71	28.0	0.11
140	401	12924 \pm 51	23.8	0.18	25281 \pm 71	29.0	0.12
160	397	12981 \pm 51	23.6	0.18	25194 \pm 71	33.2	0.13
180	394	12919 \pm 51	18.2	0.14	25182 \pm 71	31.8	0.13
200	389	12679 \pm 50	21.6	0.17	25134 \pm 71	33.6	0.13
220	382	12723 \pm 50	18.4	0.14	25103 \pm 71	34.0	0.14

D) Optimized window, LL/800 ns							
Addition of quench (μ l)	tSIE ^a	^{234}Th (13-83 keV)			^{230}Th (120-280 keV)		
		cpm $_{\beta(B)}$ ^b	cpm $_{\alpha(\alpha)}$ ^c	% spill $_{\alpha}$	cpm $_{\alpha(\alpha)}$ ^c	cpm $_{\beta(B)}$ ^b	% spill $_{\beta}$
0	432	12232 \pm 49	21.0	0.17	25359 \pm 71	7.6	0.03
20	439	12178 \pm 49	26.6	0.22	25443 \pm 71	7.2	0.03
40	436	12055 \pm 49	28.6	0.24	25297 \pm 71	11.8	0.05
60	423	12069 \pm 49	21.4	0.18	25394 \pm 71	11.6	0.05
80	419	12108 \pm 49	21.8	0.18	25440 \pm 71	10.6	0.04
100	414	12042 \pm 49	22.0	0.18	25398 \pm 71	16.4	0.07
120	408	11978 \pm 49	22.6	0.19	25240 \pm 71	15.4	0.06
140	401	11986 \pm 49	25.2	0.21	25374 \pm 71	14.6	0.06
160	397	11972 \pm 49	20.8	0.17	25211 \pm 71	17.0	0.07
180	394	11900 \pm 49	21.8	0.18	25311 \pm 71	18.4	0.07
200	389	11899 \pm 49	20.0	0.17	25263 \pm 71	16.2	0.06
220	382	11888 \pm 49	24.2	0.20	25225 \pm 71	17.2	0.07

- a* Mean tSIE for α and β emitter.
b Count rate in the β window of the β MCA.
c Count rate in the α window of the α MCA.

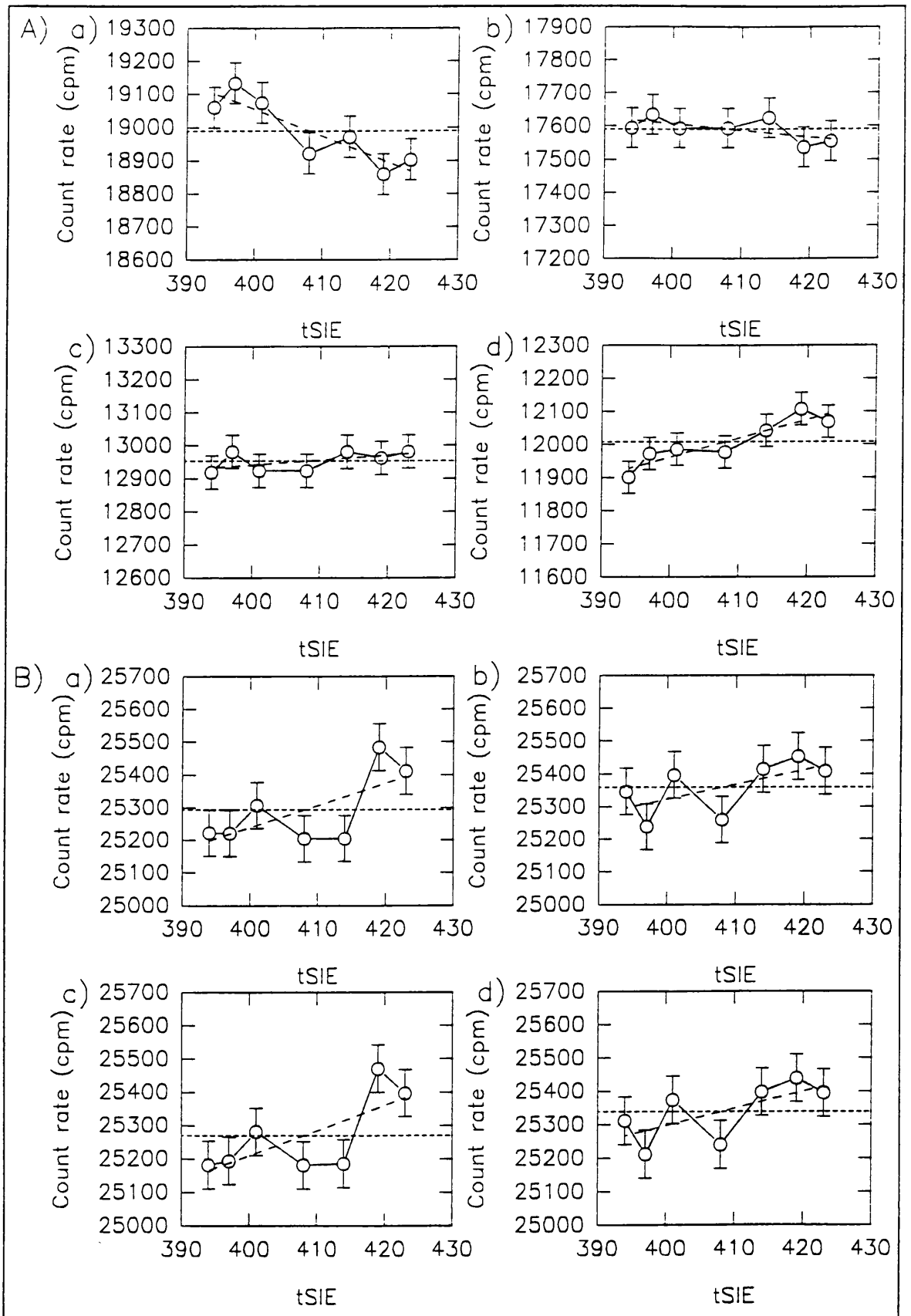


Figure 3.12: The effect of quenching on counting efficiency for ^{234}Th (A) and ^{230}Th (B) in the NCM (a,c) and LLCM (b,d) using open (a,b) and optimized (c,d) windows.

the entire data set is taken it is apparent that there is an overall upwards (open window) or downwards (optimized window) trend in the ^{234}Th counting efficiency as quenching increases. The discrepancy between these trends is due to the rate at which events are lost at the lower energy end of the spectrum, as compared to the rate at which they are gained at the higher energy end of the counting window. However, when the data are restricted to those points which fall within the experimental range, it becomes apparent that the LL/800 ns (open window) and the NCM (optimized window) fulfil the requirements for constant counting efficiency with quenching for ^{234}Th . The narrower ^{230}Th window shows that the α counting efficiency changes with quenching, due to the lower limit of the peak moving out of the window. By increasing the window to 110-280 keV, the change in counting efficiency is reduced and for the LLCM can be regarded as negligible.

The changes found in the % spills were small ($< 0.2\%$) and are not sufficiently large to account for any observed changes in counting efficiency. In addition, they are also low enough to cause no problems in changes in misclassification. The maximum % spills found here were 0.32% from the ^{230}Th spectrum into the β region of interest and 0.23% from the ^{234}Th spectrum into the α region of interest. Increasing the size of the α window from 120-280 keV to 110-280 keV (keeping the β window constant) had no effect on the % spill $_{\beta}$, but results in an increase in the % spill $_{\alpha}$ of 0.02%. However, this change is more than compensated for by the effect on the counting efficiency.

3.3.3.6 ^{238}U analysis

^{238}U was determined on a 50 ml subsample of the filtered water. Initially this was carried out by ICP-MS by taking a 9.8 ml aliquot of the sample and adding 0.2 ml ^{236}U spike (81.6 ng ml $^{-1}$). The ^{238}U working solution was diluted appropriately with 2% nitric acid (1:100 twice to give 0.005 dpm ml $^{-1}$, then 1:5 when needed to give 0.001 dpm ml $^{-1}$) to give a similar concentration and aliquots were made up as samples to run alongside the waters as a check. This procedure worked well, however a new instrument was acquired, which could not utilize samples with such a high dissolved solid

concentration. Therefore, a dilution of 0.5 ml to 10 ml with 2% nitric acid was required, but the ^{238}U data thus obtained were consistently low, both for the known activity sample and from the estimated salinity values. This was later attributed to an inaccuracy in the ^{236}U spike (T. M. Shimmield, personal communication, 1994), although the variations in calculated ^{238}U activities did not appear to be systematic. Therefore, salinity measurements were made using a salinometer (belonging to the Clyde River Purification Board, East Kilbride). These data (salinity in ‰) were converted to ^{238}U activities using the equation of Chen *et al.* (1986) (equation 3.2, section 3.2.2.3).

3.3.4 Quality control

For each batch of samples that was counted, 6-10 backgrounds and a similar number of spikes were made up as previously described (section 3.3.3.1). A background and spike were placed at the beginning and end of the batch of samples, and after every 3-4 samples. The background samples were used to determine the mean and standard deviation of the background, and the spikes to determine the relative yield.

The ^{234}Th counting efficiency, E , was determined by taking a 1 ml aliquot of the ^{238}U working solution of known activity and spiking it with 1 ml ^{230}Th working solution. This solution was then made up to 20 ml with 9M hydrochloric acid and treated in the same manner as a sample (Fig. 3.8). Four "efficiency" samples were made up in this way and counted at the end of a batch of samples. The recovery of ^{234}Th could be determined using the data from the spikes and, as the initial activity of ^{234}Th was known, the counting efficiency over the region of interest under the specific counting conditions could be determined. The mean, E , and the standard deviation, σ_E , of the four samples were used, rather than a single value, in order to take into account all the possible variations in pipetting and sample preparation.

Figure 3.13 is a schematic representation of the decay and ingrowth processes that affect the ^{234}Th activity in the sample between the time of sampling and counting.

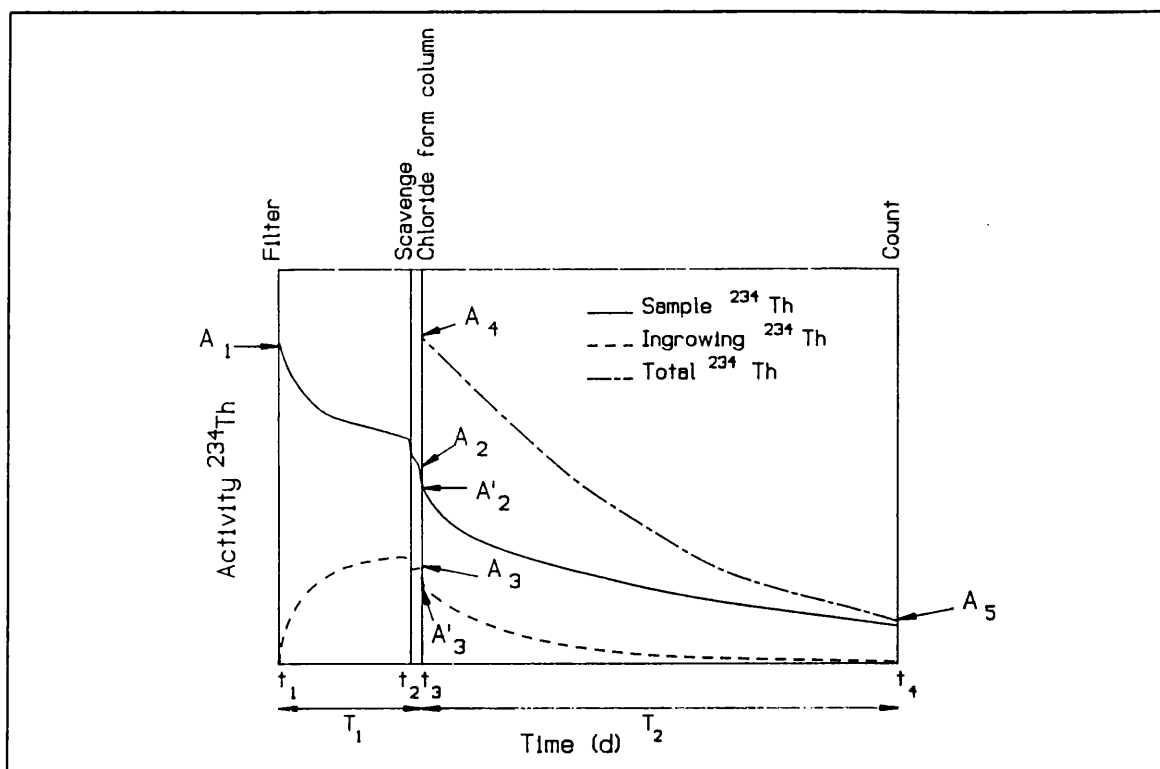


Figure 3.13: Schematic representation of decay and ingrowth processes affecting the ^{234}Th activity in a sample before counting.

After filtration at time = t_1 , ^{234}Th present in the dissolved phase of the sample (A_1) decays to A_2 , but is supplemented by ingrowth from the decay of ^{238}U (A_3). The activities, A_2 and A_3 , will both be reduced, due to incomplete recovery during the iron (III) hydroxide scavenging process (at time = t_2), to A_2' and A_3' respectively. Decay and ingrowth will continue until the time of the chloride form column (t_3), at which point uranium is removed. While the decay can be fully accounted for, the yield of ^{238}U in the scavenging step is not known, preventing further calculation of ingrowth. However, by minimizing the time interval ($t_3 - t_2$), it is possible to assume that negligible ingrowth has occurred. As this condition was met for all analyses, it was assumed that $t_3 = t_2$. From this point, A_2' and A_3' behave in the same manner and, thus, can be combined to give A_4 . After the uranium has been removed, ^{234}Th decays until the time of counting (t_4) to give A_5 . The exact method of calculation, working backwards from the observed count rate in the β window, $C_{\beta\text{obs}}$, is now described in more detail, together with the calculation of errors. σ_x is used throughout to denote the absolute error on the value

x , and S_x to denote the relative error (*i.e.* $\sigma_x \div x$).

At the end of the counting period, the Replay™ option on the counter was used to re-run the protocol with the regions of interest set at 0-120 keV (β MCA) and 110-280 keV (α MCA) (the initial count used open windows, 0-2000 keV, for both MCAs to allow full manipulation of the data at a later date). The date and time of the filtration mid-point (t_1), the addition of sample to the chloride form column (t_2) and the start of the count (t_4) for each sample were noted, and T_1 ($t_3 - t_1$) and T_2 ($t_4 - t_3$) were calculated.

The mean and standard deviation of the background for the α and β windows were determined, giving $B_\alpha \pm \sigma_{B\alpha}$ and $B_\beta \pm \sigma_{B\beta}$ respectively. The error on $C_{\beta obs}$ for the β window was calculated by assuming Poisson counting statistics (equation 3.3).

$$\sigma_{C_{\beta obs}} = \sqrt{\frac{C_{\beta obs}}{t}} \quad (3.3)$$

where t is the count time. The net count rate, $C_{\beta net}$, for the β window and its associated error were calculated using equations 3.4 and 3.5 respectively.

$$C_{\beta net} = C_{\beta obs} - B_\beta \quad (3.4)$$

$$\sigma_{C_{\beta net}} = \sqrt{\sigma_{C_{\beta obs}}^2 + \sigma_{B_\beta}^2} \quad (3.5)$$

$C_{\beta net}$ was then converted into the activity, A_5 , by equation 3.6

$$A_5 = \frac{C_{\beta net}}{E} \quad (3.6)$$

where E is the counting efficiency expressed as a fraction, and the error, σ_{A_5} , was found using equation 3.7.

$$S_{A_5} = \sqrt{\left(\frac{\sigma_{C_{net}}}{C_{net}}\right)^2 + S_E^2} \quad (3.7)$$

A_5 was then decay corrected to the time of the chloride form column, A_4 , using equation 3.8, and the error, S_{A_5} , was calculated using equation 3.9.

$$A_4 = A_5 e^{-\lambda T_2} \quad (3.8)$$

$$S_{A_4} = S_{A_5} \quad (3.9)$$

The mean and standard deviation of the spike count rate in the α window, Sp_α and σ_{Sp_α} , were determined. The background was subtracted from both Sp_α and $C_{\alpha obs}$ (observed count rate of the sample in the α window) using equation 3.4, giving Sp_{net} and $C_{\alpha net}$ respectively, and the errors, $\sigma_{Sp_{net}}$ and $\sigma_{C_{\alpha net}}$, were calculated using equation 3.5. The yield ratio, Y , was determined using equation 3.10 and the error, S_Y , using equation 3.11.

$$Y = \frac{C_{\alpha net}}{Sp_{net}} \quad (3.10)$$

$$S_Y = \sqrt{\left(\frac{\sigma_{C_{\alpha net}}}{C_{\alpha net}}\right)^2 + \left(\frac{\sigma_{Sp_{net}}}{Sp_{net}}\right)^2} \quad (3.11)$$

The term Y includes all losses of ^{234}Th from the sample from the time of filtration. Now,

$$A_4 = A_3' + A_2'$$

but A_3' , the activity of ingrown ^{234}Th minus chemical losses, is not known. However,

$$A_3' = A_3 \times Y$$

and

$$A_2' = A_2 \times Y$$

Therefore,

$$A_4 = (A_3 \cdot Y) + (A_2 \cdot Y)$$

and, hence

$$\frac{A_4}{Y} = A_2 + A_3$$

A_4/Y was determined and the error was found using equation 3.12.

$$S_{\frac{A_4}{Y}} = \sqrt{S_{A_4}^2 + S_Y^2} \quad (3.12)$$

A_4/Y , in dpm, was then corrected for volume, V , using equation 3.13, to give Z in dpm l^{-1} , and the error, S_Z , was found using equation 3.14.

$$Z = \frac{\frac{A_4}{Y}}{V} \quad (3.13)$$

$$S_Z = \sqrt{\left(\frac{S_{A_4}}{Y}\right)^2 + \left(\frac{\sigma_V}{V}\right)^2} \quad (3.14)$$

The activity of ^{234}Th resulting from the decay of ^{238}U in the sample, between times t_1 and t_2 , is A_3 and was found using equation 3.15

$$A_3 = A_U(1 - e^{-\lambda T_1}) \quad (3.15)$$

where A_U is the activity of ^{238}U in the dissolved phase (in dpm l^{-1}) and λ is the decay constant of ^{234}Th , and the error, S_{A_3} , using equation 3.16

$$S_{A_3} = S_{A_U} \quad (3.16)$$

A_2 , and its error, σ_{A_2} , were found using equations 3.17 and 3.18 respectively.

$$A_2 = Z - A_3 \quad (3.17)$$

$$\sigma_{A_2} = \sqrt{(S_Z \cdot Z)^2 + (S_{A_3} \cdot A_3)^2} \quad (3.18)$$

Finally, the activity at time t_1 , A_1 (later referred to as A_{Th} , was found by applying equation 3.19, and the error, $\sigma_{A_{Th}}$, by using equation 3.20.

$$A_1 = A_{Th} = A_2 e^{\lambda T_1} \quad (3.19)$$

$$\sigma_{A_{Th}} = S_{A_{Th}} \cdot A_{Th} = S_{A_2} \cdot A_{Th} \quad (3.20)$$

For particulate samples, it was assumed that $A_U = 0$, and hence $A_3 = 0$. Therefore, the calculation was simplified and a single decay correction was needed.

The effect on the errors experienced for marine samples of using the LLCM and the NCM, with and without the optimized windows was compared for the 2250 CA α/β and the 2550 TR/AB (a) (Table 3.11). The samples had been collected during an October 1992 cruise to the Northeast Atlantic (more details of the sampling procedures and analysis of the results can be found in section 4.3.1). The α counting window was 110-280 keV in all cases and the count time 200 min.

Table 3.11 shows that using the optimized window reduces the relative errors when the NCM is used (A and B). However, when the LLCM with $DBB = 800$ ns is turned on there is no benefit from using the optimized window and relative errors generally increase. The optimized window was found by maximizing the E^2/B figure of merit, but these samples are not close to the limit of detection, and so maximizing this factor becomes less important, which should be remembered when considering the results shown in section 3.3.2 (Figure 3.7 and Table 3.1).

Table 3.11: Effect on errors of using the normal count mode (NCM) and low-level count mode (LLCM) with and without optimized windows for the 2250 CA α/β and 2550 TR/AB (a). Errors are quoted at the 1σ level of confidence.

A) 2250 CA α/β NCM								
Sample	0-120 keV				15-117 keV			
	A_{Th}^p ^a (dpm l ⁻¹)	Relative error (%)	A_{Th}^d ^b (dpm l ⁻¹)	Relative error (%)	A_{Th}^p ^a (dpm l ⁻¹)	Relative error (%)	A_{Th}^d ^b (dpm l ⁻¹)	Relative error (%)
CH1/1	0.18 ± 0.09	50.0	0.92 ± 0.10	10.9	0.19 ± 0.07	36.9	0.86 ± 0.08	9.3
CH1/2	0.30 ± 0.11	37.2	0.88 ± 0.09	10.3	0.36 ± 0.09	25.0	0.87 ± 0.08	9.2
CH1/3	1.08 ± 0.11	10.2	-- ^c	-- ^c	1.20 ± 0.10	8.4	-- ^c	-- ^c
CH1/4	1.25 ± 0.12	9.6	0.79 ± 0.12	15.2	1.36 ± 0.11	8.1	0.61 ± 0.10	16.4
CH1/5	0.57 ± 0.11	19.3	1.40 ± 0.11	7.9	0.76 ± 0.10	13.2	1.27 ± 0.10	7.9
CH1/6	-- ^d	-- ^d	0.72 ± 0.11	15.3	0.38 ± 0.09	23.7	0.73 ± 0.09	12.4
CH1/7	0.56 ± 0.14	25.0	1.43 ± 0.09	6.3	0.54 ± 0.11	20.4	1.46 ± 0.08	5.5
CH1/8	-- ^d	-- ^d	0.79 ± 0.14	17.7	-- ^d	-- ^d	0.62 ± 0.12	19.4
CH1/9	1.90 ± 0.15	7.9	0.59 ± 0.18	30.5	1.94 ± 0.13	6.7	0.59 ± 0.15	25.4
CH1/10	0.81 ± 0.10	12.4	0.41 ± 0.12	29.3	0.82 ± 0.08	9.8	0.32 ± 0.10	31.3
CH1/11	0.73 ± 0.12	16.5	0.34 ± 0.10	29.4	0.70 ± 0.10	14.3	0.40 ± 0.09	22.5
CH1/12	0.36 ± 0.09	25.0	-- ^c	-- ^c	0.42 ± 0.08	19.1	-- ^c	-- ^c
CH1/13	0.80 ± 0.11	13.8	2.20 ± 0.15	6.8	0.75 ± 0.09	12.0	0.64 ± 0.11	17.2

B) 2550 TR/AB (a) NCM								
Sample	0-120 keV				13-83 keV			
	A_{Th}^p ^a (dpm l ⁻¹)	Relative error (%)	A_{Th}^d ^b (dpm l ⁻¹)	Relative error (%)	A_{Th}^p ^a (dpm l ⁻¹)	Relative error (%)	A_{Th}^d ^b (dpm l ⁻¹)	Relative error (%)
CH1/1	0.18 ± 0.09	50.0	0.91 ± 0.10	11.0	0.16 ± 0.06	37.5	0.80 ± 0.07	8.8
CH1/2	0.41 ± 0.11	26.9	0.86 ± 0.09	10.5	0.43 ± 0.08	18.6	0.85 ± 0.07	8.3
CH1/3	1.23 ± 0.11	9.0	-- ^c	-- ^c	1.21 ± 0.09	7.5	-- ^c	-- ^c
CH1/4	1.45 ± 0.13	9.0	0.60 ± 0.11	13.4	1.45 ± 0.10	6.9	0.54 ± 0.09	16.7
CH1/5	0.75 ± 0.11	14.7	1.46 ± 0.11	7.6	0.84 ± 0.09	10.7	1.36 ± 0.09	6.6
CH1/6	0.55 ± 0.12	21.8	0.93 ± 0.12	12.9	0.49 ± 0.08	16.4	0.83 ± 0.09	10.9
CH1/7	0.58 ± 0.14	24.2	1.46 ± 0.09	6.2	0.80 ± 0.10	12.5	1.53 ± 0.08	5.3
CH1/8	-- ^d	-- ^d	1.16 ± 0.13	11.2	0.26 ± 0.09	34.6	1.20 ± 0.10	8.4
CH1/9	1.81 ± 0.14	7.8	0.57 ± 0.19	33.4	1.79 ± 0.11	6.2	0.51 ± 0.13	25.5
CH1/10	0.73 ± 0.10	13.7	-- ^d	-- ^d	0.82 ± 0.07	8.6	0.18 ± 0.09	50.0
CH1/11	0.67 ± 0.12	17.9	0.36 ± 0.10	27.8	0.71 ± 0.09	12.7	0.40 ± 0.07	17.5
CH1/12	0.31 ± 0.09	19.1	-- ^c	-- ^c	0.29 ± 0.06	20.7	-- ^c	-- ^c
CH1/13	1.08 ± 0.11	10.2	0.63 ± 0.13	20.7	0.81 ± 0.08	9.9	0.45 ± 0.09	20.0

C) 2550 TR/AB (a) LL/800 ns

Sample	0-120 keV				13-83 keV			
	A_{Th}^p ^a (dpm l ⁻¹)	Relative error (%)	A_{Th}^d ^b (dpm l ⁻¹)	Relative error (%)	A_{Th}^p ^a (dpm l ⁻¹)	Relative error (%)	A_{Th}^d ^b (dpm l ⁻¹)	Relative error (%)
CH1/1	0.32 ± 0.06	18.8	0.74 ± 0.07	9.5	0.31 ± 0.06	19.4	0.72 ± 0.08	11.1
CH1/2	0.49 ± 0.07	14.3	0.91 ± 0.07	7.7	0.47 ± 0.08	17.0	0.82 ± 0.08	9.8
CH1/3	1.23 ± 0.09	7.3	-- ^c	-- ^c	1.26 ± 0.10	8.0	-- ^c	-- ^c
CH1/4	1.36 ± 0.10	7.4	0.90 ± 0.09	10.0	1.31 ± 0.11	8.4	0.44 ± 0.09	20.5
CH1/5	0.78 ± 0.08	10.3	1.49 ± 0.10	6.7	0.72 ± 0.09	12.5	1.07 ± 0.10	9.4
CH1/6	0.41 ± 0.07	17.1	0.77 ± 0.08	10.4	0.32 ± 0.08	25.0	0.67 ± 0.09	13.5
CH1/7	0.82 ± 0.09	11.0	1.32 ± 0.09	6.8	0.73 ± 0.10	13.7	1.31 ± 0.09	6.8
CH1/8	0.19 ± 0.08	42.1	1.33 ± 0.10	7.5	-- ^d	-- ^d	1.27 ± 0.11	8.7
CH1/9	2.08 ± 0.13	6.3	0.38 ± 0.11	29.0	1.93 ± 0.14	7.3	0.55 ± 0.14	25.5
CH1/10	0.79 ± 0.07	8.8	0.38 ± 0.08	21.1	0.79 ± 0.08	10.2	0.33 ± 0.10	30.1
CH1/11	0.70 ± 0.08	11.5	0.38 ± 0.07	18.4	0.68 ± 0.09	13.2	0.34 ± 0.08	23.6
CH1/12	0.36 ± 0.06	16.7	-- ^c	-- ^c	0.36 ± 0.07	19.5	-- ^c	-- ^c
CH1/13	0.70 ± 0.07	10.0	0.94 ± 0.09	9.6	0.70 ± 0.08	11.5	0.50 ± 0.10	20.0

- a* Particulate fraction of the sample.
b Aqueous fraction of the sample.
c Sample lost during chemical separation.
d Below limit of detection.

The errors shown in Table 3.11C using the open β window (the count conditions employed for marine samples) range between 6.3 and 42.1%, with the mean being 13.3%. These errors are higher than ideally would be the case. Therefore, an investigation into some of the factors affecting the errors was undertaken.

The effect of count time on the errors experienced with samples was examined by entering different count times (100 min, 400 min and 600 min, as well as the true count time of 200 min) into the spreadsheet used to calculate results and looking at the effect on the final results for the six estuarine samples previously described (Fig. 3.10) (Table 3.12). The samples were counted in the 2550 TR/AB (b) using the LLCM, DBB = 800 ns with PDD = 110 for 200 min.

Table 3.12: The effect of counting time on the errors for duplicate estuarine samples. Errors are quoted at the 1σ level of confidence.

A) Count time = 100 min				
Sample	A_{Th}^p (dpm l ⁻¹)	Relative error (%)	A_{Th}^d (dpm l ⁻¹)	Relative error (%)
LG1	0.60 ± 0.11	18.3	0.11 ± 0.10	90.9
LG2	0.53 ± 0.11	20.8	0.08 ± 0.14	175
HB1	0.38 ± 0.08	21.1	-- ^c	-- ^c
HB2	0.43 ± 0.09	20.9	-- ^c	-- ^c
AR1	0.28 ± 0.13	46.4	-- ^c	-- ^c
AR2	0.43 ± 0.12	27.9	0.13 ± 0.09	69.2
B) Count time = 200 min				
Sample	A_{Th}^p (dpm l ⁻¹)	Relative error (%)	A_{Th}^d (dpm l ⁻¹)	Relative error (%)
LG1	0.60 ± 0.08	13.3	0.11 ± 0.07	63.6
LG2	0.53 ± 0.08	15.1	0.08 ± 0.11	138
HB1	0.38 ± 0.06	15.8	-- ^c	-- ^c
HB2	0.43 ± 0.07	16.3	-- ^c	-- ^c
AR1	0.28 ± 0.10	35.7	-- ^c	-- ^c
AR2	0.43 ± 0.09	20.9	0.13 ± 0.07	53.8
C) Count time = 400 min				
Sample	A_{Th}^p (dpm l ⁻¹)	Relative error (%)	A_{Th}^d (dpm l ⁻¹)	Relative error (%)
LG1	0.60 ± 0.07	11.7	0.11 ± 0.06	54.5
LG2	0.53 ± 0.07	13.2	0.08 ± 0.09	113
HB1	0.38 ± 0.05	13.2	-- ^c	-- ^c
HB2	0.43 ± 0.05	11.6	-- ^c	-- ^c
AR1	0.28 ± 0.08	28.6	-- ^c	-- ^c
AR2	0.43 ± 0.08	18.6	0.13 ± 0.05	38.5
D) Count time = 600 min				
Sample	A_{Th}^p (dpm l ⁻¹)	Relative error (%)	A_{Th}^d (dpm l ⁻¹)	Relative error (%)
LG1	0.60 ± 0.06	10.0	0.11 ± 0.06	54.5
LG2	0.53 ± 0.06	11.3	0.08 ± 0.08	100
HB1	0.38 ± 0.05	13.2	-- ^c	-- ^c
HB2	0.43 ± 0.05	11.6	-- ^c	-- ^c
AR1	0.28 ± 0.08	28.6	-- ^c	-- ^c
AR2	0.43 ± 0.07	16.3	0.13 ± 0.05	38.5

- a Particulate fraction of the sample.
- b Aqueous fraction of the sample.
- c Below limit of detection.

The data in Table 3.12 for both dissolved and particulate thorium show that increasing the count time from 100 (mean relative error = 54.5%) to 200 min (mean = 41.4%) reduces the errors by approximately 13%, which in turn will have an effect on the limits of detection for the method. This improvement reaches 20% if the count time is increased to 400 min (mean = 33.7%). However, a count time of 600 min (mean = 31.6%) results in only another 2% reduction in the errors. In addition, the increased delay before counting that will occur for the later samples in a batch has not been taken into account. A 400 min count is probably the optimum in terms of balancing the precision against decay as, within this period, less than 1% of the total ^{234}Th activity decays away allowing the use of a single time for decay correction.

The above data were also manipulated in a spreadsheet to simulate the effect on the errors of changing the sample volume to 5 l and 20 l. The results are shown in Table 3.13 and indicate that the errors are inversely and linearly related to the volume, *i.e.* doubling the volume results in an approximate halving of the errors. For the particulate fractions only, the mean relative error is 38.7% for 5 l samples, 19.5% for 10 l samples and 10.5% for 20 l samples. However, if values of 20 l and 400 min are entered for volume and count time respectively, the resultant errors are not significantly different from those in Table 3.13C, indicating that the net count rate plays a greater role in the errors than the count time.

The net count rate can be increased either by using larger sample volumes or by reducing the elapsed time before counting. This latter point could be achieved if a greater part (or indeed all) of the analysis could be carried out while at sea. Furthermore, detailed analysis of the errors at each step in the calculation shows that two steps are responsible for large increases in the relative error,

Table 3.13: The effect of sample volume on the errors associated with duplicate estuarine samples, counted for 200 min. Errors are quoted at a 1σ level of confidence.

A) Volume = 5 l				
Sample	A_{Th}^p ^a (dpm l ⁻¹)	Relative error (%)	A_{Th}^d ^b (dpm l ⁻¹)	Relative error (%)
LG1	0.60 ± 0.16	26.7	-- ^c	-- ^c
LG2	0.53 ± 0.16	30.2	-- ^c	-- ^c
HB1	0.38 ± 0.12	31.6	-- ^c	-- ^c
HB2	0.43 ± 0.13	30.2	-- ^c	-- ^c
AR1	0.28 ± 0.20	71.4	-- ^c	-- ^c
AR2	0.43 ± 0.18	41.9	-- ^c	-- ^c
B) Volume = 10 l				
Sample	A_{Th}^p ^a (dpm l ⁻¹)	Relative error (%)	A_{Th}^d ^b (dpm l ⁻¹)	Relative error (%)
LG1	0.60 ± 0.08	13.3	0.11 ± 0.07	63.6
LG2	0.53 ± 0.08	15.1	0.08 ± 0.11	138
HB1	0.38 ± 0.06	15.8	-- ^c	-- ^c
HB2	0.43 ± 0.07	16.3	-- ^c	-- ^c
AR1	0.28 ± 0.10	35.7	-- ^c	-- ^c
AR2	0.43 ± 0.09	20.9	0.13 ± 0.07	53.8
C) Volume = 20 l				
Sample	A_{Th}^p ^a (dpm l ⁻¹)	Relative error (%)	A_{Th}^d ^b (dpm l ⁻¹)	Relative error (%)
LG1	0.60 ± 0.04	6.7	0.11 ± 0.04	36.4
LG2	0.53 ± 0.05	9.4	0.08 ± 0.05	62.5
HB1	0.38 ± 0.03	7.9	-- ^c	-- ^c
HB2	0.43 ± 0.04	9.3	0.04 ± 0.05	125
AR1	0.28 ± 0.05	17.9	-- ^c	-- ^c
AR2	0.43 ± 0.05	11.6	0.13 ± 0.04	30.8

- a* Particulate fraction of the sample.
b Aqueous fraction of the sample.
c Below limit of detection.

namely subtracting the background, B_β , from the $C_{\beta\text{obs}}$ and subtracting the ingrown activity, A_3 , from Z (*i.e.* $A_4/(Y \times V)$). The impact of these steps could be reduced by (i) reducing the background of the counter and (ii) minimizing T_1 (*i.e.* the elapsed time before the chloride form column). The former approach is not possible with the counters used in the present study, but other LS counters are now available with enhanced background reduction capabilities, for example the Packard Tri-Carb® 2750 TR/LL employs a BGO (bismuth germanate - $\text{Bi}_4\text{Ge}_3\text{O}_{12}$) cosmic guard. Cosmic rays that interact with this guard produce PMT anode pulses that are much longer in duration than either α or β pulses produced by the cocktail, enabling effective discrimination against background events (Passo and Cook, 1994). A brief trial of this instrument has shown that, using the same background composition and the LLCM with $\text{DBB} = 800$ but no α/β separation, backgrounds of 4.50 cpm are achievable over the 0-120 keV window, compared with ~ 11 cpm for the 2550 TR/AB.

As stated above, each batch of samples was accompanied by 6-10 background vials, which were counted under the same conditions as the samples. As 200-400 min counts do not provide good statistics for this low number of counts (~ 0.1 cpm in the α window and ~ 11 cpm in the β window - using the 2550 TR/AB (b) LL/800 ns and 0-120 window), the mean and standard deviation of the backgrounds were used in the calculations to improve the accuracy of the data. The use of the standard deviation as the error also allows small differences between vials and their contents to be taken into account. The variability in background count rates for the 2550 TR/AB (b) in the LLCM, $\text{DBB} = 800$ ns, $\text{PDD} = 110$ and β window of 0-120 keV was examined by making up 10 background samples and counting each of them for 400 min on four occasions. The mean background, for both the α and β counting windows, was found for each sample and also for each counting period, along with the standard deviation (Fig. 3.14). These data imply that variability between vials is no greater than variability between different counting periods, indicating that the use of the mean of several different background samples is a valid procedure.

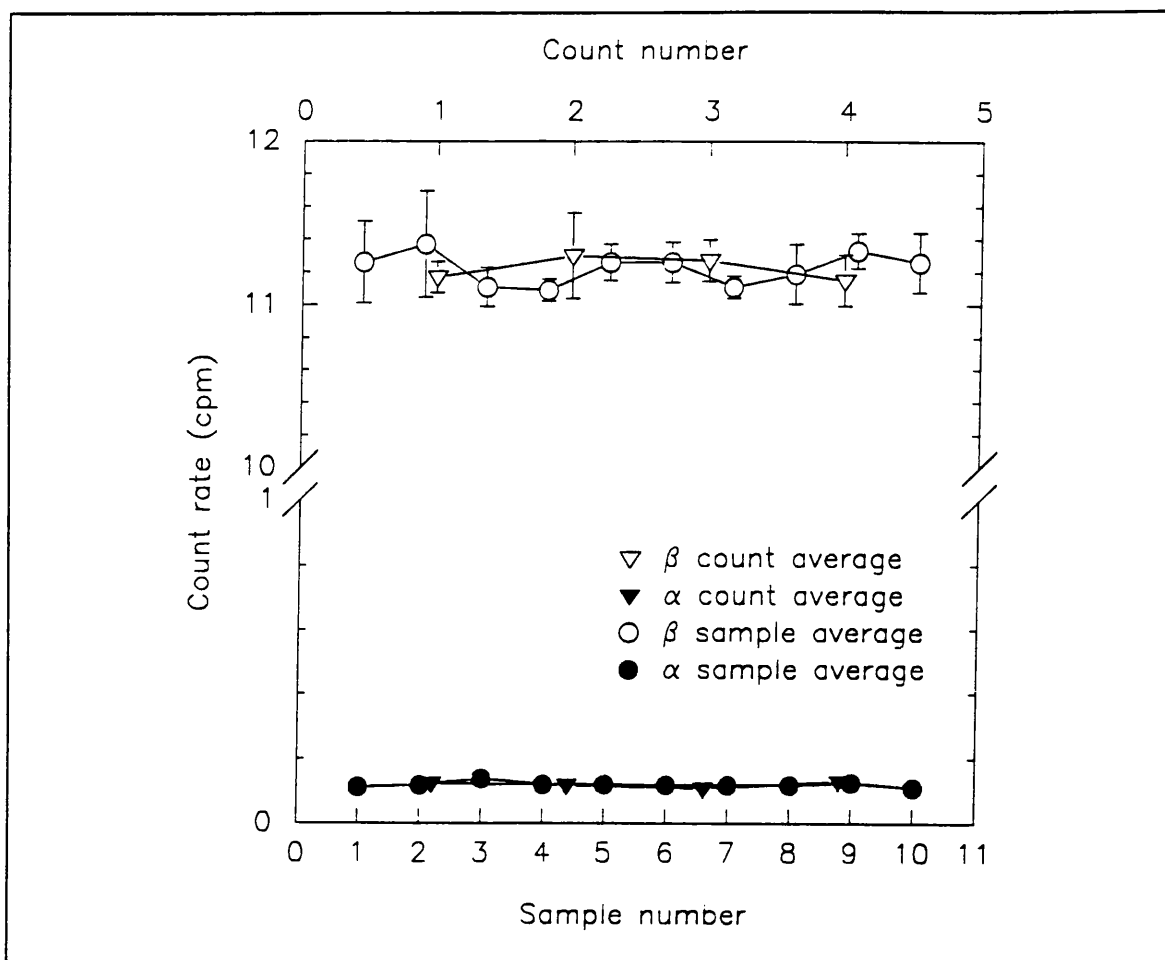


Figure 3.14: The variation in background standards between different vials and different counts. Errors are 1σ .

These background samples do not take into account any thorium activity derived from the analytical reagents and, therefore, reagent blanks (samples RB1-8) were analysed to check for this source of contamination. Each reagent blank sample consisted of 1 ml ^{230}Th working solution in 25 ml concentrated hydrochloric acid and 10 ml iron carrier solution. Four samples (RB1-4) were made up with an iron solution that had not been extracted into DIPE and four samples (RB5-8) used iron solution that had been DIPE extracted. The solution was reduced in volume, then made up to 50 ml with 9M hydrochloric acid before adding it to a chloride form column. The remaining treatment was as for samples and they were counted on the 2550 TR/AB (b) LLCM, DBB = 800 ns and PDD = 110 for 400 min (β window = 0-120 keV) on 3 occasions approximately 14, 33 and 35 days after the chloride form column. If systematic contamination with ^{234}Th was occurring, the count rate would be

expected to decrease with time. However, the data in Table 3.14 show no observable decreasing trend, indicating that the reagents were free of detectable contamination.

Table 3.14: Reagent blanks counted on three occasions using the 2550 TR/AB (b) in the LL/800 ns. Samples RB1-4 were made using Fe carrier that had not been DIPE extracted and samples RB5-8 were made up with Fe carrier that had. Errors are quoted at the 1σ level of confidence.

Sample	Net cpm		
	Count 1	Count 2	Count 3
RB1	-0.05 ± 0.21	-0.30 ± 0.21	0.05 ± 0.22
RB2	0.32 ± 0.22	-0.33 ± 0.21	0.08 ± 0.22
RB3	0.13 ± 0.22	-0.17 ± 0.21	-0.21 ± 0.21
RB4	0.30 ± 0.22	0.18 ± 0.22	0.14 ± 0.22
Mean \pm (standard error)	0.175 ± 0.173	-0.155 ± 0.234	0.015 ± 0.155
RB5	0.32 ± 0.22	-0.23 ± 0.21	0.18 ± 0.22
RB6	0.33 ± 0.22	-0.04 ± 0.21	0.08 ± 0.22
RB7	0.00 ± 0.21	-- ^a	-0.29 ± 0.21
RB8	-0.07 ± 0.21	-- ^a	-0.36 ± 0.21
Mean \pm (standard error)	0.145 ± 0.210	-0.135 ± 0.134	-0.098 ± 0.267

^a Not determined.

Currie (1968) defined L_D to be the level of the net signal which, *a priori*, can be expected to lead to detection (equation 3.21).

$$L_D = 2.71 + 4.65\sqrt{\mu_B} \quad (3.21)$$

where μ_B is the mean background expressed in counts. Dividing this value by the count time, T, gives the minimum detectable count rate (equation 3.22).

$$L_D \text{ (cpm)} = \frac{2.71 + 4.65\sqrt{\mu_B}}{T} \quad (3.22)$$

Based on the data illustrated in Figure 3.14, the mean background for 2550 TR/AB (b) over the β window (0-120 keV) with LL/800 ns and PDD=110 is 11.22 cpm over a 400 min counting period. This equates to an L_D of 0.79 cpm (net count rate). If typical values of the counting efficiency (99%) and sample volume (10 l) are employed the limit of detection is 0.08 dpm l⁻¹. This implies that a minimum of 3.2% of the total theoretical ²³⁴Th activity in the open ocean of 2.5 dpm l⁻¹ must be in the particulate phase to ensure detection. If the volume is increased to 20 l, the limit of detection falls to 0.04 dpm l⁻¹ and only 1.6% of the ²³⁴Th has to be on the particulate phase. As the errors on a 20 l sample are also halved, relative to a 10 l sample, it seems that 20 l samples are generally preferable. Using the approximate background obtainable with the 2750 TR/LL (*i.e.* 4.50 cpm over 400 min), the limit of detection would be 0.05 dpm l⁻¹ for a 10 l sample, which is close to that obtainable using a 20 l sample.

In order to validate the method, 5 replicate 20 l samples were collected from the Firth of Clyde at Greenock - an estuarine environment with a high suspended material load. The samples were filtered, acidified and spiked immediately upon return to the laboratory. One was analysed immediately and the remaining samples were analysed at intervals (10, 12, 19 and 29 d after filtration) to observe the ingrowth of ²³⁴Th. Counting was performed using the 2550 TR/AB (a) in the NCM for 200 min. ²³⁸U was determined by ICP-MS and found to be 2.27 dpm l⁻¹. The observed ingrowth was plotted against the predicted value (assuming no ²³⁴Th is present initially) (Fig. 3.15). This assumption is shown to be incorrect, as the regression of the data intersects the y-axis at 0.19 dpm l⁻¹ implying that 8.4% of the maximum ²³⁴Th activity (2.27 dpm l⁻¹) remained in the dissolved phase, despite the presence of a high particulate load. However, the two lines (theoretical and measured) should still converge at 2.27 dpm l⁻¹, despite the incorrect initial assumption. The observed value at this point is 2.19 dpm l⁻¹, which

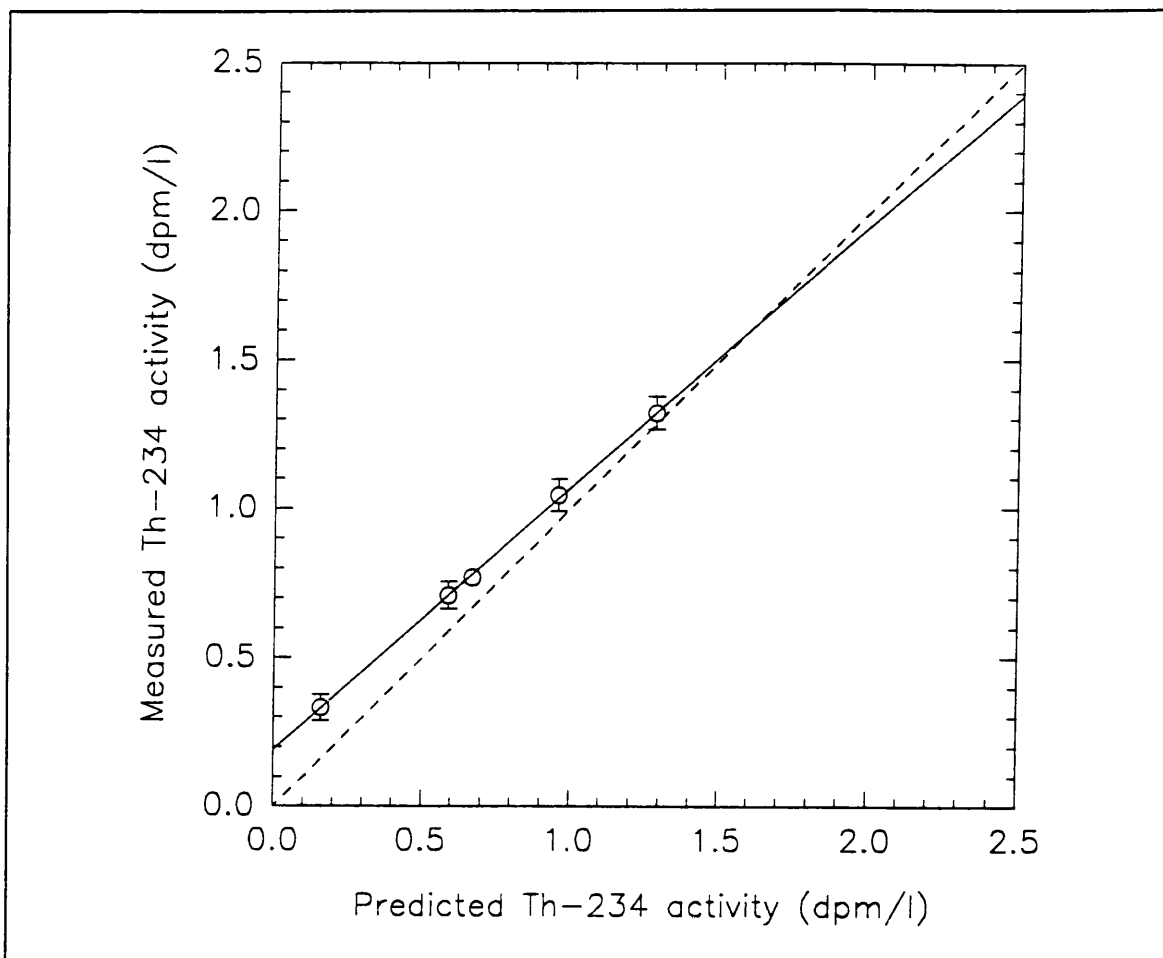


Figure 3.15: Ingrowth of ^{234}Th into filtered estuarine water samples. Errors are 1σ .

is within the analytical uncertainty of the method.

3.4 CONCLUSIONS

α/β LSS has been demonstrated to be a suitable tool for ^{234}Th analysis in the presence of a ^{230}Th yield tracer. For seawater analysis, sample volumes of 10 l can be employed, but unless a substantial part of the analysis can be performed at sea, a volume of 20 l is preferable since it will result in lower errors. It was found that the elapsed time prior to the separation of uranium was critical to the error and, therefore, performing at least the first part of the chemistry while at sea is essential for precise results. The separation chemistry is similar to that routinely used for ^{234}Th determination via gas proportional counting, but the problems associated with electrodeposition and obtaining a thin

source are eliminated. Much shorter counting times than for either gas proportional counting or γ -spectrometry are required. Nitromethane quenching has a slight effect on α counting efficiencies over the range of 390-430 tSIE units, but this will be discussed further in Chapter 4 with regard to marine samples.

The biggest problem with using LSS is the relatively high β background, compared to either gas proportional counting or γ -spectrometry, as it affects both the limit of detection and the errors. However, the use of electronic background reduction has reduced the background to ~ 11 cpm and increased the E^2/B figure of merit, which results in a limit of detection of 0.08 dpm l^{-1} for a 10 l sample. More modern LS counters have enhanced background reduction capability, which could have a significant impact on this method, for example with the Packard Tri-Carb® 2750 TR/LL a detection limit of 0.05 dpm l^{-1} was obtained.

The method, as it stands, is not entirely suitable for the shipboard analysis of small seawater samples. However, several improvements could potentially be included to enhance the simplicity of the separation chemistry. These include the use of small scale manganese oxide scavenging systems, such as a column packed with manganese impregnated fibres, to replace the iron (III) hydroxide precipitation step, allowing smaller volumes of acid to be used at later stages.

CHAPTER 4: APPLICATIONS OF $^{234}\text{Th}/^{238}\text{U}$ DISEQUILIBRIUM IN THE MARINE ENVIRONMENT

4.1 INTRODUCTION

The following chapter starts with an overview of the types of study that have employed $^{234}\text{Th}/^{238}\text{U}$ disequilibrium to elucidate kinetic data on the world's oceans (section 4.2). The short half-life of ^{234}Th ($t_{1/2} = 24.1$ d) confines its use in marine tracer studies to areas with a high particle flux or to areas in which thorium has been concentrated, resulting in $^{234}\text{Th}/^{238}\text{U}$ activity ratios that are neither close to zero nor close to unity (section 1.4.3). These include coastal regions (*e.g.* Huh *et al.*, 1993), which experience both large sedimentary fluxes with a terrigenous source and high rates of biological production, the euphotic zone (*e.g.* Coale and Bruland, 1987) in which biological production occurs, and the bottom sediments in both coastal and deep-sea environments (*e.g.* Aller and DeMaster, 1984). Particle flux studies make use of the depletion of ^{234}Th with respect to its parent, whereas studies of bottom sediments employ unsupported or excess ^{234}Th activities, which result from a flux of thorium rich particles to the sediment surface.

The remaining sections (sections 4.3.1 and 4.3.2) cover two small scale studies, carried out as part of the present work, employing the α/β LSS method of ^{234}Th analysis discussed in Chapter 3. These studies were chosen more to evaluate the potential of the method, than to provide comprehensive oceanographic data. The first examines the seasonal variation in particle fluxes in the Northeast Atlantic and the Firth of Clyde and the second uses ^{234}Th to follow the scavenging processes occurring around a hydrothermal vent site on the Mid-Atlantic Ridge (MAR).

Much of the following discussion focuses on the partitioning of thorium between the dissolved and particulate phases of seawater. It should be noted, however, that "particulate phase" and "dissolved phase" are operationally defined terms. Many studies have defined the dissolved phase to

include any material that passes through either a 0.45 μm filter (*e.g.* McKee *et al.*, 1986) or a 0.2 μm filter (*e.g.* Kershaw and Young, 1988). This convention is now changing due to an increasing awareness of the role of colloidal material in scavenging processes (*e.g.* Moran and Buesseler, 1993), leading to a more recent definition of the dissolved phase being that which passes through a 10,000 nominal molecular weight (NMW) filter, with the colloidal fraction being that which passes through a 0.2 μm filter but is retained by the 10,000 NMW filter.

4.2 SURVEY OF APPLICATIONS

The major applications for $^{234}\text{Th}/^{238}\text{U}$ disequilibrium have focused on either elucidating the flux of carbon in the world's oceans (*e.g.* Lambert *et al.*, 1991; Buesseler *et al.*, 1992a) or modelling the behaviour of reactive pollutants in coastal environments (*e.g.* Santschi *et al.*, 1980; Kershaw and Young, 1988). In the former case, the particles studied are biogenic in nature, whereas in the latter, the particles are both biogenic and terrigenous, in varying proportions according to the location of the study. In addition, some studies have been made of sedimentation and sediment reworking (*e.g.* McKee *et al.*, 1984; Martin and Sayles, 1987). Therefore, the following discussion has been divided into the categories of sedimentary processes, carbon fluxes and pollutant modelling. However, the boundaries between these areas are not clearly defined, and some work falls into more than one category. The work discussed does not provide a comprehensive survey of all the oceanographic studies reported which employ ^{234}Th as a tracer, but illustrates its potential by including a diverse range of applications.

4.2.1 Sedimentary processes

McKee and co-workers have studied $^{234}\text{Th}/^{238}\text{U}$ disequilibrium in continental shelf areas near to the mouths of the Amazon River (McKee *et al.*, 1985 and 1986) and the Yangtze River (McKee *et al.*, 1984), which experience high inputs of terrigenous material. The Yangtze study examined surface

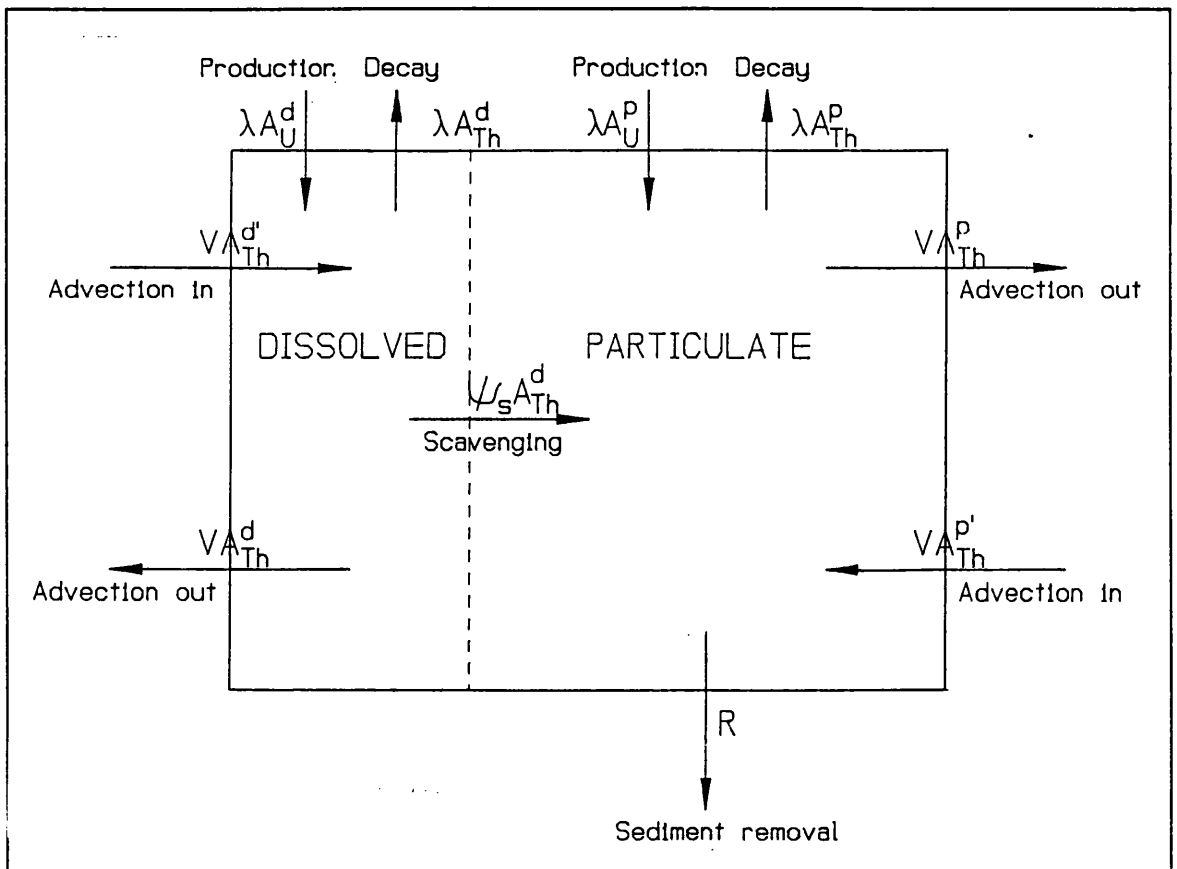


Figure 4.1: Two dimensional model of thorium scavenging (after McKee *et al.*, 1984).

water and sediment ^{234}Th concentrations along a transect across the continental shelf and highlighted the need for horizontal transport terms in modelling this near-shore environment (Figure 4.1 illustrates the model used by McKee *et al.*). The residence time, with respect to scavenging of ^{234}Th in the dissolved phase, was found to decrease to a minimum as the sediment concentration increased to 100 mg l^{-1} , at which level all the available ^{234}Th was in the particulate phase.

The Amazon study, on the other hand, was a temporal study examining surface and bottom water ^{234}Th concentrations close to the Amazon estuary, over several tidal cycles. McKee *et al.* compared the validity of a steady-state or equilibrium model (as discussed in section 1.4.3) and a kinetic model, in which it was assumed that the equilibrium position had not been reached and that scavenging was an irreversible process. It was found that the variability of suspended sediment concentrations over the tidal cycle meant that the kinetic model fitted the observed data more closely.

However, if averaged over several tidal cycles, the equilibrium model could also be used. In both studies, the residence time for ^{234}Th in the water column, with respect to scavenging, ranged from 0.3 d to 4 d, indicating the usefulness of this radionuclide in modelling sedimentation processes in the near-shore environment.

Although most of the scavenging of ^{234}Th occurs in the euphotic region of the ocean, with the result that by a depth of 300 m most of the ^{234}Th is in the dissolved state and total ^{234}Th is in equilibrium with ^{238}U (Coale and Bruland, 1987; Buesseler *et al.*, 1992b) due to the small particulate loads (Aller and DeMaster, 1984) and low settling rates, it has been found that $^{234}\text{Th}/^{238}\text{U}$ disequilibrium can be used effectively to measure the very low sedimentation rates that occur at the deep-sea floor (Aller and DeMaster, 1984). This is due to the fact that the low particle concentrations in the open ocean result in high specific activities of ^{234}Th and high $^{234}\text{Th}_{\text{xs}}$ (*i.e.* ^{234}Th unsupported by decay of its parent nuclide) activities of the order of 1000-39,000 dpm g^{-1} of ashed filter for surface waters (Krishnaswami *et al.*, 1976), 2000 dpm g^{-1} at 300-400 m depths (Moore *et al.*, 1981) and 2000-3000 dpm g^{-1} at 3500 m depths (Bacon and Rutgers van der Loeff, 1989). Thus, Aller and DeMaster (1984) found measurable $^{234}\text{Th}_{\text{xs}}$ in sediments to a depth of 5 cm in the Panama Basin, which has a depth of overlying water of 3990 m. This would allow the detection of sedimentation rates of a few $\mu\text{g cm}^{-2} \text{d}^{-1}$ and of bioturbation in the surface layers of the sediment. In general, ^{234}Th can provide an independent means of checking the accuracy of sediment traps. Several studies have shown good correlation between data obtained from both sediment traps and ^{234}Th activities (*e.g.* Moore *et al.*, 1981). However, an independent validation is important as the accuracy of sediment traps in the surface ocean has been called into question (Buesseler, 1992).

Martin and Sayles (1987) carried out a detailed, seasonal survey of $^{234}\text{Th}_{\text{xs}}$ concentrations in the sediments of Buzzard's Bay, Massachusetts, a coastal area with an overlying water depth of 15 m. The depth to which $^{234}\text{Th}_{\text{xs}}$ occurred varied between 3-5 cm in the summer months and ~ 2 cm

over the winter months. These variations were found to be due primarily to the effects of biological activity within the sediments, resulting in sediment reworking. Seasonal variations in the flux of particulate material to the sediment surface were also inferred from longer residence times of ^{234}Th in the water column over the winter months, associated with the decreased concentration of resuspended sediments over this period. An important conclusion of this study was that the rates of reworking rapidly changed between the seasons, with a time-scale of approximately one month. This allowed the use of ^{234}Th as an effective tracer in conjunction with steady-state models.

Below a depth of ~ 300 m in seawater, total ^{234}Th is expected to be in equilibrium with ^{238}U (Buesseler *et al.*, 1992b). However, marked disequilibrium can occur in the bottom layer of the deep-ocean in areas with a bottom nepheloid layer (BNL) (a layer of increased turbidity, resulting from higher suspended sediment concentrations) (Bacon and Rutgers van der Loeff, 1989). Bacon and Rutgers van der Loeff (1989) observed that particulate ^{234}Th increased with proximity to the sediment-water interface in an area with a BNL, whereas both the dissolved and total fractions decreased, allowing them to speculate as to the possible mechanism creating the turbidity. Lateral transport was rejected as allowing insufficient exchange with the sediment and an alternative, excessive turbulence preventing the settling out of sediments, was also rejected owing to the observed decrease in total ^{234}Th , which is inconsistent with this model. The final suggestion, which is consistent with the observed data, is that bioturbation and resuspension were occurring locally.

4.2.2 Carbon fluxes

Atmospheric carbon dioxide enters the world's oceans by exchange at the air-sea interface, whereupon it enters into equilibrium with other inorganic carbon species, including bicarbonate, carbonate, and carbonic acid (Libes, 1992). The bicarbonate carbon can be taken up by phytoplankton and enter the marine organic carbon cycle (Fig 4.2), which describes the processes of uptake and eventual fate of the carbon (Chester, 1990). It has been estimated that $\sim 5\%$ of the carbon taken up

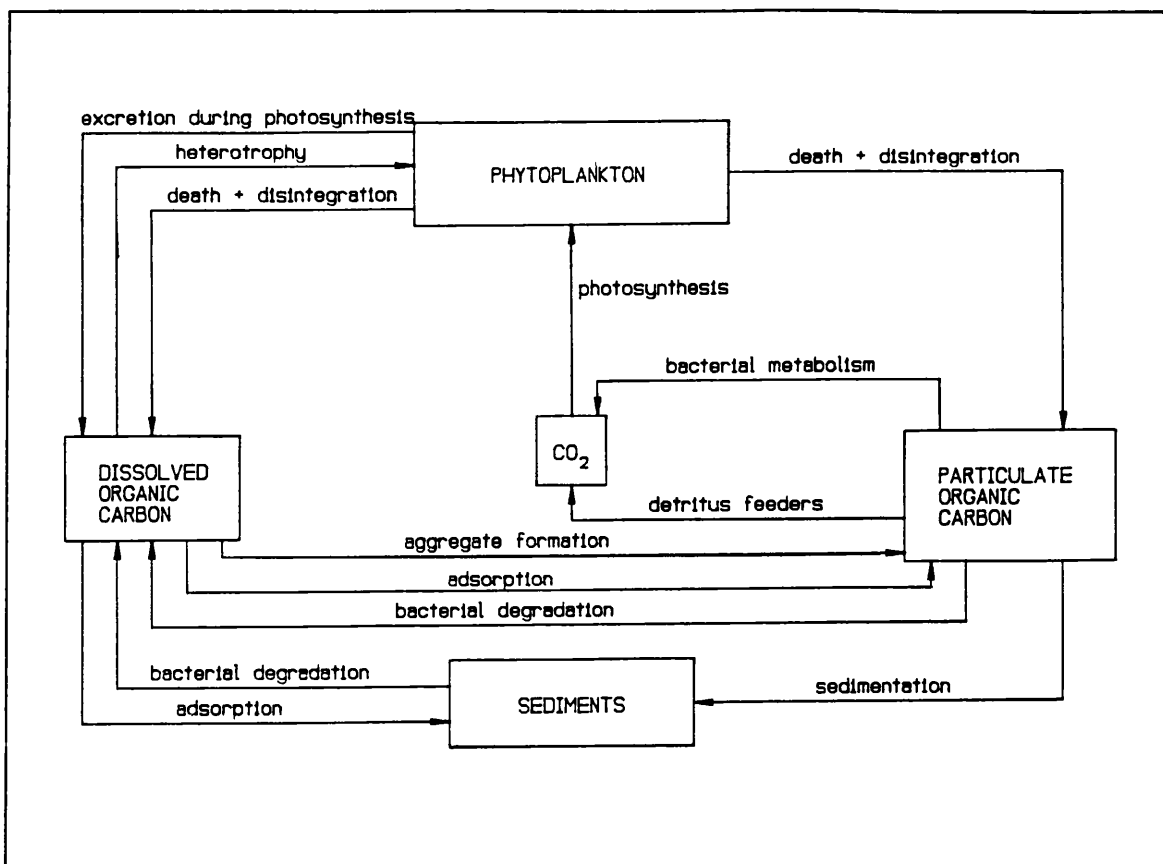


Figure 4.2: Schematic of the marine organic carbon cycle (after Chester, 1990).

in global, annual phytoplankton production is lost to the seafloor as particulate organic carbon (Chester, 1990). Otherwise, much of the carbon is recycled in the surface layer of the ocean. The balance between these processes is of growing interest as concern over global atmospheric carbon concentrations increases, requiring more detailed data on the potential of the ocean to act as a carbon sink. As many of the relevant processes take place over days rather than months, ²³⁴Th can be used to trace the fate of organic carbon in the water column. The evolution of the use of ²³⁴Th/²³⁸U disequilibria in carbon flux studies is outlined below.

²³⁴Th/²³⁸U disequilibrium was first used to study production phenomena by Matsumoto (1975), following the work by Broecker *et al.* (1973) on ²²⁸Th disequilibrium with its parent ²²⁸Ra. These studies showed that thorium is preferentially taken up by biota in the surface layers of the ocean, mimicking the behaviour of the nutrient species nitrate and phosphate (section 1.4.1). Bhat *et al.* (1969) observed

an increase in the $^{234}\text{Th}/^{238}\text{U}$ activity ratio to greater than unity in the mid-region of the water column, which was explained as being due to the release of ^{234}Th from particulate matter by the processes of disaggregation or dissolution.

Tanaka *et al.* (1983) studied the influence of biological processes on $^{234}\text{Th}/^{238}\text{U}$ disequilibrium in a coastal environment (Funka Bay, Japan), by analysing unfiltered water samples at varying depths and monthly intervals in conjunction with other parameters such as dissolved oxygen and dissolved silica. Again, a subsurface maximum in the $^{234}\text{Th}/^{238}\text{U}$ activity ratio was observed. However, this group concluded that decomposition of organic matter could not account for the effect, but that it was the result of physical and biological breakdown of large particles into smaller particles with slower settling velocities. The calculated ^{234}Th inventories correlated well with the occurrence of phytoplankton blooms in the bay, indicating that this nuclide could be used effectively as an indicator of biological activity. However, it was found that the ^{234}Th activities changed sufficiently rapidly to make steady-state models inapplicable and alternatively, a non-steady-state model was used to calculate residence times.

A series of studies of open-ocean production have used $^{234}\text{Th}/^{238}\text{U}$ disequilibrium to constrain, more precisely, the mechanisms of scavenging and removal of biogenic material from the surface layers of the ocean. Coale and Bruland (1985) demonstrated that the rate at which thorium is scavenged (*i.e.* transferred from the dissolved to the particulate phase) is a function of primary production and suggested that the loss of particulate material is controlled by the abundance of grazing zooplankton. This latter conclusion was supported by Schmidt *et al.* (1992), who found that particulate ^{234}Th activities were not correlated with phytoplankton masses, but with grazing zooplankton masses, in particular of *Salpa fusiformis*. In a later study, Coale and Bruland (1987) found that it was possible to distinguish stratification within the euphotic zone *via* the $^{234}\text{Th}/^{238}\text{U}$ disequilibrium. A distinction was made between an upper, oligotrophic zone, in which much of the production was based on recycled nutrients, and a lower, mixed layer, in which a greater proportion of the production was

"new", based on observations of the flux of particulate material from each of these zones. In each of these studies, a simple, steady state model (as equation 1.19, section 1.4.3) was used to calculate residence times of both dissolved and particulate ^{234}Th .

In section 1.4.3, a partitioned box model was described which divided the ^{234}Th pool into the dissolved phase, small suspended particulate material and large sinking particulate material (Fig. 1.9, equations 1.23, 1.24 and 1.25). Honeyman and Santschi (1989) developed a theoretical model of trace metal scavenging, based on evidence from the thorium isotopes, which showed the importance of the colloidal phase in transferring material from the dissolved to the particulate phase and explained anomalous observations of high "dissolved" phase concentrations of thorium isotopes. The validity of this theoretical approach has been complemented by laboratory studies and observations in the field of the behaviour of ^{234}Th . For example, Niven and Moore (1988) conducted experiments in which the K_d (distribution coefficient) values for seawater suspensions containing varying concentrations of organic colloidal material (phytoplankton exudates) and particulate alumina were determined, and found that colloidal material played a significant role in scavenging. With no alumina present, the colloidal material adsorbed up to 40% of the available ^{234}Th . In the presence of 5.0 mg Al l^{-1} , the K_d for scavenging varied with the concentration of carbon, between 4.3×10^5 (for 0 mg C l^{-1}) and 1.2×10^5 (for 2.5 mg C l^{-1}). ^{234}Th was chosen for these experiments due to its high specific activity, which allowed sufficient activity to be employed for straightforward measurement, without exceeding naturally occurring concentrations of thorium.

Baskaran *et al.* (1992) divided seawater samples collected in the Gulf of Mexico into several fractions, namely $> 0.4 \mu\text{m}$ (*i.e.* particulate), $10,000 \text{ Dalton}-0.4 \mu\text{m}$ (*i.e.* colloidal) and $< 10,000 \text{ Dalton}$ (*i.e.* dissolved). A significant proportion of the thorium was found to occur in the colloidal fraction (up to 80%) and the ^{234}Th scavenging rate constants were found to correlate well with the fraction associated with colloidal material. Moran and Buesseler (1992), in a vertical profile study of surface

waters in the Northwest Atlantic, found that colloidal (10,000 NMW-0.2 μm) material accounted for ~ 10% of the total ^{234}Th - a similar level to that of the small particulate fraction (0.2-53 μm), with ~ 80% occurring in the dissolved phase (< 10,000 NMW). Significantly, the colloidal fraction of ^{234}Th was found to have a residence time of only 10 days, implying that organic carbon is rapidly cycled in the surface layers of the open ocean.

In order to estimate carbon and nitrogen fluxes during a bloom event in the North Atlantic, Buesseler *et al.* (1992a) obtained ^{234}Th activities in a depth profile over a time period of two months. This time sequence allowed the use of a non-steady-state model (as equation 21, section 1.4.3), a more accurate approach during these rapidly changing conditions. The model comprised several layers, each fed by loss of particulate material from the layer above (Fig. 3.3). Carbon and nitrogen fluxes were estimated by combining ^{234}Th residence times obtained from the model and C/ ^{234}Th and N/ ^{234}Th ratios obtained from sediment trap samples. Although the authors felt that the sediment trap data were of dubious quality, the ^{234}Th data provided a straightforward means of calculating these important parameters (*i.e.* C and N fluxes).

Despite the success of these studies, Lambert *et al.* (1991) have demonstrated that caution should be applied when using $^{234}\text{Th}/^{238}\text{U}$ disequilibrium to estimate biogenic fluxes in areas which experience significant fluxes of terrigenous material. In a study of the northwestern Mediterranean, they found that ^{234}Th fluxes were poorly correlated with total carbon fluxes. Only by taking into account aluminium fluxes (as an indicator of terrigenous material - the Mediterranean experiences periodic inputs of Saharan dust) could ^{234}Th be used to predict the biogenic flux of material.

4.2.3 Reactive pollutants

Coastal regions of the marine environment are often subject to high input levels of pollutants, for example, heavy metals associated with sewage, organic pollutants and anthropogenic radionuclides. The aim of discharging these pollutants into the ocean is to allow their dispersal, such

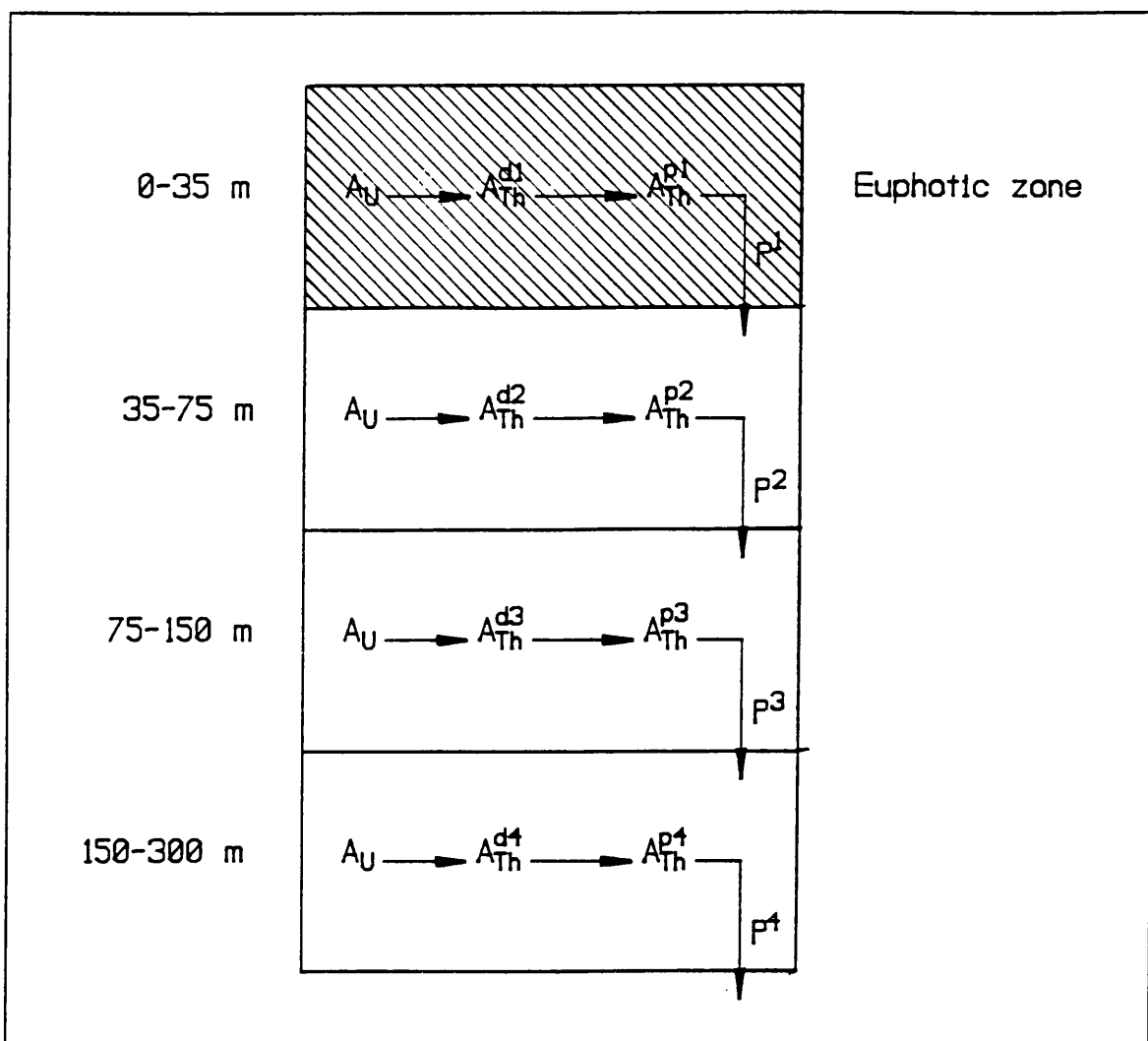


Figure 4.3: Schematic of a multi-layer box model (after Buesseler, 1992a).

that they no longer present a pollution hazard (the dilute and disperse mechanism). Coastal environments also have high rates of sedimentation and biological production and, hence, large particle fluxes (Bacon and Rutgers van der Loeff, 1989). As some of these pollutants have a high particle reactivity, it is necessary to determine whether they are remaining in the dissolved phase for a sufficiently long period for the dilute and disperse mechanism to work, or whether concentration of pollutants by particle scavenging and deposition within near-shore sediments is occurring. If the latter mechanism is dominant, the possibility remains that biological concentration and exposure to human populations *via* the food chain may occur (Santschi *et al.*, 1980).

One method for studying these processes is *via* the use of ^{234}Th . It is often simpler to develop

a model of particle scavenging based on ^{234}Th data, than on concentrations of the pollutant itself for the reasons that were outlined in section 1.4.3, namely ease of detection, known source term and the timing element provided by radioactive decay (McKee *et al.*, 1984). Santschi *et al.* (1980) found that, in a model ecosystem, thorium isotopes could be used to simulate the behaviour of the reactive, pollutant elements iron, lead, americium, chromium (III) and mercury. In addition, Boniforti (1987) proposed, on the basis of detailed analysis of the physico-chemical properties of the actinides and lanthanides, that thorium could be used effectively to model the behaviour of plutonium in the marine environment.

The Santa Monica Basin is a deep (~ 900 m) basin off the coast of southern California, in which the flow of water and particulate material is highly restricted below a depth of 420 m (Huh *et al.*, 1993). Water flowing into the Santa Monica Basin receives a large input of sewage derived pollutants, with the possibility that particle reactive species could be trapped in the basin by settling particles. By analysis of thorium isotopes, including ^{234}Th , Huh *et al.* (1993) determined that the rate of removal to the basin sediments of particle reactive species was small with respect to the residence time of the water body as it passes through the basin. Thus, it could be inferred that the anticipated dispersal mechanism was working, a conclusion supported by the low concentrations of contaminant metals found in the basin sediments.

Anthropogenic radionuclides are often discharged, under licence, into the marine environment from nuclear power plants and nuclear fuel production and reprocessing plants. An example of this situation is the discharge of fission and activation products from the nuclear fuel reprocessing plant at Sellafield into the Irish Sea. Plutonium and americium are particle reactive and have been found to be concentrated in the bottom sediments of the Irish Sea, the distribution being influenced by the sediment type (Pentreath *et al.*, 1984). However, it has been found that the distribution of plutonium and americium does not entirely follow anticipated patterns, *i.e.* sediments with a smaller particle size

are expected to contain a higher concentration of radionuclides. Therefore, Kershaw and Young (1988) decided to model the behaviour of plutonium and americium with naturally occurring ^{234}Th . Although the supply of ^{234}Th is not subject to the same constraints as Sellafield discharges, *i.e.* a point source and temporal fluctuations (discharges occur twice daily at high tide), $^{234}\text{Th}/^{238}\text{U}$ disequilibrium was found to provide an insight into the scavenging processes that occur in the coastal environment of the Irish Sea and partially to explain anomalously high concentrations of the nuclides of interest in certain areas.

4.3 APPLICATIONS OF THE α/β LSS ^{234}Th METHOD TO MARINE TRACER STUDIES

The applications discussed below for the α/β LSS method of ^{234}Th determination, developed in the present work, were chosen to evaluate the potential range and associated problems with the method in its present state of development.

4.3.1 Partitioning of ^{234}Th in the Northeast Atlantic and Firth of Clyde

4.3.1.1 Introduction

A number of studies of Sellafield-derived ^{137}Cs , in combination with salinity data, have allowed the northwards flow of Irish Sea water to be monitored. After passing through the North Channel, part of the Irish Sea water enters the Clyde Sea Area, a well-mixed water body that also has freshwater input from the Clyde estuary and a number of sea lochs (Fig. 3.10) (Baxter *et al.*, 1979; McKinley *et al.*, 1981a). Salinity data have indicated that the average composition of water in this area is 92% Irish Sea derived, 7% Atlantic and 1% freshwater (Baxter *et al.*, 1979).

Irish Sea/Clyde Sea water (termed simply Irish Sea water hereafter) then continues northwards along the Scottish coast. Again, there are three water sources in this region - Irish Sea, Atlantic and freshwater run-off (although other than in the Firth of Lorne area, this last contribution is generally small (McKay *et al.*, 1986)) (Fig. 4.4). Between the spring and autumn months, the three

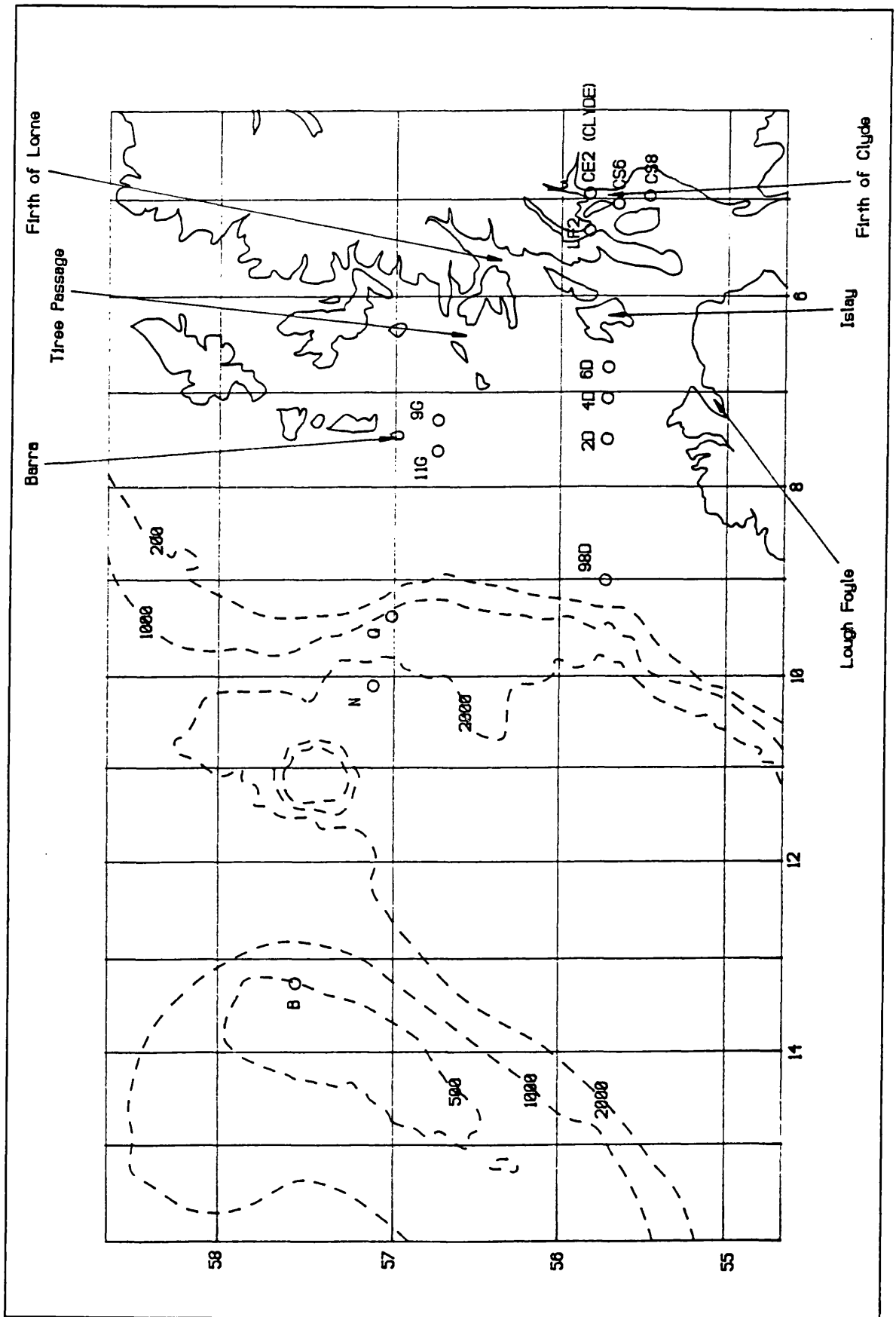


Figure 4.4: Location of Northeast Atlantic and Firth of Clyde sampling stations.

water bodies can be distinguished by temperature and salinity profiles, the Atlantic and near-shore water being stratified, while Irish Sea water is well-mixed throughout the water column (McKinley *et al.*, 1981*b*). Measurements of ^{137}Cs in surface waters have shown that the Irish Sea water passes the west coast of Islay, then passes through the Tiree Passage before the current splits, taking the majority of this water through the Minch, while the remainder passes to the west of Barra Head and travels up the west coast of the Outer Hebridean islands (Bradley *et al.*, 1988) (Fig. 4.4). During the winter months this pattern is less distinct, due to increased freshwater run-off (principally from the Firth of Clyde) and incursions of Atlantic water (McKay *et al.*, 1986; Bradley *et al.*, 1988).

These conditions cause a strong front, called the Islay front, to develop over the summer months to the west of Islay at the boundary of the higher salinity, colder Atlantic water and the lower salinity, warmer coastal water (McKay *et al.*, 1986). Atlantic water is rich in nutrients and, therefore, this boundary with the warmer, but nutrient poor, coastal water, creates suitable conditions for phytoplankton production, with enhanced production expected on the Atlantic side of the front (Lalli and Parsons, 1992).

The continental shelf waters in this area experience two, seasonally variable, inputs of particulate material, *i.e.* biogenic and terrigenous. It is expected that there are marked differences in particulate load, both across the continental shelf and with the changing seasons, that could be followed by the associated $^{238}\text{U}/^{234}\text{Th}$ disequilibrium. By examining ^{234}Th partitioning between the dissolved and particulate phases of surface samples along two transects crossing the continental shelf (Fig. 4.4), an attempt was made to observe changes in rates of scavenging and particle fluxes from these waters. The more northerly of these transects was sampled on three occasions (once in March and twice in September) in order to correlate changes in scavenging with seasonal effects. A depth profile was also taken at one point, in the open ocean, to examine the possible change in the rate of scavenging with depth. Surface water samples were collected from a variety of locations in the Firth

of Clyde (Figs. 3.10 and 4.4), both from a ship and from land, in order to examine the changes in particle flux as a function of proximity to a freshwater input. Sedimentation rates for the Firth of Clyde sea lochs have been found to be in the range $0.008\text{-}0.40\text{ g cm}^{-2}\text{ y}^{-1}$ using ^{210}Pb dating techniques (Shimmiel, 1993). This indicates that particle fluxes are high, due to the large input of terrigenous material, implying that high rates of scavenging could be expected in most of this area

4.3.1.2 Experimental methods

Samples (10 l) were collected on three occasions: September/October 1992 (cruise CH97/92), March 1993 (cruise CH101B/93) and September 1993 (cruise CH105/93) from locations in the Northeast Atlantic (Fig 4.4), along two surface transects crossing the continental shelf edge, and in the Firth of Clyde on cruises onboard the NERC vessel RRS *Challenger*. (The cruise numbers are derived in the following way: CH indicates the vessel *Challenger*, the first number is the cruise number and the second is the year.) Surface water samples were collected by pumping through a clean seawater system, while samples from depth were collected in 30 l, messenger-operated, Niskin bottles. In addition, 10 l samples were collected during late February, 1993 at Helensburgh, Loch Goil and Arrochar (jointly named SL/93 - sea loch samples, 1993) (Fig. 3.10) from piers extending into deep water. Samples have been numbered using letters to indicate where they were collected (CH is *Challenger*, HB is Helensburgh, etc.) and consecutive numbers. After filtration, they have also been designated W (water) or P (particulate).

In all cases, samples were immediately filtered, spiked with ^{230}Th and acidified and had iron carrier added (Fig 3.8). Some of the samples collected during the CH97/92 cruise were taken to the aluminium hydroxide precipitation step while at sea (samples CH1W-CH8W). The remaining parts of the analyses were performed on return to the laboratory, including that of the particulates. The first two sets of particulate analyses were carried out using the ashing and acid digestion method, while the last set was digested using the microwave digestion system (section 3.3.3.2). ^{238}U analyses were

carried out on the aqueous phase using the ICP-MS technique for CH97/92 samples, but via salinity determinations for all other samples. The ^{238}U activity in the particulate samples was assumed to be zero, based on the conservative behaviour of this element (section 1.4.1). While this is not a rigorously correct procedure, the aim of the study was to illustrate the use of the ^{234}Th method and insufficient time was available to perform the requisite number of particulate ^{238}U analyses.

Samples from cruise CH97/92 were counted using the 2550 TR/AB (a), whereas all other samples were counted using the 2550 TR/AB (b). CH97/92 samples were counted for 200 min in the LLCM with DBB = 800 ns, PDD = 100; CH101B/93 and SL/93 samples were counted in the LLCM with DBB = 800 ns and PDD = 110, the former for 400 min and the latter for 200 min; CH105/93 samples were counted for 4 x 100 min in the LLCM with DBB = 700 ns and PDD = 110. In all cases, backgrounds and spikes, as described in section 3.3.4, were counted amongst the samples and four efficiency determinations were made on each occasion. The 0-120 keV window in the β MCA was used in all cases, as was the 110-280 keV window in the α MCA.

4.3.1.3 Northeast Atlantic: results and discussion

The results from the three sampling cruises are given in Table 4.1. The particulate samples CH22P-CH31P were all below the limit of detection due to the length of time that elapsed between sampling and counting (~ 40 d). All other samples were above the limit of detection (0.08 dpm l^{-1}). The station numbers given in Table 4.1 and Figure 4.4 correspond to those given in McKay *et al.* (1986) and Bradley *et al.* (1988).

The relative errors associated with the dissolved ^{234}Th activities ranged between 3.0% and 42.9%, the mean being 13.3%. Comparing the errors experienced for the CH97/92 samples and CH101B/93 samples shows the benefit of increasing the counting time to 400 min. The true extent of this reduction in the errors is obscured by the fact that the mean time between filtering and the uranium separation for CH97/92 samples was 3.3 d, but for CH101B/93 samples was 8.2 d (the time

Table 4.1: Results of ^{234}Th analysis for Northeast Atlantic samples collected during cruises CH97/92, CH101B/93 and CH105/93. Errors are quoted at the 1σ level of confidence.

A) Cruise CH97/92 (September 25th - October 6th 1992)							
Sample	Sampling station	Depth (m)	Particulate phase		Dissolved phase		Dissolved ^{238}U activity (dpm l $^{-1}$)
			tSIE	$A_{\text{Th}}^{\text{p}, \text{a}}$ (dpm l $^{-1}$)	tSIE	$A_{\text{Th}}^{\text{d}, \text{b}}$ (dpm l $^{-1}$)	
CH1	9G	0	418	0.32 ± 0.06	419	0.74 ± 0.07	2.58 ± 0.02
CH2	11G	0	401	0.49 ± 0.07	413	0.91 ± 0.07	2.59 ± 0.02
CH3	Q	0	417	1.23 ± 0.09	-- ^d	-- ^c	-- ^d
CH4	N	0	416	1.36 ± 0.10	396	0.90 ± 0.09	2.56 ± 0.03
CH5	B	0	413	0.78 ± 0.08	399	1.49 ± 0.10	2.60 ± 0.02
CH6	B	50	418	0.41 ± 0.07	413	0.77 ± 0.08	2.59 ± 0.02
CH7	B	100	421	0.82 ± 0.09	413	1.32 ± 0.09	2.61 ± 0.02
CH8	B	150	417	0.19 ± 0.08	409	1.33 ± 0.10	2.60 ± 0.03
CH9	B	180	428	2.08 ± 0.13	407	0.38 ± 0.11	2.58 ± 0.03
CH10	6D	0	415	0.79 ± 0.07	417	0.38 ± 0.08	2.50 ± 0.04
CH11	4D	0	418	0.70 ± 0.08	417	0.38 ± 0.07	2.54 ± 0.04
CH12	2D	0	422	0.36 ± 0.06	-- ^d	-- ^c	2.56 ± 0.04
CH13	98D	0	420	0.70 ± 0.07	395	0.94 ± 0.09	2.60 ± 0.05

B) Cruise CH101B/93 (March 14th - March 18th 1993)							
Sample	Sampling station	Depth (m)	Particulate phase		Dissolved phase		Dissolved ^{238}U activity (dpm l $^{-1}$)
			tSIE	$A_{\text{Th}}^{\text{p}, \text{a}}$ (dpm l $^{-1}$)	tSIE	$A_{\text{Th}}^{\text{d}, \text{b}}$ (dpm l $^{-1}$)	
CH14	9G	0	428	0.27 ± 0.07	428	0.70 ± 0.04	2.44 ± 0.01
CH15	11G	0	431	0.54 ± 0.07	426	0.60 ± 0.04	2.45 ± 0.01
CH16	Q	0	430	0.54 ± 0.16	425	1.42 ± 0.05	$2.45 \pm 0.01^{\text{e}}$
CH17	N	0	428	-- ^f	424	1.99 ± 0.06	$2.45 \pm 0.01^{\text{e}}$

C) Cruise CH105/93 (September 3rd - September 16th 1993)							
Sample	Sampling station	Depth (m)	Particulate phase		Dissolved phase		Dissolved ^{238}U activity (dpm l $^{-1}$)
			tSIE	$A_{\text{Th}}^{\text{p}, \text{a}}$ (dpm l $^{-1}$)	tSIE	$A_{\text{Th}}^{\text{d}, \text{b}}$ (dpm l $^{-1}$)	
CH22	B	0	-- ^d	-- ^f	415	0.89 ± 0.09	2.43 ± 0.01
CH23	B	150	-- ^d	-- ^f	414	1.03 ± 0.09	2.42 ± 0.01
CH24	N	0	-- ^d	-- ^f	412	0.32 ± 0.12	2.43 ± 0.01
CH25	Q	0	-- ^d	-- ^f	416	0.21 ± 0.09	2.44 ± 0.01
CH26	11G	0	-- ^d	-- ^f	415	0.63 ± 0.09	2.39 ± 0.01
CH27	9G	0	-- ^d	-- ^f	414	1.05 ± 0.11	2.40 ± 0.01

<i>a</i>	²³⁴ Th activity in the particulate fraction of sample.
<i>b</i>	²³⁴ Th activity in the aqueous fraction of sample.
<i>c</i>	Sample lost during analysis.
<i>d</i>	Not determined.
<i>e</i>	²³⁸ U activity estimated from nearby stations, due to insufficient sample.
<i>f</i>	Below limit of detection - 0.08 dpm l ⁻¹ (see section 3.3.4).

between uranium separation and counting was similar for both sets of samples at 9.7 and 9.8 d respectively). The increase in errors for the CH105/93 samples was due to an even longer delay (mean = 10.5 d) before uranium separation. For the particulate samples, the range of relative errors was between 6.3 and 42.1%, the mean being 15.0%. These values are substantially higher than for the dissolved ²³⁴Th, attributable to the generally lower activities found in the particulate phase and to the longer times that elapsed before counting (10.8 and 21.6 d for CH97/92 and CH101B/93 samples respectively). These data indicate that if counting cannot be performed within a few days of sampling, more accurate results would be obtained by using 20 l samples, bringing the errors into a more suitable range for further manipulation.

In section 3.3.3.5, it was found that quenching had a small effect on the α counting efficiency over the maximum range experienced for marine samples, namely 395 (sample CH1W) to 432 (sample CH19P) tSIE units (Tables 4.1 and 4.4). The data presented in Tables 4.1 and 4.4 were calculated using the 110-280 keV α window, but the 120-280 keV α window yielded identical results and errors. Although the former window produced a less pronounced effect on α counting efficiency in the quenching experiment (Fig. 3.12 and Table 3.10), the lack of variation between these samples implies that quenching has not had a serious effect on the results. In addition, the greatest spread of tSIEs was for the first set of analyses to be performed (CH97/92 samples), with subsequent analyses producing a range of only 20 units.

Examining the total ²³⁴Th activity (*i.e.* total = dissolved + particulate) along each transect and comparing the values with the dissolved ²³⁸U activities, as activity ratios, provides an indication of the

degree of disequilibrium that exists at each point (Fig. 4.5). For all samples, the total $^{234}\text{Th}/^{238}\text{U}$ activity ratio is less than unity, indicating that net removal of ^{234}Th is occurring. The northern transect (Fig. 4.4) (samples CH1-5 from cruise CH97/92 and samples CH14-17 from cruise CH101B/93) showed increasing total $^{234}\text{Th}/^{238}\text{U}$ activity ratios with increasing distance from land (Fig. 4.5A), with those samples west of 10°W tending towards a value of 0.9, implying that removal is fastest close to shore, where terrigenous particles are most significant. The same trend occurred for both the September 1992 (cruise CH97/92) and March (cruise CH101B/93) samples (Fig. 4.5A), although the distribution between the dissolved and particulate phases was different, with the latter samples containing a greater proportion of the ^{234}Th in the dissolved phase. Although particulate data for the September 1993 (cruise CH105/93) transect are not available, the low activity of ^{234}Th in the dissolved phase around 9°W suggests that enhanced scavenging was occurring in this region.

The southern transect (Fig. 4.4) (samples CH10-13) showed a similar trend to the CH97/93 northern transect (Fig. 4.5B), although there appeared to be a greater degree of removal of ^{234}Th from the water column, due perhaps to the proximity of the Irish coast. These data suggest that although scavenging by terrigenous material is causing removal of ^{234}Th from the water column, particularly during the winter months and close to the shore, the effect of biogenic particles on scavenging can still be detected.

The profile (samples CH5-9) showed no overall trend with increasing depth (Fig. 4.6), although the deepest sample at 180 m is striking in the very high particulate $^{234}\text{Th}/^{238}\text{U}$ activity ratio relative to other samples and a corresponding low dissolved $^{234}\text{Th}/^{238}\text{U}$ ratio. One possible cause of this phenomenon could be the resuspension of sediments, providing increased opportunities for scavenging to occur. A similar effect has been observed in the Irish Sea by Kershaw and Young (1988).

To gain some insight into the processes that are occurring along the two surface transects,

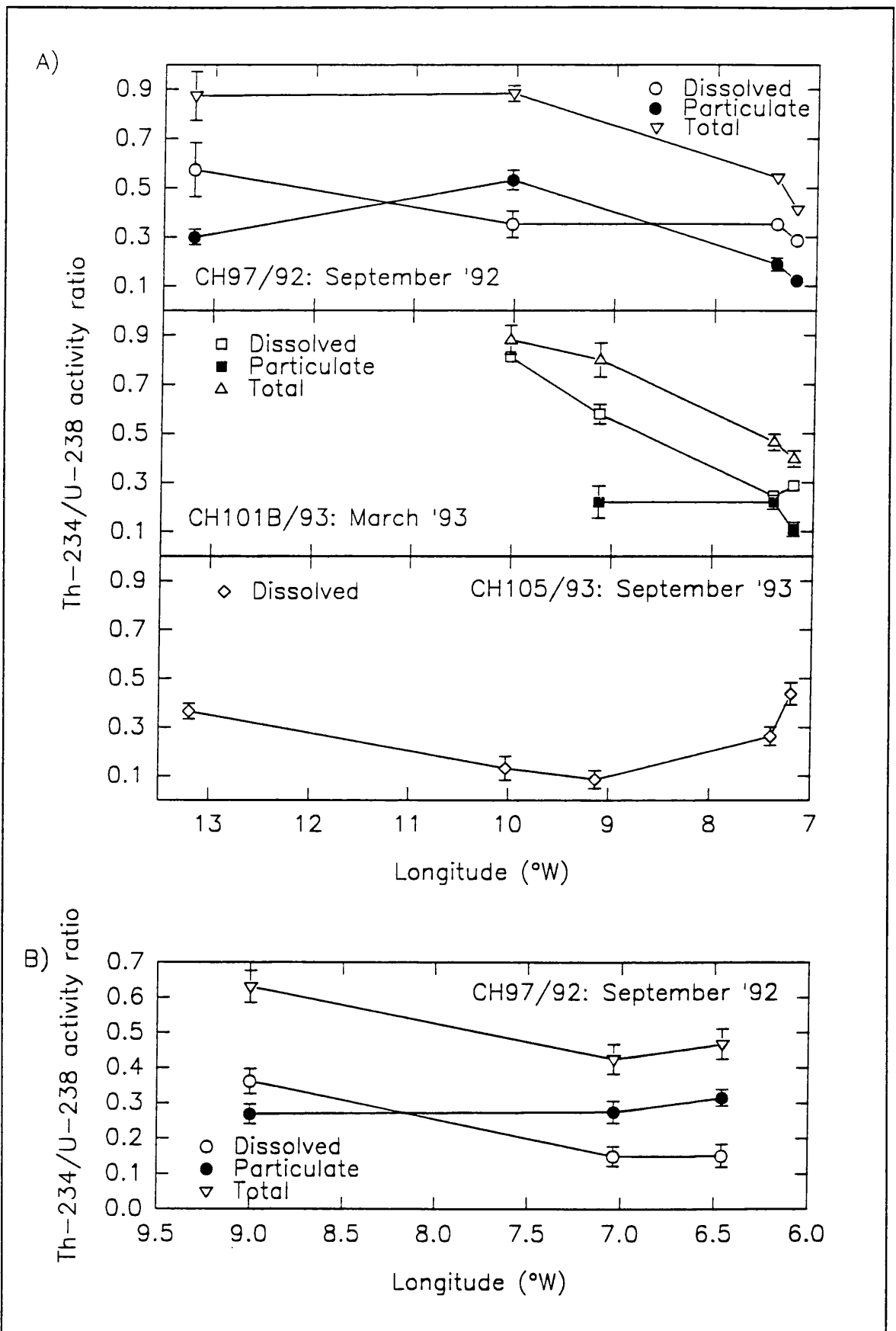


Figure 4.5: $^{234}\text{Th}/^{238}\text{U}$ activity ratios for the two transects: A) northern and B) southern.

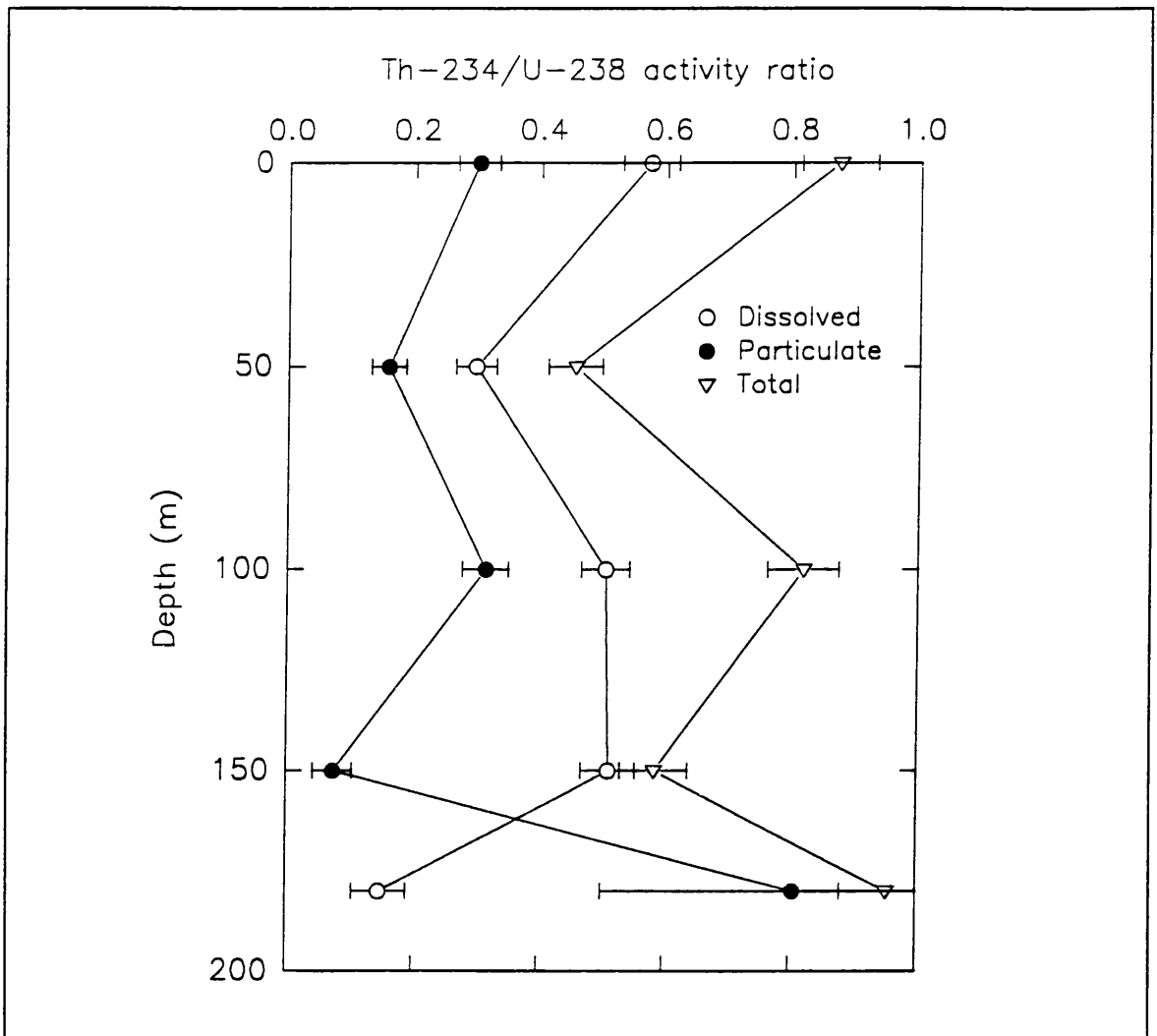


Figure 4.6. $^{234}\text{Th}/^{238}\text{U}$ activity ratios for the depth profile sampled during cruise CH97/92 at Station B.

a steady-state model (equation 1.19, section 1.4.3) was applied to the data for ^{234}Th in the dissolved and particulate phases. The assumptions that this simple model are based upon should be reiterated at this point to emphasize its limitations in a coastal environment. Firstly, it is assumed that supply of ^{234}Th to the dissolved phase is solely from the decay of its parent and removal is either to the particulate phase *via* scavenging processes or by radioactive decay. Removal by scavenging from the dissolved phase becomes supply to the particulate phase and removal occurs *via* sinking, grazing or radioactive decay. Thus, it is assumed that no horizontal transport occurs of either dissolved or particulate material and that no vertical advection or diffusion of dissolved ^{234}Th occurs. Buesseler

(1991) suggested that these assumptions are valid in situations where the particle flux is significantly greater than the neglected transport terms, such as in the open ocean. Application of a model that includes horizontal advection terms, such as that employed by McKee *et al.* (1984), requires a knowledge of ^{234}Th activities in the underlying sediments and was therefore not possible in the present study. However, as the principal currents in this area run south-north (Bradley *et al.*, 1988), it is possible to assume negligible horizontal advection across the shelf, parallel to the transects (Fig. 4.4). Residence times for dissolved and particulate ^{234}Th were calculated using equations 4.1 and 4.2 respectively (Coale and Bruland, 1985)

$$\tau_d = \frac{A_{\text{Th}}^d}{J_{\text{Th}}} \quad (4.1)$$

$$\tau_p = \frac{A_{\text{Th}}^p}{P_{\text{Th}}} \quad (4.2)$$

where J_{Th} and P_{Th} are the rates of removal from the dissolved and particulate phases respectively; A_{Th}^d and A_{Th}^p are the activities of ^{234}Th in the dissolved and particulate phases; and τ_d and τ_p are residence times. The results from these calculations are given in Table 4.2 and Figures 4.7 and 4.8.

Figure 4.7 shows the effect of increasing distance from land on the rate of removal of ^{234}Th from the particulate and dissolved phases for the northern transect (7°W is the point closest to the Scottish coast and 14°W is the furthest (Fig. 4.4)). For both the March (cruise CH101B/93) and September (cruise CH97/92) transects, the rate of removal, P_{Th} , of particulate material from the water column decreases significantly with distance from shore, as the influence of terrigenous material is reduced. A steady-state is apparently reached at approximately 10°W after which there is no further decrease, the same pattern being observed in both March and September. The more southerly transect (Fig 4.7) shows little change with increasing longitude, and the rates of removal are generally

Table 4.2: Rate of removal and residence times for ^{234}Th in the dissolved and particulate phases for Northeast Atlantic samples collected along surface transects during cruises CH97/92, CH101B/93 and CH105/93. Errors are quoted at the 1σ level of confidence.

A) Cruise CH97/92 (September 25th - October 6th 1992)						
Sample	Sampling station	Depth (m)	J_{Th}^a (dpm l ⁻¹ d ⁻¹)	P_{Th}^b (dpm l ⁻¹ d ⁻¹)	τ_d^c (d)	τ_p^d (d)
CH1	9G	0	0.053 ± 0.002	0.044 ± 0.002	14.0 ± 1.4	7.3 ± 1.4
CH2	11G	0	0.048 ± 0.002	0.034 ± 0.002	18.8 ± 1.7	14.3 ± 2.2
CH4	N	0	0.048 ± 0.003	0.009 ± 0.003	18.9 ± 2.2	157.6 ± 50.3
CH5	B	0	0.032 ± 0.003	0.009 ± 0.004	46.7 ± 5.3	82.2 ± 33.2
CH10	6D	0	0.061 ± 0.003	0.038 ± 0.003	6.2 ± 1.3	20.7 ± 2.3
CH11	4D	0	0.062 ± 0.002	0.042 ± 0.002	6.1 ± 1.1	16.7 ± 2.1
CH13	98D	0	0.048 ± 0.003	0.028 ± 0.003	19.7 ± 2.2	25.4 ± 3.7
B) Cruise CH101B/93 (March 14th - March 18th 1993)						
Sample	Sampling station	Depth (m)	J_{Th}^a (dpm l ⁻¹ d ⁻¹)	P_{Th}^b (dpm l ⁻¹ d ⁻¹)	τ_d^c (d)	τ_p^d (d)
CH14	9G	0	0.050 ± 0.001	0.042 ± 0.001	14.0 ± 0.9	6.4 ± 1.7
CH15	11G	0	0.053 ± 0.001	0.038 ± 0.001	11.3 ± 0.8	14.3 ± 1.9
CH16	Q	0	0.030 ± 0.001	0.014 ± 0.001	47.9 ± 2.9	38.3 ± 12.0
CH17	N	0	0.013 ± 0.001	0.008 ± 0.002	150.4 ± 20.2	-- ^e
C) Cruise CH105/93 (September 3rd - September 16th 1993)						
Sample	Sampling station	Depth (m)	J_{Th}^a (dpm l ⁻¹ d ⁻¹)	P_{Th}^b (dpm l ⁻¹ d ⁻¹)	τ_d^c (d)	τ_p^d (d)
CH22	B	0	0.044 ± 0.003	-- ^e	20.1 ± 2.3	-- ^e
CH24	N	0	0.061 ± 0.003	-- ^e	5.3 ± 2.0	-- ^e
CH25	Q	0	0.064 ± 0.003	-- ^e	3.3 ± 1.4	-- ^e
CH26	11G	0	0.051 ± 0.003	-- ^e	12.4 ± 1.9	-- ^e
CH27	9G	0	0.039 ± 0.003	-- ^e	27.0 ± 3.6	-- ^e

- a* Rate of removal from the dissolved phase.
b Rate of removal from the particulate phase.
c Residence time in the dissolved phase.
d Residence time in the particulate phase.
e Not determined.

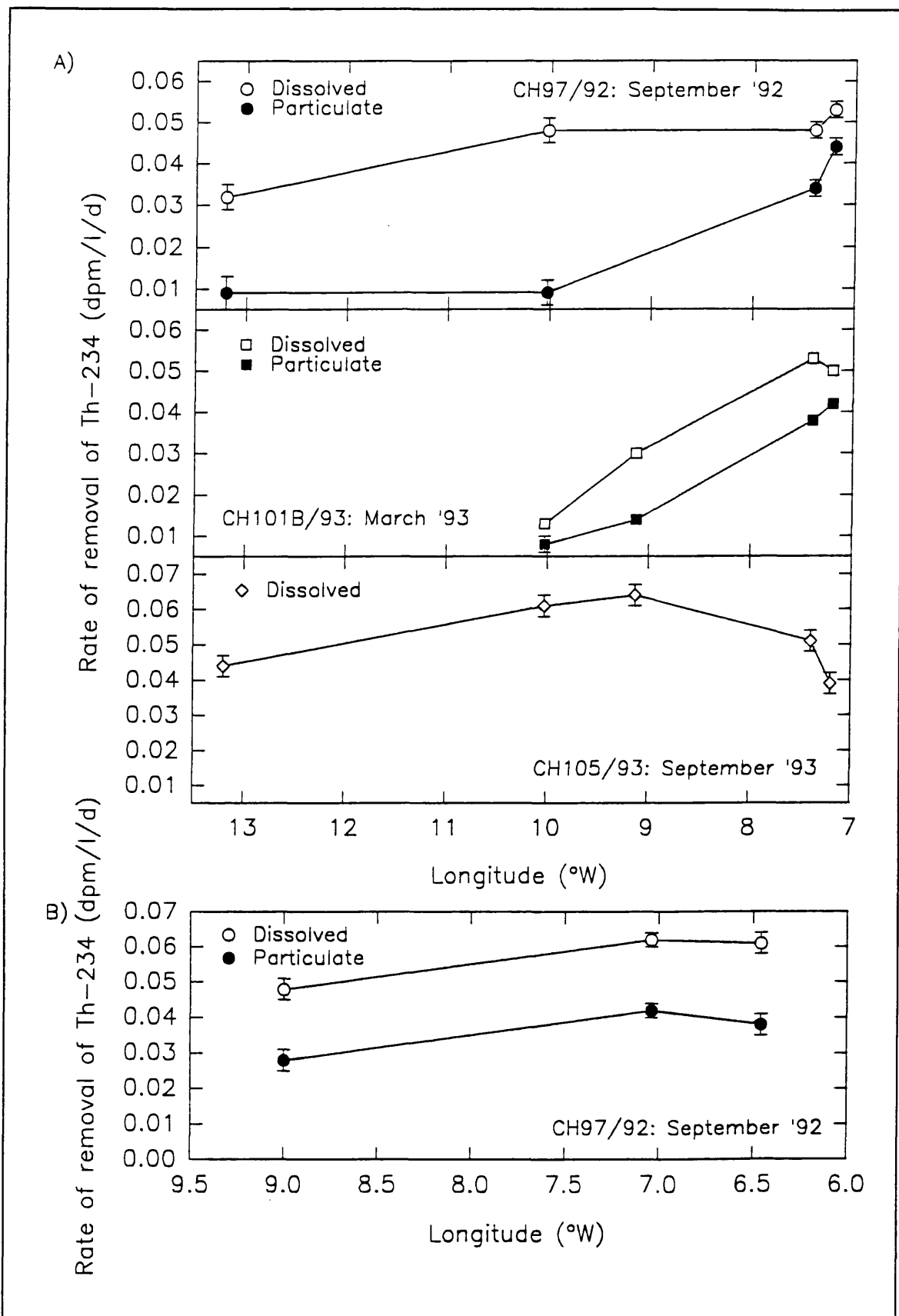


Figure 4.7: Rate of removal for ^{234}Th in the dissolved and particulate phase with increasing distance from land. A) northern transect and B) southern transect.

higher and the residence times (Fig 4.8) in the particulate phase are significantly lower. The proximity of the northern Irish coast, as previously mentioned, means that the longitude cannot be used effectively as a measure of distance from shore. Higher inputs of terrigenous material relative to the northern transect occur in this area, which is consistent with the generally higher freshwater input from the northern Irish coast, notably from Lough Foyle, than from the west coast of Scotland (McKinley *et al.*, 1981*b*).

The rate of removal from the dissolved phase (or scavenging) shows two distinctly different trends for the March (cruise CH101B/93) and September (cruises CH97/92 and CH105/93) samples (Fig. 4.7). The March samples show a rapid decrease in the rate of scavenging with distance from shore, implying that terrigenous material is the principal scavenging agent, a conclusion that is consistent with the low biological production at this time of year. The September 1993 northern transect (Fig. 4.7A), on the other hand, increases to a maximum at a distance from the coast, while the September 1992 northern transect has its maximum at the most easterly point.

These trends can be explained when more detailed information on the salinity are studied (data taken from the appropriate cruise reports). For the southern transect (Fig. 4.4), there was a marked salinity gradient, indicating the presence of the boundary between the two water bodies, between stations 4D (sample CH11) and 2D (sample CH12), corresponding to the maximum rate of scavenging. Unfortunately, sample CH12W was lost during analysis, which blurs the exact position of the maximum. For the northern transect (Fig. 4.4) during the September 1992 cruise (CH97/92), the water boundary was situated to the east of station 9G (sample CH1), whereas during the September 1993 cruise (CH105/93) it was located between stations 9G (sample CH14) and 11G (sample CH15) (Fig. 4.7A). This difference is reflected in the rate of removal from the dissolved phase, which reaches a maximum in the region of the front. The fact that, even with the relatively coarse sampling resolution of the data, it is possible to detect an increase in scavenging rates, probably

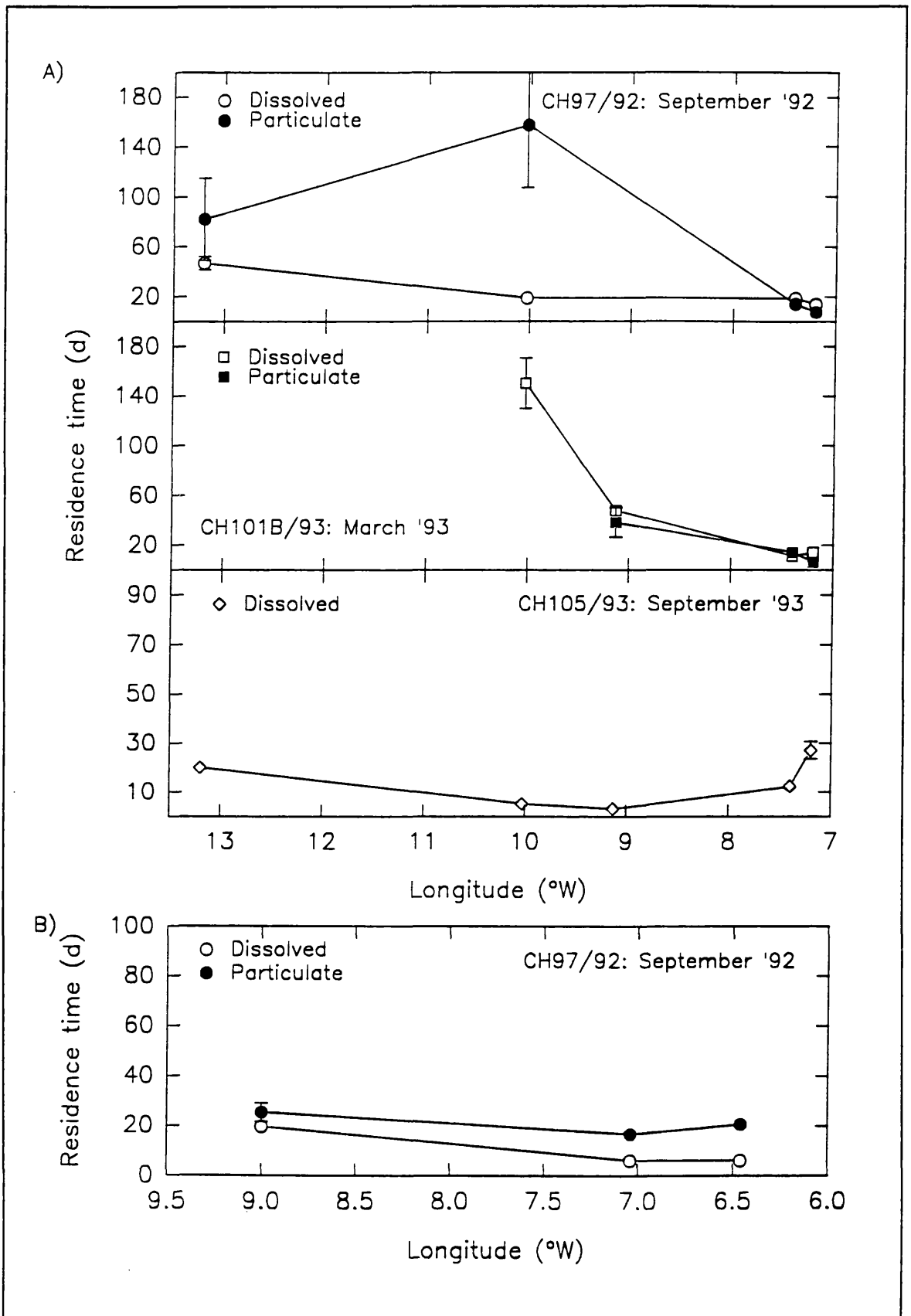


Figure 4.8: Residence times for ^{234}Th in the dissolved and particulates phases with increasing distance from land. A) northern transect and B) southern transect.

associated with enhanced productivity along the front, indicates that $^{234}\text{Th}/^{238}\text{U}$ disequilibrium is a useful tool in production studies, even in coastal waters with relatively high inputs of terrigenous material.

Residence times varied between 6.1 and 150.4 d for dissolved ^{234}Th and 6.4 and 157.6 d for particulate ^{234}Th (Table 4.2 and Fig. 4.8). These can be compared with the data obtained by other groups working in continental shelf environments using steady-state approximations. Tanaka *et al.* (1983) found residence times of between 27 and 125 d for ^{234}Th in unfiltered water from Funka Bay, Japan. Moran and Buesseler (1993) found residence times of $\tau_d = 0.47$, τ_c (residence time in colloidal material) = 1.91 d and $\tau_p = 33.6$ d at a station in the Gulf of Maine, with 251 m water depth at the sampling station. In deeper water at the edge of the continental shelf (3660 m), Morn and Buesseler (1993) found that these values varied to 0.006-0.54 d, 2.98-3.15 d and 98.11-142.78 d for dissolved, colloidal and particulate ^{234}Th respectively. Coale and Bruland (1987) found still greater residence times in the upper mixed layer (0-45 m) of the Pacific, with τ_d ranging between 50 and 447 d and τ_p varying between 16 and 412 d. The values obtained in the present study agree with these ranges, with stations closer to shore producing residence times closer to the results of Tanaka *et al.* (1983) and the near-shore samples of Moran and Buesseler (1993), while the true Atlantic stations produced values closer to those found in the Pacific (Coale and Bruland, 1987) and western Atlantic (Moran and Buesseler, 1993).

The data from the profile were treated slightly differently, in that the supply to the particulate phase was augmented for the deeper points by sinking material from the point above (as with the model employed by Buesseler *et al.* (1992b)). Thus, the equation now employed to calculate the rate of removal of ^{234}Th from the particulate phase by sinking is equation 4.3.

$$P_{Th}^i = J_{Th}^i + P_{Th}^{i-1} - A_{Th}^{Pi} \lambda_{Th} \quad (4.3)$$

where i indicates data for depth = i and $i-1$ is the depth of the samples above. The results from these

calculations are given in Table 4.3 and Figure 4.9.

Table 4.3: Rates of removal and residence times for ^{234}Th from the dissolved and particulate phases from a depth profile at station B in the Northeast Atlantic. Errors are quoted at the 1σ level of confidence.

A) Cruise CH97/92 (September 25th - October 6th 1992)					
Sample	Depth (m)	J_{Th}^a (dpm l ⁻¹ d ⁻¹)	τ_d^b (d)	P_{Th}^c (dpm l ⁻¹ d ⁻¹)	τ_p^d (d)
CH5	0	0.032 ± 0.003	46.7 ± 5.3	0.009 ± 0.004	82.2 ± 33.2
CH6	50	0.052 ± 0.002	14.7 ± 1.7	0.050 ± 0.005	8.2 ± 1.6
CH7	100	0.037 ± 0.003	35.6 ± 3.5	0.064 ± 0.006	12.9 ± 1.9
CH8	150	0.037 ± 0.003	36.4 ± 4.0	0.095 ± 0.007	2.0 ± 0.9
CH9	180	0.063 ± 0.003	6.0 ± 1.8	0.098 ± 0.009	21.2 ± 2.3
B) Cruise CH105/93 (September 3rd - September 16th 1993)					
Sample	Depth (m)	J_{Th}^a (dpm l ⁻¹ d ⁻¹)	τ_d^b (d)	P_{Th}^c (dpm l ⁻¹ d ⁻¹)	τ_p^d (d)
CH22	0	0.044 ± 0.003	20.1 ± 2.4	-- ^e	-- ^e
CH23	150	0.040 ± 0.003	25.8 ± 2.8	-- ^e	-- ^e

- a* Rate of removal from the dissolved phase.
- b* Residence time in the dissolved phase.
- c* Rate of removal from the particulate phase.
- d* Residence time in the particulate phase.
- e* Not determined.

The rate of removal from the dissolved phase was approximately constant with increasing depth, with the exception of the last point at 180 m, at which there was a significant increase. There was more variability in the residence times for the dissolved ^{234}Th , but again there was a sharp decrease to 6.01 d at 180 m. These observations are consistent with enhanced removal of ^{234}Th by resuspended sediment close to the bottom as discussed earlier. The rate of removal from the particulate phase steadily increases with depth until 150 m and is then approximately constant. The very low rate of removal and corresponding long residence time at the surface is consistent with the

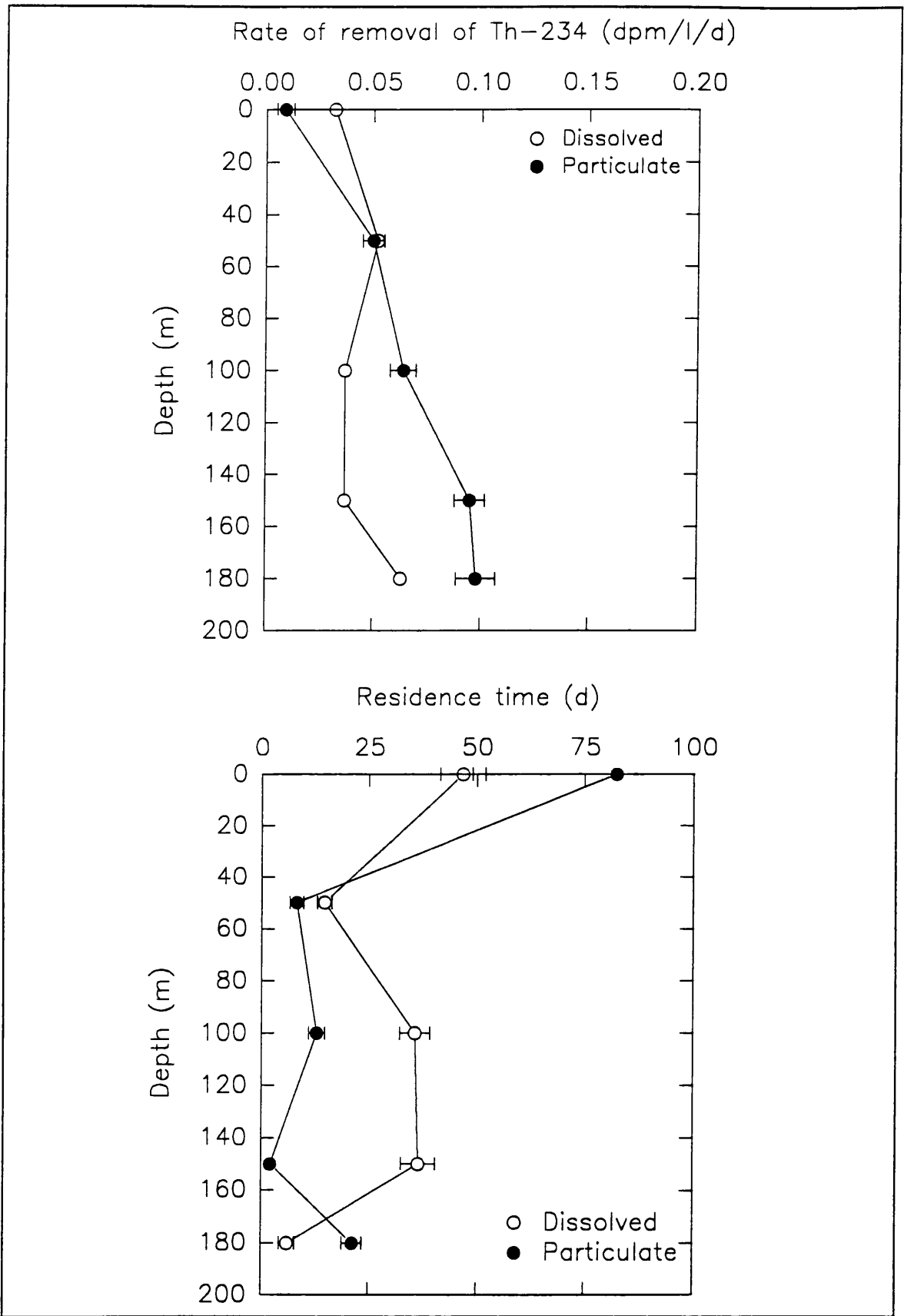


Figure 4.9: Rate of removal and residence times of dissolved and particulate ²³⁴Th with increasing depth at Station B (cruise CH97/92).

small input of particulate material at this station, which is in the open Atlantic at a distance from the front and, hence, from the main area of production in this region. Although the sedimentation rate is low, as particles sink through the water column they continue to scavenge thorium from the dissolved phase, as shown by the increasing rate of removal and reduced residence times with depth. This is perhaps another weakness with the modelling approach adopted, in that non-reversible scavenging is assumed to occur, with no account taken of potential dissolution or desorption as the particle sinks. For the deepest point, however, the residence time of the particulate ^{234}Th increases once again, which is another indication of resuspension from the sediment surface.

4.3.1.4 Firth of Clyde: results and discussion

The results from the samples taken in the Firth of Clyde are given in Table 4.4. The three duplicate analyses from the sea lochs all gave reasonable replication for the particulate phase, but the dissolved ^{234}Th activities were below the limit of detection for the method. As with the data in Table 4.1, the tSIEs were much more consistent than for the earlier samples, indicating that quenching is not a problem.

Figure 4.10 shows activity ratios for particulate, dissolved and total ^{234}Th vs. salinity, which was taken as an indicator of proximity to a freshwater source and hence land. There is possibly a slight trend towards lower activity ratios at low salinity, which would indicate greater net removal, but it is very slight and difficult to assess with any degree of confidence. The dissolved ^{234}Th concentrations from cruise CH101B/93 are significantly lower than all samples from the Northeast Atlantic stations, while the remaining values are similar to those observed at the stations closest to shore in Table 4.1. This is consistent with the far greater input of terrigenous material in the Firth of Clyde, particularly for the SL/93 samples, in which the dissolved ^{234}Th is below the limit of detection, as witnessed by significantly longer filtration times that were required for these samples. This particulate material is also rapidly sinking as demonstrated by the total ^{234}Th activities, which show

Table 4.4: Results from sea loch samples and sampling cruises (CH101B/93 and 105/93) for Firth of Clyde samples. Errors are quoted at the 1σ level of confidence.

A) SL/93 (February 1993)							
Sample	Sampling station	Depth (m)	Particulate phase		Dissolved phase		Dissolved ^{238}U activity (dpm l^{-1})
			tSIE	$A_{\text{Th}}^{\text{p } a}$ (dpm l^{-1})	tSIE	$A_{\text{Th}}^{\text{d } b}$ (dpm l^{-1})	
HB1	-- ^c	0	418	0.38 ± 0.06	421	-- ^e	2.01 ± 0.01^d
HB2	-- ^c	0	418	0.43 ± 0.07	422	-- ^e	2.01 ± 0.01
AR1	-- ^c	0	426	0.28 ± 0.10	420	-- ^e	2.24 ± 0.01
AR2	-- ^c	0	424	0.43 ± 0.09	420	-- ^e	2.24 ± 0.01^d
LG1	-- ^c	0	426	0.60 ± 0.08	421	-- ^e	2.15 ± 0.01^d
LG2	-- ^c	0	420	0.53 ± 0.08	423	-- ^e	2.15 ± 0.01

B) CH101B/93 (March 14th - March 18th 1993)							
Sample	Sampling station	Depth (m)	Particulate phase		Dissolved phase		Dissolved ^{238}U activity (dpm l^{-1})
			tSIE	$A_{\text{Th}}^{\text{p } a}$ (dpm l^{-1})	tSIE	$A_{\text{Th}}^{\text{d } b}$ (dpm l^{-1})	
CH18	CL10	0	430	0.79 ± 0.06	430	0.29 ± 0.04	2.30 ± 0.01
CH19	CL12	0	428	0.79 ± 0.06	432	0.27 ± 0.04	2.30 ± 0.01^d
CH20	CL14	0	420	0.85 ± 0.04	429	0.26 ± 0.04	2.30 ± 0.01^d
CH21	CLYDE	0	422	0.66 ± 0.05	430	0.11 ± 0.04	2.26 ± 0.01

C) CH105/93 (September 3rd - September 16th 1993)							
Sample	Sampling station	Depth (m)	Particulate phase		Dissolved phase		Dissolved ^{238}U activity (dpm l^{-1})
			tSIE	$A_{\text{Th}}^{\text{p } a}$ (dpm l^{-1})	tSIE	$A_{\text{Th}}^{\text{d } b}$ (dpm l^{-1})	
CH28	CS6	0	-- ^f	-- ^e	419	0.27 ± 0.07	2.25 ± 0.01
CH29	CE2	0	-- ^f	-- ^e	413	-- ^e	2.23 ± 0.01
CH30	CS8	0	-- ^f	-- ^e	422	0.34 ± 0.08	2.25 ± 0.01
CH31	LF2	0	-- ^f	-- ^e	416	0.33 ± 0.07	2.25 ± 0.01

- a* ^{234}Th activity in the particulate fraction of the sample.
b ^{234}Th activity in the aqueous fraction of the sample.
c Not applicable.
d ^{238}U activity estimated from nearby stations, due to insufficient sample for analysis.
e Below the limit of detection.
f Not determined.

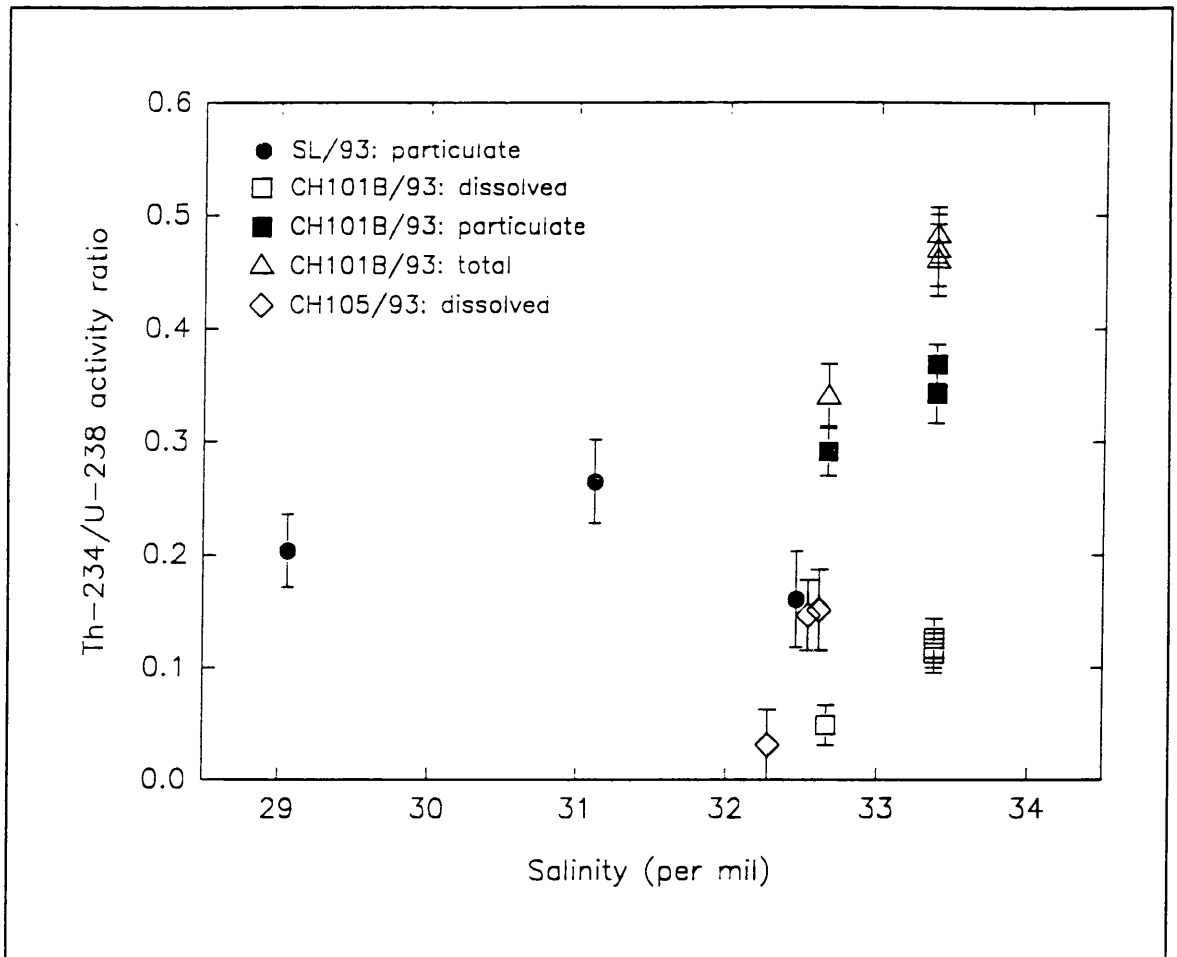


Figure 4.10: $^{234}\text{Th}/^{238}\text{U}$ activity ratios for the Firth of Clyde samples vs. salinity.

significant net removal. It is not possible to assess the influence of seasonality on these data, due both to lack of repetitive sampling from the same location and to the similarity between data points.

As there is a high particle flux in the Firth of Clyde, it is not strictly valid to use a steady-state model, due to the non-equilibrium conditions. However, insufficient data were collected on a temporal basis for a non-equilibrium model to be applied. In addition, while horizontal advection can be assumed to be negligible even on the continental shelf, it is certainly present in this tidal environment. Therefore, it is with caution that the data given in Table 4.4 have been put into the same model as used for the Northeast Atlantic data, bearing in mind that the results thus gained (Table 4.5 and Fig. 4.11) cannot be directly compared with other studies unless they too use a steady-state assumption.

There appears to be a slight increase in τ_p with increasing salinity and a larger increase in

Table 4.5: Rate of removal and residence times for Firth of Clyde samples calculated using a steady-state model. Errors are quoted at the 1σ level of confidence.

A) SL/93 (February 1993)						
Sample station	Sampling Depth (m)	J_{Th}^a (dpm l ⁻¹ d ⁻¹)	τ_d^b (d)	P_{Th}^c (dpm l ⁻¹ d ⁻¹)	τ_p^d (d)	
HB1	-- ^e	0	-- ^f	-- ^f	0.046 ± 0.003	8.3 ± 1.4
HB2	-- ^e	0	-- ^f	-- ^f	0.044 ± 0.003	9.7 ± 1.7
AR2	-- ^e	0	-- ^f	-- ^f	0.048 ± 0.002	8.9 ± 1.9
LG1	-- ^e	0	-- ^f	-- ^f	0.041 ± 0.002	14.5 ± 2.1
LG2	-- ^e	0	-- ^f	-- ^f	0.044 ± 0.003	12.0 ± 2.0
B) CH101B/93 (March 14th - March 18th 1993)						
Sample station	Sampling Depth (m)	J_{Th}^a (dpm l ⁻¹ d ⁻¹)	τ_d^b (d)	P_{Th}^c (dpm l ⁻¹ d ⁻¹)	τ_p^d (d)	
CH18	CL10	0	0.058 ± 0.001	5.0 ± 0.7	0.035 ± 0.001	22.5 ± 1.9
CH19	CL12	0	0.058 ± 0.001	4.6 ± 0.7	0.036 ± 0.001	22.2 ± 1.9
CH20	CL14	0	0.059 ± 0.001	4.4 ± 0.7	0.034 ± 0.001	24.8 ± 2.5
CH21	CLYDE	0	0.062 ± 0.001	1.8 ± 0.7	0.043 ± 0.001	15.4 ± 1.3
C) CH105/93 (September 3rd - September 16th 1993)						
Sample station	Sampling Depth (m)	J_{Th}^a (dpm l ⁻¹ d ⁻¹)	τ_d^b (d)	P_{Th}^c (dpm l ⁻¹ d ⁻¹)	τ_p^d (d)	
CH28	CS6	0	0.057 ± 0.002	4.7 ± 1.3	-- ^e	-- ^e
CH29	CE2	0	-- ^f	-- ^f	-- ^e	-- ^e
CH30	CS8	0	0.055 ± 0.003	6.2 ± 1.5	-- ^e	-- ^e
CH31	LF2	0	0.055 ± 0.002	6.0 ± 1.3	-- ^e	-- ^e

- a* Rate of removal from the dissolved phase.
b Residence time in the dissolved phase.
c Rate of removal from the particulate phase.
d Residence time in the particulate phase.
e Not applicable.
f Below limits of detection.

τ_p for the Firth of Clyde samples (Fig. 4.11). As rates of scavenging are already high in this area, there is not a sufficiently large range of samples to observe a significant change. However, the increase in

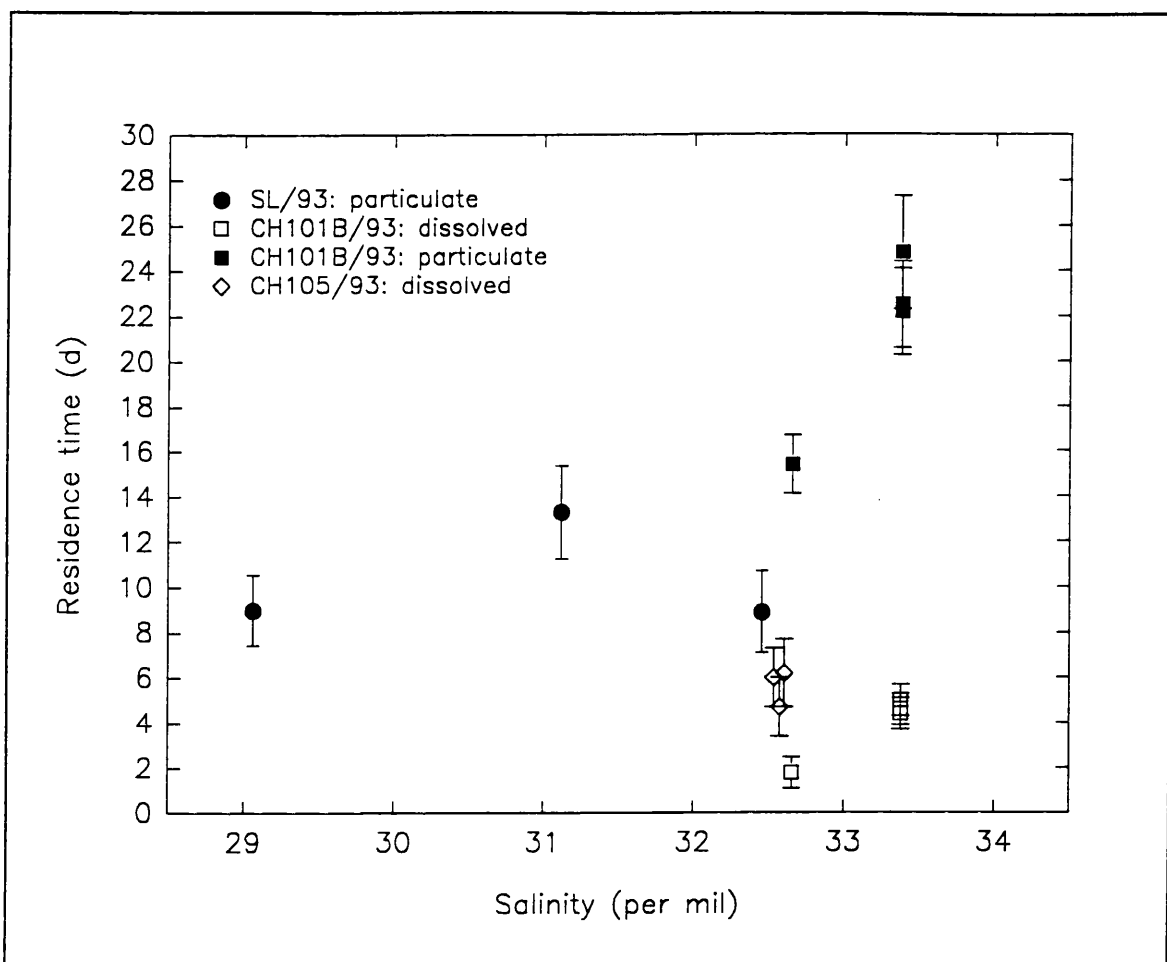


Figure 4.11: Residence times for ^{234}Th in the dissolved and particulate phases for the Firth of Clyde samples vs. salinity.

residence time for particulate ^{234}Th , as the freshwater component decreases, is indicative of more rapid sinking of material closer to shore, with the finer grained material being carried into the open Firth, where salinities are higher. These data can be compared to those of Kershaw and Young (1988) from the Irish Sea of $\tau_d = 0.5\text{-}7.7$ d and $\tau_p = 7\text{-}50$ d; McKee *et al.* (1984) from the Yangtze shelf of $\tau_d = 0.33\text{-}3.90$ d and $\tau_p = 0.46\text{-}11.2$ d; Moran and Buesseler (1993) for Buzzards Bay, Massachusetts of $\tau_d = 0.91\text{-}3.63$ d, $\tau_c = 0.11\text{-}0.68$ d and $\tau_p = 0.86\text{-}8.86$ d and Battaglia *et al.* (1988) for the Mediterranean of $\tau_d = 1.8$ d and $\tau_p = 18.6$ d for a sample depth of 30 m. The values determined within the present work are consistent with those found for other areas with relatively high sedimentation rates.

4.3.2 Hydrothermal vents in the Mid-Atlantic Ridge

4.3.2.1 Introduction

Hydrothermal activity occurs in regions of ocean-floor spreading, when seawater permeates into newly-formed crust through cracks and fissures and is heated by the proximity of a magma chamber (Bearman, 1992). The seawater and rock interact to produce a hot (~ 350°C), acidic (pH ~ 4), reducing fluid that is significantly different in composition to deep-ocean water, typically being enriched in iron, manganese, silica and many other trace and rare earth elements, while being depleted with respect to magnesium and sulphate (*e.g.* Edmond *et al.*, 1979; Von Damm *et al.*, 1985; Campbell *et al.*, 1988). The hydrothermal fluid rises to the surface and is issued at localized vents (Libes, 1992), where it immediately reacts with the alkaline, oxic seawater to produce copious quantities of metal sulphides and oxides, giving rise to the name "black smokers" (Bearman, 1992; Libes, 1992). Although there are considerable geological differences between the spreading centres in the Pacific and Atlantic oceans, such as rate of spreading and depth of the magmatic heat source, it has been found that the chemistry of hydrothermal vent fluids is similar at both (Campbell *et al.*, 1988).

The plume of material emanating from a vent is significantly more buoyant than the surrounding water, owing to its higher temperature, and rises in a plume several hundred meters above the sea-floor (German *et al.*, 1991*a*). As the plume rises, surrounding water is entrained and carried upwards until neutral buoyancy is attained, at which point an effluent layer, typically a few hundred meters thick, is formed with a distinct hydrothermal signature (Lupton *et al.*, 1985). $^3\text{He}/^4\text{He}$ ratios of material derived from the mantle are ten times greater than that in the atmosphere and it has been found that both ^3He and manganese concentrations can serve as highly sensitive tracers of water that has a hydrothermal origin (Lupton *et al.*, 1980) allowing both detection of hydrothermal activity (Jenkins *et al.*, 1980) and lateral dispersion to be followed. Temperature measurements alone

do not provide a sufficiently high degree of sensitivity to trace hydrothermal plumes, as the effluent layer is very dilute - measurements of this layer directly above the Endeavour vent field on the Juan de Fuca Ridge in the Pacific indicated that it consisted of only 0.01% vent water, 30% ambient seawater from that depth and 70% entrained water brought up from depth (Lupton *et al.*, 1985) - and further dilution will occur as the plume travels further from its origin. Although manganese has sources other than the mantle, particularly close to the continents, manganese anomalies in sediments adjacent to the East Pacific Rise have been shown to correspond to mid-water currents (Klinkhammer and Hudson, 1986). However, the MAR hydrothermal vents give rise to plumes that do not exceed the height of the rift valley in which they are situated, which constrains lateral dispersion and, hence, the hydrothermal material is restricted in range (Klinkhammer *et al.*, 1985).

It is now recognized that hydrothermal circulation plays a significant role in determining the concentration of many elements that occur in seawater (Jenkins *et al.*, 1980). Although hydrothermal fluids are rich in many metallic elements relative to seawater, their net effect may be as a sink rather than a source, as a result of the scavenging behaviour of the iron oxyhydroxides (section 1.4.1) that make up the bulk of particles in hydrothermal plumes (German *et al.*, 1991a). Studies of the TAG hydrothermal vent area on the MAR indicated that particulate iron and dissolved manganese concentrations are closely correlated, with the effect that particulate iron can be used as an indicator of hydrothermal material in the plume (Trocine and Trefy, 1988; German *et al.*, 1991b). Although metal sulphides initially form a large proportion of hydrothermal particulates, these are soon lost from the plume either by settling or dissolution, taking associated trace metals such as cadmium or zinc with them (Trocine and Trefy, 1988). Two types of scavenging behaviour by the iron oxyhydroxide particulates have been demonstrated to occur: the rare earth elements and some trace elements, such as beryllium and yttrium, are scavenged from the seawater that dilutes the plume, whereas others, such as vanadium or chromium, are scavenged rapidly as the iron oxyhydroxides form, but no further

scavenging occurs (German *et al.*, 1990; German *et al.*, 1991b). Trace elements in this latter group are not thought to comprise a significant proportion of hydrothermal fluids and, hence, are scavenged from seawater alone (Trocine and Trefy, 1988).

Although some information on the scavenging processes that occur within the hydrothermal plume can be gained from studying trace element data, an alternative means is required to determine how quickly these processes occur. The distribution of naturally occurring radionuclides between the dissolved and particulate phases can be used to define more accurately the time scales over which scavenging occurs. Again at the TAG site, German *et al.* (1991a) studied the effect of hydrothermal scavenging on activities of ^{234}Th , ^{230}Th , ^{228}Th , ^{231}Pa and ^{210}Pb in the particulate phase and ^{230}Th and ^{228}Th in the dissolved phase. These nuclides all showed considerable scavenging from the dissolved phase, with scavenging continuing as the plume dispersed. A model based on ^{230}Th activities included the assumption that the residence time for particles in the neutrally buoyant plume was ~ 1 month, and found that up to 75% of particles were recycled, *i.e.* re-entrained particulate material that had previously settled out of the plume (German *et al.*, 1991a). If processes within the plume have such rapid rates, it is implied that models based on $^{234}\text{Th}/^{238}\text{U}$ disequilibria would be more applicable.

4.3.2.2 Experimental methods

Samples were collected by C. R. German, of the Institute of Oceanographic Sciences - Deacon Laboratory (IOSDL), during the RRS *Charles Darwin* cruise (CD77/93) to the Mid-Atlantic Ridge in March/April 1993. Three hydrothermal vent fields were sampled, namely MARK (23°N), TAG (26°N) and Broken Spur (29°N) and samples were taken at depths ranging between 2688 and 3444 m. Approximately 1000 l of seawater were sampled at each point by pumping it firstly through a filter (293 mm diameter, 1.0 μm Nuclepore) and then sequentially through two manganese dioxide cartridges (a and b) using Stand-Alone Pumps (SAPs). The filters were leached with ~ 60 ml concentrated nitric acid at Bristol University and the manganese dioxide cartridges with 1500 ml

recirculating 1.5M nitric acid followed by 1500 ml 1.5M hydrochloric acid, which were subsequently combined, at IOSDL - techniques used with quantitative yields for these sample types on previous occasions (German *et al.*, 1991a; Thomson *et al.*, 1993). Aliquots of each solution (10 ml filter solutions and 300 ml manganese cartridge solutions) representing ~ 200 and 100 l seawater respectively were sent to the SURRC for ^{234}Th analysis by α/β LSS.

Upon arrival at the SURRC, each solution was spiked with ^{230}Th (50 dpm for (b) cartridges and 100 dpm for (a) cartridges and filter solutions) and iron (III) carrier was added (3 mg Fe^{3+} for the manganese dioxide cartridges, 2 mg Fe^{3+} for the filters). These ^{230}Th activities were chosen to be significantly in excess of the ^{230}Th occurring in the sample (German *et al.*, 1991a). The samples were then left for a minimum of 24 h to allow equilibration of the spike. The (a) and (b) solutions were reduced to < 150 ml by gentle heating, before transferring with distilled water rinses to a 200 ml centrifuge bottle. The filter solutions were transferred to 50 ml centrifuge tubes with no volume reduction. All samples were treated in the same manner from this point onwards. The pH was raised to ~ 7 with concentrated ammonium hydroxide to precipitate iron (III) hydroxide, to scavenge thorium from solution, and the sample was shaken vigorously for several minutes. The samples were centrifuged for 6-10 min at 4500 rpm and the supernatant liquid poured off. The precipitate was washed with ~ 50 ml distilled water and centrifuged as before. The precipitate was dissolved in a small quantity of 9M hydrochloric acid and made up to 50 ml with distilled water. The procedure was repeated, but with the precipitate being dissolved finally in 50 ml 9M hydrochloric acid. From this point onwards, samples were treated as for seawater samples (Fig 3.8), with the counting being performed in the 2550 TR/AB (b), for 400 min in the LLCM with DBB = 800 ns and PDD = 110. A β window of 0-120 keV and an α window of 120-280 keV were applied. A total of 16 backgrounds and 16 spikes (as described in section 3.3.3.1) were counted amongst the samples. It was assumed that ^{238}U activities in both the manganese cartridge and filter samples were negligible based on previous work

(German *et al.*, 1991a).

4.3.2.3 Results and discussion

Results were calculated as described in section 3.3.4 and are given in Table 4.6. Yields for the filter analyses ranged between 78 and 90%, with a mean of 86%, and for the manganese cartridge analyses between 77 and 100%, with a mean of 88%. For the manganese cartridges, tSIEs ranged between 406 and 424 and for the filters between 403 and 427. These ranges are consistent with those found for seawater samples and are within the limits required to avoid problems associated with quenching. The mean elapsed time between sampling and the start of counting was 64.76 d for the particulate samples and 44.2 d for the dissolved samples. Overall, the relative errors ranged between 2.1 and 6.3% for particulate samples and 1.2 and 2.0% for dissolved samples. These data together indicate that the separation chemistry employed was suitable for these sample types, which contained large quantities of dissolved metals, in particular iron and manganese, and these did not present any difficulties with subsequent counting procedures. German *et al.* (1991a) used a high-purity germanium γ detector for analysis of ^{234}Th in untreated filter samples upon return to the laboratory, which required count times of ~ 24 h and resulted in relative errors of between 5 and 8%. The errors between the two methods compare favourably when it is considered that the sample volume employed for the analysis in the present work was approximately one fifth that employed in German *et al.* (1991a) and the count time was considerably shorter.

The most readily apparent point of interest about these data is the cartridge scavenging efficiencies, which were calculated using equation 3.1. These are highly variable and several are negative, indicating that more thorium was deposited on the second cartridge than the first and hence that the cartridges were not behaving in a consistent manner. Data obtained for these cartridges pertaining to other thorium isotopes is consistent with that obtained for ^{234}Th , indicating that this was not caused by an analytical problem associated with the ^{234}Th analysis (C. R. German, personal

Table 4.6: Results from hydrothermal vent samples collected at the MARK, TAG and Broken Spur sites. Errors are quoted at the 1σ level of confidence.

A) MARK site												
Sample	Latitude (°N)	Longitude (°W)	Water depth (m)	Sampling depth (m)	Volume sampled (l)	²³⁴ Th adsorbed onto MnO ₂ (dpm l ⁻¹)	Cartridge efficiency (%)	Dissolved ²³⁴ Th activity ^a (dpm l ⁻¹)	Particulate ²³⁴ Th activity (dpm l ⁻¹)	Total ²³⁴ Th activity ^a (dpm l ⁻¹)		
314Ba	23° 22.07'	44° 56.96'	3532	3444	1333	0.44 ± 0.01	32.44	0.74 ± 0.01	0.12 ± 0.01	0.86 ± 0.01		
314Bb						0.30 ± 0.01						
317Ta	23° 22.14'	44° 57.06'	3538	3307	1093	0.63 ± 0.02 (0.36 ± 0.01) ^b	49.22	0.95 ± 0.02 (0.77 ± 0.02) ^b	0.15 ± 0.01	1.10 ± 0.02 (0.92 ± 0.02) ^b		
317Tb						0.32 ± 0.01 (0.41 ± 0.01) ^b						
317Ba				3407	1260	0.37 ± 0.01	40.44	0.59 ± 0.01	0.11 ± 0.01	0.70 ± 0.01		
317Bb						0.22 ± 0.01						
323Ta	23° 22.09'	44° 57.12'	3497	3366	1288	0.36 ± 0.01	7.04	0.69 ± 0.01	0.12 ± 0.01	0.81 ± 0.01		
323Tb						0.33 ± 0.01						
323Ba				3409	1260	0.32 ± 0.01	-9.03	0.67 ± 0.01	0.10 ± 0.01	0.77 ± 0.01		
323Bb						0.35 ± 0.01						
329Ba	23° 22.15'	44° 57.16'	3468	3293	1175	0.32 ± 0.01 (0.55 ± 0.01) ^b	-13.07	0.68 ± 0.01 (0.83 ± 0.02) ^b	0.08 ± 0.01 ^c	0.76 ± 0.01 (0.91 ± 0.02) ^b		
329Bb						0.36 ± 0.01 (0.28 ± 0.01) ^b						
B) TAG site												
Sample	Latitude (°N)	Longitude (°W)	Water depth (m)	Sampling depth (m)	Volume sampled (l)	²³⁴ Th adsorbed onto MnO ₂ (dpm l ⁻¹)	Cartridge efficiency (%)	Dissolved ²³⁴ Th activity ^a (dpm l ⁻¹)	Particulate ²³⁴ Th activity (dpm l ⁻¹)	Total ²³⁴ Th activity ^a (dpm l ⁻¹)		
403Ta	26° 08.24'	44° 49.58'	3641	3340	784	0.33 ± 0.01	-83.38	0.93 ± 0.02	1.47 ± 0.03	2.40 ± 0.04		
403Tb						0.60 ± 0.01						
403Ba				3440	933	0.31 ± 0.01	13.63	0.58 ± 0.01	0.59 ± 0.02	1.17 ± 0.02		

communication, 1994). Although these cartridges came from a commercial source, it is apparent that there is either a general problem with their use or that this particular batch did not have adequate quality checks made. Many groups have employed these cartridges for thorium analysis in a variety of oceanographic settings, apparently without problem, and German *et al.* (1991a) used these cartridges successfully in a previous study of hydrothermal vents, with a mean scavenging efficiency of $80 \pm 5\%$, which implies that this is not an unsuitable application for their use. However, Thomson *et al.* (1993) reported similar difficulties to those reported here in a study of ^{210}Pb and proposed that either manganese was being stripped from the (a) cartridge and being redeposited on the (b) cartridge or that channelling of the water flow was occurring, with the effect that the maximum scavenging efficiency was not occurring. Thus, it is uncertain whether the problem is an isolated incident or indicative of a more widespread problem.

If cartridge efficiencies are ignored, as they must be since the calculation used to derive them is based on the assumption of equal scavenging by (a) and (b) cartridges, the dissolved ^{234}Th values determined can be seen as minimum values. Thus, a limited amount of data can be derived, although it is of no use in the development of a scavenging model for hydrothermal vent systems. Figure 4.12 shows the data for the three sites, with the TAG and Broken Spur sites both showing increased ^{234}Th in the particulate phase at plume height (3340 and 2827 m respectively), although this is very slight in the latter case. The lack of a distinct change in scavenging efficiency at the plume height for the MARK samples is attributable to the particulate iron concentrations. These range between 4.0 and 58.0 nmol l^{-1} for TAG, 2.0 and 13.6 nmol l^{-1} for Broken Spur and 2.7 and 5.3 nmol l^{-1} for MARK samples (C. R. German, personal communication, 1994). As iron oxyhydroxides are responsible for thorium scavenging, if iron concentrations fall so will scavenging efficiency and the activity of thorium in the particulate phase will drop. This also accounts for the difference in particulate ^{234}Th activities between the present work for the MARK and Broken Spur samples and those reported in German *et*

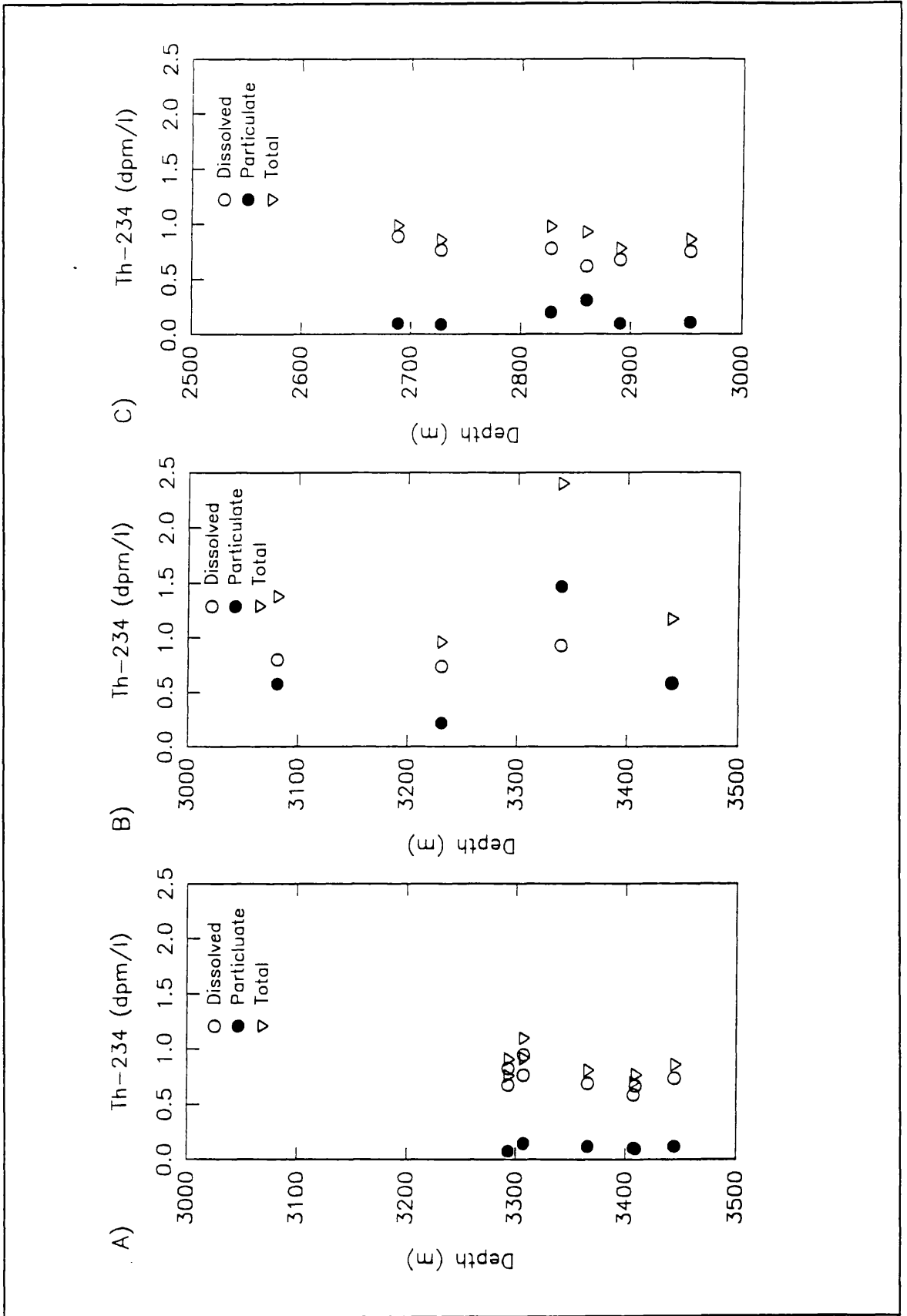


Figure 4.12: Depth profiles of samples taken at the Mid-Atlantic Ridge. A) MARK site, B) TAG site and C) Broken Spur site. Errors (1σ) are smaller than the symbols unless shown.

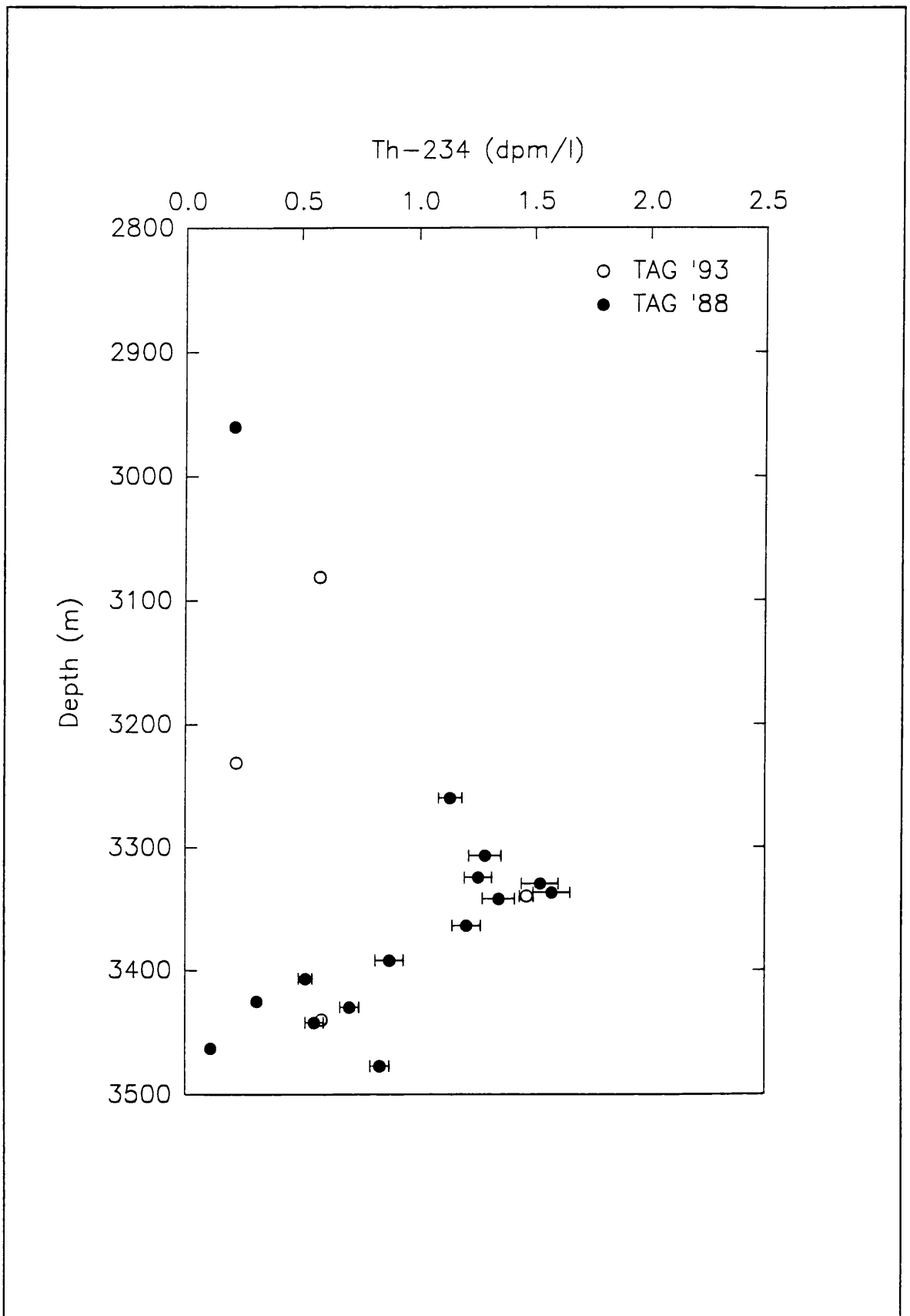


Figure 4.13: Particulate ^{234}Th data from the TAG site for 1988 (from German et al., 1991a) and 1993. Errors (1σ) are smaller than the symbol unless shown.

al. (1991a) for the TAG site, when the particulate iron concentrations ranged between 1 and 212 nmol l⁻¹. Figure 4.13 gives a comparison between ²³⁴Th data for the TAG site from the present work and from German *et al.* (1991a), which were collected in 1988. Although the present data set is much more restricted than in the previous work, the general trend is similar and there appears to be reasonable agreement between the two sampling occasions. This provides further evidence that the α/β LSS technique for ²³⁴Th measurements is applicable to this type of samples.

4.4 CONCLUSIONS

The applications discussed in this chapter have shown that α/β LSS is a method that can be used effectively for ²³⁴Th analysis in coastal, open ocean and hydrothermal samples with a reasonable degree of accuracy. Quenching has not been found to be a problem with the sample types studied, despite indications to the contrary, from examining the effects of nitromethane over the same tSIE range (390-430) (section 3.3.3.5). When marine samples were analysed, no apparent change in the results could be found by using either of two α counting windows (*i.e.* 110-280 keV or 120-280 keV). In addition, as the separation chemistry was refined, the range of tSIEs dropped to ~ 20 units. At this level, quenching did not appear to affect α or β counting efficiencies or PSD. The discrepancy observed between the nitromethane study (section 3.3.3.5) and the marine samples is probably due either to nitromethane not being the quenching agent in these samples, which could bring about significantly different results (see section 2.3.2), or to the size of changes induced in the count rate, if small the effect on the final result will be masked in subsequent calculations.

The majority of particulate and dissolved ²³⁴Th concentrations from the Northeast Atlantic were above the limit of detection for this method. However, the dissolved ²³⁴Th concentrations from the Firth of Clyde were below the limit of detection, due high sedimentation rates in this area. If 20 l samples had been taken, all samples would have been within the limit of detection. Although the sampling

resolution for the Northeast Atlantic was low, it was still possible to determine the point at which the highest scavenging rate occurred, which corresponded to the position of the front between open ocean and coastal waters. Thus, the detection limit for this method allows its use in this type of marine environment.

The study of hydrothermal vents has shown that serious problems can arise with the use of manganese cartridges to sample thorium from large volumes of seawater, calling into question the validity of their use. However, if other thorium isotopes are to be analysed and the use of manganese cartridges is necessary, then a subsample can be used for ^{234}Th analysis by α/β LSS with no further problems. The separation chemistry developed for seawater and suspended material continued to be effective for the hydrothermal vent samples, despite high concentrations of manganese and other metals, as indicated by the tSIEs and chemical yields. The greater counting efficiency found with LSS than for γ -spectrometry negates the need to carry out the analysis while at sea, even if only subsamples are analysed (*i.e.* 100-200 l), or alternatively manganese cartridges could be avoided and 100 l samples taken for later processing (the iron (III) hydroxide precipitation being performed at sea for ease of transport).

CHAPTER 5: CONCLUSIONS

The efficiency with which α and β events are allocated to their separate MCAs was found to be highly dependent on the shapes of the PMT anode pulse shapes and the light output of the cocktail. Several factors were found to be of particular importance in optimizing α/β separation:

- cocktail composition - the use of a cocktail containing a "slow" solvent such as DIN or naphthalene enhances event separation.
- quenching - this should be constant or, if necessary, its effects quantified using the quenching impurities present in the sample matrix, as different quenching agents have different effects.
- glass vials - these produce better event separation than plastic vials, although energy resolution can be poorer.

In general, PSD can be vulnerable to small variations in sample composition, which could lead to erroneous results if not detected. Therefore, in determining the degree of misclassification, it is desirable to use standards (*i.e.* the pure α emitter and the pure β emitter) that are as close as possible in composition to the samples.

α/β LSS was found to be a useful tool in the analysis of ^{234}Th in marine samples. Sample sizes of 10 l were successfully employed, with a resulting limit of detection of 0.08 dpm l⁻¹. The limit of detection could easily be reduced either by increasing the sample size to 20 l or by using an instrument with enhanced background reduction. Advantages over both β -counting and γ -spectrometry included the smaller sample sizes and shorter counting times (400 min for α/β LSS). The analytical method that was developed is still not fully suitable for shipboard analysis, as it involves excessive chemical manipulation. However, the use of small manganese dioxide columns to replace the initial preconcentration steps showed potential. Their use could result in a significant reduction in the

volumes of acid required for the remaining part of the procedure and, hence, allow the complete analysis to be performed at sea.

Although, in general, the level of quenching was found to be critical in maintaining a constant degree of α/β separation, within the tSIE range found for marine samples in this study, neither the ^{234}Th nor ^{230}Th counting efficiencies were affected. In addition, with practice, a near constant degree of quenching could be achieved, covering ~ 20 tSIE units.

For the 10 l samples collected in the Northeast Atlantic, the mean relative error for the dissolved ^{234}Th activity was 13.3% and for the particulate ^{234}Th activity it was 15.0%. It was shown that increasing the count time from 200 to 400 min had a significant effect on reducing the errors. In addition, the elapsed time between sampling and the separation of ^{238}U by ion exchange was critical if reasonable errors were to be obtained. This implies that it is necessary to perform at least the initial stages of the chemical purification while at sea, even for relatively short cruises. The background of the instrument was also shown to be an important contributor to both the limit of detection for the method and the errors obtained. While the instrument employed in this study had a β background of ~ 11 cpm, in the region of interest, a more modern instrument with enhanced background reduction could give a β background of just 4.5 cpm.

The study of particle fluxes in the Northeast Atlantic showed that $^{234}\text{Th}/^{238}\text{U}$ disequilibrium can be used to detect higher rates of thorium scavenging by particles, associated with a front. Despite the coarse resolution of the sampling, the technique was sufficiently precise to allow differences to be detected both with distance from shore and with season. Samples taken in the Firth of Clyde were, in general, close to the detection limit for this method. However, increasing the sample size to 20 l would have overcome this difficulty and allowed more precise quantification of the scavenging rates in this area.

The study of hydrothermal vents allowed two main conclusions to be drawn. Firstly, the

method developed for the analysis of seawater and marine particulate material was also suitable for the analysis of leached manganese dioxide cartridges. The greater counting efficiency of LSS allowed the ^{234}Th analysis to be performed on return to the laboratory, negating the need for a sea-going γ -detector. Secondly, the manganese cartridges employed in this work resulted in inconsistent scavenging efficiencies for thorium, which prevented further use of the data.

To summarise, a thorough survey of the parameters affecting α/β LSS has shown those which are important in optimising performance. α/β separation was achieved to a high degree (approximately 0.1% misclassification). α/β LSS was shown to be a useful technique for the analysis of ^{234}Th in marine samples and, with a little more work, could become a valid shipboard method.

REFERENCES

- Abuzeida, M., Arebi, B. H., Zolaterov, Y. A. and Komarov, N. A. 1987 Selective liquid scintillation method of uranium α -spectrometry. *Journal of Radioanalytical and Nuclear Chemistry, Articles* 116(2): 285-289.
- Adams, F. and Dams, R. 1970 *Applied Gamma-Ray Spectrometry*. Oxford, Pergamon Press: 751 p.
- Adu, J. K. and Oades, J. M. 1974 Suspension counting of ^{14}C in soil, soil extracts and plant materials by liquid scintillation. In: Stanley, P. E. and Scroggins, B. A., eds., *Liquid Scintillation Counting. Recent Developments*. New York, Academic Press: 207-221.
- Agno, M., Chiozzotto, M. and Querzoli, R. 1950 Scintillations in liquids and solutions. *Physical Review* 79: 720.
- Aldrich 1992 *Catalogue Handbook of Fine Chemicals*. Gillingham, England, Aldrich Chemical Company Limited: 1968 p.
- Aller, R. C. and DeMaster, D. J. 1984 Estimates of particle flux and reworking at the deep sea floor using $^{234}\text{Th}/^{238}\text{U}$ disequilibrium. *Earth and Planetary Science Letters* 67: 308-318.
- Alessio, M., Allegri, L., Bella, F. and Improta, S. 1976 Study of the background characteristics by means of a high efficiency liquid scintillation counter. *Nuclear Instruments and Methods* 137: 537-543.
- Alessio, M., Allegri, L., Bella, F. and Improta, S. 1978 Influence of quenching on the background of liquid scintillation counters. *Nuclear Instruments and Methods* 157: 579-582.
- Alexander, T. K. and Goulding, F. S. 1961 An amplitude-insensitive system that distinguishes pulses of different shapes. *Nuclear Instruments and Methods* 13: 244-246.
- Anderson, E. C. 1958 The Los Alamos human counters. In: Bell, C. G. and Hayes, F. N., eds., *Liquid Scintillation Counting*. London, Pergamon Press: 211-219.

- Anderson, R., Cook, G. T., MacKenzie, A. B. and Harkness, D. D. 1991 The determination of Th-234 in water column studies by liquid scintillation counting. *In: Ross, H. H., Noakes, J. E. and Spaulding, J. D., eds., Liquid Scintillation Counting and Organic Scintillators*. Chelsea, Michigan, Lewis Publishers: 461-470.
- Anderson, R. F. and Fler, A. P. 1982 Determination of natural actinides and plutonium in marine particulate material. *Analytical Chemistry* 54: 1142-1147.
- Anderson, R. F., Bacon, M. P. and Brewer, P. G. 1983 Removal of Th-230 and Pa-231 from the open ocean. *Earth and Planetary Science Letters* 62: 7-23.
- Atkins, P. W. 1986 *Physical Chemistry, 3rd ed.* Oxford, Oxford University Press: 857 p.
- Bacon, M. P. and Rosholt, J. N. 1982 Accumulation rates of Th-230, Pa-231, and some transition metals on the Bermuda Rise. *Geochimica et Cosmochimica Acta* 46: 651-666.
- Bacon, M. P. and Rutgers van der Loeff, M. M. 1989 Removal of thorium-234 by scavenging in the bottom nepheloid layer of the ocean. *Earth and Planetary Science Letters* 92(2): 157-164.
- Baskaran, M., Santschi, P. H., Benoit, G. and Honeyman, B. D. 1992 Scavenging of Th isotopes by colloids in seawater of the Gulf of Mexico. *Geochimica et Cosmochimica Acta* 56: 3375-3388.
- Basson, J. K. and Steyn, J. 1954 Absolute alpha standardization with liquid scintillator. *Proceedings of the Physical Society* A67: 297-298.
- Battaglia, A., Martinotti, W. and Queirazza, G. 1988 $^{234}\text{Th}/^{238}\text{U}$ disequilibrium to estimate the mean residence time of thorium isotopes in a coastal marine environment. *In: Guary, J. C., Guegueniat, P. and Pentreath, R. J., eds., Radionuclides: A Tool for Oceanography*. London, Elsevier Applied Science: 143-152.
- Baxter, M. S., McKinley, I. G., MacKenzie, A. B. and Jack, W. 1979 Windscale radiocaesium in the Clyde Sea area. *Marine Pollution Bulletin* 10: 116-120.
- Bearman, G., ed. 1992 *The Ocean Basins: Their Structure and Evolution*. Oxford, Pergamon

- Press/The Open University: 171 p.
- Berlman, I. B. 1971 *Handbook of Fluorescence Spectra of Aromatic Molecules*. New York, Academic Press: 471 p.
- Berlman, I. B., Grismore, R. and Oltman, B. G. 1963 Study of α/β ratios of organic scintillation solutions. *Transactions of the Faraday Society* 59: 2010-2015.
- Bhat, S. G., Krishnaswami, S., Lal, D., Rama, and Moore, W. S. 1969 Th-234/U-238 ratios in the ocean. *Earth and Planetary Science Letters* 5: 483-491.
- Birks, J. B. 1951a Scintillations from organic crystals: specific fluorescence and relative response to different radiations. *Proceedings of the Physical Society* A64: 874-877.
- Birks, J. B. 1951b The specific fluorescence of anthracene and other organic materials. *Physical Review* 84: 364-365.
- Birks, J. B. 1964 *The Theory and Practice of Scintillation Counting*. Oxford, Pergamon Press: 662 p.
- Birks, J. B. 1970 Physics of the liquid scintillation process. In: Bransome, E. D., ed., *The Current Status of Liquid Scintillation Counting*. New York, Grune and Stratton, Inc.: 3-12.
- Birks, J. B. 1974 Towards an understanding of the scintillation process in organic molecular systems. In: Stanley, P. E. and Scroggins, B. A., eds., *Liquid Scintillation Counting. Recent Developments*. New York, Academic Press: 1-38.
- Birks, J. B. and Aladekomo, J. B. 1963 The photo-dimerization and excimer fluorescence of 9-methyl anthracene. *Photochemistry and Photobiology* 2: 415-418.
- Birks, J. B. and Kuchela, N. N. 1961 Energy transfer in organic systems II: solute-solute transfer in liquid solutions. *Proceedings of the Physical Society* 77: 1083-1094.
- Bollinger, L. M. and Thomas, G. E. 1961 Measurement of the time dependence of scintillation intensity by a delayed-coincidence method. *Review of Scientific Instruments* 32(9): 1044-1050.
- Bond, C. W. 1984 Liquid scintillation counting: elimination of spurious results due to static electricity.

International Journal of Applied Radiation and Isotopes 35(6): 550-551.

- Boniforti, R. 1987 Lanthanides, uranium, and thorium as possible simulators of the behaviour of transuranics in the aquatic environment. *The Science of the Total Environment* 64(1-2): 181-189.
- Bouwer, E. J., McKlveen, J. W. and McDowell, W. J. 1979 A solvent extraction-liquid scintillation method for assay of uranium and thorium in phosphate-containing materials. *Nuclear Technology* 42: 102-111.
- Bradley, P. E., Economides, B. E., Baxter, M. S. and Ellett, D. J. 1988 Sellafield radiocaesium as a tracer of water movement in the Scottish coastal zone. In: Guary, J. C., Guegueniat, P. and Pentreath, R. J., eds., *Radionuclides: A Tool for Oceanography*. London, Elsevier Applied Science: 281-293.
- Bray, G. A. 1960 A simple efficient liquid scintillator for counting aqueous solutions in a liquid scintillation counter. *Analytical Biochemistry* 1: 279-285.
- Broecker, W. S., Kaufman, A. and Trier, R. M. 1973 The residence time of thorium in surface seawater and its implications for the fate of reactive pollutants. *Earth and Planetary Science Letters* 20: 35-44.
- Broecker, W. S. and Peng, T.-H. 1982 *Tracers in the Sea*. Palisades, New York, Lamont-Doherty Geological Observatory: 690 p.
- Brooks, F. D. 1956 Organic scintillators. *Progress in Nuclear Physics* 5: 252-313.
- Brooks, F. D. 1958 Scintillation counters with pulse shape selection to distinguish neutrons from gamma-rays. In: Bell, C. G. and Hayes, F. N., eds., *Liquid Scintillation Counting*. London, Pergamon Press: 268-269.
- Brooks, F. D. 1979 Development of organic scintillators. *Nuclear Instruments and Methods* 162: 477-505.

- Broser, I. and Kallmann, H. 1947 Über die Angerung von Leuchtstoffen durch schnelle Korpuskularteilchen I. Eine neue Methode zur Registrierung und Energiemessung. *Zeitschrift für Naturforschung* 2A(8): 439-440.
- Buesseler, K. O. 1991 Do upper-ocean sediment traps provide an accurate record of particle flux? *Nature* 353: 420-423.
- Buesseler, K. O., Bacon, M. P., Cochran, J. K. and Livingston, H. D. 1992a Carbon and nitrogen export during the JGOFS North Atlantic Bloom Experiment estimated from ^{234}Th : ^{238}U disequilibrium. *Deep-Sea Research* 39(7/8): 1115-1137.
- Buesseler, K. O., Cochran, J. K., Bacon, M. P., Livingston, H. D., Casso, S. A., Hirschberg, D., Hartman, M. C. and Fleer, A. P. 1992b Determination of thorium isotopes in seawater by non-destructive and radiochemical procedures. *Deep-Sea Research* 39: 1103-1114.
- Burnett, W. C. and Tai, W.-C. 1992 Determination of radium in natural waters by alpha liquid scintillation. *Analytical Chemistry* 64: 1691-1697.
- Burns, P. D. and Steiner, R., eds. 1991 *Advanced Technology Guide for LS 6000 Series Scintillation Counters*. Bulletin No. 7885. Fullerton, California, Beckman Instruments: 66 p.
- Bush, E. T. 1963 General applicability of the channels ratio method of measuring liquid scintillation counting efficiencies. *Analytical Chemistry* 35(8): 1024-1029.
- Buzinny, M. G., Zelensky, A. V. and Los', I. P. 1993 Beta-spectrometric determination of ^{90}Sr in water, milk and other samples with an ultra-low level liquid scintillation counter. *In*: Noakes, J. E., Schönhofer, F. and Polach, H. A., eds., *Liquid Scintillation Spectrometry 1992*. Tuscon, Arizona, Radiocarbon: 439-446.
- Campbell, A. C., Palmer, M. R., Klinkhammer, G. P., Bowers, T. S., Edmond, J. M., Lawrence, J. R., Casey, J. F., Thompson, G., Humphris, S., Rona, P. and Karson, J. A. 1988 Chemistry of hot springs on the Mid-Atlantic Ridge. *Nature* 335: 514-519.

- Carrasco, C. H. and McKlveen, J. W. 1985 A new scheme for liquid scintillation pulse-shape discrimination. *Transactions of the American Nuclear Society* 50: 23-24.
- Case, G. N. and McDowell, W. J. 1982 An improved sensitive assay for polonium-210 by use of a background-rejecting extractive liquid-scintillation method. *Talanta* 29: 845-848.
- Chester, R. 1990 *Marine Geochemistry*. London, Unwin Hyman: 698 p.
- Chen, J. H., Edwards, R. L. and Wasserburg, R. G. 1986 ^{238}U , ^{234}U and ^{232}Th in seawater. *Earth and Planetary Science Letters* 80: 241-251.
- Clegg, S. L. and Whitfield, M. 1990 A generalized model for the scavenging of trace metals in the open ocean - I. Particle cycling. *Deep-Sea Research* 37(5): 809-832.
- Coale, K. H. and Bruland, K. W. 1985 $^{234}\text{Th}/^{238}\text{U}$ disequilibrium within the California current. *Limnology and Oceanography* 30: 22-33.
- Coale, K. H. and Bruland, K. W. 1987 Oceanic stratified euphotic zone as elucidated by ^{234}Th - ^{238}U disequilibria. *Limnology and Oceanography* 32(1): 189-200.
- Cochran, J. K. 1992 The oceanic chemistry of the uranium- and thorium-series nuclides. In: Ivanovich, M. and Harmon, R. S., eds., *Uranium-series Disequilibrium: Applications to Earth, Marine and Environmental Sciences, 2nd ed.* Oxford, Clarendon Press: 334-395.
- Cochran, J. K., Buesseler, K. O., Bacon, M. P. and Livingston, H. D. 1993 Thorium isotopes as indicators of particle dynamics in the upper ocean - results from the JGOFS North-Atlantic Bloom Experiment. *Deep-Sea Research* 40(8): 1569-1595.
- Cook, G. T. and Anderson, R. 1991 The determination of ^{241}Pu by liquid scintillation spectrometry using the Packard 2250CA. *Journal of Radioanalytical and Nuclear Chemistry, Letters* 154(5): 319-330.
- Cook, G. T. and Anderson, R. 1992 A radiocarbon dating protocol for use with Packard scintillation counters employing burst-counting circuitry. *Radiocarbon* 34(3): 381-388.

- Cook, G. T. and Anderson, R. 1993 Assessment of new features on a commercial liquid scintillation spectrometer for radiocarbon dating. *In: Noakes, J. E., Schönhofer, F. and Polach, H. A., eds., Liquid Scintillation Spectrometry 1992.* Tucson, Arizona, Radiocarbon: 17-21.
- Cook, G. T., Bury, S. J., Anderson, R., MacKenzie, A. B. and Thomson, J. *In preparation* A novel ^{234}Th measurement technique applied to euphotic zone production studies.
- Cross, P. and McBeth, G. W. 1976 Liquid scintillation alpha particle assay with energy and pulse shape discrimination. *Health Physics* 30: 303-306.
- Currie, L. A. 1968 Limits for qualitative detection and quantitative determination. *Analytical Chemistry* 40(3): 586-593.
- Czirr, J. B. 1963 The α/β ratio of several organic scintillators. *Nuclear Instruments and Methods* 25: 106-108.
- Dahlberg, E. 1982 Quench correction in liquid scintillation counting by a combined internal standard-samples channels ratio technique. *Analytical Chemistry* 54: 2082-2085.
- Daehnick, W. and Sherr, R. 1961 Pulse shape discrimination in stilbene scintillators. *Review of Scientific Instruments* 32(6): 666-670.
- De Filippis, S. J. and van Caeter, S. C. 1985 A novel approach to external standardization in liquid scintillation counting. *Transactions of the American Nuclear Society* 50: 22-23.
- Dyer, A. 1974 *An Introduction to Liquid Scintillation Counting.* London, Heyden: 111 p.
- Ediss, C. 1980 A multichannel analyzer interface for a Beckman 9000 liquid scintillation counter. *In: Peng, C.-T., Horrocks, D. L. and Alpen, E. L., eds., Liquid Scintillation Counting. Recent Applications and Development. Volume 1: Physical Aspects.* New York, Academic Press: 281-289.
- Edmond, J. M., Measures, C., McDuff, R. E., Chan, L. H., Collier, R., Grant, B., Gordon, L. I. and Corliss, J. B. 1979 Ridge crest hydrothermal activity and the balances of the major and minor

- elements in the ocean: the Galapagos data. *Earth and Planetary Science Letters* 46: 1-18.
- Effertz, B., Neumann, K. and Englert, D. 1993 Single photomultiplier technology for scintillation counting in microplates. *In: Noakes, J. E., Schönhofer, F. and Poalch, H. A., eds., Liquid Scintillation Spectrometry 1992*. Tucson, Arizona, Radiocarbon: 37-42.
- Einarsson, S. A. 1992 Evaluation of a prototype low-level scintillation multisample counter. *Radiocarbon* 34(3): 366-373.
- Elliott, J. C. 1984 Effect of vial composition and diameter on determination of efficiency, background, and quench curves in liquid scintillation counting. *Analytical Chemistry* 56: 758-761.
- Elliott, J. C. and van Mourik, B. 1987 A performance comparison of select alkylbenzene and detergent based liquid scintillation cocktails. *Applied Radiation and Isotopes* 38(8): 629-633.
- Faure, G. 1986 *Principles of Isotope Geology, 2nd ed.* New York, John Wiley and Sons: 589 p.
- Fleischer, R. L. 1980 Isotopic disequilibrium of uranium: alpha-recoil damage and preferential solution effects. *Science* 207: 979-981.
- Friedlander, G., Kennedy, J. W., Macias, E. S. and Miller, J. M. 1981 *Nuclear and Radiochemistry, 3rd ed.* New York, John Wiley and Sons: 684 p.
- Fujii, H., Takiue, M. and Ishikawa, H. 1989 New emulsive scintillator for liquid scintillation measurements. *Applied Radiation and Isotopes* 40(3): 235-238.
- Furst, M. and Kallmann, H. 1958 Concentration quenching of liquid scintillators. *In: Bell, C. G. and Hayes, F. N., eds., Liquid Scintillation Counting*. London, Pergamon Press: 237-245.
- German, C. R., Klinkhammer, G. P., Edmond, J. M., Mitra, A. and Elderfield, H. 1990 Hydrothermal scavenging of rare earth elements in the ocean. *Nature* 345(6275): 516-518.
- German, C. R., Fleer, A. P., Bacon, M. P. and Edmond, J. M. 1991a Hydrothermal scavenging at the Mid Atlantic Ridge: radionuclide distributions. *Earth and Planetary Science Letters* 105: 170-181.

- German, C. R., Cambell, A. C. and Edmond, J. M. 1991*b* Hydrothermal scavenging at the Mid Atlantic Ridge: modification of trace element dissolved fluxes. *Earth and Planetary Science Letters* 107: 101-114.
- Gibson, J. A. B. 1980 Modern techniques for measuring the quench correction in a liquid scintillation counter: a critical review. *In: Peng, C.-T., Horrocks, D. L. and Alpen, E. L., eds., Liquid Scintillation Counting. Recent Applications and Development. Volume 1: Physical Aspects.* New York, Academic Press: 153-172.
- Grau Carles, A. and Grau Malonda, A. 1994 Alpha/beta separation in liquid scintillation gel samples. *Nuclear Instruments and Methods in Physics Research A* 345(1): 102-106.
- Guan, S. and Xie, Y. 1992 Instrumentation and software for low-level liquid scintillation counting radiocarbon dating. *Radiocarbon* 34(3): 374-380.
- Haas, H. and Trigg, V. 1991 Low-level scintillation counting with a LKB Quantalus counter establishing optimal parameter settings. *In: Ross, H. H., Noakes, J. E. and Spaulding, J. D., eds., Liquid Scintillation Counting and Organic Scintillators.* Chelsea, Michigan, Lewis Publishers: 669-675.
- Hayes, F. N. 1956 Liquid scintillators: attributes and applications. *International Journal of Applied Radiation and Isotopes* 1: 46-56.
- Hayes, F. N. and Gould, R. G. 1953 Liquid scintillation counting of tritium-labelled water and organic compounds. *Science* 117: 480-482.
- Hayes, F. N., Hiebert, R. D. and Schuch, R. L. 1952 Low energy counting with a new liquid scintillation solute. *Science* 116: 140.
- Hayes, F. N., Ott, D. G. and Kerr, V. N. 1956 Pulse-height comparison of secondary solutes. *Nucleonics* 14(1): 42-45.
- Hayes, F. N., Ott, D. G., Kerr, V. N. and Rogers, B. S. 1955*a* Pulse height comparison of primary solutes. *Nucleonics* 13(12): 38-41.

- Hayes, F. N., Rogers, B. S. and Sanders, P. C. 1955b Importance of solvent in liquid scintillators. *Nucleonics* 13(1): 46-48.
- Health and Safety Executive 1992 *EH40 / 92 Occupational Exposure Limits 1992*. London, HMSO: 46 p.
- Helf, S. 1958 Round-table on 'Suspension Counting'. In: Bell, C. G. and Hayes, F. N., eds., *Liquid Scintillation Counting*. London, Pergamon Press: 96-100.
- Hiebert, R. D. and Watts, R. J. 1953 Fast coincidence circuit for H³ and C¹⁴ measurements. *Nucleonics* 11(12): 38-41.
- Higashimura, T., Yamada, O., Nohara, N. and Shidei, T. 1962 External standard method for the determination of the efficiency in liquid scintillation counting. *International Journal of Applied Radiation and Isotopes* 13: 308-309.
- Hiller, A., Anderson, R. and Cook, G. T. 1994 Effects of a range of quenching agents on ¹⁴C-benzene counting efficiency when employing pulse shape analysis. In: *Advances in Liquid Scintillation Spectrometry 1994*. Tuscon, Arizona, Radiocarbon: in press.
- Hogg, A. G. 1993 Performance and design of 0.3-ml to 10-ml synthetic silica liquid scintillation vials for low-level ¹⁴C determination. In: Noakes, J. E., Schönhofer, F. and Polach, H. A., eds., *Liquid Scintillation Spectrometry 1992*. Tuscon, Arizona, Radiocarbon: 135-142.
- Hogg, A. G. and Noakes, J. E. 1992 Evaluation of high-purity synthetic silica vials in active and passive vial holders for liquid scintillation counting of benzene. *Radiocarbon* 34(3): 394-401.
- Honeyman, B. D. and Santschi, P. H. 1989 A Brownian-pumping model for oceanic trace metal scavenging: evidence from Th isotopes. *Journal of Marine Research* 47(4): 951-992.
- Hopkins, J. L. 1951 Electron energy studies with the anthracene scintillation counter. *Review of Scientific Instruments* 22(1): 29-33.
- Horrocks, D. L. 1963 Interaction of fission fragments with organic scintillators. *Review of Scientific*

- Instruments* 34(9): 1035-1040.
- Horrocks, D. L. 1964a Liquid scintillator-methods for calculation of average energy required to produce one photoelectron. *Nuclear Instruments and Methods* 27: 253-258.
- Horrocks, D. L. 1964b Alpha particle energy resolution in a liquid scintillator. *Review of Scientific Instruments* 35(3): 334-340.
- Horrocks, D. L. 1970 Pulse shape discrimination with organic scintillators. *Applied Spectroscopy* 24(4): 397-405.
- Horrocks, D. L. 1974 *Applications of Liquid Scintillation Counting*. New York, Academic Press: 346 p.
- Horrocks, D. L. 1976a Absolute disintegration rate determination of beta-emitting radionuclides by the pulse height shift-extrapolation method. *In: Noujaim, A. A., Ediss, C. and Weibe, L. I., eds., Liquid Scintillation Science and Technology*. New York, Academic Press: 185-198.
- Horrocks, D. L. 1976b The mechanisms of the liquid scintillation process. *In: Noujaim, A. A., Ediss, C. and Weibe, L. I., eds., Liquid Scintillation Science and Technology*. New York, Academic Press: 1-16.
- Horrocks, D. L. 1985 Studies of background sources in liquid scintillation counting. *International Journal of Applied Radiation and Isotopes* 36(8): 609-617.
- Huh, C.-A., Ku, T.-L., Luo, S., Landry, M. R. and Williams, P. M. 1993 Fluxes of Th isotopes in the Santa Monica Basin, offshore California. *Earth and Planetary Science Letters* 116(1-4): 155-164.
- Jenkins, W. J., Rona, P. A. and Edmond, J. M. 1980 Excess ^3He in the deep water over the Mid-Atlantic Ridge at 26°N: evidence of hydrothermal activity. *Earth and Planetary Science Letters* 49: 39-44.
- Kaihola, L. 1993 Glass vial background reduction in liquid scintillation counting. *The Science of the Total Environment* 130/131: 297-304.

- Kaihola, L., Kojola, H. and Heinonen, A. 1992 A minivial for small-sample ^{14}C dating. *Radiocarbon* 34(3): 402-405.
- Kaihola, L. and Oikari, T. 1991 Some factors affecting alpha particle detection in liquid scintillation spectrometry. In: Ross, H. H., Noakes, J. E. and Spaulding J. D., eds., *Liquid Scintillation Counting and Organic Scintillators*. Chelsea, Michigan, Lewis Publishers: 211-218.
- Kallmann, H. and Accardo, C. A. 1950 Coincidence experiments for noise reduction in scintillation counting. *Review of Scientific Instruments* 21(1): 48-51.
- Kallmann, H. and Furst, M. 1951 Fluorescent liquids for scintillation counters. *Nucleonics* 8(3): 32-39.
- Kallmann, H. and Furst, M. 1958 The basic processes occurring in the liquid scintillator. In: Bell, C. G. and Hayes, F. N., eds., *Liquid Scintillation Counting*. London, Pergamon Press: 3-22.
- Keller, C. 1988 *Radiochemistry*. Chichester, England, Ellis Horwood Ltd.: 208 p.
- Kershaw, P. and Young, A. 1988 Scavenging of ^{234}Th in the eastern Irish Sea. *Journal of Environmental Radioactivity* 6(1): 1-23.
- Kessler, M. J., ed. 1989 *Liquid Scintillation Analysis. Science and Technology*. Meriden, Connecticut, Packard Instrument Co.: 184 p.
- Kessler, M. 1990 Time-resolved liquid scintillation counting. *Radiocarbon* 32(3): 381-386.
- King, T. A. and Voltz, R. 1966 The time dependence of scintillation intensity in aromatic materials. *Proceedings of the Royal Society (London)* A289: 424-439.
- Klein, R. C. and Gershey, E. L. 1990 "Biodegradable" liquid scintillation counting cocktails. *Health Physics* 59(4): 461-470.
- Klinkhammer, G. and Hudson, A. 1986 Dispersal patterns for hydrothermal plumes in the South Pacific using manganese as a tracer. *Earth and Planetary Science Letters* 79: 241-249.
- Klinkhammer, G., Rona, P., Greaves, M. and Elderfield, H. 1985 Hydrothermal manganese plumes in the Mid-Atlantic Ridge rift valley. *Nature* 314: 727-731.

- Kobayashi, Y. and Maudsley, D. V. 1974 Recent advances in sample preparation. *In: Stanley, P. E. and Scroggins, B. A., eds., Liquid Scintillation Counting. Recent Developments.* New York, Academic Press: 189-205.
- Kojola, H., Polach, H., Nurmi, J., Oikari, T. and Soini, E. 1984 High resolution low-level liquid scintillation β -spectrometer. *International Journal of Applied Radiation and Isotopes* 35(10): 949-952.
- Kopp, D. M. and Kopp, M. K. 1991 PERALS datamap, a new method for simultaneous counting and separation of alpha and beta/gamma activity using PERALS spectrometry. *Transactions of the American Nuclear Society* 64: 25-27.
- Krishnaswami, S., Lal, D. and Somayajulu, B. L. K. 1976 Investigations of gram quantities of Atlantic and Pacific surface particulates. *Earth and Planetary Science Letters* 32: 403-419.
- Ku, T.-L., Knauss, K. G. and Mathieu, G. G. 1977 Uranium in the open ocean: concentration and isotopic composition. *Deep-Sea Research* 24: 1005-1017.
- Lalli, C. M. and Parsons, T. R. 1993 *Biological Oceanography: An Introduction.* Oxford, Pergamon Press: 301 p.
- Lambert, C. E., Fowler, S., Miquel, J. C., Buat-Menard, P., Dulac, F., Nguyen, H. V., Schmidt, S., Reyss, J. L. and La Rosa, J. 1991 Th-234: an ambiguous tracer of biogenic particle export from northwestern Mediterranean surface waters. *In: Kershaw, P. J. and Woodhouse, D. S., eds., Radionuclides in the Study of Marine Processes.* London, Elsevier Applied Science: 116-128.
- Langmuir, D. 1978 Uranium solution-mineral equilibrium at low temperatures with applications to sedimentary ore deposits. *Geochimica et Cosmochimica Acta* 42: 547-569.
- Laustriat, G. 1968 The luminescence decay of organic scintillators. *Molecular Crystals* 4: 127-145.
- Laustriat, G., Voltz, R. and Klein, J. 1970 Influence of solvent on scintillation yield. *In: Bransome, E.*

- D., ed., *The Current Status of Liquid Scintillation Counting*. New York, Grune and Stratton: 13-24.
- Lederer, C. M. and Shirley, V. S., eds. 1978 *Table of Isotopes, 7th ed.* New York, John Wiley and Sons: 1599 p.
- Libes, S. M. 1992 *An Introduction to Marine Biogeochemistry*. New York, John Wiley and Sons: 734 p.
- Livingston, H. D. and Cochran, J. K. 1987 Determination of transuranic and thorium isotopes in ocean water: in solution and in filterable particles. *Journal of Radioanalytical and Nuclear Chemistry, Articles* 115(2): 299-308.
- Long, E., Kohler, V. and Kelly, M. J. 1976 Heterogeneous counting on filter support media. In: Noujaim, A. A., Ediss, C. and Weibe, L. I., eds., *Liquid Scintillation Science and Technology*. New York, Academic Press: 47-69.
- Lupton, J. E., Delaney, J. R., Johnson, H. P. and Tivey, M. K. 1985 Entrainment and vertical transport of deep-ocean water by buoyant hydrothermal plumes. *Nature* 316: 621-623.
- Lupton, J. E., Klinkhammer, G. P., Normark, W. R., Haymon, R., MacDonald, K. C., Weiss, R. F. and Craig, H. 1980 Helium-3 and manganese at the 21°N East Pacific Rise hydrothermal site. *Earth and Planetary Science Letters* 50: 115-127.
- Lynch, F. J. 1975 Basic limitations of scintillation counters in time measurements. *IEEE Transactions on Nuclear Science* NS-22: 58-64.
- McDowell, W. J. 1986 Alpha Counting and Spectrometry Using Liquid Scintillation Methods. *National Academy of Sciences - National Research Council: Nuclear Science Series, Radiochemistry Techniques*. Oak Ridge, Tennessee, Technical Information Center, Office of Scientific and Technical Information, U. S. Department Energy: 108 p.
- McDowell, W. J., Bouwer, E. J., McKlveen, J. W. and Case, G. N. 1980 Application of the combined

- solvent extraction-high-resolution liquid scintillation method to the determination of Th-230 and U-234,238 in phosphatic materials. *In: Peng, C.-T., Horrocks, D. L. and Alpen, E. L., eds., Liquid Scintillation Counting. Recent Applications and Development. Volume 1: Physical Aspects.* New York, Academic Press: 333-346.
- McDowell, W. J., Farrar, D. T. and Billings, M. R. 1974 Plutonium and uranium determination in environmental samples: combined solvent extraction-liquid scintillation method. *Talanta* 21: 1231-1245.
- McDowell, W. J. and McDowell, B. L. 1993 The growth of a radioanalytical method: alpha liquid scintillation spectrometry. *In: Noakes, J. E., Schönhofer, F. and Polach, H. A., eds., Liquid Scintillation Spectrometry 1992.* Tuscon, Arizona, Radiocarbon: 193-200.
- McDowell, W. J. and McDowell, B. L. 1994 *Liquid Scintillation Alpha Spectrometry.* Boca Raton, Florida, CRC Press: 184 p.
- McEvoy, A. F., Dyson, S. R. and Harris, W. G. 1972 Compatibility of commercial tissue solubilizers with three primary scintillation fluors. *International Journal of Applied Radiation and Isotopes* 23: 338.
- McKay, W. A., Baxter, M. S., Ellett, D. J. and Meldrum, D. T. 1986 Radiocaesium and circulation patterns west of Scotland. *Journal of Environmental Radioactivity* 4: 205-232.
- McKee, B. A., DeMaster, D. J. and Nittrouer, C. A. 1984 The use of $^{234}\text{Th} / ^{238}\text{U}$ disequilibrium to examine the fate of particle reactive species on the Yangtze continental shelf. *Earth and Planetary Science Letters* 68: 431-442.
- McKee, B. A., DeMaster, D. J., Nittrouer, C. A. and Curtin, T. B. 1985 The use of Th-234 to examine chemical scavenging near the Amazon River mouth. *Estuaries* 8(2B): 112A.
- McKee, B. A., DeMaster, D. J. and Nittrouer, C. A. 1986 Temporal variability in the partitioning of thorium between dissolved and particulate phases on the Amazon shelf: implications for the

- scavenging of particle-reactive species. *Continental Shelf Research* 6(1/2): 87-106.
- Mackenzie, A. B., Scott, R. D., Linsalata, P., Miekeley, N. and Coutinho de Jesus, H. 1994 Interlaboratory comparison of analytical methods for the determination of natural series uranium and thorium isotopes in rock samples. *Journal of Radioanalytical and Nuclear Chemistry, Articles* 182(1): 21-34.
- McKinley, I. G., Baxter, M. S. and Jack, W. 1981a A simple model of radiocaesium transport from Windscale to the Clyde Sea area. *Estuarine, Coastal and Shelf Science* 13: 59-67.
- McKinley, I. G., Baxter, M. S., Ellett, D. J. and Jack, W. 1981b Tracer applications of radiocaesium in the Sea of the Hebrides. *Estuarine, Coastal and Shelf Science* 13: 69-82.
- McKlveen, J. W. 1974 *Alpha radioassay using liquid scintillation with energy or pulse shape discrimination*. Packard Technical Bulletin No 19. Downers Grove, Illinois, Packard Instrument Co.: 11 p.
- McKlveen, J. W. 1976 Liquid-scintillation energy and pulse-shape detection applied to low-level alpha radioassay. *Radiation Research* 66: 199-214.
- McKlveen, J. W. and Johnson, W. R. 1975 Simultaneous alpha and beta particle assay using liquid scintillation counting with pulse-shape discrimination. *Health Physics* 28: 5-11.
- McKlveen, J. W. and McDowell, W. J. 1976 Some studies of reflector construction and electronics configurations for optimizing pulse-height and pulse-shape resolution in alpha liquid-scintillation spectrometry. *Nuclear Technology* 28: 159-164.
- Martin, W. R. and Sayles, F. L. 1987 Seasonal changes of particle and solute transport processes in nearshore sediments: $^{222}\text{Rn}/^{226}\text{Ra}$ and $^{234}\text{Th}/^{238}\text{U}$ disequilibrium at a site in Buzzards Bay, MA. *Geochimica et Cosmochimica Acta* 51(4): 927-943.
- Matsumoto, E. 1975 Th-234/U-238 radioactive disequilibrium in the surface layer of the ocean. *Geochimica et Cosmochimica Acta* 39: 205-212.

- Mirza, M. Y. 1978 Preparation of ^{230}Th and ^{234}Th tracers. *Radiochimica Acta* 25(1): 45-47.
- Momoshima, N., Nakamura, Y. and Takashima, Y. 1983 Vial effect and background subtraction method in low-level tritium measurement by liquid scintillation counter. *International Journal of Applied Radiation and Isotopes* 34(12): 1623-1626.
- Moore, R. M. and Hunter, K. A. 1985 Thorium adsorption in the ocean: reversibility and distribution amongst particle sizes. *Geochimica et Cosmochimica Acta* 49(11): 2253-2257.
- Moore, W. S. 1976 Sampling ^{226}Ra in the deep ocean. *Deep-Sea Research* 23: 647-651.
- Moore, W. S. and Reid, D. F. 1973 Extraction of radium from natural waters using manganese-impregnated acrylic fibres. *Journal of Geophysical Research* 78: 8880-8886.
- Moore, W. S., Bruland, K. W. and Michel, J. 1981 Fluxes of uranium and thorium series isotopes in the Santa Barbara Basin. *Earth and Planetary Science Letters* 53(3): 391-399.
- Moran, S. B. and Buesseler, K. O. 1992 Short residence time of colloids in the upper ocean estimated from ^{238}U - ^{234}Th disequilibria. *Nature* 359(6392): 221-223.
- Moran, S. B. and Buesseler, K. O. 1993 Size-fractionated ^{234}Th in continental shelf waters off New England: implications for the role of colloids in oceanic trace metal scavenging. *Journal of Marine Research* 51(4): 893-922.
- Nibeck, J. I., Bares, S. L. and Williams, E. S. 1980 New scintillation cocktails in response to present and future trends in liquid scintillation counting. In: Peng, C.-T., Horrocks, D. L. and Alpen, E. L., eds., *Liquid Scintillation Counting. Recent Applications and Development. Volume 1: Physical Aspects*. New York, Academic Press: 59-72.
- Niven, S. E. H. and Moore, R. M. 1988 Effect of natural colloidal matter on the equilibrium adsorption of thorium in seawater. In: Guary, J.-C., Guegueniat, P. and Pentreath, R. J., eds., *Radionuclides: A Tool for Oceanography*. Amsterdam, Elsevier Applied Science: 111-120.
- Noakes, J. E., Isbell, A. F., Stipp, J. J. and Hood, D. W. 1963 Benzene synthesis by low temperature

- catalysis for radiocarbon dating. *Geochimica et Cosmochimica Acta* 27: 797-804.
- Noakes, J. E., Neary, M. P. and Spaulding, J. D. 1974 A new liquid scintillation counter for measurement of trace amounts of ^3H and ^{14}C . In: Stanley, P. E. and Scroggins, B. A., eds., *Liquid Scintillation Counting. Recent Developments*. New York, Academic Press: 53-66.
- Noakes, J. E., Schönhofer, F., and Polach, H. A., eds. 1993 *Liquid Scintillation Spectrometry 1992*. Tuscon, Arizona, Radiocarbon: 483 p.
- Oikari, T., Kojola, H., Nurmi, J. and Kaihola, L. 1987 Simultaneous counting of low alpha and beta particle activities with liquid scintillation spectrometry and pulse shape analysis. *Applied Radiation Isotopes* 38(10): 875-878.
- Oster, G. 1966 A young physicist at seventy: Hartmut Kallmann. *Physics Today* 19: 51-54.
- Owen, R. B. 1958 The decay times of organic scintillators and their application to the discrimination between particles of differing specific ionization. *IRE Transactions on Nuclear Science* NS-5(3): 198-201.
- Owen, R. B. 1962 Pulse shape discrimination - a survey of current techniques. *IRE Transactions on Nuclear Science* NS-9(3): 285-293.
- Packard, L. E. 1958 Instrumentation for internal liquid scintillation counting. In: Bell, C. G. and Hayes, F. N., eds., *Liquid Scintillation Counting*. London, Pergamon Press: 50-66.
- Painter, K. 1974 Choice of counting vial for liquid scintillation: a review. In: Stanley, P. E. and Scroggins, B. A., eds., *Liquid Scintillation Counting. Recent Developments*. New York, Academic Press: 431-451.
- Parker, C. A. and Hatchard, C. G. 1962a Delayed fluorescence from solutions of anthracene and phenanthrene. *Proceedings of the Royal Society (London)* A269: 574-584.
- Parker, C. A. and Hatchard, C. G. 1962b Sensitised anti-Stokes delayed fluorescence. *Proceedings of the Chemical Society* 147: 386-387.

- Parus, J. L., Raab, W. and Radoszewski, T. 1993 Liquid scintillation counting of plutonium and/or americium concentrations. *In: Noakes, J. E., Schönhofer, F. and Polach, H. A., eds., Liquid Scintillation Spectrometry 1992.* Tucson, Arizona, Radiocarbon: 233-237.
- Passo, C. J. and Cook, G. T. 1994 *Handbook of Environmental Liquid Scintillation Spectrometry. A Compilation of Theory and Methods.* Meriden, Connecticut, Packard Instrument Co.: 121 p.
- Passo, C. and Kessler, M. J. 1992 *The Essentials of α/β Discrimination.* Meriden, Connecticut, Packard Instrument Co.: 24 p.
- Passo Jr., C. J. and Kessler, M. J. 1993 Selectable delay before burst - a novel feature to enhance low-level counting performance. *In: Noakes, J. E., Schönhofer, F. and Polach, H. A., eds., Liquid Scintillation Spectrometry 1992.* Tucson, Arizona, Radiocarbon: 51-57.
- Peng, C.-T. 1993 The history of liquid scintillation counting: a personal view. *In: Noakes, J. E., Schönhofer, F. and Polach, H. A., eds., Liquid Scintillation Spectrometry 1992.* Tucson, Arizona, Radiocarbon: 1-13.
- Pentreath, R. J., Lovett, M. B., Jefferies, D. F., Woodhead, D. S., Talbot, J. W. and Mitchell, N. T. 1984 Impact on public radiation exposure of transuranium nuclides discharged in liquid wastes from fuel element reprocessing at Sellafield, United Kingdom. *In: Radioactive Waste Management. Volume 5.* Vienna, IAEA: 315-329.
- Perkins, L. J. and Scott, M. C. 1979 The application of pulse shape discrimination in Ne 213 to neutron spectrometry. *Nuclear Instruments and Methods* 166: 451-464.
- Polach, H. A. 1992 Four decades of progress in ^{14}C dating by liquid scintillation counting and spectrometry. *In: Taylor, R. E., Long, A. and Kra, R. S., eds., Radiocarbon Dating After Four Decades. An Interdisciplinary Perspective.* New York, Springer-Verlag: 198-213.
- Polach, H., Robertson, S., Butterfield, D., Gower, J. and Soini, E. 1983a The 'windowless' approach to scintillation counting: low-level C-14 as an example. *In: McQuarrie, S. A., Ediss, C and*

- Wiebe, L. I., eds., *Advances in Scintillation Counting*. Edmonton, Canada, University of Alberta: 494-507.
- Polach, H., Gower, J., Kojola, H. and Heinonen, A. 1983b An ideal vial and cocktail for low-level scintillation counting. *In: McQuarrie, S. A., Ediss, C and Wiebe, L. I., eds., Advances in Scintillation Counting*. Edmonton, Canada, University of Alberta: 508-525.
- Polach, H., Kojola, H., Nurmi, J. and Soini, E. 1984 Multiparameter liquid scintillation spectrometry. *Nuclear Instruments and Methods in Physics Research B5*: 439-442.
- Polach, H., Calf, G., Harkness, D., Hogg, A., Kaihola, L. and Robertson, S. 1988 Performance of new technology liquid scintillation counters for ^{14}C dating. *Nuclear Geophysics 2(2)*: 75-79.
- Prichard, H. M., Venso, E. A. and Dodson, C. L. 1992 Liquid-scintillation analysis of ^{222}Rn in water by alpha-beta discrimination. *Radioactivity and Radiochemistry 3(1)*: 28-36.
- Pringle, R. W., Black, L. D., Funt, B. L. and Sobering, S. 1953 A new quenching effect in liquid scintillators. *Physical Review 92*: 1582-1583.
- Queirazza, G., Roveri, M., Delfanti, R. and Papucci, C. 1991 Gas exchange at the air-sea interface: a technique for radon measurements in seawater. *In: Kershaw, P. J. and Woodhead, D. S., eds., Radionuclides in the Study of Marine Processes*. London, Elsevier Applied Science: 94-104.
- Raben, M. S. and Bloembergen, N. 1951 Determination of radioactivity by solution in a liquid scintillator. *Science 114*: 363-364.
- Rapkin, E. 1970 Development of the modern liquid scintillation counter. *In: Bransome, E. D., ed., The Current Status of Liquid Scintillation Counting*. New York, Grune and Stratton: 45-68.
- Rapkin, E. and Gibbs, J. A. 1965 *Polyethylene containers for liquid scintillation spectrometry*. Technical Bulletin Number 9. Downers Grove, Illinois, Packard Instrument Co.: 7 p.
- Reed, D. W. 1984 Triton X-100 as a complete liquid scintillation cocktail for counting aqueous

- solutions and ionic nutrient salts. *International Journal of Applied Radiation and Isotopes* 35(5): 367-370.
- Reid, D. F., Key, R. M. and Schink, D. R. 1979 Radium, thorium and actinium extraction from seawater using an improved manganese-oxide-coated fibre. *Earth and Planetary Science Letters* 43: 223-226.
- Reynolds, G. T., Harrison, F. B. and Salvini, G. 1950 Liquid scintillation counters. *Physical Review* 78: 488.
- Ring, J. G. and Everett L. J. 1982 Using SIS to compute DPM by liquid scintillation counting. *Transactions of the American Nuclear Society* 43: 38-39.
- Rousch, M. L., Wilson, M. A. and Hornyak, W. F. 1964 Pulse shape discrimination. *Nuclear Instruments and Methods* 31: 112-124.
- Rundt, K. 1991 The effect on quench curve shape of the solvent and quencher in a liquid scintillation counter. In: Ross, H. H., Noakes, J. E. and Spaulding, J. D., eds., *Liquid Scintillation Counting and Organic Scintillators*. Chelsea, Michigan, Lewis Publishers: 257-268.
- Ryan, T. P., Mitchell, P. I., Vives i Battle, J., Sanchez-Cabeza, J. A., McGarry, A. T. and Schell, W. R. 1993 Low-level ^{241}Pu analysis by supported-disk liquid scintillation counting. In: Noakes, J. E., Schönhofer, F. and Polach, H. A., eds., *Liquid Scintillation Spectrometry 1992*. Tucson, Arizona, Radiocarbon: 75-82.
- Saarinen, L. and Suski, J. 1992 *Determination of Uranium Series Radionuclides Pa-231 and Ra-226 by Liquid Scintillation Counting*. Report YJT-92-20. Helsinki, Nuclear Waste Commission of Finnish Power Companies: 24 p.
- Saarinen, L. and Suksi, J. 1993 Determination of uranium series radionuclide ^{231}Pa using liquid scintillation counting. In: Noakes, J. E., Schönhofer, F. and Polach, H. A., eds., *Liquid Scintillation Spectrometry 1992*. Tucson, Arizona, Radiocarbon: 209-215.

- Salonen, L. 1993a A rapid method for monitoring of uranium and radium in drinking water. *The Science of the Total Environment* 130/131: 23-35.
- Salonen, L. 1993b Measurement of low levels of ^{222}Rn in water with different commercial liquid scintillation counters with pulse-shape analysis. In: Noakes, J. E., Schönhofer, F. and Polach, H. A., eds., *Liquid Scintillation Spectrometry 1992*. Tucson, Arizona, Radiocarbon: 361-372.
- Sanchez-Cabeza, J., Pujol, L., Merino, J., León, L., Molero, J., Vidal-Quadras, A., Schell, W. R. and Mitchell, P. I. 1993 Optimization and calibration of a low background liquid scintillation counter for the simultaneous determination of alpha and beta emitters in aqueous samples. In: Noakes, J. E., Schönhofer, F. and Polach, H. A., eds., *Liquid Scintillation Spectrometry 1992*. Tucson, Arizona, Radiocarbon: 43-50.
- Santschi, P. H., Adler, D., Amdurer, H., Li, Y.-H. and Bell, J. J. 1980 Thorium isotopes as analogues for "particle reactive" pollutants in coastal marine environments. *Earth and Planetary Science Letters* 47: 327-335.
- Sarin, M. M., Krishnaswami, S., Somayajulu, B. L. K. and Moore, W. S. 1990 Chemistry of uranium, thorium and radium isotopes in the Ganga-Brahmaputra River system: weathering processes and fluxes to the Bay of Bengal. *Geochimica et Cosmochimica Acta* 54: 1387-1396.
- Sarmiento, J. L., Hammond, D. E. and Broecker, W. S. 1976 The calculation of the counting error for ^{222}Rn scintillation counting. *Earth and Planetary Science Letters* 32: 351-356.
- Schmidt, S., Nival, P., Reyss, J.-L., Baker, M. and Buat-Menard, P. 1992 Relation between ^{234}Th scavenging and zooplankton biomass in Mediterranean surface waters. *Oceanologica Acta* 15(2): 227-231.
- Shimmield, G. B. and Price, N. B. 1988 The scavenging of U, ^{230}Th and ^{231}Pa during pulsed hydrothermal activity at 20°S, East Pacific Rise. *Geochimica et Cosmochimica Acta* 52(3): 669-677.

- Shimmiel, T. M. 1993 *A Study of Radionuclides, Lead and Lead Isotope Ratios in Scottish Sea Loch Sediments*. PhD Thesis, University of Edinburgh.
- Simonnet, G., Jacquet, M. A., Sharif, A. and Engler, R. 1981 Use of pliable plastic bags in liquid scintillation counting. *International Journal of Applied Radiation and Isotopes* 32: 539-543.
- Spate, V. L. and Langhorst, S. M. 1986 A comparison of the counting characteristics of Opti-Fluor® and Aquasol-2®: liquid scintillation cocktail. *Health Physics* 51(5): 667-671.
- Spaulding, J. D. and Noakes, J. E. 1993 Determination of ^{222}Rn in drinking water using an alpha/beta liquid scintillation counter. *In: Noakes, J. E., Schönhofer, F. and Polach, H. A., eds., Liquid Scintillation Spectrometry 1992*. Tucson, Arizona, Radiocarbon: 373-381.
- Stanley, P. E. 1980 An appraisal of liquid scintillation science and technology, 1964-1979. *In: Peng, C.-T., Horrocks, D. L. and Alpen, E. L., eds., Liquid Scintillation Counting. Recent Applications and Development. Volume 1: Physical Aspects*. New York, Academic Press: 257-271.
- Suontausta, J., Oikari, T. and Webb, S. 1993 A meltable thermoplastic scintillator. *In: Noakes, J. E., Schönhofer, F. and Polach, H. A., eds., Liquid Scintillation Spectrometry 1992*. Tucson, Arizona, Radiocarbon: 173-178.
- Takiue, M., Matsui, Y. and Fujii, H. 1991 Activity determination of simultaneously chemical and color quenched samples using a liquid scintillation counter. *Applied Radiation and Isotopes* 42(3): 241-244.
- Tanaka, N., Takeda, Y. and Tsunogai, S. 1983 Biological effect on removal of ^{234}Th , ^{210}Po and ^{210}Pb from surface water in Funka Bay, Japan. *Geochimica et Cosmochimica Acta* 47: 1783-1790.
- ter Wiel, J. 1993 Effect of viscosity on quench characteristics of solvents for liquid scintillation counting. *In: Noakes, J. E., Schönhofer, F. and Polach, H. A., eds., Liquid Scintillation Spectrometry 1992*. Tucson, Arizona, Radiocarbon: 185-191.
- ter Wiel, J. and Hegge, T. 1991 Advances in scintillation cocktails. *In: Ross, H. H., Noakes, J. E. and*

- Spaulding, J. D., eds., *Liquid Scintillation Counting and Organic Scintillators*. Chelsea, Michigan, Lewis Publishers: 51-67.
- Thomson, J. 1991 Di-isopropylnaphthalene - a new solvent for liquid scintillation counting. *In*: Ross, H. H., Noakes, J. E. and Spaulding, J. D., eds., *Liquid Scintillation Counting and Organic Scintillators*. Chelsea, Michigan, Lewis Publishers: 19-34.
- Thomson, J. 1993 Plastic scintillators: some novel applications. *In*: Noakes, J. E., Schönhofer, F. and Polach, H. A., eds., *Liquid Scintillation Spectrometry 1992*. Tuscon, Arizona, Radiocarbon: 179-184.
- Thomson, J., Colley, S., Anderson, R., Cook, G. T. and MacKenzie, A. B. 1993 ^{210}Pb in the sediments and water column of the Northeast Atlantic from 47 to 59°N along 20°W. *Earth and Planetary Science Letters* 115: 75-87.
- Thorngate, J. H. 1978 A simplified pulse-shape discrimination circuit for use in liquid-scintillation spectroscopy of alpha particles. *Health Physics* 34: 103-106.
- Thorngate, J. H. and Christian, D. J. 1977 Optimisation of the detector and associated electronics used for high-resolution liquid-scintillation spectroscopy. *Health Physics* 33: 443-448.
- Thorngate, J. H., McDowell, W. J. and Christian, D. J. 1974 An application of pulse shape discrimination to liquid scintillation counting. *Health Physics* 27: 123-126.
- Trocine, R. P. and Trefy, J. H. 1988 Distribution and chemistry of suspended particles from an active hydrothermal vent site on the Mid-Atlantic Ridge at 26°N. *Earth and Planetary Science Letters* 88: 1-15.
- van Cauter, S. 1986 *Three dimensional spectrum analysis: a new approach to reduce background of liquid scintillation counters*. Application Bulletin 006. Downers Grove, Illinois, Packard Instrument Co.: 8p.
- Venso, E. A., Prichard, H. M. and Dodson, C. L. 1993 Measurement of isotopic uranium in Texas

- drinking water supplies by liquid scintillation with alpha-beta discrimination. *In*: Noakes, J. E., Schönhofer, F. and Polach, H. A., eds., *Liquid Scintillation Spectrometry 1992*. Tucson, Arizona, Radiocarbon: 425-430.
- Voltz, R., Lopes da Silva, J., Laustriat, G. and Coche, A. 1966 Influence of the nature of ionising particles on the specific luminescence of organic scintillators. *Journal of Chemical Physics* 45(9): 3306-3311.
- Voltz, R., DuPont, H. and Laustriat, G. 1968 Radioluminescence des milieux organiques II. Vérification expérimentale de l'étude cinétique. *Journal de Physique* 29: 297-305.
- Von Damm, K. L., Edmond, J. M., Grant, B., Measures, C. I., Walden, B. and Weiss, R. F. 1985 Chemistry of hydrothermal solutions at 21°N, East Pacific Rise. *Geochimica et Cosmochimica Acta* 49: 2197-2220.
- Wei, C.-L. and Hung, C.-C. 1993 The effect of isotopic equilibration time on the determination of ^{234}Th in seawater. *Journal of Radioanalytical and Nuclear Chemistry, Letters* 175(2): 155-159.
- Wolff, T., Pfanner, K. and Springob, C. 1993 Fluorescence of 9,10-dimethylanthracene in solutions containing diisopropylanthracene and in solid cyclodextrin complexes. *Journal of Photochemistry and Photobiology A: Chemistry* 74: 247-253.
- Wright, G. T. 1956 Scintillation decay times of organic crystals. *Proceedings of the Physical Society* B69: 358-372.
- Wunderly, S. W. 1993 Simultaneous measurement of alpha and beta emissions on Ready Cap®. *In*: Noakes, J. E., Schönhofer, F. and Polach, H. A., eds., *Liquid Scintillation Spectrometry 1992*. Tucson, Arizona, Radiocarbon: 217-223.
- Wunderly, S. W. and Kauffman, J. M. 1990 New quench resistant fluors for liquid scintillation counting. *Applied Radiation and Isotopes* 41(9): 809-815.
- Yang, D. 1993 Alpha-counting with a solid scintillator. *Journal of Radioanalytical and Nuclear*

Chemistry, Letters 175(5): 393-400.

Yang, D. 1994 Calibration and quench correction for alpha liquid scintillation analysis. *In: Advances in Liquid Scintillation Spectrometry 1994*. Tuscon, Arizona, Radiocarbon: in press.

Yang, D., Zhu, Y. and Möbius, S. 1991 Rapid method for alpha counting with extractive scintillator and pulse shape analysis. *Journal of Radioanalytical and Nuclear Chemistry, Articles* 147(1): 177-189.

Yu, Y.-F., Salbu, B., Bjørnstad and Lien, H. 1990 Improvement for α -energy resolution in determination of low level plutonium by liquid scintillation counting. *Journal of Radioanalytical and Nuclear Chemistry, Letters* 145(5): 345-353.

Yu, Y.-F., Bjørnstad, H. E. and Salbu, B. 1992 Determination of plutonium-239 + plutonium-240 and plutonium-241 in environmental samples using low-level liquid scintillation spectrometry. *Analyst* 117: 439-442.

